RATES AND MECHANISMS OF CHEMICAL REACTIONS DURING FLOW OF SECONDARY TREATED SEWAGE EFFLUENT THROUGH POROUS BEDS

Thesis by

Julius Uradnisheck

In Partial Fulfillment of the Requirements

for the Degree of

Doctor of Philosophy

California Institute of Technology

Pasadena, California

1975

(Submitted May 13, 1975)

dedicated to the
great state of California

ACKNOWLEDGEMENTS

Without the guidance and support of my advisors, Dr. William H. Corcoran and Dr. Jack E. McKee, this investigation would not have been possible.

I am most appreciative of Dr. James J. Morgan's permitting me to use his atomic absorption apparatus.

I gratefully acknowledge California Institute of Technology's President's Fund for financial support of my research. I am appreciative of the ARCS Foundation of Los Angeles for scholarship support.

The ready help of George Griffith was responsible for preventing my equipment designs from materializing into Rube Goldberg Mousetraps. Bill Schuelke and Chic Nakawatase built the laboratory column and sampling apparatus and Jennifer Burkhart typed this thesis.

The easy flow of advice and equipment from other departments and JPL greatly facilitated the completion of this work.

ABSTRACT

A general theory is formulated, based on extensive experimental and theoretical work, concerning the variation of chemical species in the top aerated horizon of the soil associated with the intermittent percolation of a secondary treated sewage effluent containing aqueous ammonium ions.

Experimental data are presented to show that the variation of aqueous cations in inorganic percolating solutions is a result of the consecutive steps of rapid ion exchange of cations from the electric double layer followed by slow ion exchange of chemisorbed cations diffusing through aluminosilicate mineral structures.

High concentrations of alkaline earth salts in interstitially held solutions when the granitic sand is drained of solution are shown to be a result of desorption of cations from the sand by aqueous hydrogen ions generated by the conversion of adsorbed ammonium ions to nitrite ions by Nitrosomonas. Only a slight amount of mineral dissolution is shown to occur. Data are also presented to show that when a solution is again percolated through the sand, hydrogen ion desorption is accompanied by only minimal nitrification.

A mathematical model is presented to predict the variation of aqueous calcium, magnesium, sodium, ammonium, nitrate, nitrite, oxygen, acidity, and bicarbonate ions as well as the bacterial population densities, adsorbed cations, and gaseous constituency of a soil column and solution as an intermittent percolation process is operated.

TABLE OF CONTENTS

	Page
INTRODUCTION	1
BACKGROUND	4
EXPERIMENTAL APPARATUS	8
LABORATORY COLUMN	8
SOLUTION, GAS, AND SOIL SAMPLING	10
ARTIFICIAL SOIL	13
ROUTINE ANALYTICAL PROCEDURES	17
Aqueous Samples	17
Gaseous Samples	20
Biological Samples	21
Surface Chemical Species	23
GENERAL EXPERIMENTAL PROCEDURE	27
SPECIFIC EXPERIMENTAL PROCEDURES, RESULTS, AND CONCLUSIONS	29
GENERAL TREND OF THE INVESTIGATION	29
PRELIMINARY INVESTIGATIONS	30
Percolation of Deionized Water	30
Percolation of a Sodium Salt Solution	33
Percolation of a Calcium Salt Solution	37
Study of Extraneous Sand and Solution Chemical Species	41
Percolation of a Calcium Salt Solution	43
General Conclusions	46
MAIN BODY OF RESEARCH	47
Percolation of Deionized Water	47

Page

Percolation of a Calcium Salt Solution 60

Higher Rate Percolation 79

Percolation of Lithium and Ammonium Salt-Containing Solutions 90

Summary of Nonbiological Changes to a Percolating Solution 98

CHEMICAL PROPERTIES OF THE LABORATORY COLUMN SAND 102

Mineral Dissolution 102

Determination of Ion Exchange Distribution Coefficients 111

Specific Role of the Aqueous Hydrogen Ion 114

Proof of the Rate Controlling Step of Ion Exchange 123

Summary of the Chemical Properties of the Column Sand 126

PERCOLATION OF SOLUTIONS THROUGH A NITRIFYING COMMUNITY 131

First Wet Period 135

First Dry Period 136

Second Wet Period 137

Second Dry Period 147

Third Wet Period Start-Up 147

Third Wet Period Continued 156

Fourth Wet Period Leading Edge 162

Fifth Wet Period Bacterial Population Count 165

Extensive Dry Period Analysis 166

Consistency Check 172

Total Quantity of Aqueous Species in Interstitial Solution 174

		Page
	Bacterial Population Counts	175
	Proof of the Nitrification Mechanism	178
	Effects of Variations in the Duration of the Dry Period	188
	Source of Dry Period Aqueous Cations	193
MATHEMATICAL MODEL		201
SUMMARY, RECOMMENDATIONS, ENGINEERING SUGGESTIONS		224
REFERENCES		230
APPENDIX A:	Artificial Soil	238
APPENDIX B:	Percolating Solution Analyses	240
APPENDIX C:	Method of the Numerical Solution of the Unsteady State Variation of Aqueous Calcium and Magnesium Content of a Solution Percolating through a Packed Bed of Ion Exchange Medium	243
APPENDIX D:	Chronology of the Operation of the Laboratory Column and Analyses of Data	247
APPENDIX E:	Numerical Solutions	252
APPENDIX F:	Evaluation of Constants used in the Mathematical Model for the Intermittent Percolation Process	261
APPENDIX G:	Listing of Fortran Dry and Wet Period Mathematical Models	266
PROPOSITION:	Mathematical Model for the Selection Function of Ball Milling	294

LIST OF FIGURES

Number	Title	Page
1	Circulation of Percolating Solution for the Laboratory Sand Column	9
2	A Column Segment, Lateral View Showing Solution/Gas Sampler	11
3	A Column Segment, Radial View Showing Solution/Gas and Soil Samplers	12
4	Detailed Diagrams of the Solution/Gas and Soil Samplers	14
5	Nitrosomonas Bacteria Grown on Ammonium Salt Silica Gel Plating Compound	24
6	Nitrobacter Bacteria Grown on Nitrite Salt Silica Gel Plating Compound	25
7	Aqueous Calcium Ion Content of Deionized Water First Percolated through the Laboratory Column (37 ℓ/day)	31
8	pH of Deionized Water First Percolated through the Laboratory Column (37 ℓ/day)	32
9	Variations of Aqueous Calcium Ion Content of a 119 mg Na^{+}/ℓ Containing Solution Percolating at 33.6 ℓ/day through the Laboratory Column	35
10	Variations of pH in a 119 mg Na^{+}/ℓ Containing Solution Percolating at 33.6 ℓ/day through the Laboratory Column	36
11	Aqueous Calcium Ion Content of a 7 mg Ca^{++}/ℓ Containing Inlet Solution Percolating at 33.6 ℓ/day through the Laboratory Column	39
12	pH of a 7 mg Ca^{++}/ℓ Containing Inlet Solution Percolating at 33.6 ℓ/day through the Laboratory Column	440
13	Aqueous Calcium Ion Content of a 38 mg Ca^{++}/ℓ Containing Solution Percolating at 3.7 ℓ/day through the Laboratory Column Displacing a Deionized Water Solution	44
14	pH of a 38 mg Ca^{++}/ℓ Containing Solution Percolating at 3.7 ℓ/day through the Laboratory Column Displacing a Deionized Water Solution	45

Number	Title	Page
15	Aqueous Magnesium Ion Content of Deionized Water Percolating through the Laboratory Column	49
16.	Aqueous Sodium Ion Content of Deionized Water Percolating through the Laboratory Column	50
17	Aqueous Potassium Ion Content of Deionized Water Percolating through the Laboratory Column	51
18	Aqueous Silica Content of Deionized Water Percolating through the Laboratory Column	52
19	pH of Deionized Water Percolating through the Laboratory Column	53
20	Aqueous Calcium Ion Content of Deionized Water Percolating through the Laboratory Column	61
21	Aqueous Potassium Ion Content of a 40 mg Ca^{++}/ℓ Containing Inlet Solution Percolating through the Laboratory Column	63
22	Aqueous Silica Content of a 40 mg Ca^{++}/ℓ Containing Inlet Solution Percolating through the Laboratory Column	64
23	pH of a 40 mg Ca^{++}/ℓ Containing Inlet Solution Percolating through the Laboratory Column	65
24	Dissolved Oxygen Content of a 40 mg Ca^{++}/ℓ Containing Solution Percolating through the Laboratory Column	66
25	Aqueous Sodium Ion Content of a 40 mg Ca^{++}/ℓ Containing Inlet Solution Percolating through the Laboratory Column	68
26	Aqueous Calcium Ion Content of a 40 mg Ca^{++}/ℓ Containing Inlet Solution Percolating through the Laboratory Column	69
27	Aqueous Magnesium Ion Content of a 40 mg Ca^{++}/ℓ Containing Inlet Solution Percolating through the Laboratory Column	70
28	Theoretical Aqueous Calcium and Magnesium Ion Content of a 40 mg Ca^{++}/ℓ Containing Inlet Solution Percolating through and Ion Exchanging with a Column of Sand	74

Number	Title	Page
29	Aqueous Calcium Ion Content of a 40 mg Ca^{++}/ℓ Containing Inlet Solution Percolating at 36 ℓ/day through the Laboratory Column	80
30	Aqueous Magnesium Ion Content of a 40 mg Ca^{++}/ℓ Containing Inlet Solution Percolating at 36 ℓ/day through the Laboratory Column	81
31	Aqueous Silica Content of a 40 mg Ca^{++}/ℓ Containing Inlet Solution Percolating at 36 ℓ/day through the Laboratory Column	83
32	pH of a 40 mg Ca^{++}/ℓ Containing Inlet Solution Percolating at 36 ℓ/day through the Laboratory Column	84
33	Dissolved Oxygen Content of a 40 mg Ca^{++}/ℓ Solution Percolating at 36 ℓ/day through the Laboratory Column	85
34	Aqueous Sodium Ion Content of a 40 mg Ca^{++}/ℓ Inlet Solution Percolating at 36 ℓ/day through the Laboratory Column	86
35	Aqueous Potassium Ion Content of a 40 mg Ca^{++}/ℓ Containing Inlet Solution Percolating at 36 ℓ/day through the Laboratory Column	88
36	Aqueous Magnesium Ion Content of a Lithium and Ammonium Salt Containing Solution Percolating at Various Rates through the Laboratory Column	92
37	Aqueous Calcium Ion Content of a Lithium and Ammonium Salt Containing Solution Percolating at Various Rates through the Laboratory Column	93
38	Aqueous Sodium Ion Content of a Lithium and Ammonium Salt Containing Solution Percolating at Various Rates through the Laboratory Column	94
39	Aqueous Potassium Ion Content of a Lithium and Ammonium Salt Containing Solution Percolating at Various Rates through the Laboratory Column	95
40	Aqueous Silica Content of a Lithium and Ammonium Salt Containing Solution Percolating at Various Rates through the Laboratory Column	96
41	Quartz Surface after Two Month Treatment in 0.16 M Nitric Acid (7500 Magnification)	104

Number	Title	Page
42	Plagioclase Surface after One Month Treatment in 0.16 M Nitric Acid (7800 Magnification)	104
43	Freshly Fractured Plagioclase in Epoxy Support (79 Magnification)	105
44	Twin Fragment of Freshly Fractured Plagioclase after One Month Treatment in 0.16 M Nitric Acid (79 Magnification)	105
45	Freshly Fractured Hornblende in Epoxy Support (79 Magnification)	106
46	Twin Fragment of Freshly Fractured Hornblende after One Month Treatment in 0.16 M Nitric Acid (79 Magnification)	106
47	Freshly Fractured Hornblende (4000 Magnification)	107
48	Twin Fragment of Freshly Fractured Hornblende after One Month Treatment in 0.16 M Nitric Acid (4000 Magnification)	107
49	Plagioclase Surface after Two Month Treatment in Neutral Salt Solution (7750 Magnification)	109
50	Plagioclase Surface after Two Month Treatment in Fluoride/Phosphate Solution (4000 Magnification	109
51	Hornblende Surface after Two Month Treatment in Fluoride/Phosphate Solution (3700 Magnification)	110
52	Hornblende Surface after Two Month Treatment in Fluoride/Phosphate Solution (7000 Magnification	110
53	Ion Exchange Distributions for Calcium Ions and Four Other Cations	115
54	Apparatus for Long Duration, Constant pH Studies of Mineral/Solution Interactions	118
55	Test for an Equivalent Exchange of the Aqueous Hydrogen Ion with Cations Adsorbed to a Sand Sample	120
56	Cation Exchange Capacity of a Sand Mixture as a Function of pH	122
57	Accumulative Release of Cations from Sand Being Leached with Nitric Acid	127

Number	Title	Page
58	Carbon Dioxide and Oxygen Content of the Laboratory Column Atmosphere during the First Dry Period	138
59	Aqueous Potassium, Magnesium, and Calcium Ion Content of Feed Solution Percolating through the Laboratory Column during the Second Wet Period	140
60	pH of Feed Solution Percolating through the Laboratory Column during the Second Wet Period	141
61	Aqueous Inorganic Nitrogenous Species Content of Feed Solution Percolating through the Laboratory Column during the Second Wet Period	142
62	Dissolved Oxygen Content of Feed Solution Percolating through the Laboratory Column during the Second Wet Period	144
63	Quantity of Cations Extracted from Sand Samples Taken from the Laboratory Column at the End of the Second Wet Period	146
64	Carbon Dioxide and Oxygen Content of the Laboratory Column Atmosphere during the Second Dry Period	148
65	Aqueous Cation Concentrations in the Leading Edge Solution Starting the Third Wet Period	150
66	Aqueous Inorganic Nitrogen Species Concentrations in the Leading Edge Solution Starting the Third Wet Period	151
67	pH of the Leading Edge Solution Starting the Third Wet Period	153
68	Aqueous Silica Content of the Leading Edge Solution Starting the Third Wet Period	154
69	pH of Feed Solution Percolating through the Laboratory Column during the Third Wet Period	157
70	Aqueous Potassium, Magnesium, and Calcium Ion Content of Feed Solution Percolating through the Laboratory Column during the Third Wet Period	159
71	Dissolved Oxygen Content of Feed Solution Percolating through the Laboratory Column during the Third Wet Period	160

Number	Title	Page
72	Aqueous Inorganic Nitrogenous Species Content of Feed Solution Percolating through the Laboratory Column during the Third Wet Period	161
73	Aqueous Species Content of the Interstitial Solution of the Laboratory Column at the End of the Third Dry Period	164
74	Oxygen Content of the Laboratory Column Atmosphere during a Fourteen Day Duration Dry Period	168
75	Carbon Dioxide Content of the Laboratory Column Atmosphere during a Fourteen Day Duration Dry Period	169
76	Theoretical Oxygen and Carbon Dioxide Contents of the Laboratory Column Atmosphere during a Dry Period	171
77	Aqueous Cation Content of Leading Edge Solutions Starting Two Separate Wet Periods	173
78	Aqueous Cation Content of the Leading Edge Solution Terminating an Oxygen Deficient Laboratory Column Dry Period	179
79	Aqueous Silica Content of the Leading Edge Solution Terminating an Oxygen Deficient Laboratory Column Dry Period	180
80	Aqueous Nitrate Ion Content of the Leading Edge Solution Terminating Oxygen Deficient and Oxygen Sufficient Laboratory Column Dry Periods	182
81	Oxygen Content of the Laboratory Column Atmosphere during a Dry Period following Two Ammonium Ion Free Wet Periods	183
82	Carbon Dioxide Content of the Laboratory Column Atmosphere during a Dry Period following Two Ammonium Ion Free Wet Periods	184
83	pH of the Leading Edge Solution Terminating an Ammonium Ion Free Laboratory Column Dry Period	186
84	Aqueous Cation Contents of the Leading Edge Solution Terminating an Ammonium Ion Free Laboratory Column Dry Period	187
85	Aqueous Species Contents of the Interstitial Solution of the Laboratory Column at the End of a Fourteen Day Dry Period	189

Number	Title	Page
86	Aqueous Species Contents of the Interstitial Solution of the Laboratory Column at the End of a Five Day Dry Period	190
87	Aqueous Species Contents of the Interstitial Solution of the Laboratory Column at the End of a 2.2 Day Dry Period	191
88	Aqueous Species Contents of the Interstitial Solution of the Laboratory Column at the End of a One Day Dry Period	192
89	Aqueous Species Contents of the Interstitial Solution of the Laboratory Column at the End of a Dry Period following Calcium Ion Free Wet Periods	195
90	pH of the Leading Edge Solution Terminating a Dry Period following Lithium Ion Rich Wet Periods	198
91	Aqueous Species Contents of the Interstitial Solution of the Laboratory Column at the End of Dry Period following Lithium Ion Rich Wet Periods	199
92	Theoretical Population Densities of Nitrosomonas and Nitrobacter and Concentrations of Dissolved Oxygen and Gaseous Oxygen during Seven Day Wet Period	212
93	Theoretical Quantities of Adsorbed Ammonium Ions and Aqueous Nitrite, Nitrate, and Ammonium Ions during Seven Day Wet Period	213
94	Theoretical Quantities of Aqueous Calcium, Magnesium, Sodium, and Acidity during Seven Day Wet Period	214
95	Theoretical Quantities of Adsorbed Calcium, Magnesium, Sodium, and Hydrogen Ions during Seven Day Wet Period	215
96	Theoretical Population Densities of Nitrosomonas and Nitrobacter and Concentrations of Gaseous Carbon Dioxide and Oxygen during First Three Days of Dry Period	217
97	Theoretical Quantities of Adsorbed Ammonium Ions, Aqueous Nitrite, Nitrate, and Ammonium Ions during First Three Days of Dry Period	218
98	Theoretical Concentrations of Aqueous Calcium, Magnesium, Sodium, and Hydrogen Ions during First Three Days of Dry Period	219

Number	Title	Page
99	Theoretical Quantities of Adsorbed Calcium, Magnesium and Hydrogen Ions and Aqueous Oxygen during First Three Days of Dry Period	220

LIST OF TABLES

Number	Title	Page
1	Emission Spectrographic Analyses	42
2	Whittier Narrows Water Reclamation Plant Effluent Quality	133
3	Composition of Solution Fed Intermittently to the Laboratory Column	134

INTRODUCTION

Groundwater recharge by percolation of secondary treated sewage effluent has been practiced for centuries. In the past twenty years, population pressures have warranted the increased practice of recharging groundwater supplies with secondary treated sewage effluent throughout the world and in the United States. A solution percolating through the ground is acted upon by various physical, chemical, and biological mechanisms. Most rapid changes to the quality of the solution occur when it first enters the soil. A vast number of biological transformations to the solution's dissolved chemical species can occur; however, any one biological transformation will proceed only under a specific set of environmental conditions. Study of the quality of solution recharging groundwater supplies has been extensive (Tefflemire et al., 68; Fetter et al., 69). Rather than the present research concerning itself with the entire change of solution quality as secondary treated sewage effluent travels down through the soil and channels across acquifers to the groundwater reservoirs, the present research has centered on aqueous quality as solution percolates down through the topmost horizon of soil. Most of the chemical species dissolved in a solution intermittently percolating through a laboratory granitic sand column were studied under the specific conditions of the presence of aqueous ammonium and bicarbonate ions and lack of organic carbon compounds. The specific conditions of percolation were chosen so that a local problem with groundwater recharge by intermittent percolation of secondary treated sewage effluent could be analyzed. An understanding of the

recharge process under a specific set of conditions builds toward understanding the same process under all sets of conditions.

A rapidly growing population and subsequent demand on underground reserves requires the Los Angeles County Flood Control District (LACFCD) to augment water supplies by replenishing the natural groundwater reservoirs. Some recharge of these reservoirs is accomplished by intermittently spreading secondary treated sewage effluent on the ground's surface so that it can percolate through the soil and to the reservoirs. Undesirable increases of total dissolved solids in the percolating solution have been observed as it travels through the soil matrix. Only plausible explanations have been given for the dissolved-solids pickup. This present investigation has concentrated on a basic understanding of the chemical, biological, and physical interactions that lead to the change in Total Dissolved Solids content of solutions in a soil environment.

The results of the Los Angeles Flood Control District's spreading operation at Whittier Narrows had been carefully examined. A scaled-down version of the intermittent percolation process, as performed in the field by the LACFCD at Whittier Narrows, was operated in the laboratory so that more control could be placed on the variables influencing the chemical composition of percolating water. Such control has permitted development of a quantitative model for the change of total dissolved solids in the actual spreading operations. Development of the mathematical model required a recognition of basic processes associated with the interaction of minerals, solutions, and bacteria. Such recognition permits engineering recommendations to be made for

reducing the total dissolved solids increase of intermittently percolated treated sewage effluents. The results of this investigation relate to the discovery of heavy metals from mine tailings by acid leaching which apparently is also a chemical, physical, and biological process of percolation.

BACKGROUND

The spreading of water for the conservation of groundwater supplies first came into use in Southern California toward the beginning of the twentieth century. Usual practice then was to construct catch basins on the peripheries of river channels. Weirs jutting into the channels diverted water into spreading basins during flooding periods of the river (Mitchelson, 1). Population approximately doubled each ten years and drew a heavy demand on its subsurface water reserves. Such demand prompted the widespread practice of recharging the groundwaters. The Los Angeles County Flood Control District (LACFCD) constructed spreading facilities adjacent to the Rio Hondo and the San Gabriel Rivers in 1938 to compensate for their lining of the Rio Hondo and the Los Angeles Rivers for flood control purposes (Leonard, 2). Eleven years later the LACFCD investigated the spreading of treated sewage effluent to augment groundwater reserves.

Since 1963 groundwater quality research has been conducted by the LACFCD. Field research is conducted on a small test spreading basin between the Rio Hondo and the San Gabriel Rivers in Whittier Narrows. Effluent from the Whittier Narrows Water Reclamation Plant is diverted for spreading purposes to ascertain variations of solution quality as percolation proceeds through the soil matrix to the aquifers below. Attention will be given presently to the test basin at Whittier Narrows although one further south on the Rio Hondo was also operated (McMichael et al., 3). The Whittier Narrows test basin used by the LACFCD is a 50 by 70 foot plot of level ground circumferenced by a

two foot high levee and centered with a four-foot diameter cylindrical hole approximately ten feet deep and reinforced by a corrugated pipe. Effluent leaving the Whittier Narrows Water Reclamation Plant is diverted intermittently to flood the test basin for one week every three weeks. As the treated sewage effluent percolates through the soil, solution samples are withdrawn through the corrugated pipe at two-foot depth intervals (Reid, 5). Analysis of the samples permitted evaluations to be made on water quality as percolation of secondary sewage effluents proceeded.

Data from the original work at Whittier Narrows (McMichael et al., 3) show that toward the beginning of the 8-hour Wet Period and 16-hour Dry Period a Total Dissolved Solids (TDS) increase of 300 to 400 mg/ℓ could be expected in a solution after percolation through eight feet of soil. Leaching of soil salts was considered as an initial contributor to the TDS increase. Production of carbonate and nitrate ions by soil bacteria was given as the main continuing factor affecting the TDS. Such biological activity, in lowering the solution pH, would encourage the dissolution of carbonate and ferrous minerals and thereby would give the inundating solution a higher TDS content. A series of tests performed by the LACFCD at the Whittier Narrows test basin ten years since the initial work was reported (Reid, 4). Aqueous samplings were taken at four different times during the one-week Wet Period. Instead of 300 to 400 mg/ℓ dissolved solids being acquired by the percolating solution, 550 mg/ℓ TDS had been added to the solution by the time it had traveled eight feet into the soil. The periodicity of samplings permitted the new observation that the cumulative quantity

of dissolved solids added to the percolating solutions decreased from 550 to 80 mg/ℓ by the seventh day of the Wet Period. The same transient behavior of TDS content of percolating solutions is apparent in more recent data (Reid, 5). Reid attributed the total dissolved solids increase to a hardness increase. Production of aqueous hydrogen ions can be catalyzed by the bacteria Nitrosomonas (and Nitrococcus) according to the reaction

$$NH_4^+(aq) + \frac{3}{2}O_2 \longrightarrow NO_2^-(aq) + H_2O + 2H^+(aq) \quad .$$

Resulting hydrogen ions would drive calcium carbonate to dissolution. Reid listed the further nitrification step by Nitrobacter

$$NO_2^-(aq) + \frac{1}{2}O_2 \rightarrow NO_3^-(aq) \quad .$$

Primarily calcium, nitrate, and bicarbonate ions composed the overall TDS increase of the solution. A less important contributor to hardness, according to Reid, was the release of calcium ions by ion exchange reactions for ammonium ions.

The change of nitrogen compounds in intermittently percolated soil systems has been studied extensively. Pincince (6) investigated the nitrate content of soil at Whittier Narrows and found there to be little nitrification when solution was percolating. As soon as the solution began draining from the soil, nitrification proceeded very rapidly as air was drawn into the soil. Lance et al. (7) also showed that nitrification was extensive when soils drained of solution and that the leading edge of newly infiltrating solutions would be characterized by large concentrations of nitrate ions. Bouwer (8,9,10)

observed high aqueous nitrate ion containing peaks at the start of each new infiltration of solution into the ground and attributed the source of nitrate to nitrification of ammonium ions in cellular matter or adsorbed to the soil.

With the field work data from Whittier Narrows in mind, it would be expected that a solution of ammonium and other ions, on passing through a well aerated soil should experience ion exchange of its cations for calcium and magnesium followed in time by a conversion of its aqueous or adsorbed ammonium ions to nitrate ions. Acid resulting from this biologically catalyzed nitrification process would then promote dissolution of certain minerals, thus increasing the total dissolved solids content of the percolating solution.

EXPERIMENTAL APPARATUS

LABORATORY COLUMN

A laboratory apparatus was set up to simulate the intermittent groundwater recharge process and its operation. A column of artificial soil, approximately eight feet tall would permit such simulation. One-quarter-inch walled, six-inch inside diameter Lucite plastic was chosen as the column's material of construction to permit visual examination of the soil matrix during experimental runs. A six-inch inside diameter was sufficiently large to avoid wall effects to the flow and minimize flow distortions by solution withdrawals for sampling. Assembly and disassembly of the laboratory column was facilitated by segmenting the structure axially into eight units. Each individual segment had as its base a 70 Mesh stainless steel screen permitting each separate segment to support a one-foot layer of soil. To discourage the growth of photosynthetic organisms the entire laboratory column was enclosed in a black sheath. Except to permit radial passage of solution, the column's top segment was designed to be closed from the outside environment. Any gases that might escape the surface into the six-inch depth of solution capping the soil could be sampled through a septum at the apex of the top segment's conical enclosure. During the inundation phases (the Wet Period) of the intermittent groundwater recharge process the solution ideally stands at a constant depth. A "constant head" tank stood above the top of the column and hydraulically connected to it via a 1/2-inch inside diameter Tygon tube to maintain a constant head of 15 inches of water on the top of the laboratory column's soil (Figure 1). To force a flow of

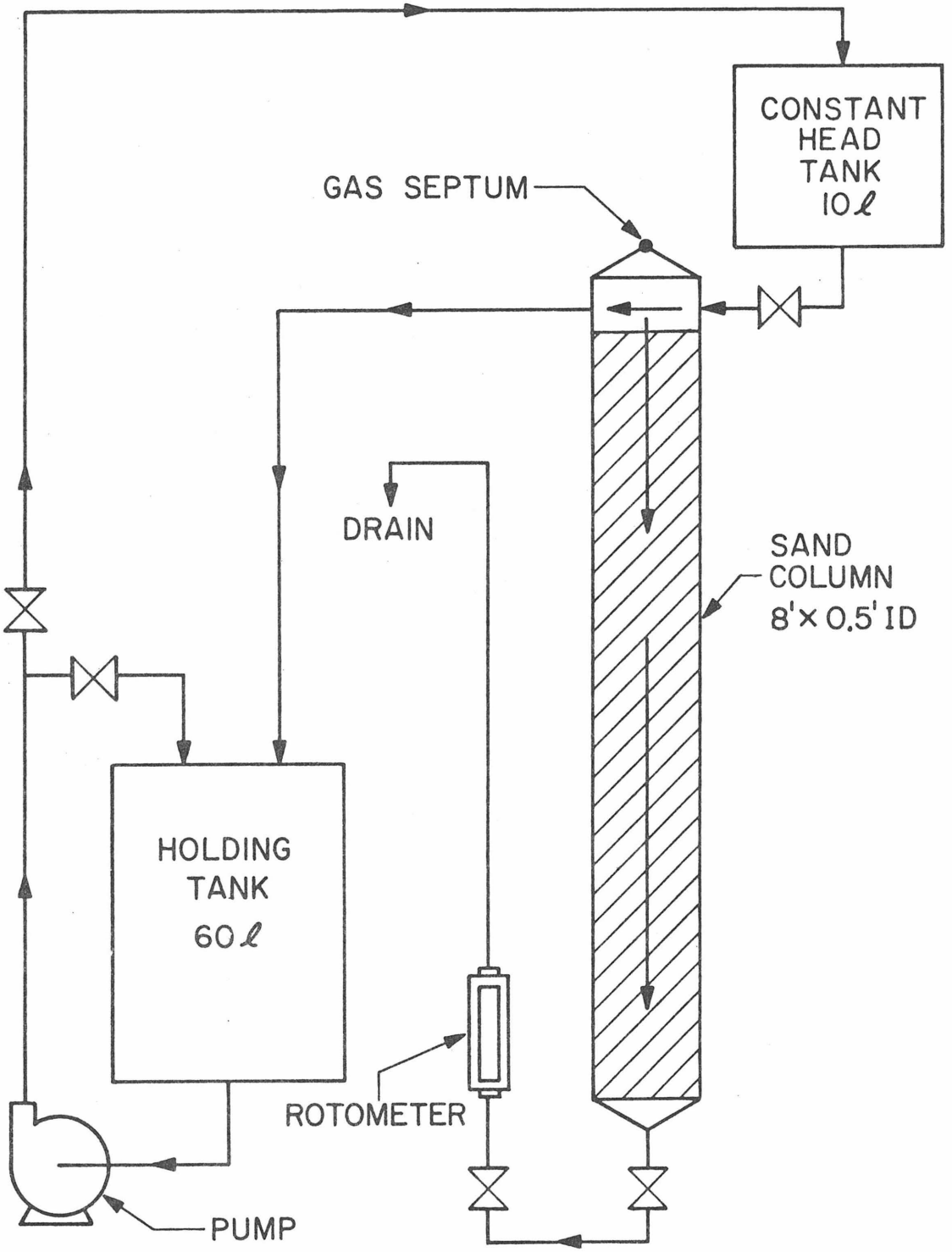

Figure 1: Circulation of Percolating Solution for the Laboratory Sand Column

550 mℓ/min. horizontally across the surface of the column's "soil", solution was pumped (Gorman-Rupp Inc.) from a large holding tank into the constant head tank at approximately 1000 mℓ/min via a 1/2-inch inside diameter Tygon tube. From there the flow was horizontal across the surface of the column's soil and out the other side of the top segment of column where it was piped back down to the holding tank. The minute quantity of solution that percolated away from the flow, across the soil surface, and down the eight-foot column was funneled through a 1/2-inch ball valve at the column's base. Flow rate of the exiting solution was controlled with a rotometer. To prevent gases from coming out of solution and interfering with the rotometer, the flow traveled out of the meter and up a tube to such a height as to maintain a seven-foot head of water on the meter. The flow was then disposed of. The laboratory column permitted solutions to travel across the surface of an artificial soil, down through that soil, and away from the soil thereby simulating the physical operations of the intermittent groundwater recharge process.

SOLUTION, GAS, AND SOIL SAMPLING

Each segment of column was supplied with a tap whose stainless steel inlet easily could be moved across the diameter of the column for solution sampling purposes (Figure 2). When the laboratory column was drained of solution, during the Dry Period, the same tap served as a gas sampling port. Immediately below the solution/gas sampler was an access for soil samples (Figure 3). Soil sampling was accomplished by screwing a hollow stainless steel rod into a solid stainless steel rod

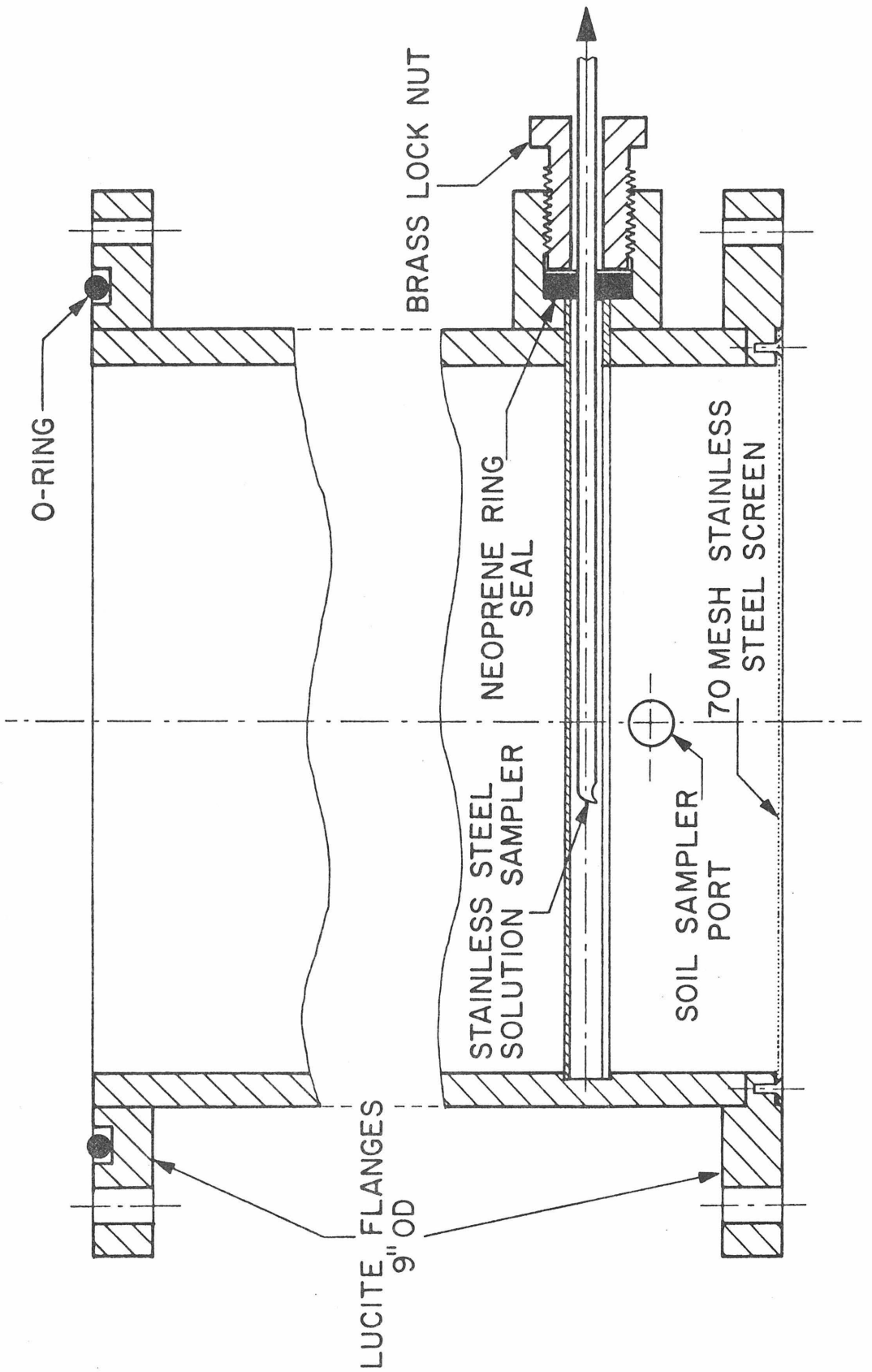

Figure 2: A Column Segment, Lateral View Showing Solution/Gas Sampler

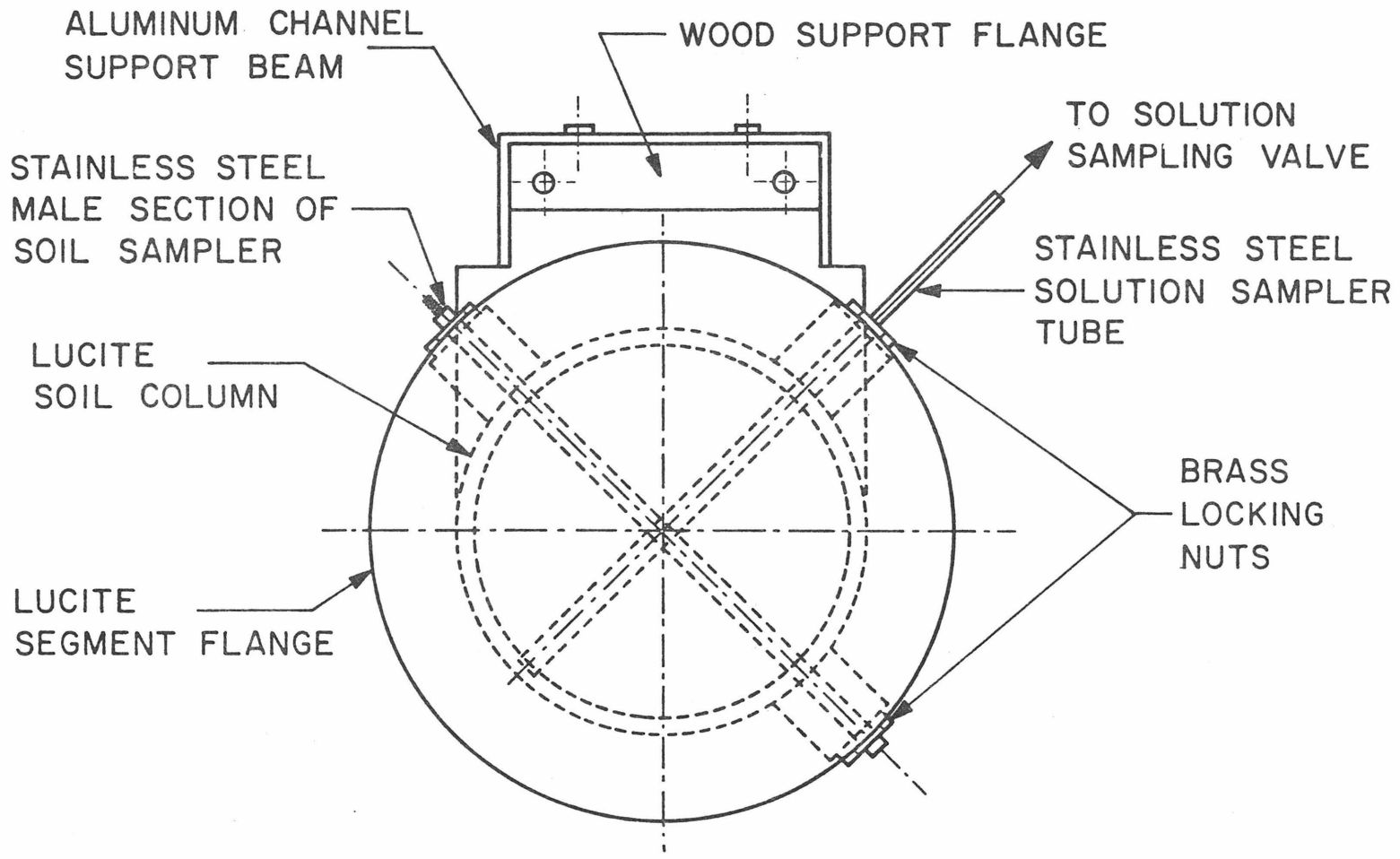

Figure 3: A Column Segment, Radial View Showing Solution/Gas and Soil Samplers

of the same diameter and already positioned horizontally through the column (Figure 4). The hollow rod was then pushed into the body of the column. When a plunger inside the hollow tube was withdrawn, approximately one gram of soil would follow the flow of solution through the tube's single opening and into the vacated cavity. The hollow rod then would be withdrawn from the column. Design of the sampler permitted soil samples to be taken only when the column was saturated with solution.

ARTIFICIAL SOIL

Filler soil for the laboratory column was chosen to approximate that in the Whittier Narrows test basin so that the Total Dissolved Solids problem of this intermittent recharge process could be simulated. The test basin is constructed on alluvium that has been deposited since the Middle Miocene Epoch. The irregularity of the fluvial deposits has given the test basin an anisotropic vertical soil profile with grain sizes varying from fine silt to sand. Although the grain's source undoubtedly was the granitic San Gabriel Mountains, the vertical soil profile was not exactly chemically homogeneous but rather varied in coloration from red to black. Instead of filling the laboratory column with material of pure origin such as crushed granite, calcite, or quartz, or of using the same soil mixture as that under the test basin, an intermediate was chosen. Sand from a Rio Hondo sand bar was collected to fill the column. Such sand originated in the San Gabriel Mountains and would be very similar to the bulk chemical composition of the soil of the Whittier Narrows test basin located 1/4-mile east of the Rio Hondo; therefore, there was a good probability that the

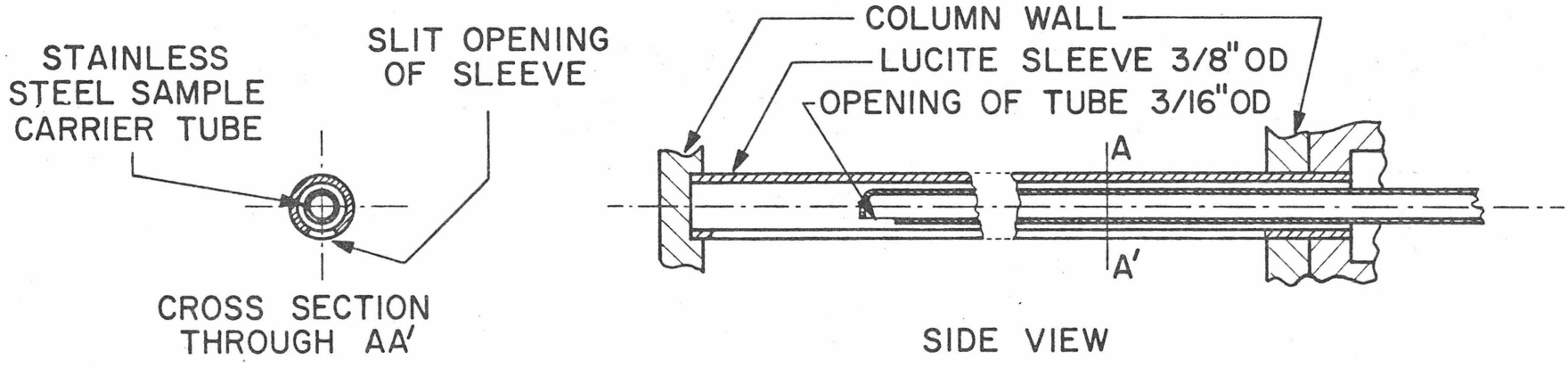

SOLUTION SAMPLER

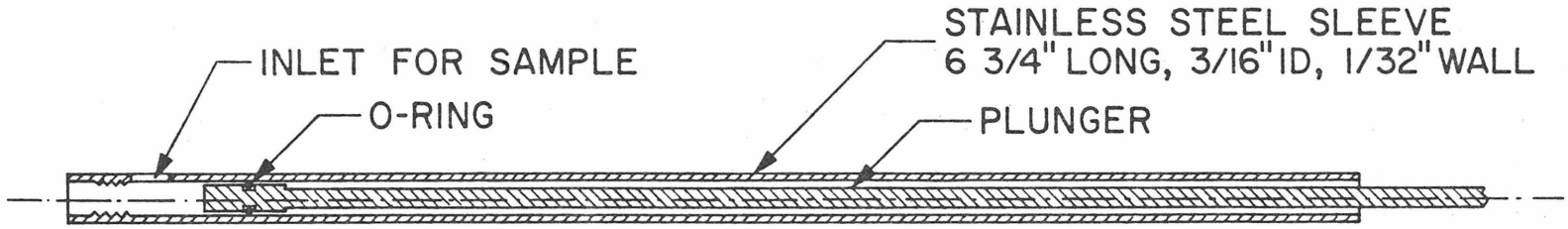

FEMALE SECTION OF
SOIL SAMPLER, SIDE VIEW

Figure 4: Detailed Diagrams of the Solution/Gas and Soil Samplers

high Total Dissolved Solids content of percolated solution associated with the Whittier Narrows test basin percolation could be duplicated in studying the intermittent groundwater recharge process.

The river sand was cleaned in water and classified. To prevent the long-term possibility of a flow-generated axial distribution of sand finer than 70 Mesh throughout the column's length, all sand finer than 65 Mesh was separated out with W. S. Tyler Company screens. Pebbles in the column's soil could cause an inconvenient flow pattern near a solution sampler or interfere with the taking of a soil sample. Sand larger than 8 Mesh was discarded. Approximately three per cent of the original river sand was removed by the two screening processes. Grain size distribution for the classified sand showed a linear form typical of unclassified natural sand when a plot was made of grain size (Mesh) versus cumulative weight (probability scale) (Appendix A). The final geometric grain size for the laboratory column's soil was 0.5 mm whereas Whittier Narrow's soil was of mean size 0.28 mm.

Although the important interfacial processes in the laboratory column will be liquid-solid in nature, the sand's surface area was determined by a method involving gas-solid interactions. A Brunauer Emmett, and Teller (BET) analysis by nitrogen adsorption yielded a surface area of 0.4 m^2/gm dry sand.† A separate analysis by krypton adsorption on a different piece of equipment yielded 0.22 m^2/gm.‡ If all the grains were perfect, nonporous spheres 0.05 cm in diameter, the surface area would be only 0.005 m^2/gm. The grains, therefore, are

† Performed by Vega Sankur, Division of Chemistry and Chemical Engineering, Caltech.

‡ Performed by Jet Propulsion Laboratory, Caltech.

either very irregular or they are extremely porous. Scanning electron micrographs typically revealed the sand to be irregularly shaped but with few fissures larger than 100 A.†

Once the laboratory column was filled with the sand, certain physical characterizations could be made on the column's solution/sand/gas system. Porosity can be considered to be of two types (Collins, 58). Total porosity includes the volume fraction that is not occupied by sand. A well packed sample of the sand outside the laboratory column gave a total porosity of 0.44 ± 0.01. Since the medium density of the sand was 2.6 ± 0.03 g/mℓ, then the bulk density would be 1.5 ± 0.3 g/mℓ. Effective porosity includes only those pore spaces that are available to fluid flowing through the porous media. Wet Period effective porosity was quantified with depth by monitoring the downward movement of a rapidly moving (1700 ℓ/day) salt solution replacing a deionized water solution in the laboratory column. Effective porosity was 0.23 at the top but leveled off to 0.35 ± 0.02 below the one-foot depth. Effective porosity for the Dry Period would be the volume fraction available for gas diffusion. Termination of a certain Dry Period was accomplished by purging the column with deionized water. The total quantity of aqueous chloride ions in the column at the end of the Dry Period was made. Under the reasonable assumption that the sand did not release aqueous chloride ions during the Dry Period and with the knowledge of the chloride ion content of the preceding Wet Period solution, the quantity of water in the column could be determined. The volume fraction of water was 0.06 ± 0.02, therefore the effective

† Performed by Ken Evans, Jet Propulsion Laboratory, Caltech.

porosity of the Dry Period was 0.38 ± 0.03.

Polarizing microscopic examination of a 0.03 mm thin section of the column's sand[†] helped characterize the sand's chemical nature. Particular attention was made to detect such rapidly dissolving minerals as calcite ($CaCO_3$) and dolomite ($MgCa(CO_3)_2$). Percentages of minerals detected were:

quartz (SiO_2)	40 ± 20
plagioclase (labradorite, andesine) $((Ca,Na)(Al,Si)AlSi_2O_8)$	20 ± 10
biotite ($K_2(Mg,Fe)_6(Si_6Al_2)O_{20}(OH)_4$)	5 ± 2
hornblende $NaCa_2[(Mg,Fe)_4Al]Al_2Si_6O_{22}(OH)_2$	3 ± 2
augite $(Ca,Mg,Fe^{++},Al)(Si,Al)O_3$	1 ± 1/2
opaques	5 ± 2
microcrystallines	25 ± 12

Detection of quartz, plagioclase, biotite, and hornblende was in accordance with the source of the sand. Although no carbonates were detected, they did exist in trace amounts in the sand by virtue of the fact the trace grains of the sand produced marked effervescence in hydrochloric acid. Clays were not detected.

ROUTINE ANALYTICAL PROCEDURES

Aqueous Samples

Solution samples from the laboratory column were collected in 50 mℓ polyethylene screw-cap bottles that previously had been washed in deionized water, 5 M nitric acid, and deionized water again. Most analyses were made directly on the contents of the polyethylene bottles.

[†] Thin section prepared by Rudy Van Heuen, Pasadena.

However, solution samples collected in 100 mℓ pyrex beakers were immediately analyzed for pH and aqueous oxygen content. Analyses for various aqueous species were performed in the following manner:

H^+ - Beckman Expandometric SS-2 gave pH values with errors of ± 0.001.

Ca^{++} - EDTA titration to a murexide indicator endpoint (Taras, 56) gave an uncertainty of ± 0.04 mg/ℓ. When aqueous sodium, magnesium, and potassium were also to be analyzed, aqueous calcium ions were quantified by atomic absorption (AA) spectroscopy (Varion Techtron, type AA-5) with an air-acetylene flame at 422.6 nm. Standardization was made against known calcium salt solutions (Taras, 56). The error of analysis was one to five per cent.

Mg^{++} - Analysis was made by flame AA spectroscopy at 285.2 nm and standardized against known magnesium salt solutions (Taras, 56). Uncertainty of the value was one to two per cent.

Na^+ - For solutions containing less than 100 mg/ℓ sodium, analysis was made by flame AA spectroscopy at 589 nm. For solutions above 100 mg/ℓ, emission spectroscopy at the same wavelength was employed. Standardization was made against sodium chloride solutions containing 2 gm K^+/ℓ. Error of analysis was two to five per cent.

K^+ - Analysis was made by flame AA spectroscopy at 766.5 nm. Standardization was against known potassium chloride solutions containing 1 gm Cs^+/ℓ. Error of analysis was one to two per cent.

Mn^{++} - Analysis was made by flame AA spectroscopy at 279.5 nm. Standardization was made against known manganese solutions (Taras, 56) and error of analysis was one to two per cent.

Iron - Analysis was made by flame AA spectroscopy at 248.3 nm against known iron salt solutions (Taras, 56). Uncertainty on the result was five per cent.

NH_4^+ - The sample was treated with $ZnSO_4$ and KOH followed by Nesslerization (Taras, 56). Solution absorbances were taken on a Beckman Model B Spectrophotometer. An error of ± 0.05 mg NH_4^+ (as nitrogen)/ℓ was typical.

NO_2^- - The sample was reacted with naphthylamine hydrochloride reagent (Taras, 56). Solution absorbances were taken and standardized against fresh nitrite salt solutions. Uncertainty of the value was ± 0.001 mg NO_2^- (as nitrogen)/ℓ.

NO_3^- - The sample was acidified and scanned from 275 to 220 mμ with a Beckman Ratio Recording Spectrophotometer. Nitrite concentrations at the same level as nitrate concentrations gave one-tenth the absorbance. Uncertainty was 10 per cent.

HCO_3^- - A titration curve was generated from pH 9.5 to 5.0 for the sample with the Radiometer system ABU12, PHM26, TT11, and SBR2c. Calibration was performed on known sodium bicarbonate solutions. An error of three per cent was realized.

Cl^- - A potentiometric curve was generated for the sample using a silver/silver chloride electrode (Taras, 56). Calibration was based on acidified sodium chloride solutions and

yielded an error of five per cent.

$Si(OH)_4$ - The molybdosilicate method (Taras, 56) gave uncertainties of ± 0.02 mg SiO_2/ℓ.

O_2 - The sample's temperature was immediately determined with a thermocouple. Aqueous oxygen content was then determined with a Beckman Fieldlab Oxygen Analyzer. Calibration was made with a solution saturated with oxygen at a known temperature. Errors in the oxygen analysis started at ± 1 mg/ℓ but later in the investigation leveled off to ± 0.2 mg/ℓ.

Gaseous Samples

Gas sampling during the Dry Period was accomplished by withdrawing a sample through the solution/gas sampling port into a 50 mℓ glass syringe. Ten feet of 1/16-inch inside diameter stainless steel tubing filled with 50-80 Mesh Porapak Q was capable of separating air, carbon dioxide, and nitrous oxide. Oxygen, nitrogen, and nitric oxide were separated in a 10-foot, 1/16-inch inside diameter stainless steel column of 60-80 Mesh molecular sieve 5A. For routine operations, only carbon dioxide, oxygen, and nitrogen were analyzed. A 0.4 mℓ gas sample could be separated into oxygen and nitrogen by operating the Porapak Q column at $0^{\circ}C$ with 20 psia helium as the carrier flowing at 1.5 mℓ/second. A 2 mℓ gas sample could be separated into carbon dioxide and air by operating the molecular sieve column at ambient temperatures with 20 psia helium as the carrier flowing at 0.67 mℓ/second. All gases were detected with a thermoconductivity detector on a Carle Instrument Company Basic Gas Chromatograph, Model 8000.

Biological Samples

Cell counting apparatus and reagents were all steam sterilized at 248°F for 30 minutes. A soil sample of approximately one gram sand, accompanied by 3 mℓ solution, was emptied into 40 mℓ of sterilized, deionized water in a 50 mℓ polyethylene centrifuge tube (sterilized for 24 hours with ultraviolet light). The tubes were individually capped and agitated at full speed on an S8223 Vortex Genie Mixer (American Hospital Supply Corporation) for two minutes to remove bacteria from the sand grains. The resulting agitated solution was then diluted 10, 100, and 1,000 times before being plated.

An accumulative count of all types of heterotrophic bacteria living at various depths in the laboratory column was ascertained by spreading 100 µℓ of the hundred and thousandfold dilutions of agitated solution on plates of nutrient agar. Colonies became visible after only 24 hours of growth on the agar in the dark. Final bacterial counts were made three or more days after the solutions were plated. The white to yellow circular colonies were primarily gram negative cocci and bacilli two to five microns in length.

Nitrosomonas and Nitrobacter are potentially important microorganisms that cause secondary treated sewage effluent to acquire a higher Total Dissolved Solids content as it percolates through the soil. Populations of both of these nitrifying autotrophs were analyzed quantitatively with depth in the laboratory column. A silica based compound, free of organic compounds, was used as the plating medium to discourage heterotrophic bacterial growth. Work of Pramer (57) served as a basis for the preparation of the silica substrate. A

Biological Samples

Cell counting apparatus and reagents were all steam sterilized at 248°F for 30 minutes. A soil sample of approximately one gram sand, accompanied by 3 mℓ solution, was emptied into 40 mℓ of sterilized, deionized water in a 50 mℓ polyethylene centrifuge tube (sterilized for 24 hours with ultraviolet light). The tubes were individually capped and agitated at full speed on an S8223 Vortex Genie Mixer (American Hospital Supply Corporation) for two minutes to remove bacteria from the sand grains. The resulting agitated solution was then diluted 10, 100, and 1,000 times before being plated.

An accumulative count of all types of heterotrophic bacteria living at various depths in the laboratory column was ascertained by spreading 100 µℓ of the hundred and thousandfold dilutions of agitated solution on plates of nutrient agar. Colonies became visible after only 24 hours of growth on the agar in the dark. Final bacterial counts were made three or more days after the solutions were plated. The white to yellow circular colonies were primarily gram negative cocci and bacilli two to five microns in length.

Nitrosomonas and Nitrobacter are potentially important microorganisms that cause secondary treated sewage effluent to acquire a higher Total Dissolved Solids content as it percolates through the soil. Populations of both of these nitrifying autotrophs were analyzed quantitatively with depth in the laboratory column. A silica based compound, free of organic compounds, was used as the plating medium to discourage heterotrophic bacterial growth. Work of Pramer (57) served as a basis for the preparation of the silica substrate. A

solution of 30 gm sodium metasilicate in 300 mℓ water was passed through 200 mℓ of IR-120 C.P. (Mallinckrodt Chemical Works) cation exchange resin which had previously been purged with 1:1 N HCl. The resulting silicic acid solution was acidified further to pH 1 with concentrated HCl and sterilized. Extensive reports on the preparation of culture media (Lewis et al., 59; Loveless et al., 11; Lees, 12; Dessers et al., 13; Laudelout et al., 14) and plating media (Engel et al., 15; Delwiche et al., 60) for Nitrosomonas and Nitrobacter exist. The plating media used was similar to the chemical environment from which the bacteria would be collected. An ammonium salt-containing solution was prepared with the following salts and concentrations (mg/ℓ):

$CaCl_2$	560
$MgSO_4$	238
$MnCl_2 \cdot 4H_2O$	8
$K_2HPO_4 \cdot 3H_2O$	65.2
KH_2PO_4	59.3
$NaHCO_3$	1382
$(NH_4)_2SO_4$	8000

A nitrite salt-containing solution was prepared of similar constituency except ammonium sulfate was replaced by 600 mg/ℓ $NaNO_2$. After sterilization, the Nitrosomonas plating mixture was prepared by raising the pH of an equal volume mixture of silicic acid solution and the ammonium salt solution to 6.0 with potassium hydroxide. The resulting solution was poured into 9 cm diameter culture dishes; gelling occurred in less than 10 minutes. A similar procedure was followed for the Nitrobacter plating compound except that nitrite solution, instead of ammonium salt

solution, was used. One hundred μℓ of the ten and hundredfold dilutions of the agitated solution were plated. Within one week of incubation in darkness, minute specks were visible on the plates. A final count of the specks, made two weeks after the plating, yielded the population densities of Nitrosomonas and Nitrobacter in the laboratory column.

The plate containing ammonium salt should permit only Nitrosomonas bacteria to multiply (Stanier, 16) and similarly Nitrobacter should be the only bacteria that could grow in the nitrite salt containing medium. Actually there do exist various genuses that could populate the same plates (Breed, 17). Nitrifying bacteria colonies were single-cell thick transparent star-shaped masses approximately 3 mm in diameter. Colonies growing on the ammonium enriched medium were gram positive, nonmotile rods 1.0 by 2.0 microns. These rods were loosely joined together on chains of up to six rods (Figure 5). The nitrite ion-enriched silica gel plating medium grew single-cell thick masses of gram-positive rods of similar geometry. These rods however, were not primarily chained (Figure 6). The behavior of the colony to its being manipulated with a wire and the regularity of distance between cells suggested each cell was surrounded by a 1 μ-thick slime layer. These descriptions strongly suggest the former bacteria as being Nitrosomonas and the latter as Nitrobacter (Breed, 17) as was the intent of each medium.

Surface Chemical Species

Analysis of the distribution of cationic chemical species adsorbed to the surface of sand required the use of sand whose surface was

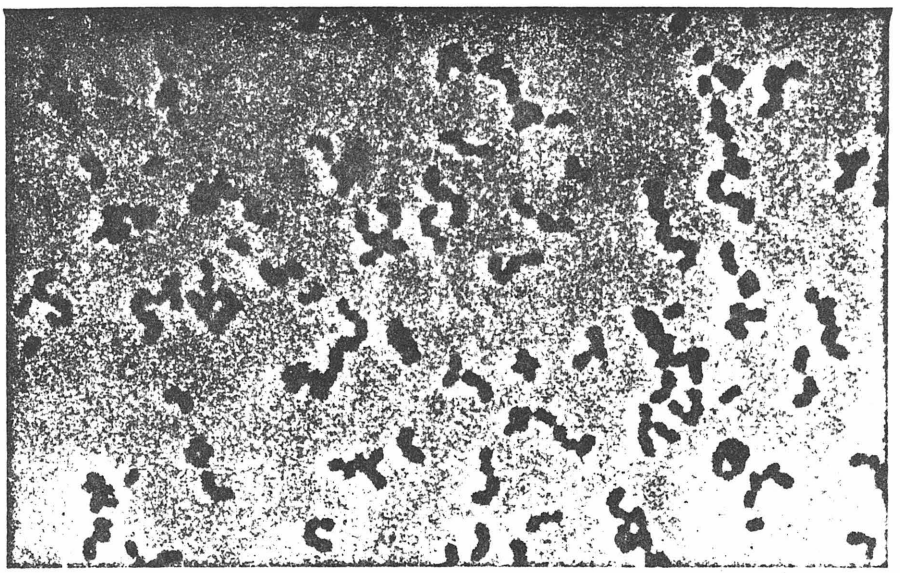

Cells from Center of 5 mm
Diameter Colony

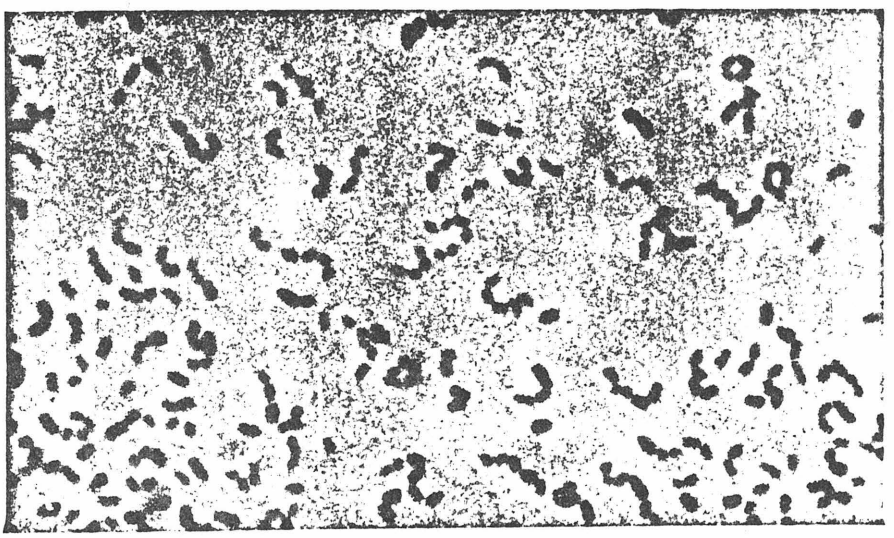

Cells from Edge of Colony

Figure 5: Nitrosomonas Bacteria Grown on Ammonium Salt Silica Gel Plating Compound

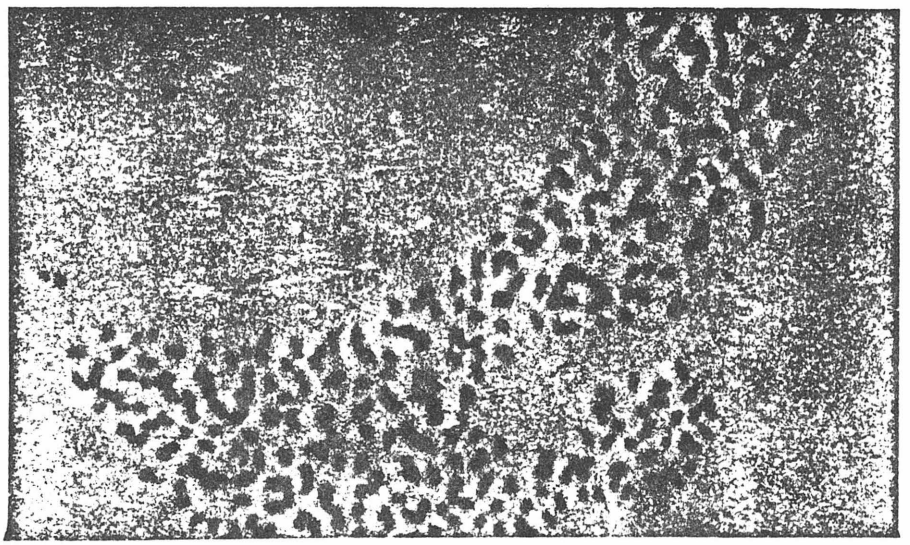

Figure 6: Nitrobacter Bacteria Grown on Nitrite Salt Silica Gel Plating Compound

adsorbed with just one cation. For the preparation of such a sand, sand was leached for three days with a salt solution of the appropriate cation. Immediately after the leaching step, the sand was washed in 200 mℓ of acetone in less than two minutes and rapidly dried in a stream of air. Such procedure would leave a sand surface undisturbed by possible dissolution of the sand.

The procedure for the determination of the quantity of cations adsorbed to the surface of sand (in equilibrium with a specifically prepared solution) was followed in a manner that would avoid the possibility that sand dissolution would alter the chemical composition of solution immediately in contact with the sand surface. A sand sample was leached by the specifically prepared solution, but not dried (Barber et al., 18). The moist sand was weighed and frozen. Later, the sand was leached for four hours with 0.01 M ammonium acetate solution (0.01 M barium chloride was used when adsorbed ammonium ions were being determined). Analysis of the leachate and knowledge of the composition and quantity of solution film originally on the moist sand yielded the quantity of cations adsorbed to the surface (Sivasubramaniam et al., 19) even if the sand itself were dissolving to yield more aqueous cations.

GENERAL EXPERIMENTAL PROCEDURE

Wet Period procedure essentially called for the permitting of a solution to flow, at constant rate, through the experimental column so that samples of the percolating solution could be taken with depth and time. Usually the feed solution was prepared by diluting a more concentrated solution one-hundredfold to give a 50 ℓ feed stock. A well-mixed feed solution was insured by circulating the solution between the holding and constant head tanks for several minutes before flow was permitted into the column itself. The first flow into and down the laboratory column usually ran at the average rate of 670 ℓ/day until the solution reached the column's base. Flow was then set at a much lower rate by adjusting the rotometer. Nine solution samples could be taken at nine depth intervals in less than 15 minutes. To terminate the Wet Period, flow of solution into the column's top segment was diverted. Flow leaving the base was disconnected from the rotometer and permitted to exit to the drain. Emptying lasted approximately 30 minutes; however, even a week after the end of the Wet Period tiny sporadic flows would periodically be released.

The Dry Period was considered to have begun as soon as solution flow to the column was stopped and draining had begun. Easy access of air to the soil was insured by removing the conical roof from the column's top segment. Gas samples, taken through the solution/gas sampling ports were immediately analyzed. The entire gaseous interior of the column could be sampled and quantified in less than one hour. The Dry Period usually lasted two weeks. Even though the 1/2-inch ball valve at the column's base remained open, the bottom two feet of

the column's soil usually remained waterlogged throughout the Dry Period.

SPECIFIC EXPERIMENTAL PROCEDURES, RESULTS, AND CONCLUSIONS

GENERAL TREND OF THE INVESTIGATION

Experimental investigations with the laboratory column were begun as soon as a minimal knowledge of the intermittent percolation process would permit. The preliminary investigations permitted the investigator to make most of his mistakes and yet to acquire a feel for the operation of the laboratory column and the relative importance of various basic processes at work. It was learned that ion exchange reactions were important enough that the initial condition of the surface of the sand would have to be quantified in order to predict mathematically transient changes to the cationic character of a solution percolating through the sand. The main body of research can essentially be viewed as composed of three areas of investigation. One area centered on the general nonbiological interaction between the percolating solution and sand system. Another area of investigation was a detailed examination of the interactions of a granitic sand sample and an aqueous solution outside of the laboratory column. The third basic area of investigation of the main body of research focused on the general overall interactions of physical, chemical, and biological agents with a percolating solution, thereby permitting a theory to be developed on the mechanism of the addition of large quantities of dissolved solids to percolating secondary treated sewage effluent and the intermittent groundwater recharge process in general.

PRELIMINARY INVESTIGATIONS

Percolation of Deionized Water

Total Dissolved Solids content of secondary treated sewage effluent percolating through the top 10 feet of soil at the Whittier Narrows test basin has been reported to be increasing mainly in the form of hardness. By one mechanism, the calcium and magnesium ions of hardness are driven into solution by ion exchange with the solution's ammonium ions. The major increase of hardness is attributed to dissolution of carbonate minerals due to a continuous production of aqueous hydrogen ions by the nitrification reactions during the percolation process.

The present run ascertained the change of aqueous calcium ions in a solution percolating through the column when no aqueous ammonium ions could exchange calcium into solution nor be converted to nitrite ions with an accompanying production of carbonate-dissolving hydrogen ions. Nine solution samples were drawn simultaneously at one-foot intervals as demineralized water percolated down through the column at 37 ℓ/day. Data on the concentration of aqueous calcium and hydrogen ions were taken at three time periods.

A production of 0.5 mg Ca^{++}/ℓ per foot of travel existed throughout the 37.5 hours of the run (Figure 7). In general, there was a decrease of aqueous hydrogen ions in the solution as it traveled down through the sand (Figure 8). The solution was acidified in the top foot of travel. Thereafter it became increasingly alkaline until the five-foot depth was reached. At that depth a leveling off of pH rise was apparent even though calcium ions were still being added to the

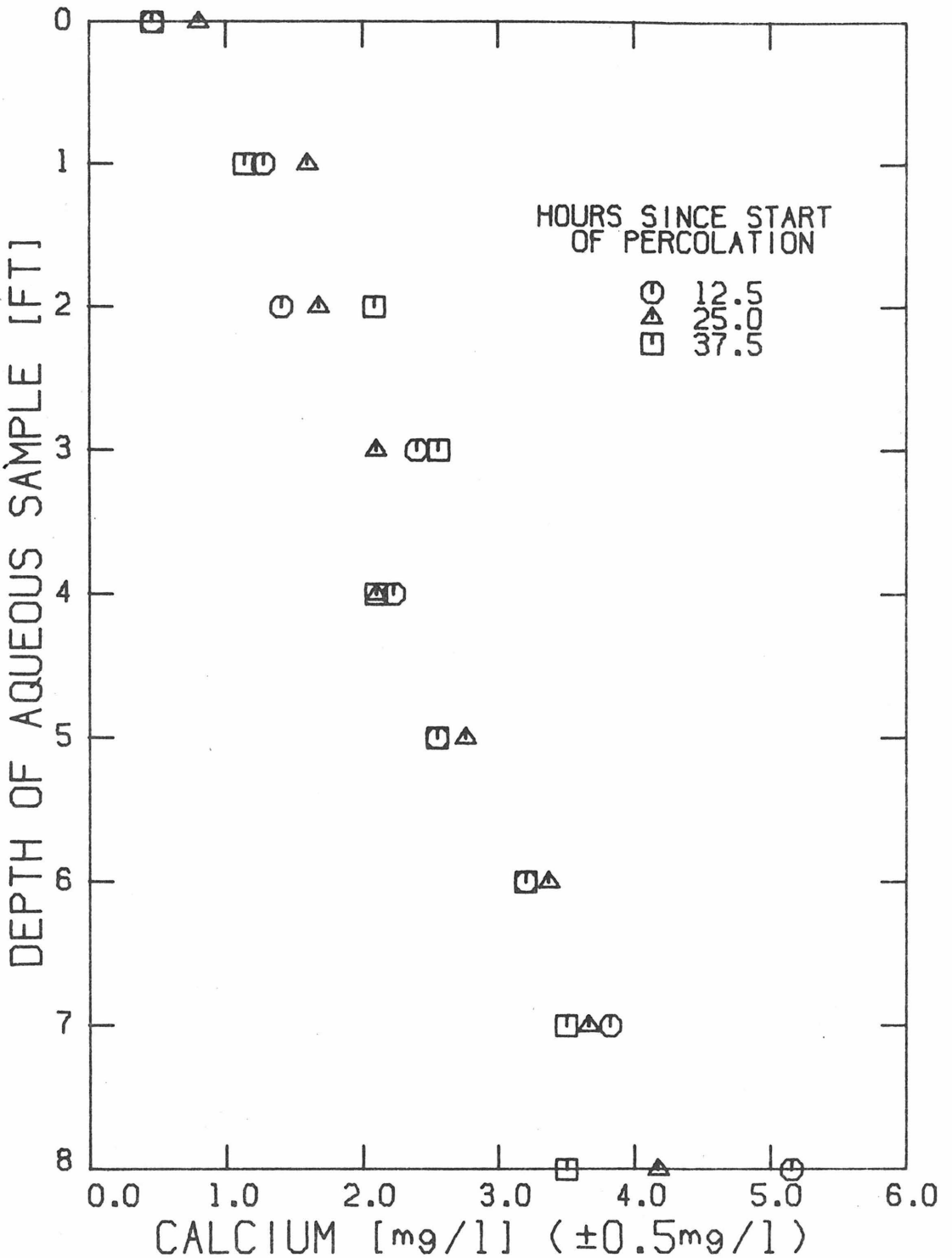

Figure 7: Aqueous Calcium Ion Content of Deionized Water First Percolated through the Laboratory Column (37 ℓ/day)

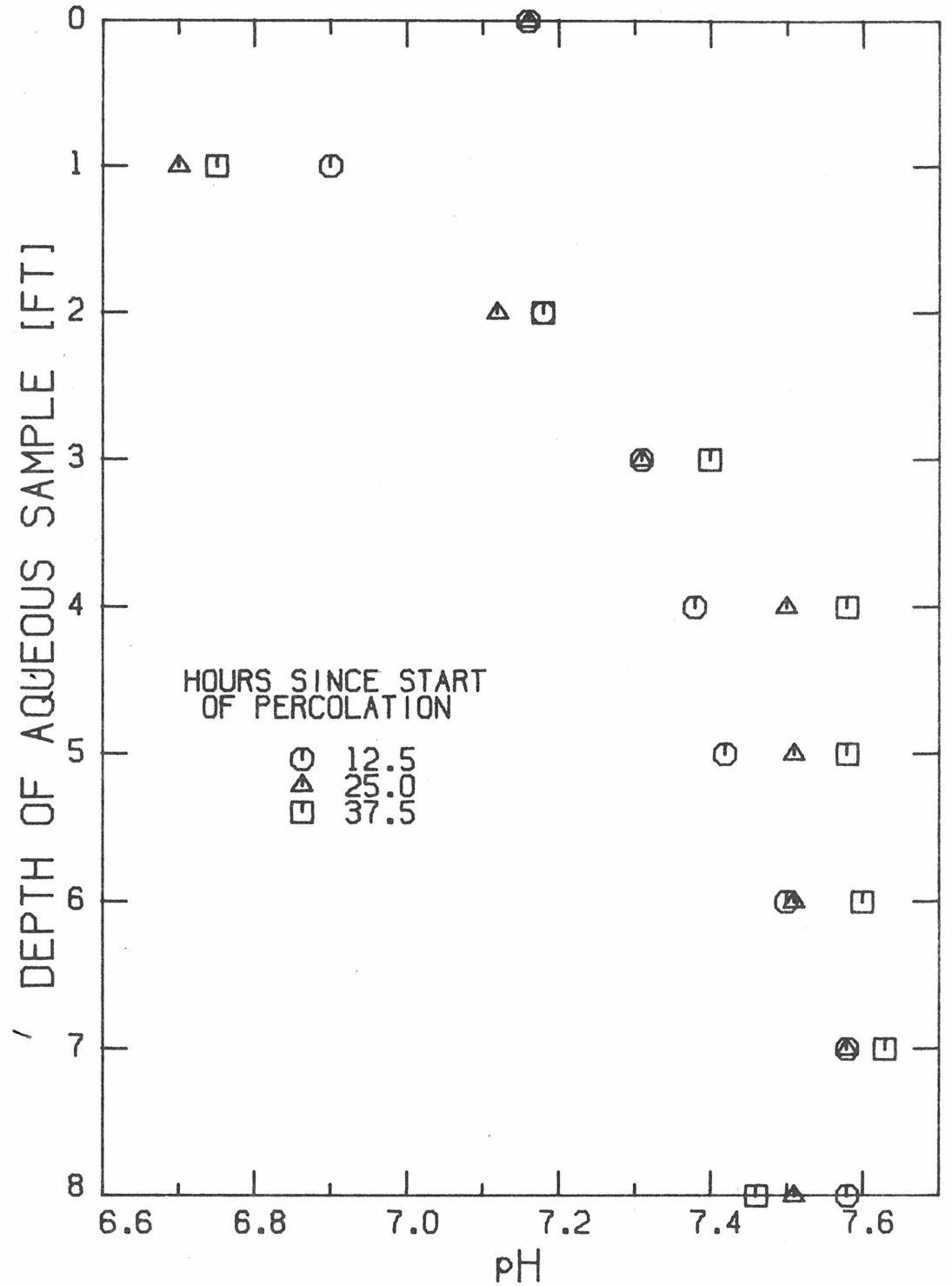

Figure 8: pH of Deionized Water First Percolated through the Laboratory Column (37 ℓ/day)

solution at 0.5 mg Ca^{++}/ℓ.

Electroneutrality of the percolating solution requires that the appearance of 0.22 meq Ca^{++}/ℓ of the effluent solution be matched by the disappearance of 0.22 meq/ℓ of another cation or the appearance of 0.22 meq/ℓ of an aqueous anion. By virtue of the fact that deionized water was being percolated, the only cation that could disappear from the solution would be the hydrogen ion. Because less than a tenth of a per cent of the 0.22 meq/ℓ can be matched by the disappearance of aqueous hydrogen, then there must have been an addition of some aqueous anion species to the percolating solution

This run brings out the fact that, in the absence of nitrification reactions and substantial ion exchange reactions, the maximum rate of release of aqueous calcium ions would be 10^{-4} mg Ca^{++}/gm sand·hr. Furthermore, the ability of the column's mineral assemblage to alter solution acidity is but very slight.

Percolation of a Sodium Salt Solution

Ion exchange of aqueous ammonium ions for calcium and magnesium ions was partially blamed as being a slight cause of dissolved solids acquired by a percolating solution. Motivation for percolating a sodium salt solution through the column was to exhibit the rate and extent of ion exchange reactions in which the column's sand could participate.

The surface chemical constituency of the sand was the same as that after the end of the previous run of 37.5 hours of percolation of demineralized water. A feed solution of 119 mg Na^{+}/ℓ (typical sodium ion

level of the Whittier Narrows' secondary treated sewage effluent) was percolated through the laboratory column at 33.6 ℓ/day. Percolation lasted for 25 hours during which time two sets of depth profile concentrations of aqueous calcium and hydrogen were taken.

A pronounced appearance of aqueous calcium ions occurs in the percolating solution when up to 31 mg Ca^{++}/ℓ was added (Figure 9). Even during the short 12.5 hour interval between samplings there was a drop-off of rate of calcium ion addition to the percolating solution. Aqueous hydrogen ions were removed from the percolating solution (Figure 10) until a pH of 7.0 was reached at the three-foot depth. Below three feet, acidity of the solution increased throughout the remainder of travel down through the column. With time, there was a tendency for the consumption of acid to diminish at the column's top even though the addition of acids further down was constant.

Since no analysis was made for aqueous sodium ions, it can only be theorized that these graphs represent the ion exchange of sodium ions for calcium ions. Since the outlet concentration of aqueous calcium ions varied from 31 to 22 mg Ca^{++}/ℓ, then the amount of calcium that was released from the column's sand averaged 0.4 μeq/gm dry sand. Considering the entire run's release of aqueous calcium ions, the sand's capacity to hold calcium must be at least 1.0 μeq/gm. If the ion exchange reaction between solid exchangers $\overline{Na}$ and $\overline{Ca}$ and aqueous species Na^{+} and Ca^{++} is

$$\overline{Ca} + 2Na^{+} \underset{k_1}{\overset{k_2}{\rightleftharpoons}} 2\overline{Na} + Ca^{++} \qquad (1)$$

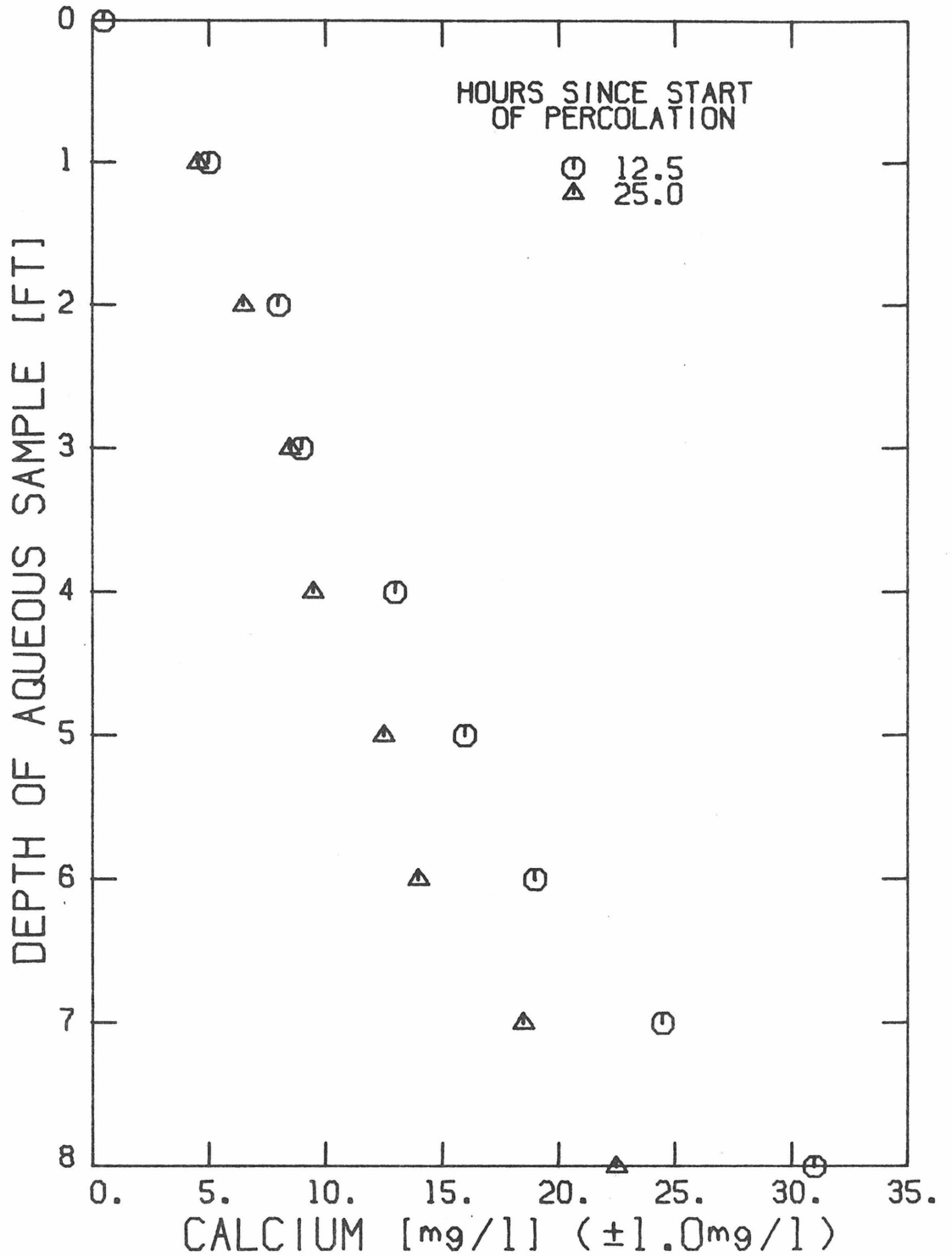

Figure 9: Variations of Aqueous Calcium Ion Content of a 119 mg Na^+/ℓ Containing Solution Percolating at 33.6 ℓ/day through the Laboratory Column

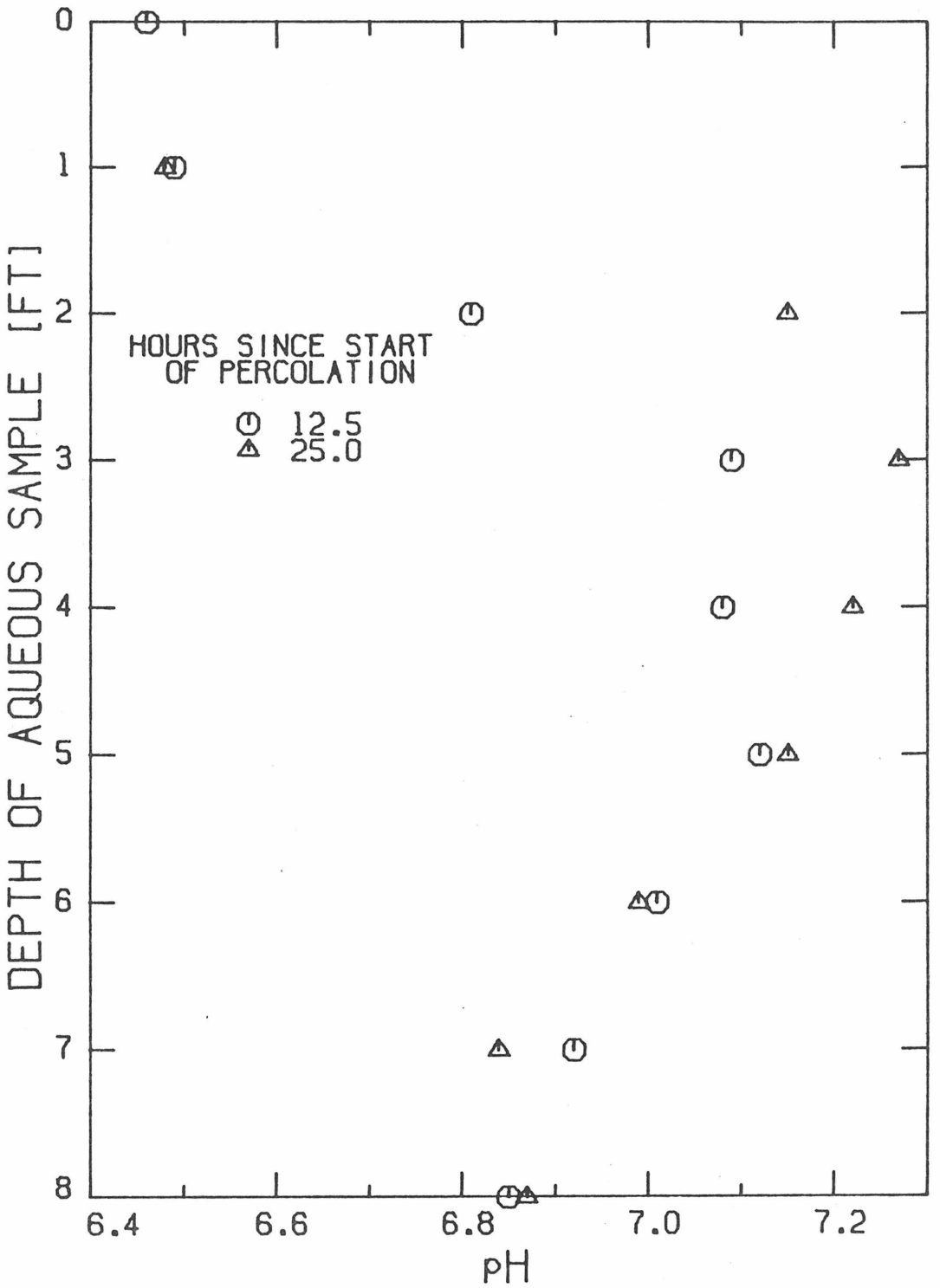

Figure 10: Variations of pH in a 119 mg Na^+/ℓ Containing Solution Percolating at 33.6 ℓ/day through the Laboratory Column

then the concentration of aqueous calcium ions, Ca, in the percolating solution with depth, z, (neglecting axial diffusion through the column) is describable by

$$-\frac{\partial Ca}{\partial z} = \alpha(K_1\ Na^2\ \overline{Ca} - K_2\ Ca\ \overline{Na}^2) + \beta\ \frac{\partial Ca}{\partial t} \quad . \qquad (2)$$

where α and β are constants, K_1 and K_2 are rate constants of reaction (1), $\overline{Na}$ and $\overline{Ca}$ are the concentrations of adsorbed cations, and Na and Ca are aqueous cation activities. Because the initial surface concentrations are not known, quantitative use of the above mass balance equation cannot be made. It is clear, however, that the sand surface could not have been devoid of sodium species. If calcium species were dominant on the sand, then there would be a larger rate of addition of calcium ions at the top of the column than at the bottom. Of course the data show the reverse to be true and therefore there must have been liberal quantities of sodium ions adsorbed to the sand surface at the start of this percolation.

Percolation of a Calcium Salt Solution

A long duration study of changes to a percolating solution of 7 mg Ca^{++}/ℓ was undertaken. The sand surface chemical constituency would be the same as that at the end of the 25-hour flow of 119 mg Na^{+}/ℓ solution. The sand's surface should be approximately half-to-fully saturated with sodium ions. Over a period of 50 hours the flow of solution was maintained at a constant at 33.6 ℓ/day. Six depth samplings of solutions were taken.

The depth profiles of aqueous calcium ion concentration can be

described as a set of breakthrough curves traveling down the column. These breakthrough curves connect an aqueous calcium ion concentration of 7.1 mg/ℓ with one of 3.6 mg/ℓ (Figure 11). Neglecting the top segment of column, the aqueous hydrogen ion content depth profiles also are breakthrough type curves connecting pH 6.5 with pH 7.5 (Figure 12). The hydrogen curves appeared to move down the column in conjunction with the calcium ion profiles.

Assuming the prevalent process is an ion exchange of aqueous calcium ions for sodium, certain numerical results can be concluded. The average rate of travel of the breakthrough curve is 0.13 ± 0.03 ft/hour down the column. Since the porosity of the column is 0.44, then 0.25 ± 0.06 μeq Ca^{++}/gm was adsorbed by the sand along with 0.0004 ± 0.0001 μeq H^{+}/gm. Sand located above any breakthrough curve represents sand that has come to equilibrium with the inlet solution. Since the inlet solution is devoid of aqueous sodium ions, then the sand above any breakthrough curve must have negligible sodium adsorbed to its surface. Sand below the breakthrough curve is in equilibrium with the aqueous calcium ion (3.6 mg/ℓ) and sodium (3.85 mg/ℓ) released in the breakthrough curve region of the column. If only sodium is released when aqueous calcium ions are adsorbed by the sand, then the quantity of sodium ions on the sand below the breakthrough curve must be 0.25 ± 0.06 μeq Na^{+}/gm. If "x" is the total capacity of the sand to hold cations, in μeq/gm, then the equilibrium coefficient, K_{eq}, for the exchange reaction (1) can be defined as

$$K_{eq} = \frac{Na^2 \overline{Ca}}{Ca \overline{Na}^2} \qquad (3)$$

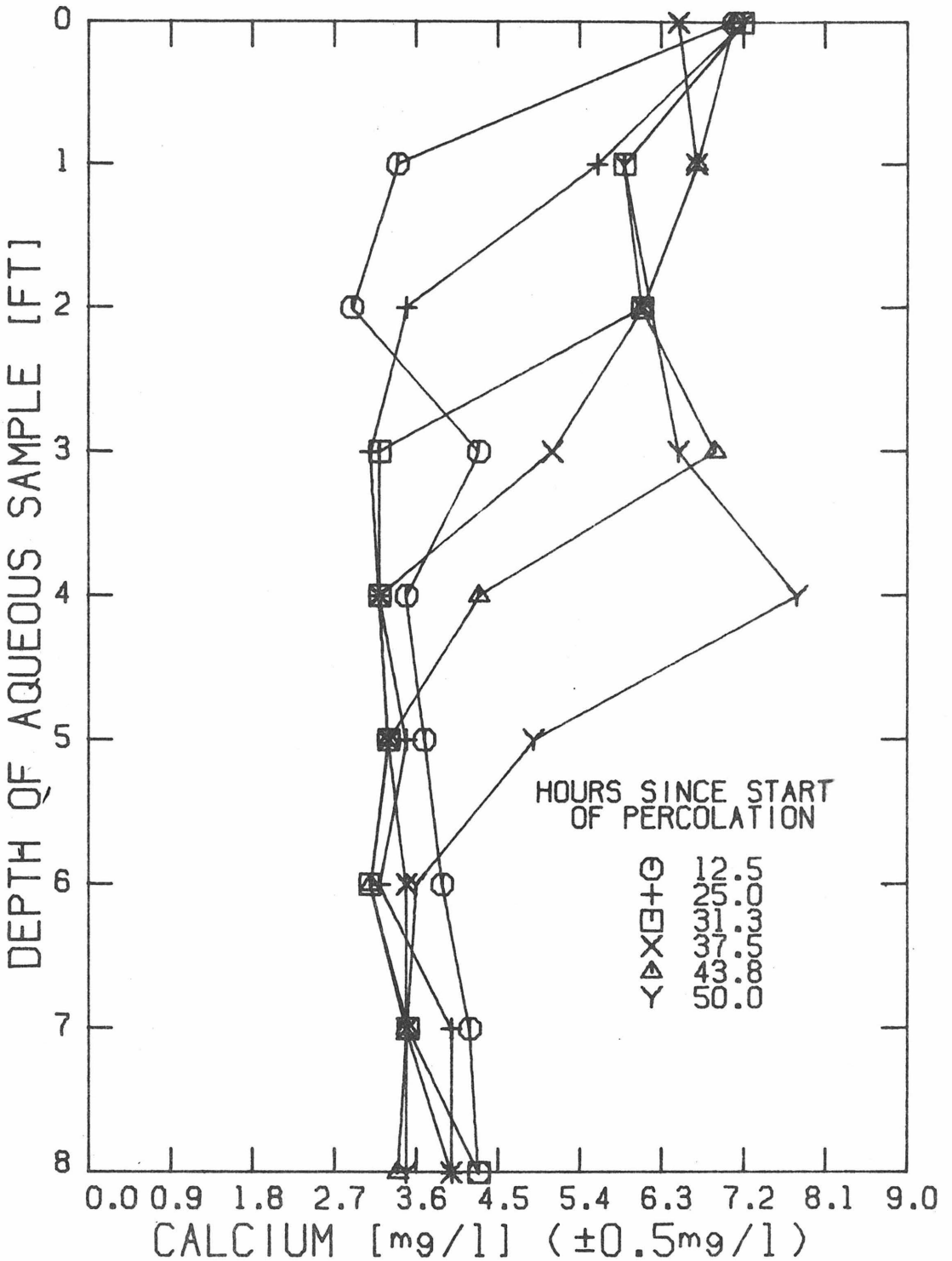

Figure 11: Aqueous Calcium Ion Content of a 7 mg Ca^{++}/ℓ Containing Inlet Solution Percolating at 33.6 ℓ/day through the Laboratory Column

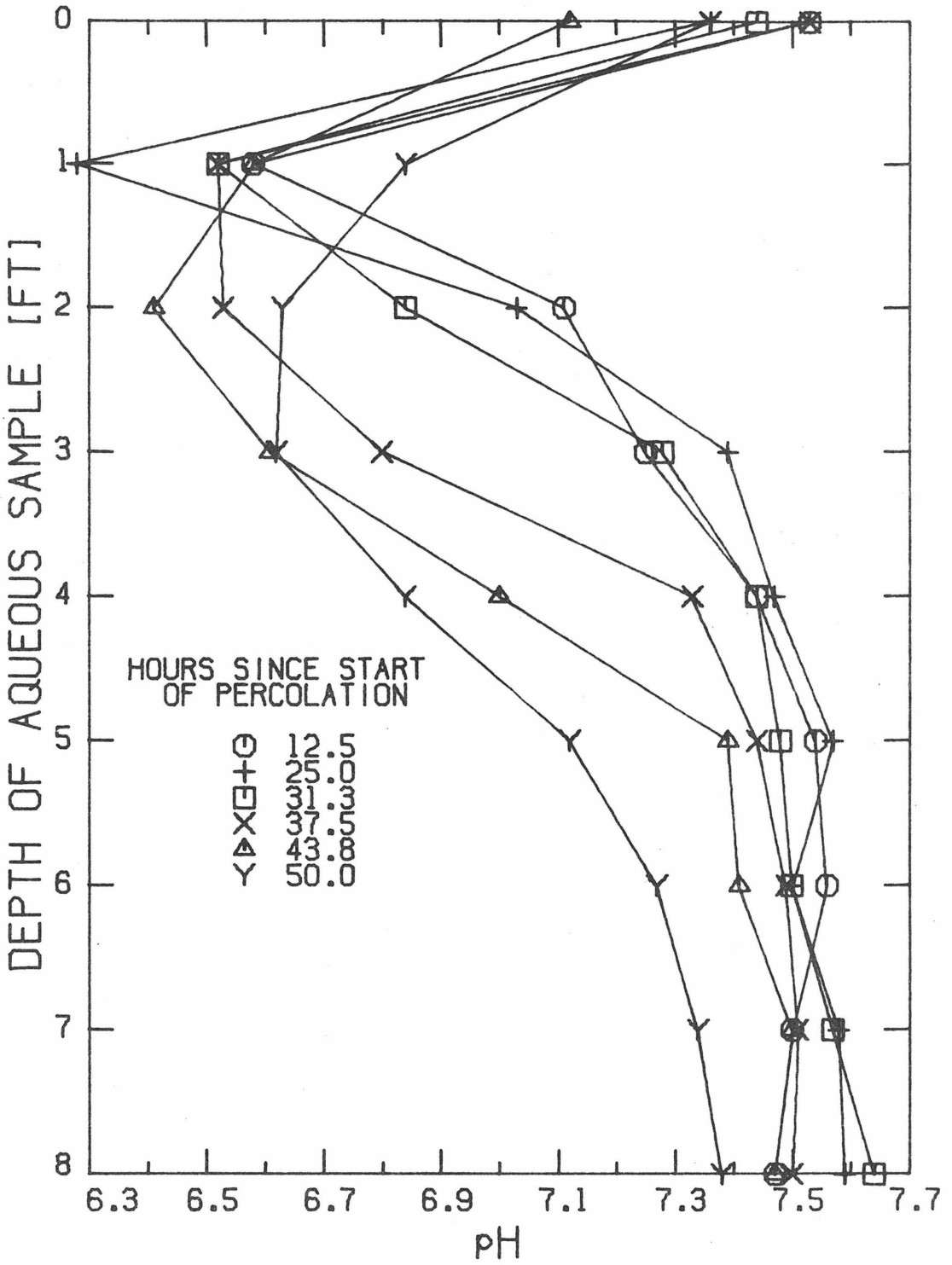

Figure 12: pH of a 7 mg Ca^{++}/ℓ Containing Inlet Solution Percolating at 33.6 ℓ/day through the Laboratory Column

and evaluated as

$$K_{eq} = 5(x - 0.25)[\text{mM gm}/\mu\text{eq}] \quad . \qquad (4)$$

Study of Extraneous Sand and Solution Chemical Species

So far, the only ion investigated that would be released by the laboratory's sand was calcium. However the column's minerals are known to contain calcium, sodium, potassium, magnesium, iron, zirconium, and probably manganese. The standard chemical formulas of minerals in the laboratory column are purely ideal and any number of cationic substitutions could occur in the mineral. To head off the possibility that an important cation might have been neglected in considerations of the interaction of the minerals and a percolating solution, a sample of the column's sand was vaporized in an electric arc and its emission spectrum was analyzed for most metallic elements.† Also, effluent from the column during the percolation of a 40 mg Ca^{++}/ℓ solution was taken and evaporated to dryness under an infrared lamp. The residue was also submitted for analysis for many extraneous cations.

There were no surprises in the composition of the sand itself (Table 1). The presence of certain cations in the solution is important. The relative abundance of barium ions in the percolating solution is assumed to represent an impurity in the feed solution. However the abundance of iron, manganese, and copper in the solution relative to their relative quantities in the mineral material itself possibly means that the minerals of these cations are more accessible

† Performed by Mrs. E. Bingham, Geology, Caltech.

Table 1

Emission Spectrographic Analyses

Element[†]	Sand ppm/ ppm Sr	Solution mg/ℓ / mg/ℓ Sr
Mg	3.7	100
Fe	1.2	1
Ti	1.2	trace
Ba	0.85	3
Sr	1.00	1
Mn	0.22	17
Zr	0.11	1
Cu	0.06	0.5
V	0.03	1
Cr	0.03	0.3
Ga	0.02	0.2
Sc	0.01	0.3

[†] Certain elements are not tabulated due to their being difficult to analyze or their being too abundant.

to dissolution. Possibly the accessory minerals are coatings on the surface of other minerals.

Percolation of Calcium Salt Solution

Again, a calcium salt solution was percolated through the column. This time the concentration was higher at 37 to 38 mg Ca^{++}/ℓ with a flow rate of only 3.7 ℓ/day. The initial condition of the sand was that after two weeks of deionized water flow, for which the column effluent contained 4 mg Ca^{++}/ℓ. The column was initially full of deionized water. During the run, samplings were taken every 12 hours and analyzed for calcium, pH, and carbonate.

pH profiles show a breakthrough curve moving down the column at approximately 0.17 ft/hr. and connecting solution of pH 6.3 with pH 6.9. When the curve had swept through the column in 60 hours, the pH profiles were quite constant at pH 6.3. Curves representing the quantity of aqueous calcium ions in the percolating solution with time appeared to have two breakthrough curves. One curve was similar to the pH breakthrough curve in that it traveled down through the column at the rate of 0.17 ft/hr. The second breakthrough curve moved at a much slower rate down the column. The slow moving curve connected solution of 38 mg Ca^{++}/ℓ with 27 ± 1 mg Ca^{++}/ℓ; the other curve joined solution of 30 ± 4 mg Ca^{++}/ℓ with 3 ± 2 mg Ca^{++}/ℓ. On top of all the many inflections of the calcium ion profiles was a gradual increase of 0.5 mg $Ca^{++}/\ell \cdot ft$. Carbonate ion concentrations (see Appendix B) increased in the percolating solution at a constant rate of 0.0667 mM/ft.

Both the pH breakthrough curve and the fast moving calcium ion

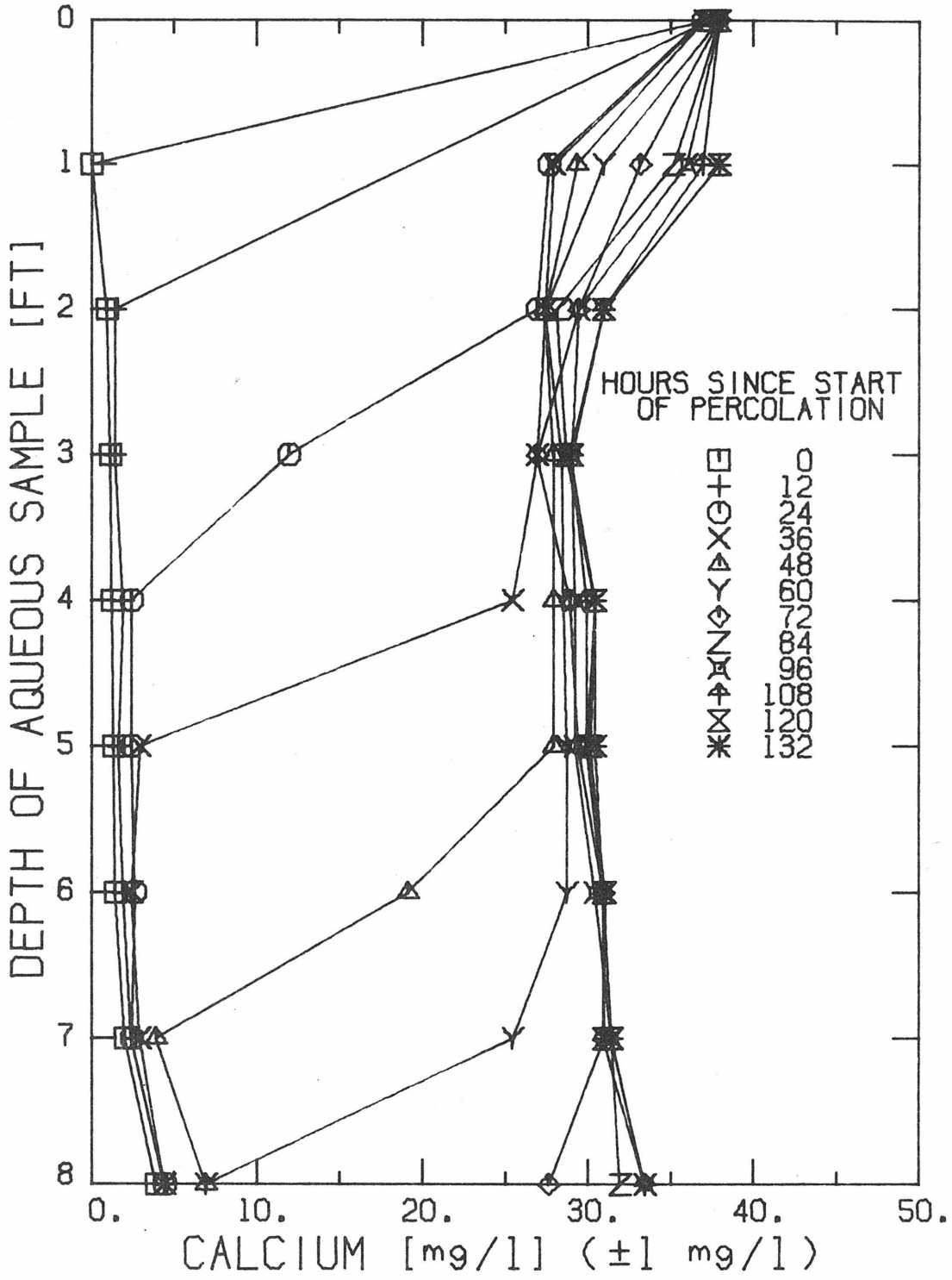

Figure 13: Aqueous Calcium Ion Content of a 38 mg Ca^{++}/ℓ Containing Solution Percolating at 3.7 ℓ/day through the Laboratory Column Displacing a Deionized Water Solution

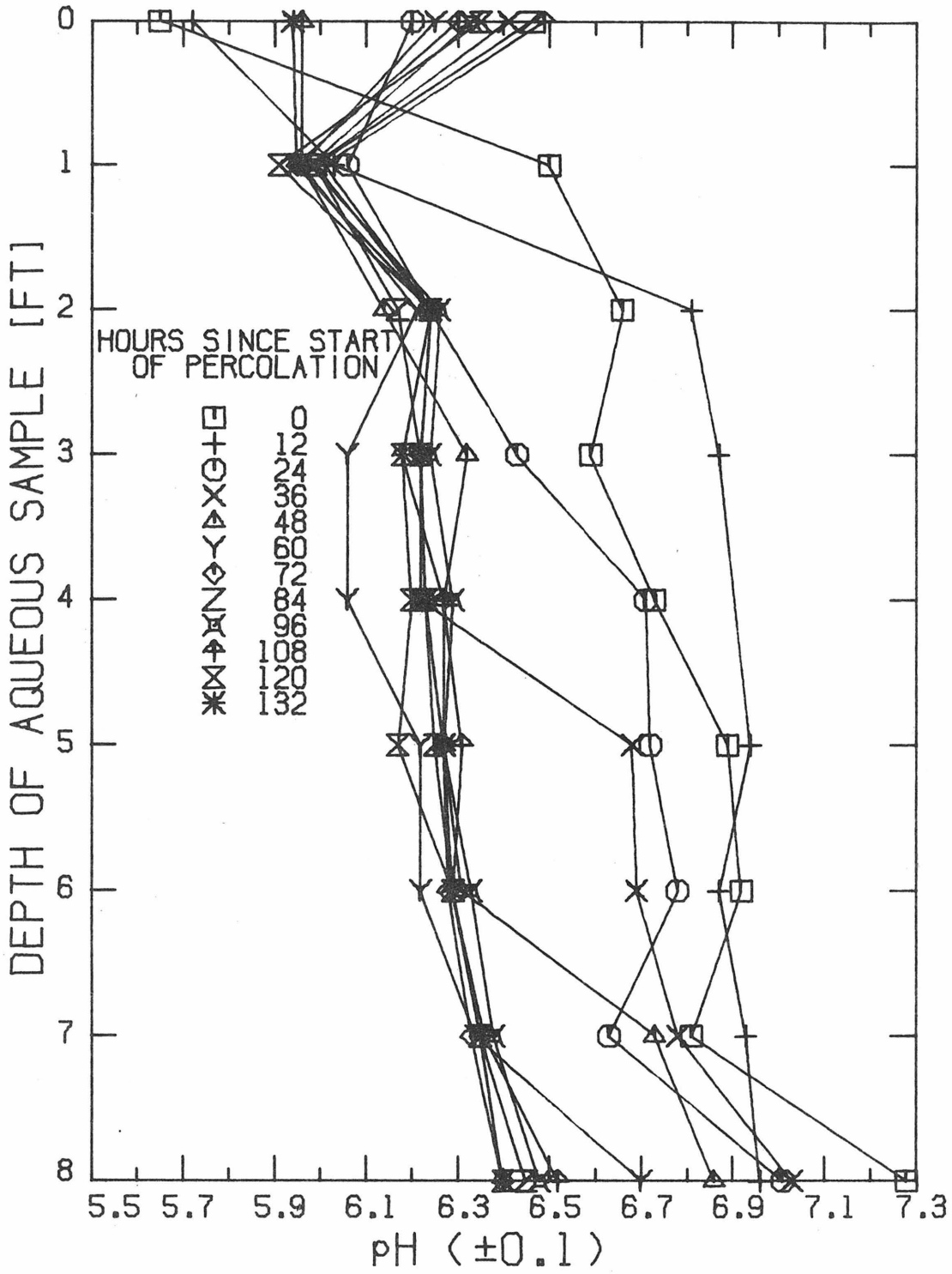

Figure 14: pH of a 38 mg Ca^{++}/ℓ Containing Solution Percolating at 3.7 ℓ/day through the Laboratory Column Displacing a Deionized Water Solution

breakthrough curve are the leading edge of the calcium salt solution as it displaces the deionized water solution already in the column. The smaller calcium ion breakthrough curve represents the boundary between sand that is in equilibrium with the incoming solution and sand in equilibrium with the column's effluent. The quantity of calcium ions that must be added to the sand so that it will be in equilibrium with the influent determines the rate at which the breakthrough curve travels down the column. The data show that 1.2 μeq Ca^{++}/gm was added. Gradual upward inflections in the calcium ion profiles are assumed due to genuine dissolution of a calcium-containing mineral. The addition of carbonate ions to the percolating solution suggests that mineral to be calcium carbonate.

General Conclusions

The preliminary investigation revealed several important points relative to the addition of dissolved solids to a percolating solution. When a neutral solution passes through the laboratory column, aqueous calcium would be released at less than 10^{-4} mg Ca^{++}/gm·hr. Calcium carbonate is the partial source of the aqueous calcium ions. Rate of release of calcium ions did not appreciably vary with pH between the range 6.3 and 7.7. If bacterial nitrification is going to cause a large increase of the rate of release of calcium ions to the percolating solution similar to the situation at the Whittier Narrows test basin, the pH will have to be dropped considerably below 6.3.

Ion exchange reactions are rapid and extensive enough to be important transient factors in the cationic constituency of a percolating

solution. Cationic exchange capacity of the sand is at least 1.2 μeq/gm. Besides sodium and calcium, the aqueous hydrogen ion can also participate in ion exchange reactions with the column's sand.

Ion exchange reactions must be considered if a mathematical model is to predict the variation of aqueous species in a percolating solution under non-steady-state conditions. Verification of the role of ion exchange reactions requires that, at least, all the concentrations of all prominent ions in the aqueous phase be known.

MAIN BODY OF RESEARCH

Percolation of Deionized Water

This run represented a situation of dissolution of the column's minerals in a near neutral environment in the absence of biological interference. Later, when a biological community would be established in the column, effect on the dissolved solids content of the solution by bacteria would be immediately obvious.

Chemical interactions between the mixture of minerals of the laboratory column and a percolating solution was undertaken with the addition of two more sampling ports at the 1/4- and 1/2-foot depth positions. Biological production of acids and bases was to be avoided as much as possible during this run. Bacteria were deactivated in the column, in a manner that would be harmless to future colonies to be grown, by percolating deionized water at 11 ℓ/day. Oxygen content of the percolating solution gradually rose from a minimum value of 2 mg O_2/ℓ to 8 mg O_2/ℓ over a period of one month. Except for traces of organic compounds and light coming into the top segment, there would be

no energy sources to support bacterial growth capable of altering the chemical properties of the percolating solution.

Aqueous species monitored, in consideration of the constituency of the sand's minerals, were sodium, magnesium, calcium, potassium, manganese, iron, and silica. Deionized water percolated through the column for two weeks at 11.1 ℓ/day. Only the last two days of percolation were monitored.

In no sample was the aqueous manganese or iron concentration higher than 0.01 mg/ℓ. Detectable aqueous species exhibited time independent, unimodally-increasing concentrations as the solution percolated down through the column. The rate of addition of aqueous species decreased with depth of travel. Aqueous magnesium concentrations leveled off at 0.9 mg/ℓ as did sodium ion values at 0.2 ± 0.01 mg/ℓ (Figures 15 and 16). Potassium ions were added to the solution throughout the column at approximately the same rate (Figure 17). Large experimental errors on aqueous silica content did not hide the fact that approximately 1.5 ± 0.3 mg SiO_2/ℓ had been acquired by the column's effluent (Figure 18). The solution was acidified in the top three inches of sand but was driven back toward neutrality in the remainder of flow (Figure 19).

The well oxidized condition of the percolating solution (8 mg O_2/ℓ) and its neutral pH required $Fe(OH)_3$ and MnO_2 to be the stable forms of iron and manganese in the column (Stumm et al., 20). Aqueous species concentrations of iron or manganese in equilibrium with either of the minerals is negligibly small and consistent with observations.

Generation of aqueous cations from aluminosilicate minerals by ion exchange or by dissolution is but a subtle distinction. Assuming

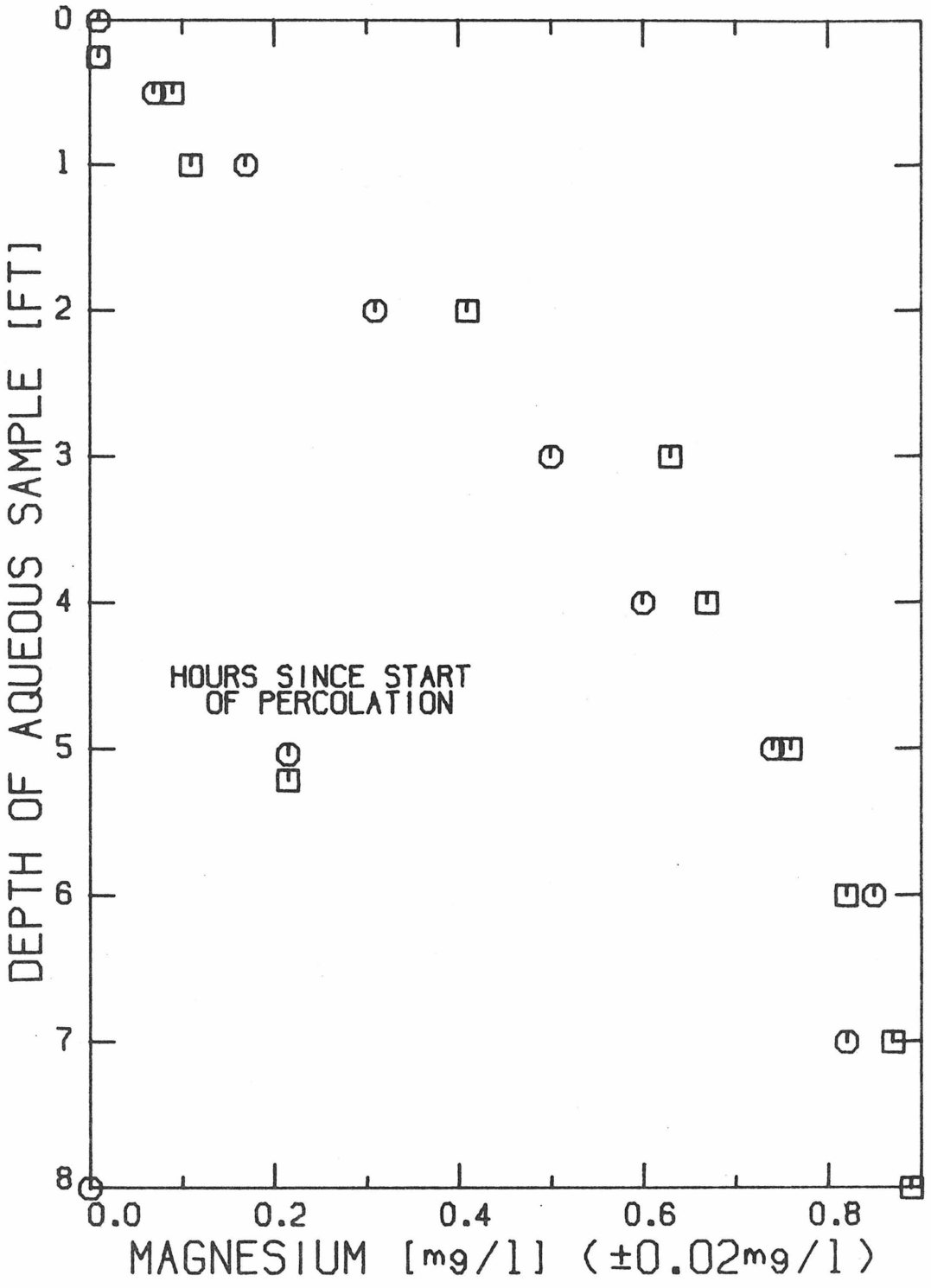

Figure 15: Aqueous Magnesium Ion Content of Deionized Water Percolating through the Laboratory Column

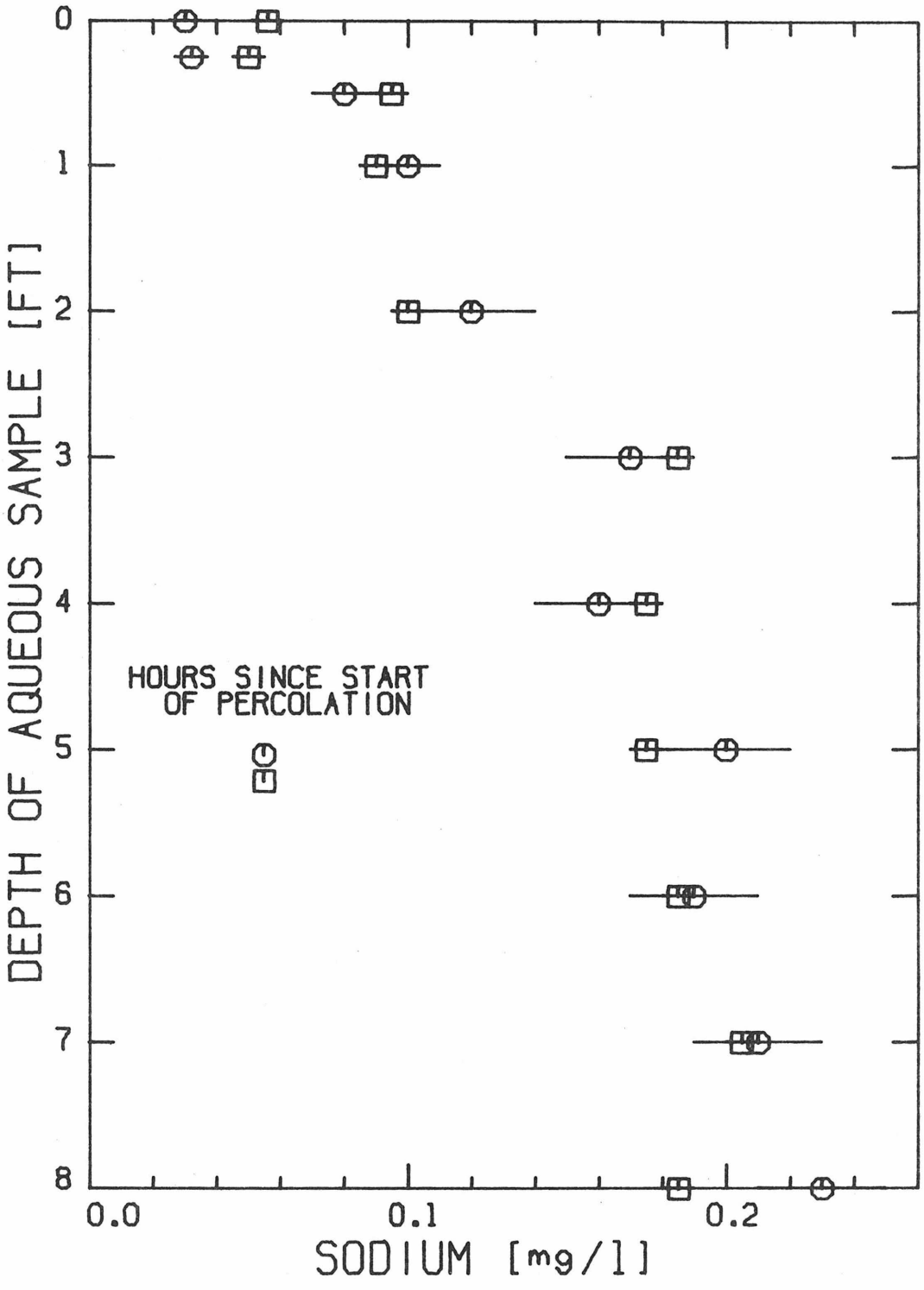

Figure 16: Aqueous Sodium Ion Content of Deionized Water Percolating through the Laboratory Column

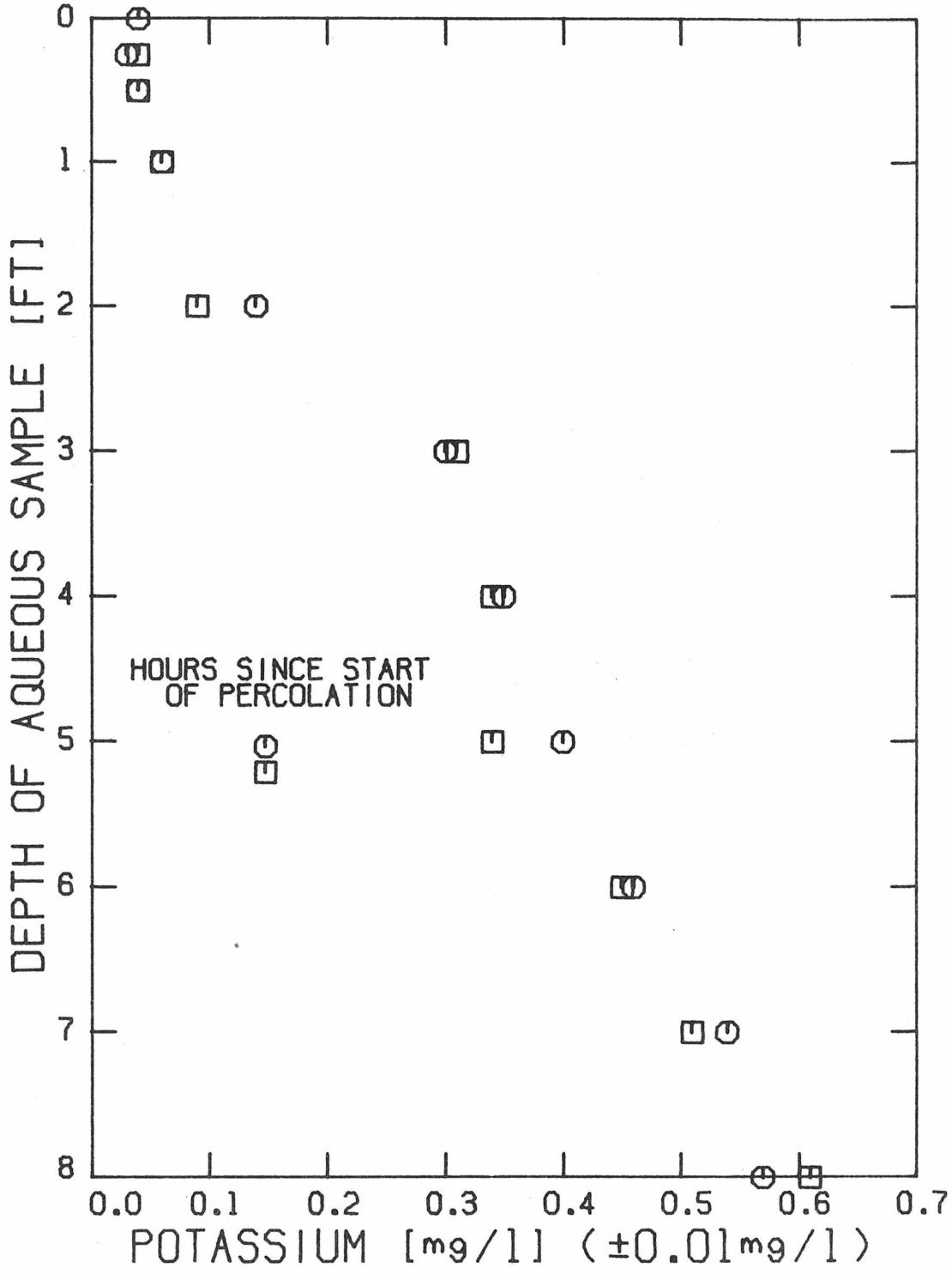

Figure 17: Aqueous Potassium Ion Content of Deionized Water Percolating through the Laboratory Column

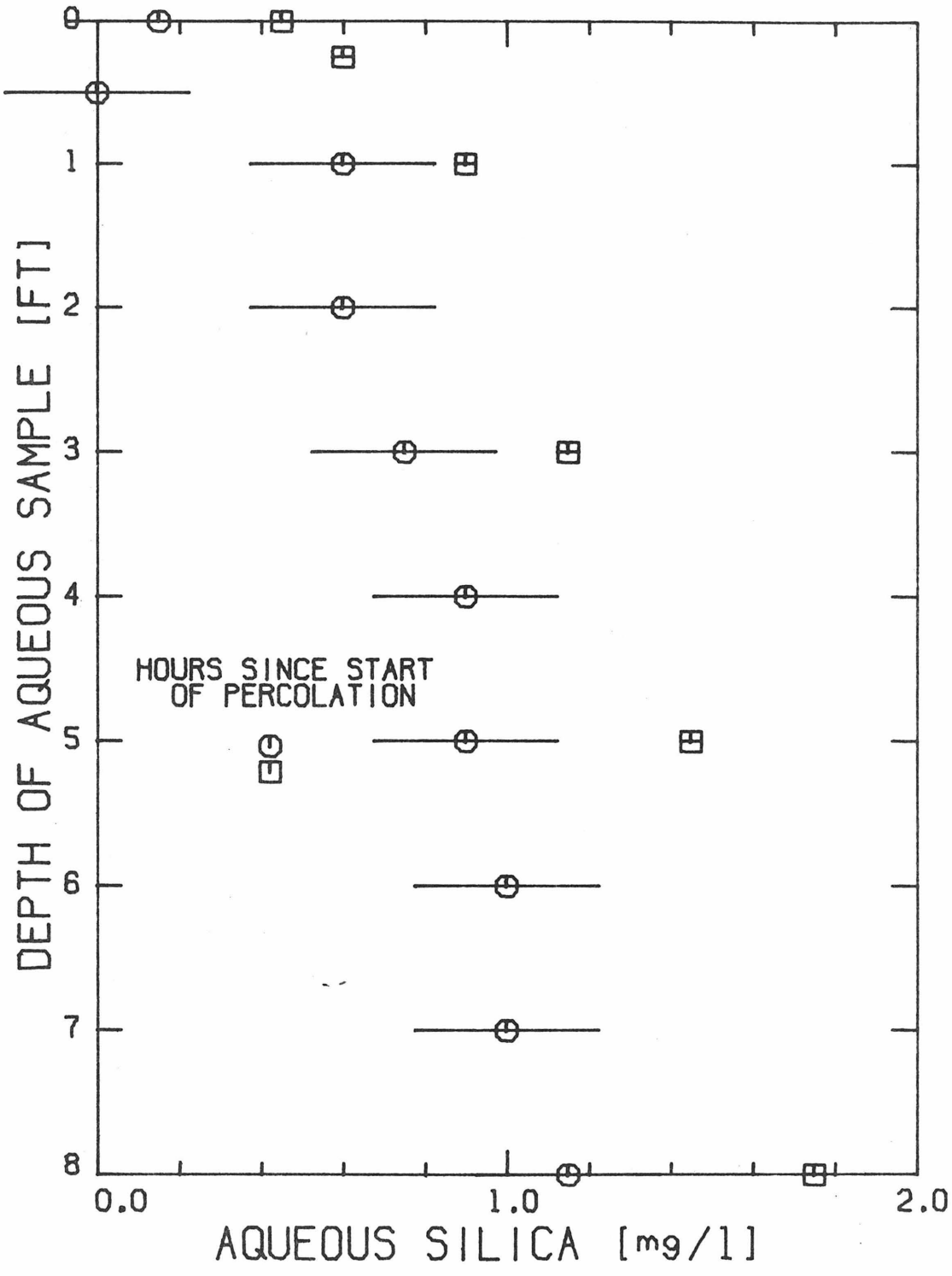

Figure 18: Aqueous Silica Content of Deionized Water Percolating through the Laboratory Column

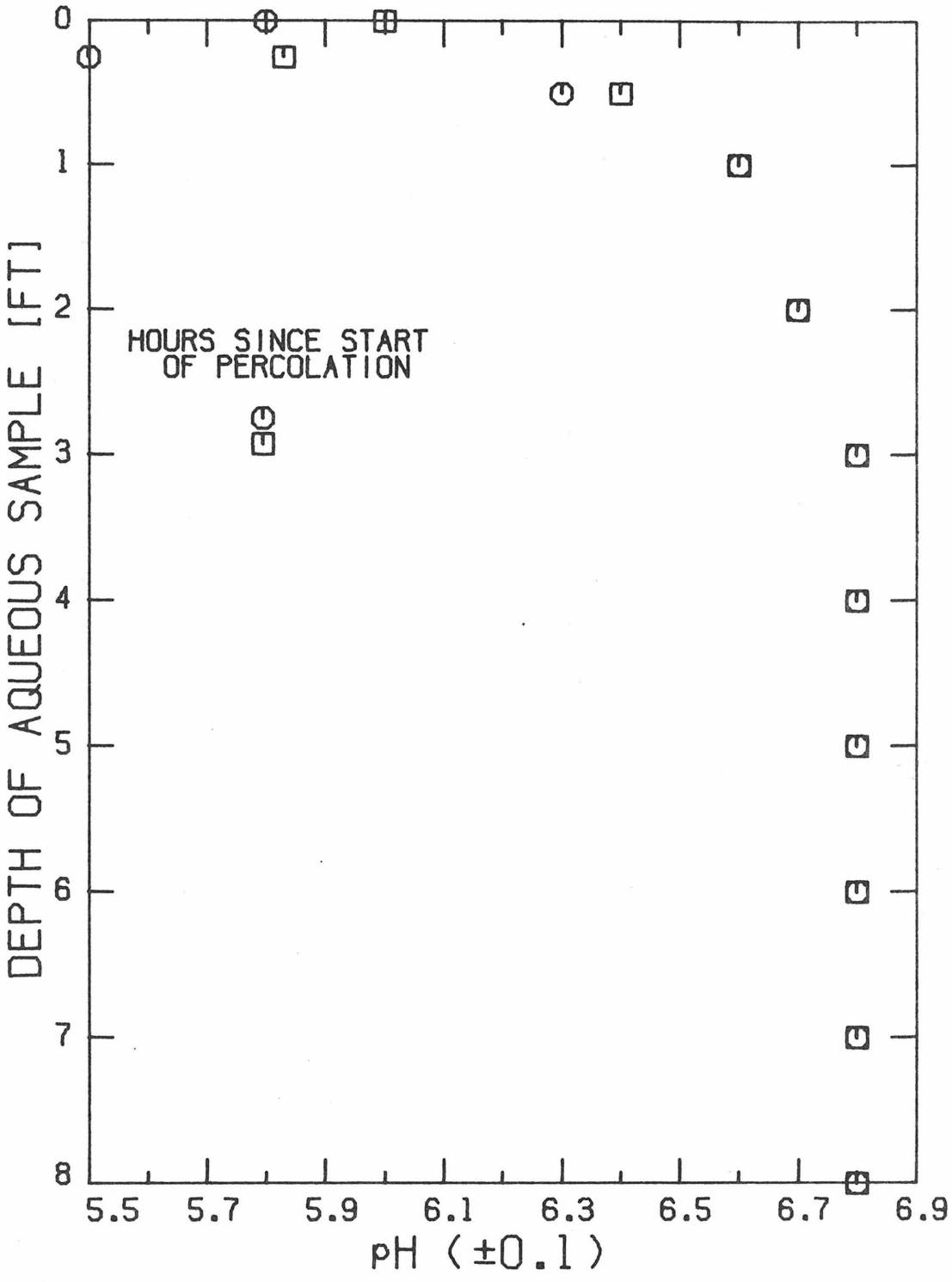

Figure 19: pH of Deionized Water Percolating through the Laboratory Column

the microscopic examination of the sand to be thorough, the source of cations by dissolution can be only aluminosilicate minerals. Overall dissolution reactions of such aluminosilicate minerals as plagioclase ($(Ca,Na)(Al,Si)AlSi_2O_8$), biotite ($K_2(Mg,Fe)_6(Si_6Al_2)O_{20}(OH)_4$), or hornblende ($NaCa_2[(Mg,Fe)_4Al]Al_2Si_6O_{22}(OH)_2$) will generally be one, or a combination of, the following in a well-oxidized neutral aqueous environment:

$$\text{aluminosilicate(s)} + H^+(aq) = \text{Fe,Mn wreckage(s)} + \text{silica(aq)} + \text{alumina(aq)} + \text{cation}^+(aq) \quad (5)$$

$$\text{aluminosilicate(s)} + H^+(aq) = \text{Fe,Mn wreckage(s)} + \text{silica(aq)} + \text{alumina wreckage(s)} + \text{cation}^+(aq) \quad (6)$$

$$\text{aluminosilicate(s)} + H^+(aq) = \text{Fe,Mn wreckage(s)} + \text{clay(s)} + \text{cation}^+(aq) \quad (7)$$

The specific path of dissolution taken will be dependent on the concentration of aqueous silica and alumina adjacent to the dissolving aluminosilicate surface. Minerals in contact with fresh free-flowing solutions will dissolve according to reaction path (5) where the Fe,Mn-wreckage would represent trace quantities of iron and manganese oxides, hydroxides, and oxyhydroxides. Neutral solutions percolating through a soil rapidly saturate with respect to aluminum hydroxide, gibbsite ($Al(OH)_3$). Eventually, as further dissolution occurs, a high enough aqueous silica concentration will prevail that further dissolution of minerals will yield clays (reaction 7). In the absence of high cationic activities the clay will typically be a member of the kaolin group ($Al_4Si_4O_{10}(OH)_8$). The present run was of high enough silica

concentration that a combination of reaction paths 2 and 3 would be thermochemically possible down through the laboratory column:

$$\text{aluminosilicate(s)} + H^{+}\text{(aq)} = \text{Fe,Mn, and clay wreckages(s)} + \text{silica(aq)} + \text{cation}^{+}\text{(aq)} \quad (8)$$

Such a dissolution mechanism gives the aqueous hydrogen ion and cations the attribute of ion exchangers. Pure ion exchange reactions, however, do not involve change of the solid exchanger's structure. The question of whether the source of cations in percolating solutions at Whittier Narrows is due to ion exchange or to mineral dissolution is of great importance, and the eventual separation of the two mechanisms is imperative.

The appearance of aqueous silica in the present investigation's solution cannot be by the ion exchange path since its aqueous species is neutral. $Si(OH)_4$ is the only aqueous species possible over the entire pH range that will exist in the percolating solution (pH 4.5 to 8.5). Aqueous silica appears in the solution due only to actual mineral dissolution.

Simplification of the source mechanism of aqueous silica is accomplished by neglecting dissolution of quartz. The overall reaction of solid silica phases with water is:

$$SiO_2(s) + 2H_2O = Si(OH)_4(aq)$$

$Si(OH)_4$ can dissociate or polymerize into at least five other aqueous species (Lagerström et al., 30). As long as the solution pH is between 2 and 9, $Si(OH)_4$ concentration is unaffected by pH. Much study has

been given the solubility of quartz due to discrepancies between data caused by a more soluble metastable, amorphous silica phase or micro-crystalline quartz (Moore et al., 53). The present discussion is focused on the macrocrystalline silica mineral, quartz, of solubility 12 mg SiO_2/ℓ. Only the dissolution portion of the quartz water reaction needs to be considered since the silica content of the solution of this run was well below saturation of any solid silica phase. Change of concentration of aqueous silica in a batch reaction of quartz and water can be described by:

$$\frac{d\ SiO_2}{dt} = k_1\sigma \quad , \tag{9}$$

The dissolution reaction itself controls the overall rate of transfer of silica away from the crystal quartz due to the smallness of the reaction rate constant, k_1, (4×10^{-11} $mg/cm^2 \cdot hr$)(van Lier et al., 31; Henderson et al., 32). Using the BET analyzed surface area for σ, quartz could have contributed only 0.006 mg SiO_2/ℓ to the laboratory column's effluent 1.5 mg SiO_2/ℓ. Therefore quartz can be neglected as a factor affecting the percolating solution's pH or aqueous silica concentration.

Dissolution of aluminosilicate minerals must be the reason for the addition of aqueous silica molecules to the percolating solution. The least complex dissolution of the aluminosilicates of the column's sand would be via reaction path (5). However a more complex situation arises by considering the possibility of incongruent dissolution. The aluminum-to-silicon molar ratio for the aluminosilicate minerals of the column is approximately unity. Congruent dissolution (reaction path 5) should yield an aqueous effluent alumina activity of 0.75 mg Al^{+++}/ℓ.

Maximum solubility of the hydrated aluminum hydroxide gibbsite ($Al_2O_3\ 3H_2O$) in the pH range of the present run is 0.0007 mg Al^{+++}/ℓ (Gardner, 36). Gibbsite, therefore, must be a product of the incongruent dissolution of the parent aluminosilicate throughout the length of the column. Furthermore, subsequent data show that aqueous aluminum concentration is at least less than 0.01 mg Al^{+++}/ℓ thus negating the possibility that a more soluble amorphous gibbsite (Wollast, 29) and slow gibbsite crystallization rate could permit a higher aqueous alumina concentration. As aqueous silica concentrations increase further, another solid mineral, kaolinite, could precipitate by reaction of aqueous silica and gibbsite:

$$4Al_2O_3 \cdot 3H_2O(s) + 4Si(OH)_4(aq) = Al_4Si_4O_{10}(OH)_8(s) + 10H_2O\ .$$

Theoretically 1.2 mg SiO_2/ℓ is all the aqueous silica necessary to start the formation of kaolinite from gibbsite (Stumm et al., 20). By observation of natural water systems Garrels (37) listed 10 mg SiO_2/ℓ as the minimum silica concentration. According to Weaver (38), six kaolin phases exist. Due to the unknown kinetics of the reaction, it is difficult to state which phase will prevail as a solution percolates through the column. From a thermodynamic point of view, if equilibrium has been reached, 1.2 mg SiO_2/ℓ would be the maximum concentration the percolating solution could attain. Therefore, minerals above the three-foot depth must incongruently dissolve to gibbsite and those below the same depth will dissolve incongruently to kaolinite.

It has been proposed (Helgeson, 33; Wollast, 29) that products of incongruent dissolution form a coating on the parent mineral, hindering

the flow of products and reactants of dissolution. If the overall rate of release of aqueous silica is controlled by diffusion through an amorphous coating, then a steady state representation of aqueous silica in a percolating solution will be described by:

$$[SiO_2](z) = [SiO_2]_0^1 (1 - \exp(-ADz/uL)) \qquad (10)$$

where

$[SiO_2](z)$ = aqueous silica concentration as a function of depth, z

$[SiO_2]_0^1$ = aqueous silica concentration at interface of parent mineral and coating

D = diffusion coefficient of silica through the coating = 3.6×10^{-11} cm^2/hr (Wollast, 29)

L = thickness of coating = 10^{-7} cm.

Because diffusion through the surface coating is assumed to control the overall rate of release of silica from the parent aluminosilicate, then the interfacial aqueous silica concentration will be in equilibrium with both the parent and the coating mineral. In the case of albite ($NaAlSi_3O_8$) in contact with either gibbsite or kaolinite, that concentration is approximately 10 mg SiO_2/ℓ (Stumm et al. 20). Therefore,

$$[SiO_2](z) \simeq 10(1 - \exp(0.01z)) \quad . \qquad (11)$$

If the products of incongruent dissolution do not adhere to the parent mineral, the overall release of silica will be governed by

$$[SiO_2](z) = [SiO_2]_0^2 (1 - \exp(-ak_1z/u)) \qquad (12)$$

where

k_1 = rate constant of dissolution

$[SiO_2]_0^2$ = aqueous silica concentration in equilibrium with both gibbsite and kaolinite.

Either equation could represent the change of aqueous silica concentration of percolating solutions if reasonable guesses for the constants of the equations were made.

Incongruent dissolution of any aluminosilicate mineral reaction (8) in a near neutral deionized environment will produce the same equivalents of alkali ions as it will consume hydrogen ions. 0.003 μeq H^+/ℓ was removed from the percolating solution; yet, 0.26 μeq cations/ℓ were added. Conservation of the solution's electroneutrality requires that an anion be released with the cations to the extent of 0.257 μeq/ℓ. Because the column had been inundated for a month with solution, the dissolving mineral-salt releasing anions and cations must at least be only sparsely soluble or else it would have dissolved away its trace occurrence in the laboratory column. Calcium or magnesium carbonate or phosphate minerals are the possible source of released anions. Sodium and potassium ionic salt minerals found in nature are not sparsely soluble. Sodium and potassium ions are undoubtedly products of the breakdown of aluminosilicate minerals. Both sodium and calcium exist in the plagioclase structure to preserve electroneutrality in the structure composed of four member chains of SiO_2 tetrahedra partially replaced by alumina. Sodium additions to the percolating solution would result from the breakdown of plagioclase and variation of the rate of addition of sodium with depth should follow that of

aqueous silica. Potassium ions probably originate from biotite at a rate dependent on the diffusion of potassium ions out from between the aluminosilicate sheets that form biotite (Reed et al., 39).

This run specifies the upper bound to the rate at which cations and silica would be released to a neutral percolating solution. Calcium ions are released (Figure 20) presumably by dissolution of carbonates at the maximum rate of 3×10^{-5} mg/gm·hr. Possibly by dissolution of carbonates and hornblende, magnesium is released at the maximum rate of 1×10^{-5} mg/gm·hr. The maximum rate of addition of sodium ions to a percolating deionized solution is 2×10^{-6} mg/gm·hr; potassium's rate is 5×10^{-6} mg/gm·hr. The release of silica is a direct result of dissolution of the column's aluminosilicates. Forty per cent of the column's sand can be neglected as a supplier of the aqueous silica because quartz is extremely slow at dissolving. As a result of this run, the effects, if any, of bacterial activity on the dissolved solids content of a percolating solution will be readily apparent.

Percolation of a Calcium Salt Solution

Preliminary findings show that, despite its coarseness, the sand of the column is an excellent cation exchange medium. This run was intended to exhibit the importance of cation exchange reactions on a large array of aqueous species. The first step of dissolution of a fresh mineral surface is an ion exchange of the mineral's cation for the hydrogen ion (Helgeson et al. 35). The sodium and calcium of plagioclase could be replaced by the aqueous hydrogen ion without much alteration of the alumina/silica bonds. Similarly, potassium of biotite is weakly held as an interlayer ion. Potassium is replaced

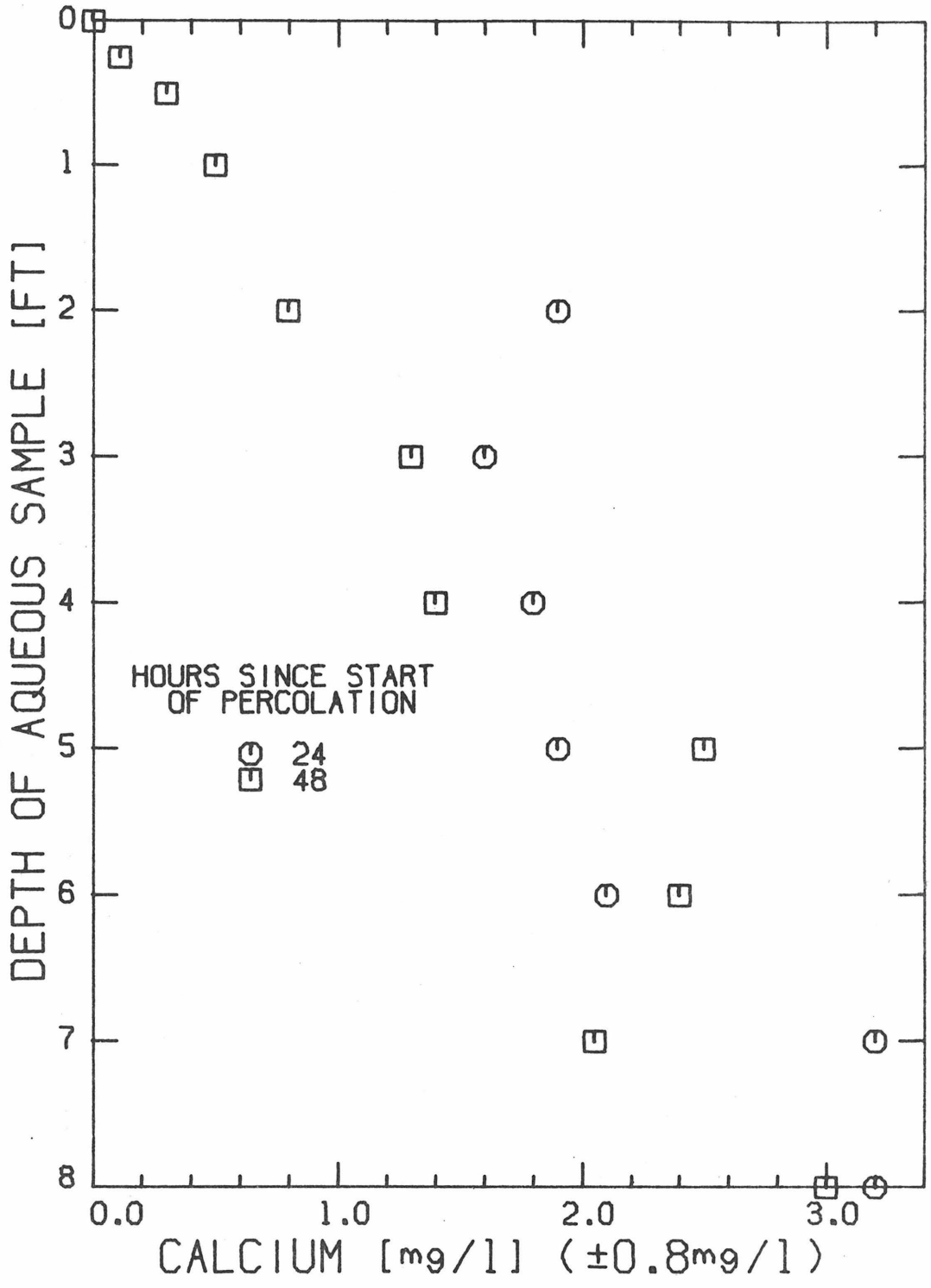

Figure 20: Aqueous Calcium Ion Content of Deionized Water Percolating through the Laboratory Column

by the hydronium ion to give vermiculite (Frye, 44) in the early stage of dissolution of biotite. The effect of a counter ion on the release of cations from the column's mineral assemblage must be examined more closely.

The counter ion used in this run was calcium in a calcium chloride solution of 40 mg Ca^{++}/ℓ. It is important to remember that previously deionized water had been purging the column for two weeks. At the rate of 11.1 ℓ/day the calcium solution percolated for 197 hours during which time the aqueous composition of the solution with depth was determined at seven time intervals. Analysis was again made after another 235 hours of flow at 36 ℓ/day, followed by 75 hours at 11.1 ℓ/day of the same 40 mg Ca^{++}/ℓ solution.

Aqueous silica, oxygen, potassium, and hydrogen concentrations of the percolating solution were essentially time independent whereas sodium and especially calcium and magnesium aqueous levels were not. The rate of addition of potassium ions to the solution (Figure 21) more than tripled over the rate when deionized water was percolated (Figure 17). As previously experienced, the rate of addition of aqueous potassium ions decreased with depth. Aqueous silica levels (Figure 22) were unaffected by the increased ionic strength of the percolating solution. pH (Figure 23) followed the same general pattern as when deionized water was percolated (Figure 19). In the top six inches 0.005 meq acid/ft was added to the incoming solution and the final constant pH for the remainder of flow was 6.1 instead of 6.7. There also existed a definite consumption of 2.5 mg O_2/ℓ (Figure 24) from the solution in the top segment of the column with a gradual readdition

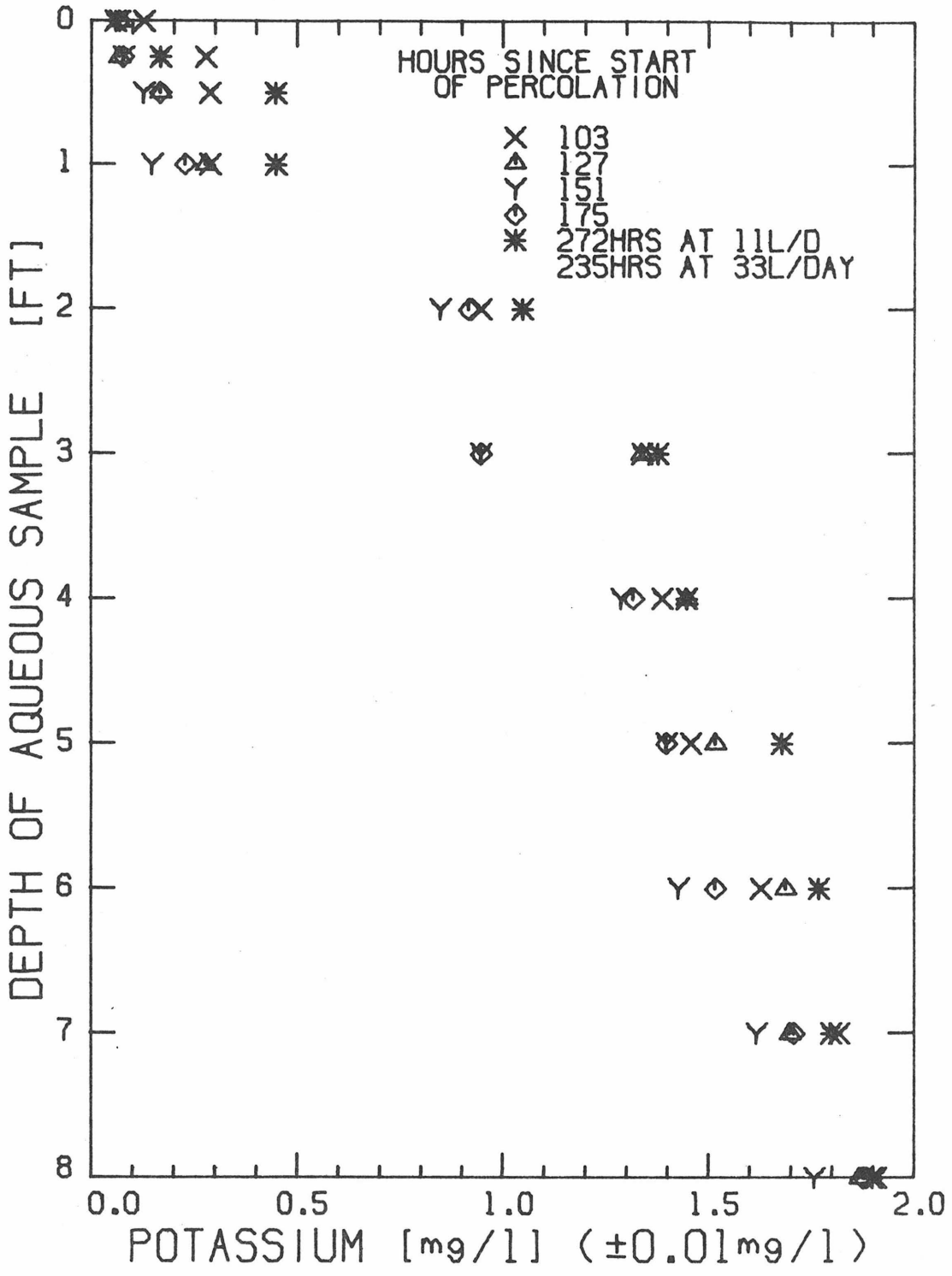

Figure 21: Aqueous Potassium Ion Content of a 40 mg Ca^{++}/ℓ Containing Inlet Solution Percolating through the Laboratory Column

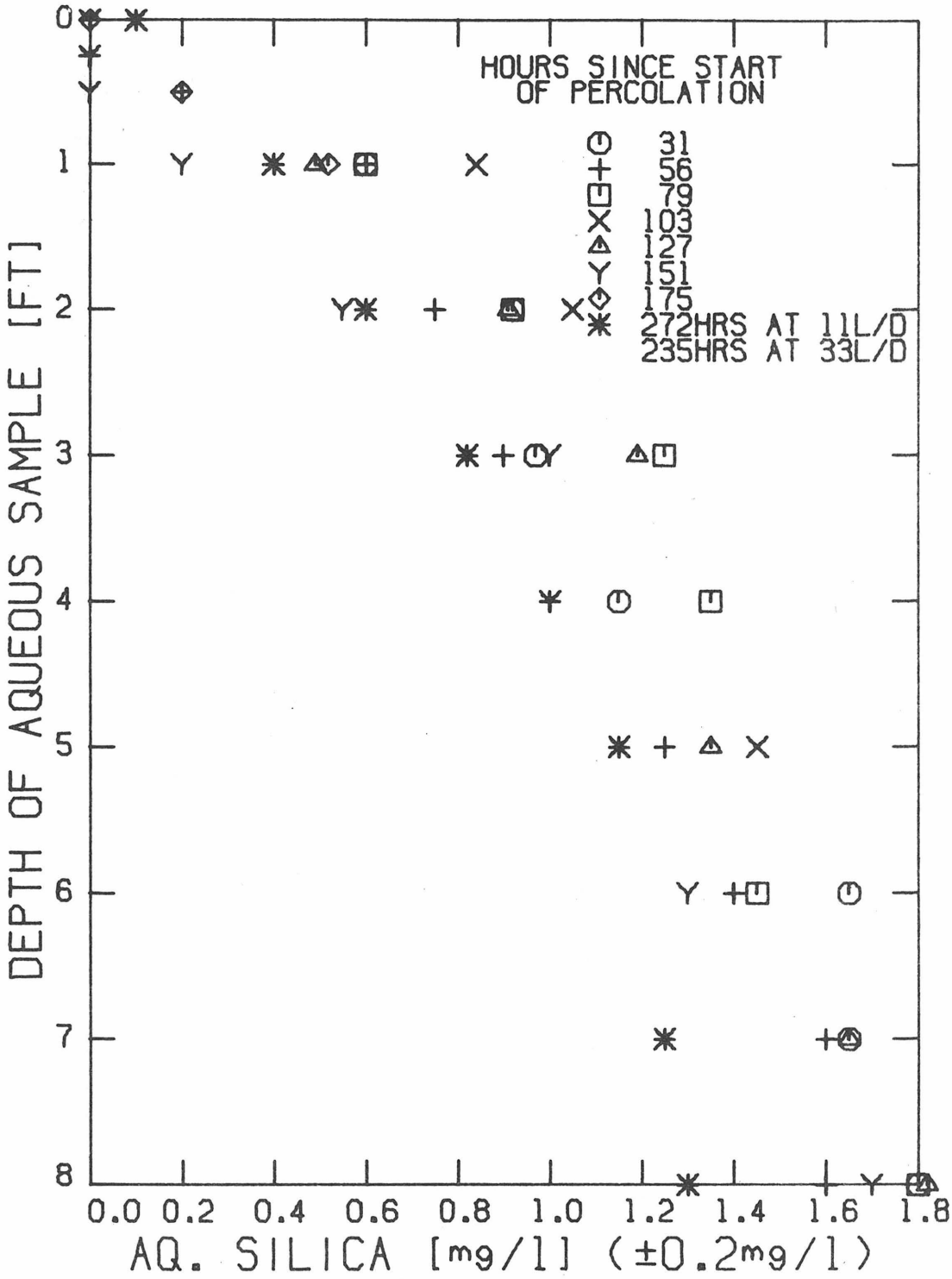

Figure 22: Aqueous Silica Content of a 40 mg Ca^{++}/ℓ Containing Inlet Solution Percolating through the Laboratory Column

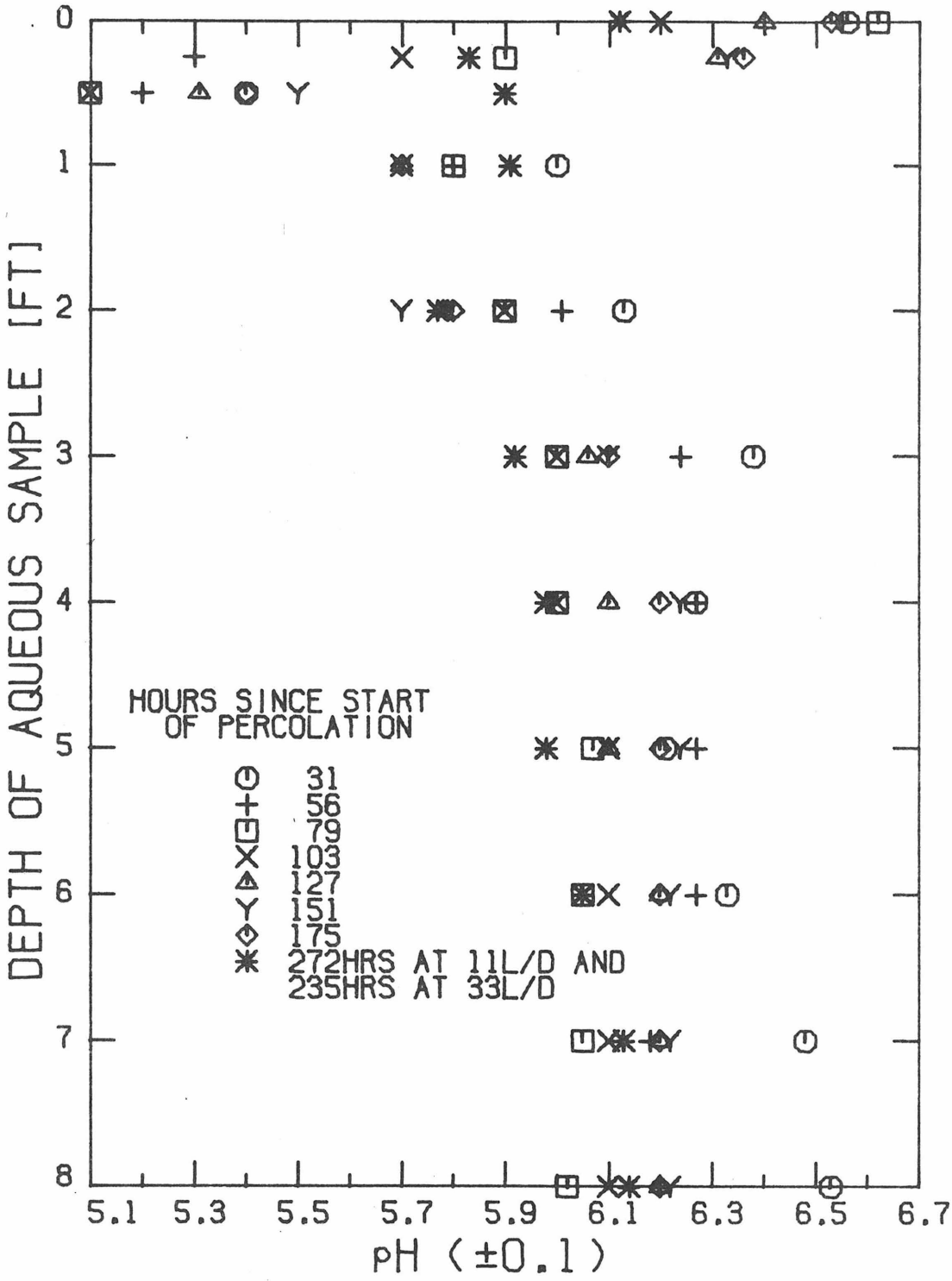

Figure 23: pH of a 40 mg Ca^{++}/ℓ Containing Inlet Solution Percolating through the Laboratory Column

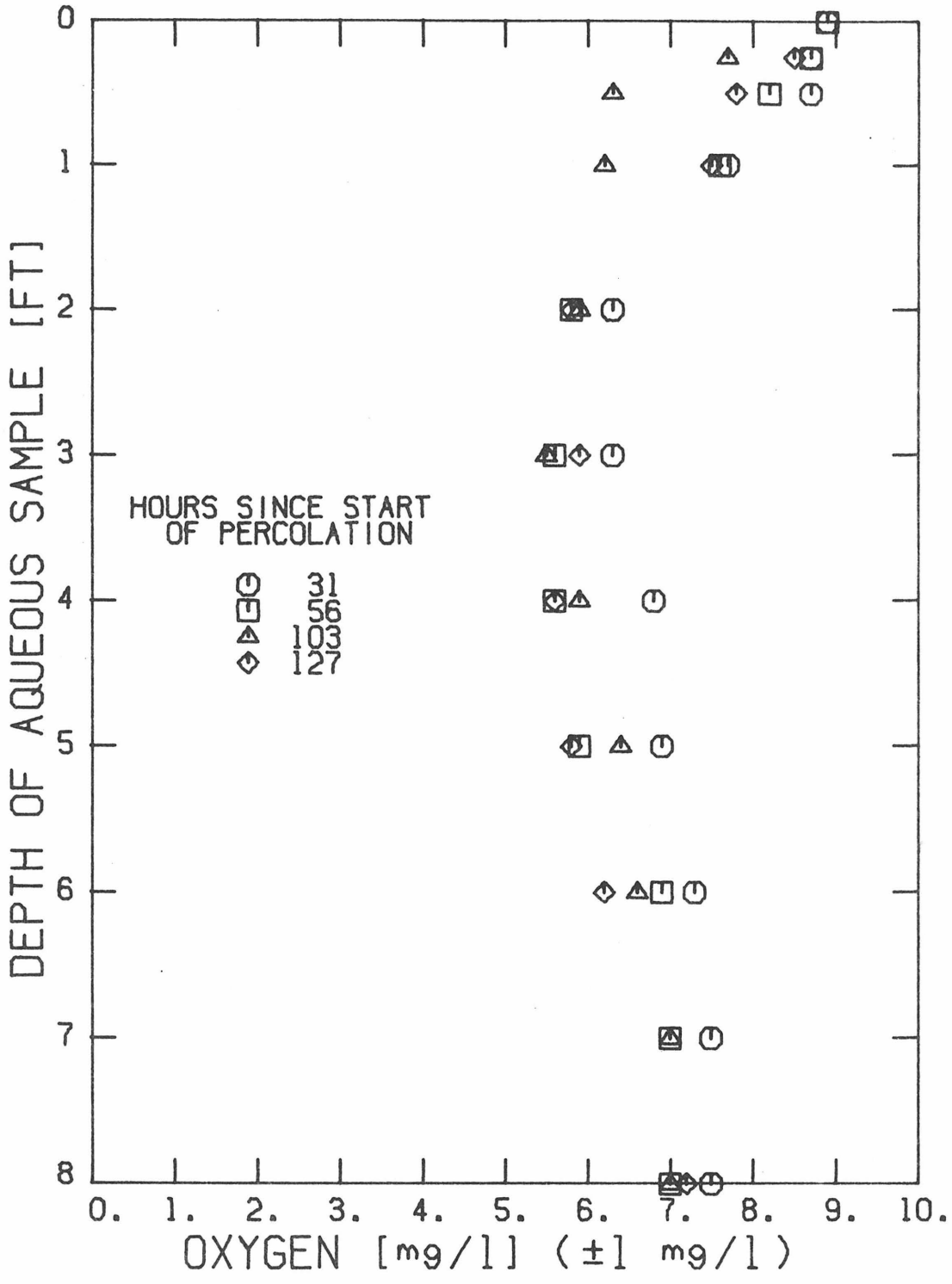

Figure 24: Dissolved Oxygen Content of a 40 mg Ca^{++}/ℓ Containing Solution Percolating through the Laboratory Column

of oxygen throughout the remainder of flow. Sodium ions appeared in the solution (Figure 25) at a rate three times that of the deionized water run (Figure 16). After extensive percolation, the quantity of sodium ions acquired by the calcium salt solution matched that of the deionized water percolation. Calcium ion level of the solution dropped through the breakthrough curve from 40 mg Ca^{++}/ℓ to a quasi-equilibrium value of 29 to 31 mg Ca^{++}/ℓ (Figure 26). Magnesium levels generally rose at some depth through its breakthrough curve from 0 to 7 mg Mg^{++}/ℓ (Figure 27). After extensive percolation, the calcium and magnesium ion breakthrough curves had traveled down and out the column and the quasiequilibrium concentrations of 29.5 ± 0.5 and 7.1 ± 0.3 mg/ℓ, respectively, gave way to the inlet values with a gradual upward movement of concentrations with depth.

One of the more interesting aspects of this run is the variation of aqueous magnesium and calcium content of the percolating solution. Aqueous calcium and magnesium ions are coupled in ion exchange. The sum of equivalents per liter of aqueous calcium and magnesium ion levels is, to within ten per cent, a constant throughout the column. The complete variation of the concentrations of aqueous calcium and magnesium of the percolating calcium chloride solution can be described by considering a mass balance for both species and making certain assumptions. Neglect any radial distribution in the column by considering only the average concentration taken radially through the solution. An effective diffusivity coefficient will account for axial molecular diffusion and dispersion. The effective porosity will be assumed to equate superficial fluid velocity with its average linear velocity.

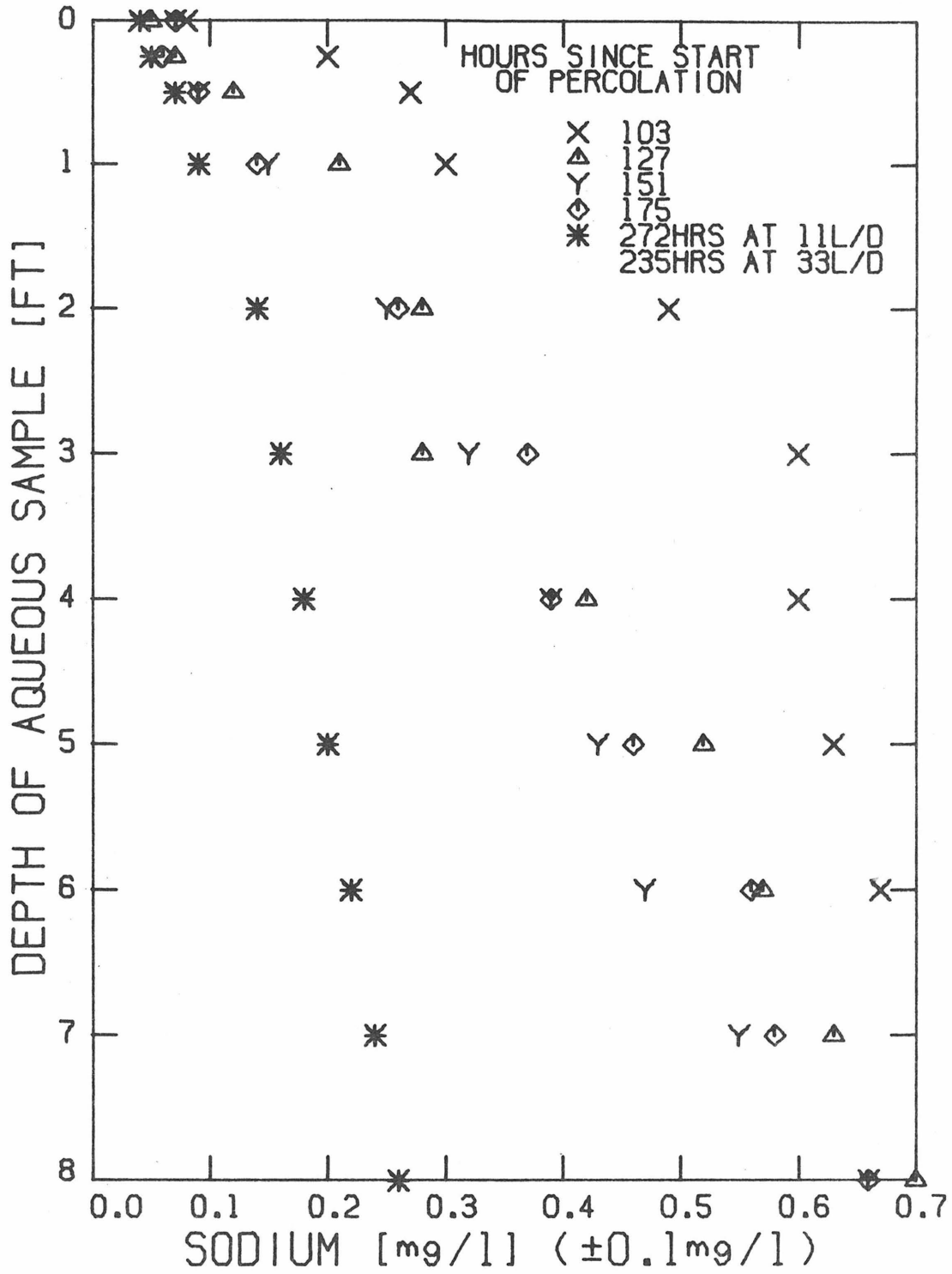

Figure 25: Aqueous Sodium Ion Content of a 40 mg Ca^{++}/ℓ Containing Inlet Solution Percolating through the Laboratory Column

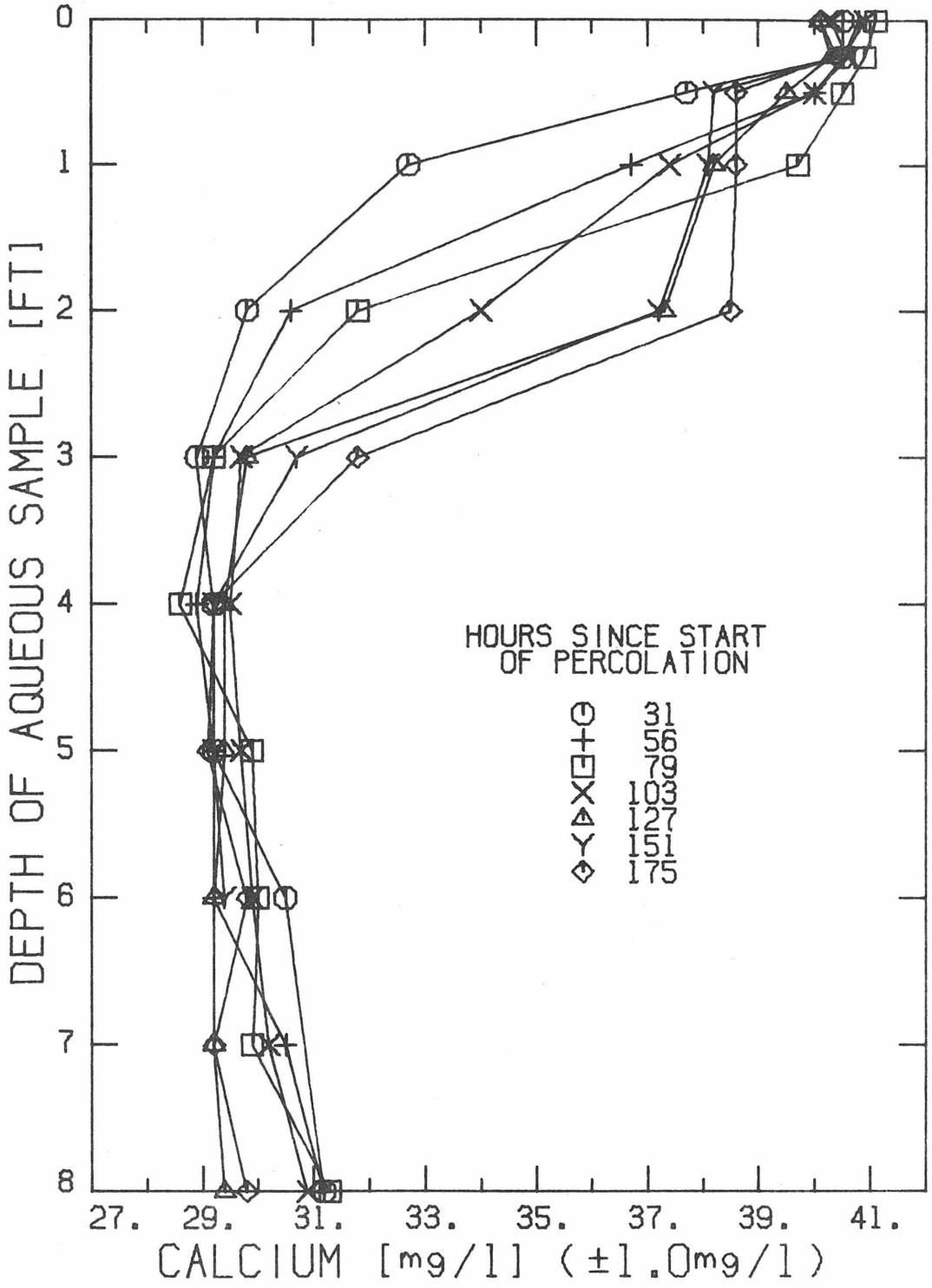

Figure 26: Aqueous Calcium Ion Content of a 40 mg Ca^{++}/ℓ Containing Inlet Solution Percolating through the Laboratory Column

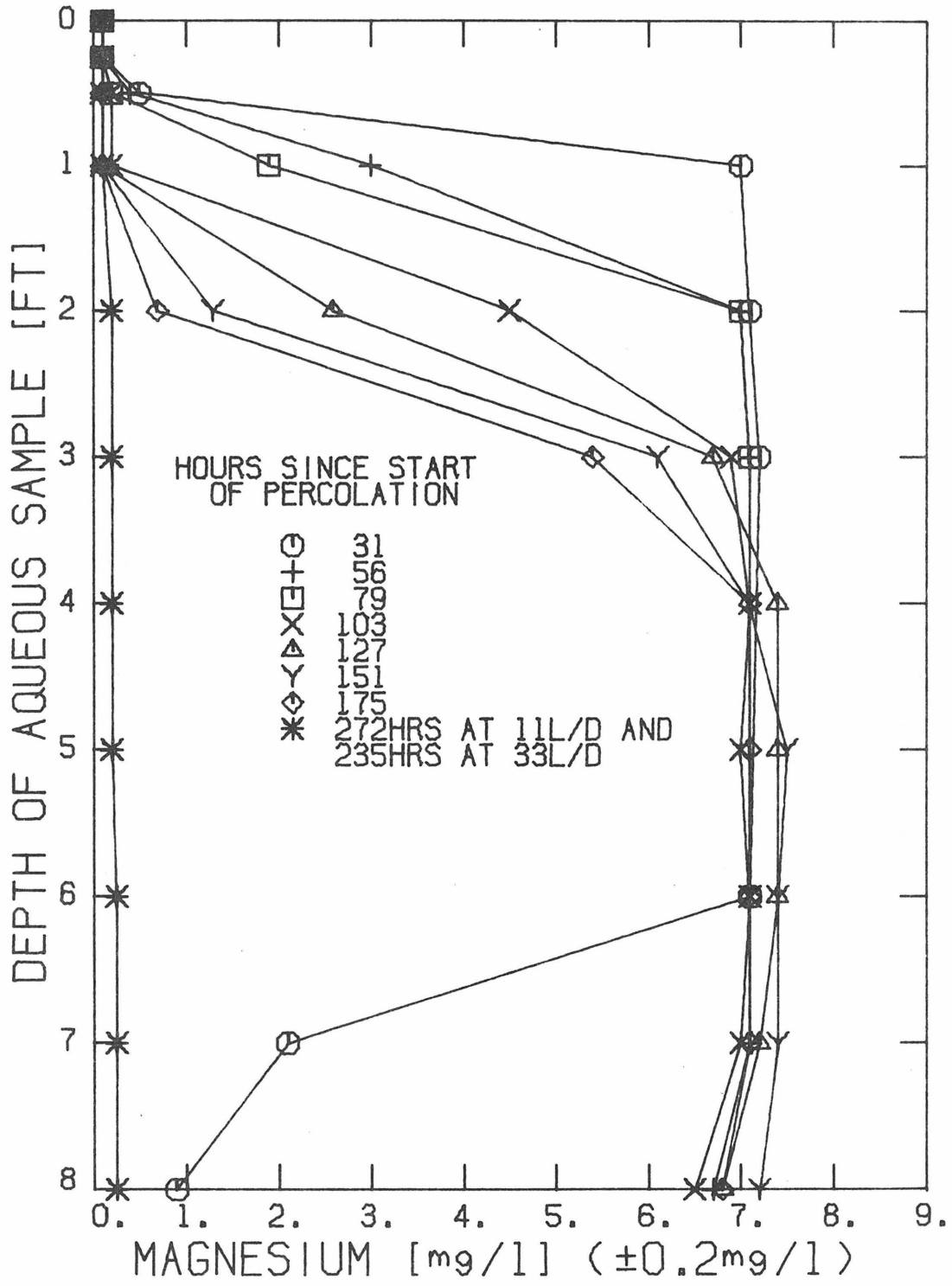

Figure 27: Aqueous Magnesium Ion Content of a 40 mg Ca^{++}/ℓ Containing Inlet Solution Percolating through the Laboratory Column

The differential mass balance for the aqueous phase calcium ion is

$$-\frac{u}{P_E}\frac{\partial Ca}{\partial z} + D_E\frac{\partial^2 Ca}{\partial z^2} = \frac{\partial Ca}{\partial t} - R_{d,Ca} - R_{i,Ca} \qquad (13)$$

Dissolution of any solid phase will be assumed to take place well below saturation and therefore the rate of production of aqueous calcium ions will not be a function of the concentration of aqueous calcium but rather constant

$$R_{d,Ca} = \frac{1 - P_L}{P_E} S_s d_{Ca} \qquad (14)$$

where d_{Ca} is the dissolution constant, S_s is the surface area, and P_L and P_E are porosities. The most prominent ion exchange reaction is,

$$Ca^{++}(aq) + \overline{Mg} \underset{k_2}{\overset{k_1}{\rightleftharpoons}} \overline{Ca} + Mg^{++}(aq) \; . \qquad (15)$$

If the reaction itself controls the overall rate of mass transfer, the production of aqueous calcium ions will be governed by the rate expression,

$$-R_{i,Ca} = k_1 \, Ca \, x_{Mg} - k_2 \, Mg \, x_{Ca} = \frac{\partial x_{Ca}}{\partial t} \; . \qquad (16)$$

A similar set of equations then exists for the magnesium ion.

A steady state situation is one in which aqueous species at a fixed depth are constant of time and in equilibrium with the solid cation exchangers. The steady state expression for equation (13) is

$$-\frac{u}{P_E}\frac{dCa}{dz} + D_E\frac{d^2 Ca}{dz^2} = -R_{d,Ca} \; . \qquad (17)$$

If an inlet solution contains only salts of calcium and magnesium of respective concentrations Ca_I and Mg_I, the integration of (17) is

$$Ca(z) = Ca_I + \frac{R_{d,Ca} P_E}{u} z \quad . \tag{18}$$

Prior to the present run, the sand had been percolated by deionized water. Since the prevalent cations appearing in solution during that run were calcium and magnesium, then it is reasonable to assume the initial solid cation exchanger of the sand for this run was composed entirely of calcium and magnesium. A distribution coefficient will be assumed constant and defined by

$$K_{eq} = \frac{Mg\ x_{Ca}}{x_{Mg}\ Ca} \quad . \tag{19}$$

During the deionized water run when a small quantity of aqueous calcium and magnesium (Ca_I and Mg_I) was percolated through the column, the equilibrium solid cation exchange ratio at various depths is predictable by use of the distribution coefficient and equation (18),

$$x_{Ca}/x_{Mg}]_0 = 0.608\ K_{eq} \frac{Ca_I + \frac{R_{d,Ca} P_E}{u} z}{Mg_I + \frac{R_{d,Mg} P_E}{u} z} \quad . \tag{20}$$

Electroneutrality of the aqueous phase of the present run will be maintained, therefore,

$$20\left(Mg_{II} - Mg + \frac{R_{d,Mg} P_E\ z}{u}\right) = 12.2\left(Ca - Ca_{II} - \frac{R_{d,Ca} P_E\ z}{u}\right) \quad . \tag{21}$$

A newly infiltrating solution of salt concentration Ca_{II} amd Mg_{II} percolating down through the column will eventually have changed its aqueous cationic ratios until they are in equilibrium with the solid cation exchange ratio $x_{Ca}/x_{Mg}]_0$ given by equation (20). This

quasiequilibrium solution, existing below the breakthrough curve, will have a calcium concentration as defined by (19), (20), and (21) to be

$$Ca_{quasi}(z) = \frac{1.64\left(Mg_{II} + \frac{R_{d,Mg}P_E z}{u}\right) + Ca_{II} + \frac{R_{d,Ca}P_E a}{u}}{1 + 1.64\,\frac{\left(Mg_I + \frac{R_{d,Mg}P_E z}{u}\right)}{\left(Ca_I + \frac{R_{d,Ca}P_E z}{u}\right)}} \qquad (22)$$

$Mg_{quasi}(z)$ is found by use of equation (19). Equation (22) predicts for this run a Ca_{quasi}(8 feet) of 30 mg Ca^{++}/ℓ which is in good agreement with the actual value of 30.4 ± 0.7 mg Ca^{++}/ℓ.

Prediction of the unsteady state variation of aqueous calcium and magnesium ion concentrations in the percolating solution requires the use of equations (13) and (16) as well as similar differential mass balances for magnesium. These equations cannot be solved analytically. The result of the numerical solution (Appendix C), as represented in Figure (28), shows 24-hour interval profiles of the aqueous concentrations of the percolating solution at various depths in the column. The initial calcium ion concentration falls from its inlet value through the breakthrough curve to some quasiequilibrium value along the line AA' which is also defined by equation (22). The large inflection below the quasiequilibrium values represents the interface between the newly infiltrating 40 mg Ca^{++}/ℓ and the deionized water that was previously occupying the column. By the eighth day the calcium breakthrough curve has reached the three-foot depth. Calcium ion concentrations in the percolating solution above that breakthrough curve are represented by equation (18). As for the magnesium ion concentrations, the first day profile shows the inlet concentration of magnesium rise through

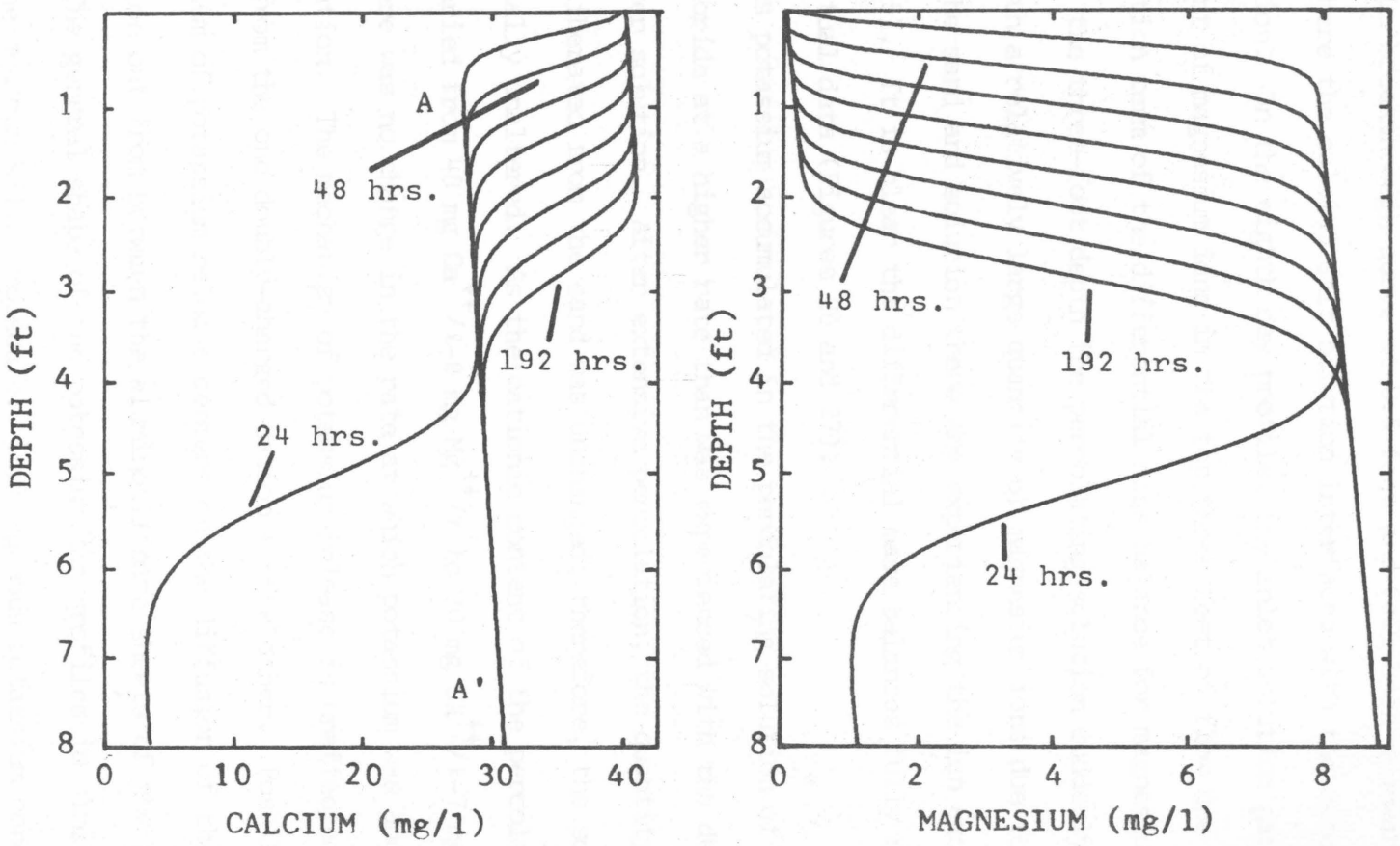

Figure 28: Theoretical Aqueous Calcium and Magnesium Ion Content of a 40 mg Ca^{++}/ℓ Containing Inlet Solution Percolating through an Ion Exchanging with a Column of Sand

the magnesium breakthrough curve at 0.5 feet and fall back downward at five feet where the calcium salt solution interfaces with the deionized water solution. On the eighth day profile, the inlet solution gains a slight amount of magnesium ions in the top three feet of flow due to the dissolution term of the differential mass balance for magnesium. However, at the three-foot depth the percolating solution suddenly is supplied with a relatively large quantity of magnesium ions due to the fact that the sand and solution there are experiencing the ion exchange reaction (15). It is clear the differential mass balances fully represent the actual data (Figures 26 and 27).

Aqueous potassium accumulated in the percolating solution of calcium chloride at a higher rate than was experienced with the deionized water solution. After extensive percolation, the quantity of potassium liberated from the sand was unchanged; therefore, the source was essentially unaltered. As the cationic content of the percolating solution varied from 40 mg Ca^{++}/ℓ-0 mg Mg^{++}/ℓ to 30 mg Ca^{++}/ℓ-7 mg Mg^{++}/ℓ, there was no change in the rate at which potassium was added to the solution. The mechanism of potassium release is unaffected by variation from the one doubly-charged cation to the other. Possibly the mechanism of potassium release centers on the diffusion of the potassium ion out from between the aluminosilicate sheets of the biotite crystal. The general shape of the potassium ion profiles is similar to those of the aqueous silica molecule. Such aqueous potassium concentration profiles could be modeled if it were assumed that the rate controlling step of the transfer of potassium ions from the interior of the biotite crystal to the percolating solution was the internal

diffusion of the potassium ion. If this were the case, then

$$[K](z) = [K]_{eq} (1 - \exp(-A\, z/ul)) \tag{23}$$

where $[K]_{eq}$ = equilibrium concentration of potassium inside the biotite crystal

l = distance between ion exchange site and opening of the sheet.

Suppose the reaction step is

$$M_{in}^{++}(aq) + 2K_{in} \underset{k_2}{\overset{k_1}{\rightleftharpoons}} M_{in} + 2K_{in}^{+}(aq) \tag{24}$$

where $M_{in}^{++}(aq)$ is the aqueous calcium or magnesium concentration at the reaction site. Since an equilibrium coefficient is assumed of the form,

$$K_{eq} = \frac{[K_{in}]^2 x_M}{[M_{in}]\, x_K} \tag{25}$$

then

$$[K]_{eq} = \frac{K_{eq}[M_{in}]}{x_M} x_K \tag{26}$$

This implies that

$$\frac{d[K](z)}{dz} \propto [M_{in}] \tag{27}$$

The concentration of calcium and magnesium ions in the deionized water was approximately 0.10 mM between the five and eight-foot depths where potassium ions were being released at 4.1×10^{-6} mg K^+/gm·hr. The quantity of calcium and magnesium ions in the present run was 1 mM. If indeed the overall rate is controlled by the diffusion of the potassium ion out from between the aluminosilicate sheet of biotite, then the

internal concentration of aqueous calcium and magnesium ions will be 1 mM. The rate of release should, therefore, be 1.3×10^{-5} mg K^+/gm·hr; it actually was 8.6×10^{-6} mg K^+/gm·hr.

Aqueous sodium ions initially were released by the minerals of the sand at triple the rate of the deionized water run. However, after extensive percolation of the 40 mg Ca^{++}/ℓ solution the sodium ion release fell back down to that of the deionized water run. Such time-dependent behavior of the aqueous sodium ion profiles can be modeled by a process including ion exchange of aqueous calcium ions for sodium ions with a continuous addition of sodium ions to the percolating solution. After the transient effects of the ion exchange die out, the continual addition of sodium ions remains.

Aqueous hydrogen ions in the percolating solution are susceptible to a large number of effects. Extensive possibilities will not be discussed. The percolating solution should have been totally unbuffered; however, 0.07 mM of phosphate ions were detected in the solution throughout the column. No aqueous carbonate ions were detectable. Acidification of the percolating solution in the top six inches of the column must represent the result of some bacterial activity that consumes oxygen and perhaps utilizes light. After the acidification, the pH of the solution showed a gradual climb from 5.3 to 6.2. Such a climb represents a consumption of 0.004 mM of aqueous hydrogen ions. Constancy of the asymptotic pH value of 6.1 is suggestive that the aqueous hydrogen ion's concentration is governed by ion exchange reactions rather than dissolution reactions.

Dissolution of aluminosilicates proceeded at the same rate

in the 1 mM calcium chloride solution as in a deionized water solution. Exchange of cations of a mineral's interior with aqueous hydrogen ions is the first step of dissolution; breakup of the remaining aluminosilicate superstructure is the final step. The presence of relatively high concentrations of other cations did not speed the degradation of the column's minerals despite the fact that the rate of addition of sodium, potassium, and magnesium to the solution had increased. If the reason for the aqueous silica concentration's leveling below 2 mg SiO_2/ℓ is due to the formation of a second solid phase containing silica, that second phase cannot be a magnesium or calcium-containing clay or else the equilibrium concentration of silica would have been dropped by the high concentrations of calcium of this run.

Cation exchange, even on sand grains 0.05 cm in diameter, is extensive. The duration of the transient cation exchange reactions is directly proportional to the total capacity of the medium to hold adsorbed cations. Considering the siltiness of the soil of the Whittier Narrows test plot, transient cation exchange would be of long duration. By the end of this run, cation exchange reactions involving weakly held ions have been giving way to mineral dissolution as the main continuing cause of addition of aqueous cations to the percolating solution. The minimum rate of addition of sodium and of magnesium ions was respectively 1.6×10^{-6} and 1.3×10^{-6} mg/gm·hr. Rate of release of aqueous silica by dissolution is a constant of the ionic strength of the percolating solution up to at least 3 mM. All the data of this run exhibited consistent results with data of the preliminary investigation.

Higher Rate Percolation

Certain mass transfer steps of solid-liquid reactions can be discounted as rate determining steps by observations of the effects of an increased flow rate of solution. If mass transfer of ions from a mineral is controlled by reaction or internal diffusion of ions, then a threefold increase of flow rate will leave the overall rate unchanged. If external diffusion controls, an increase of Reynold's number will tend to improve mass transport by external diffusion and increase the overall rate of dissolution or ion exchange.

To test mass transfer, the sand experiencing 197 hours of flow at 11.1 ℓ/day with 40 mg Ca^{++}/ℓ was suddenly subjected to 36 ± 6 ℓ/day flow of the same solution. During the 233 hours of the run, four sets of depth samples were taken from the column's percolating solution and analyzed.

The aqueous calcium and magnesium profiles, as before, were time-dependent (Figures 29 and 30). Furthermore, the rate at which the breakthrough curves traveled the length of the column was tripled. The travel rate is the rate of re-equilibration of the solid cation exchange ratios with the inlet solution. Because the rate of flow was three times faster, the solid cation exchange ratios were forced to equilibrate three times faster. The behavior of these two aqueous species can be modeled merely by changing the fluid velocity used in the solution of equation (13).

Dissolution of the column's aluminosilicate minerals proceeded at the same rate as when percolation was slower. Such a response corroborates the theory that either the mineral dissolution reaction step or

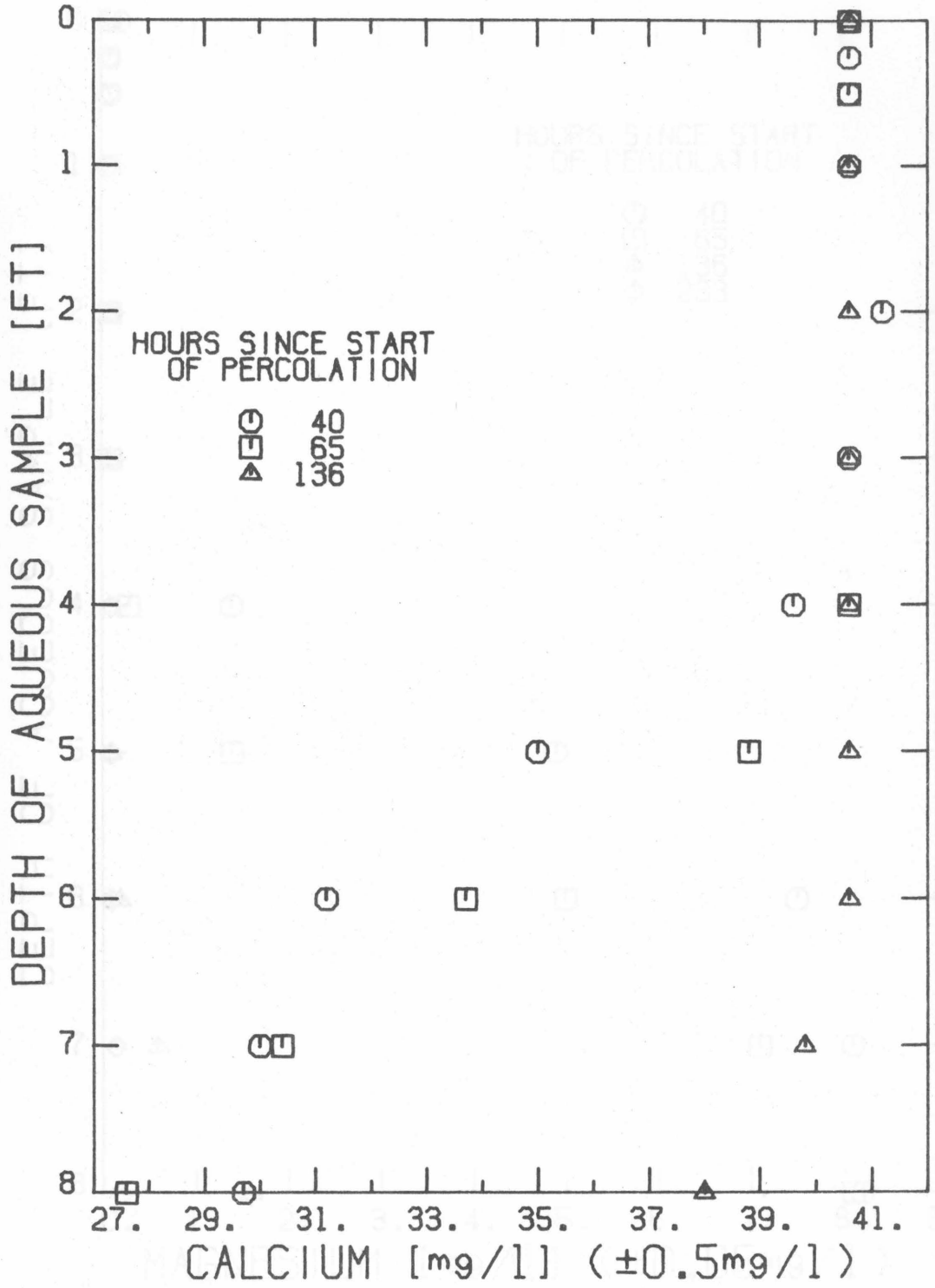

Figure 29: Aqueous Calcium Ion Content of a 40 mg Ca^{++}/ℓ Containing Inlet Solution Percolating at 36 ℓ/day through the Laboratory Column

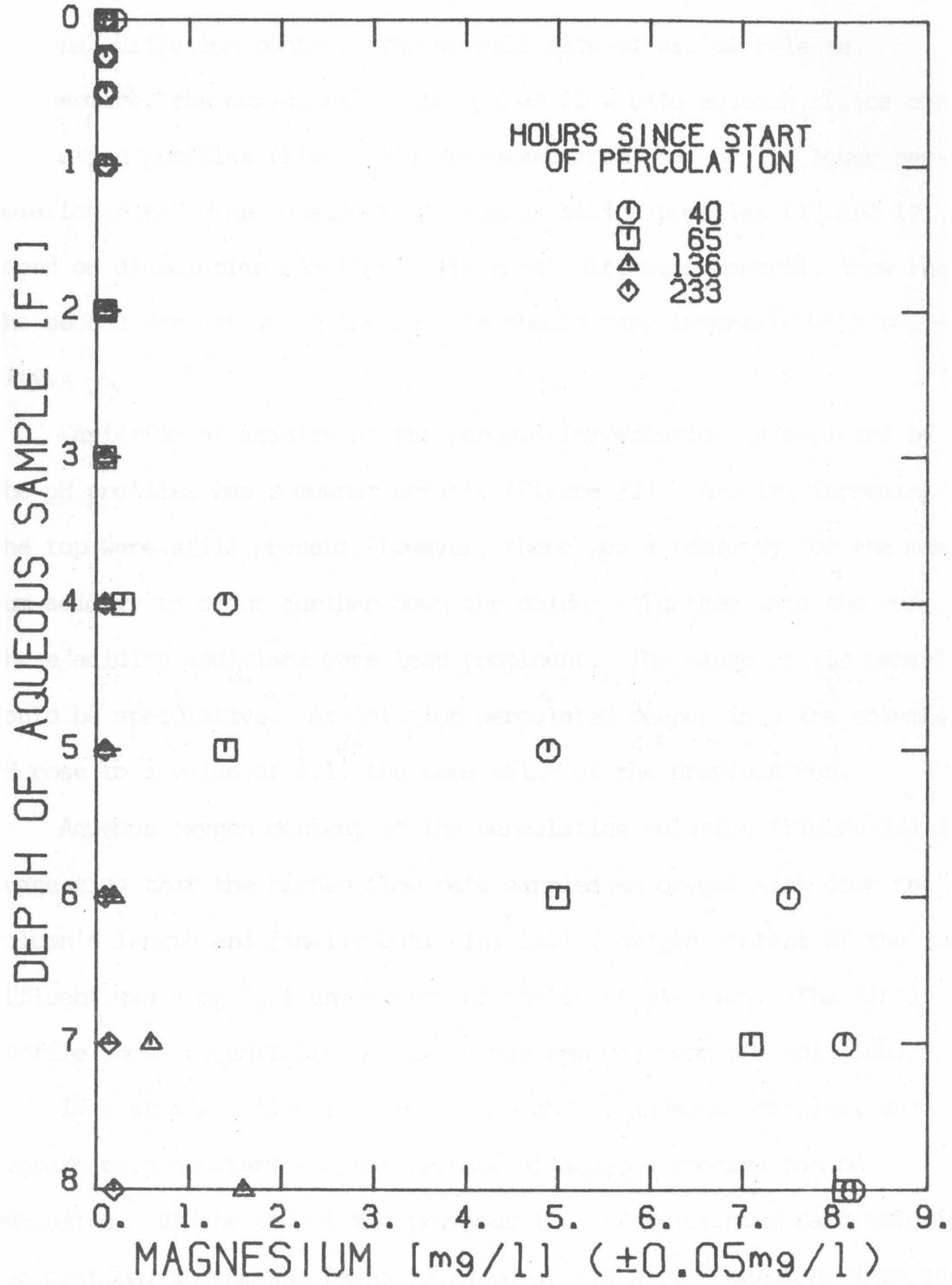

Figure 30: Aqueous Magnesium Ion Content of a 40 mg Ca^{++}/ℓ Containing Inlet Solution Percolating at 36 ℓ/day through the Laboratory Column

internal diffusion controls the overall rate of silica release. Furthermore, the curvature of the higher flow rate aqueous silica concentration profiles (Figure 31) decreases from that of the lower percolation rate. The equations of aqueous silica profiles (10 and 12), based on dissolution reaction or internal diffusion control, show that the second derivative of the profile should vary inversely with velocity.

Variation of acidity of the percolating solution as depicted by the pH profiles was somewhat erratic (Figure 32). Acidity increases at the top were still present; however, there was a tendency for the maximum acidity to occur further down the column. Further into the run these acidity additions were less prominent. The cause of the behavior would be speculative. As solution percolated deeper into the column, pH rose to a value of 6.1, the same value of the previous run.

Aqueous oxygen content of the percolating solution (Figure 33) is suggestive that the higher flow rate carried an oxygen sink down the column's length and finally out. Initially, oxygen content of the effluent was 4 mg O_2/ℓ under that of the inlet solution. The final profile shows essentially no oxygen was removed from the solution.

If a straight line is forced through the aqueous profiles, an average rate constant for the release of aqueous species can be evaluated. By the end of the previous 11.1 ℓ/day calcium salt solution percolation, sodium was being released at 4.6×10^{-6} mg/gm·hr into the solution (Figure 25). At the start of the 36 ℓ/day run its rate was 8.9×10^{-6} mg/gm·hr (Figure 34). This increase of 70 per cent can be associated with the ion exchange portion of the sodium release process.

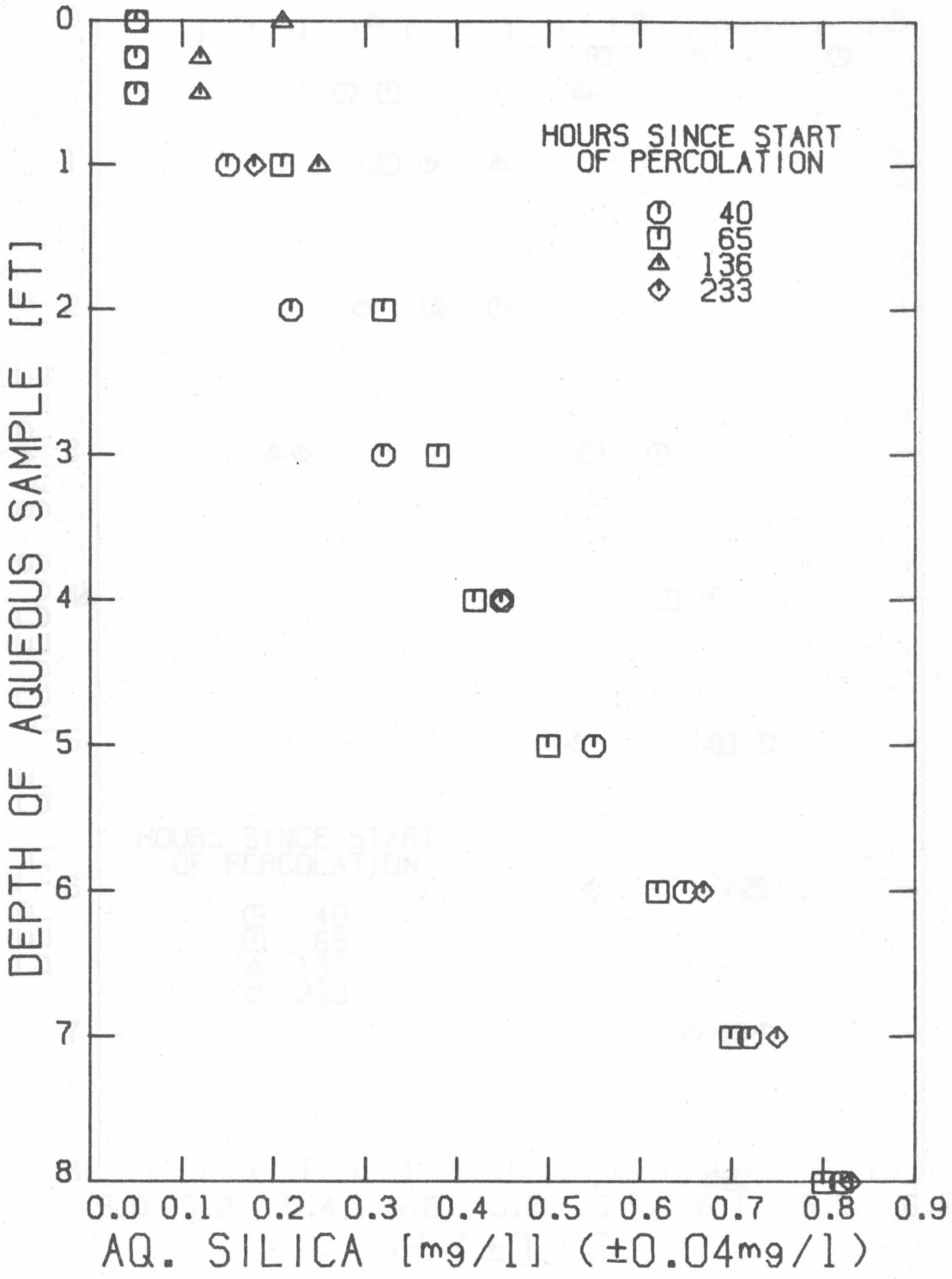

Figure 31: Aqueous Silica Content of a 40 mg Ca^{++}/ℓ Containing Inlet Solution Percolating at 36 ℓ/day through the Laboratory Column

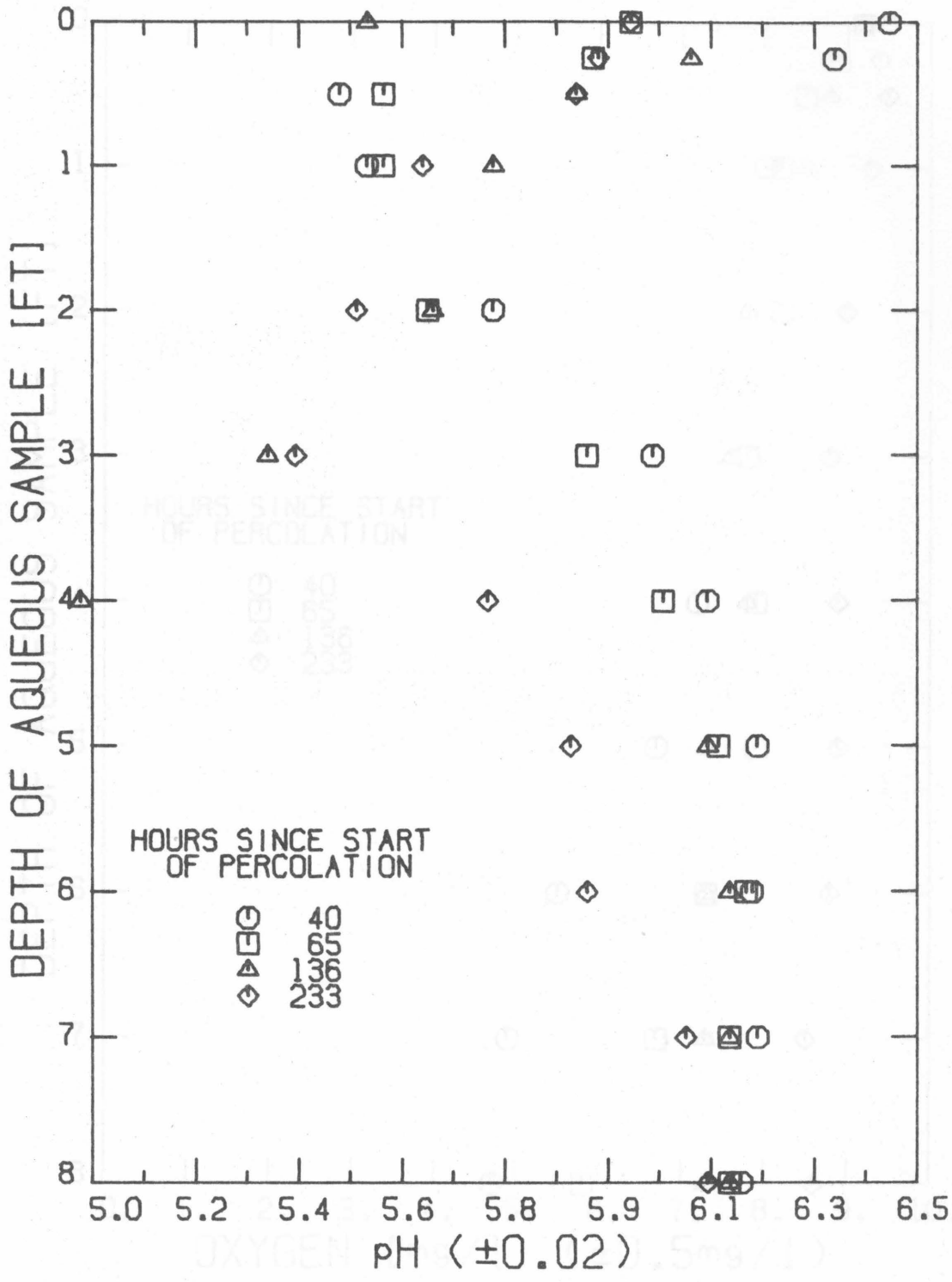

Figure 32: pH of a 40 mg Ca^{++}/ℓ Containing Inlet Solution Percolating at 36 ℓ/day through the Laboratory Column

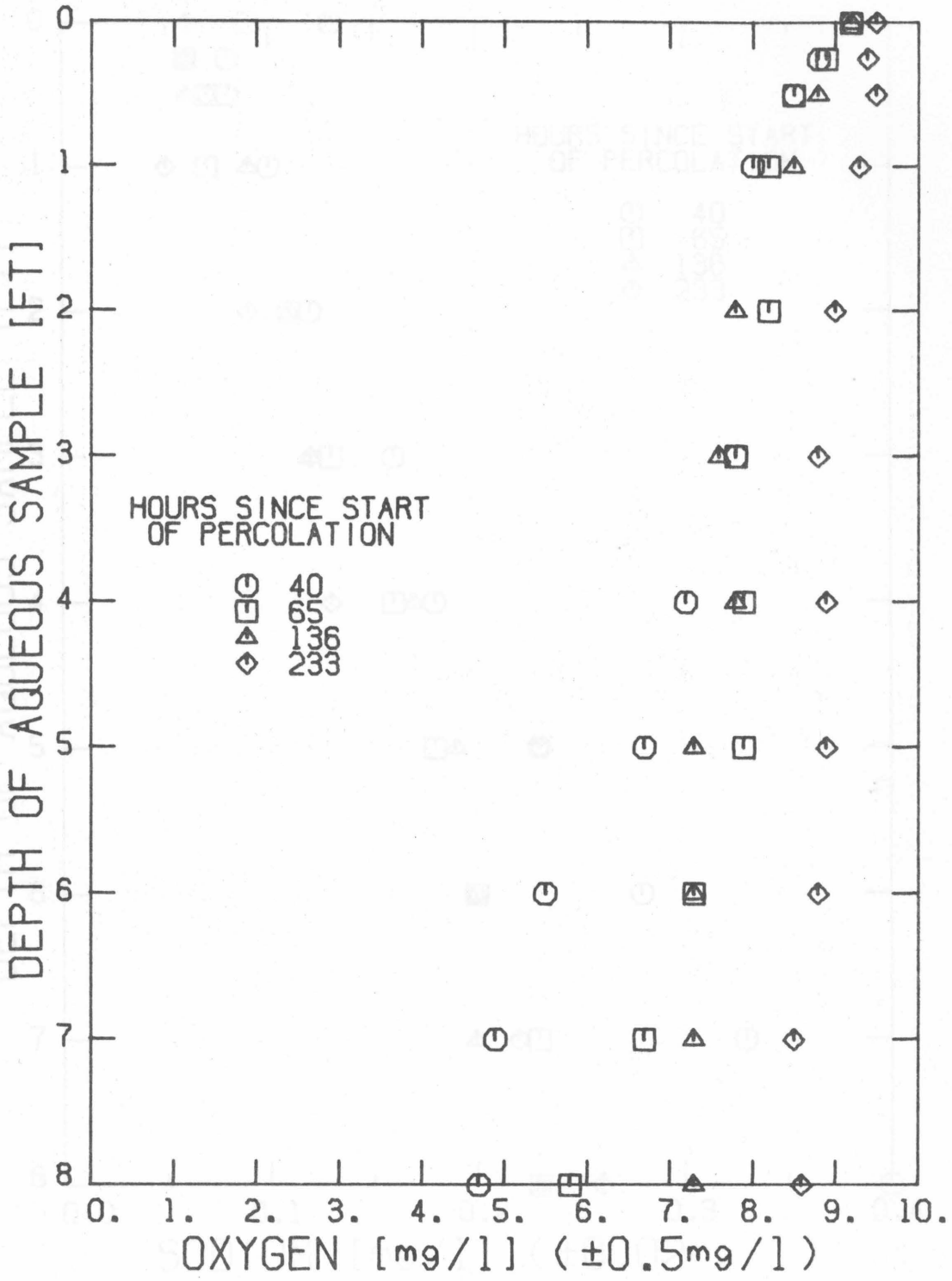

Figure 33: Dissolved Oxygen Content of a 40 mg Ca^{++}/ℓ Solution Percolating at 36 ℓ/day through the Laboratory Column

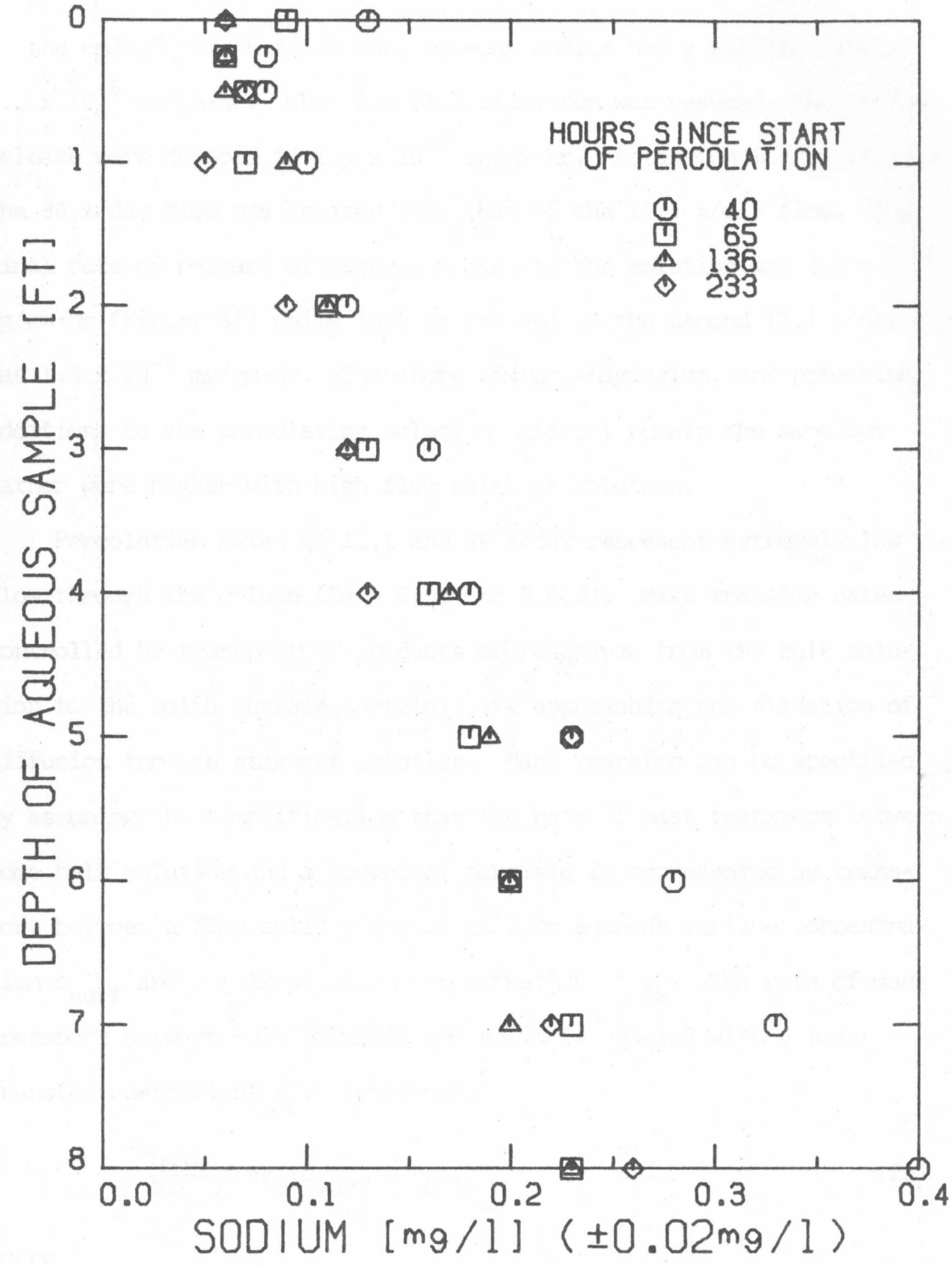

Figure 34: Aqueous Sodium Ion Content of a 40 mg Ca^{++}/ℓ Inlet Solution Percolating at 36 ℓ/day through the Laboratory Column

At the end of the 36 ℓ/day run, aqueous sodium had a release rate of 3.2×10^{-6} mg/gm·hr. When the 11.1 ℓ/day run was resumed, the sodium release rate dropped to 1.4×10^{-6} mg/gm·hr. Potassium ion release in the 36 ℓ/day flow was greater than that of the 11.1 ℓ/day flow. The final rate of release of magnesium ions to the solution was 2.9×10^{-6} mg/gm·hr (Figure 35) while that at the end of the second 11.1 ℓ/day run was 1.3×10^{-6} mg/gm·hr. Therefore sodium, magnesium, and potassium additions to the percolating solutions did not remain the same but rather were higher with high flow rates of solution.

Percolation rates of 11.1 and 36 ℓ/day represent extremely low flow through the column (Re = 0.004 to 0.012). Mass transfer rates controlled by transport of products or reactants from the bulk solution to the solid surface certainly are approaching the situation of diffusion through stagnant solution. Mass transfer can be specified by assuming the simplification that the rate of mass transport between some bulk solution and a spherical particle is represented by transport between a flat solid plane of uniform aqueous surface concentration c_{surf} and a bulk solution concentration c_{bulk}. The rate of mass transport between bulk solution and solid is equated with a mass transfer coefficient k_c. Therefore,

$$\frac{\partial c_{bulk}}{\partial t} = a k_c (c_{surf} - c_{bulk}) \qquad (28)$$

where

a = surface area of mass transfer per volume solvent.

As Reynold's number approaches zero for a packed bed of effective porosity P_E the mass transfer coefficient approaches a constant value;

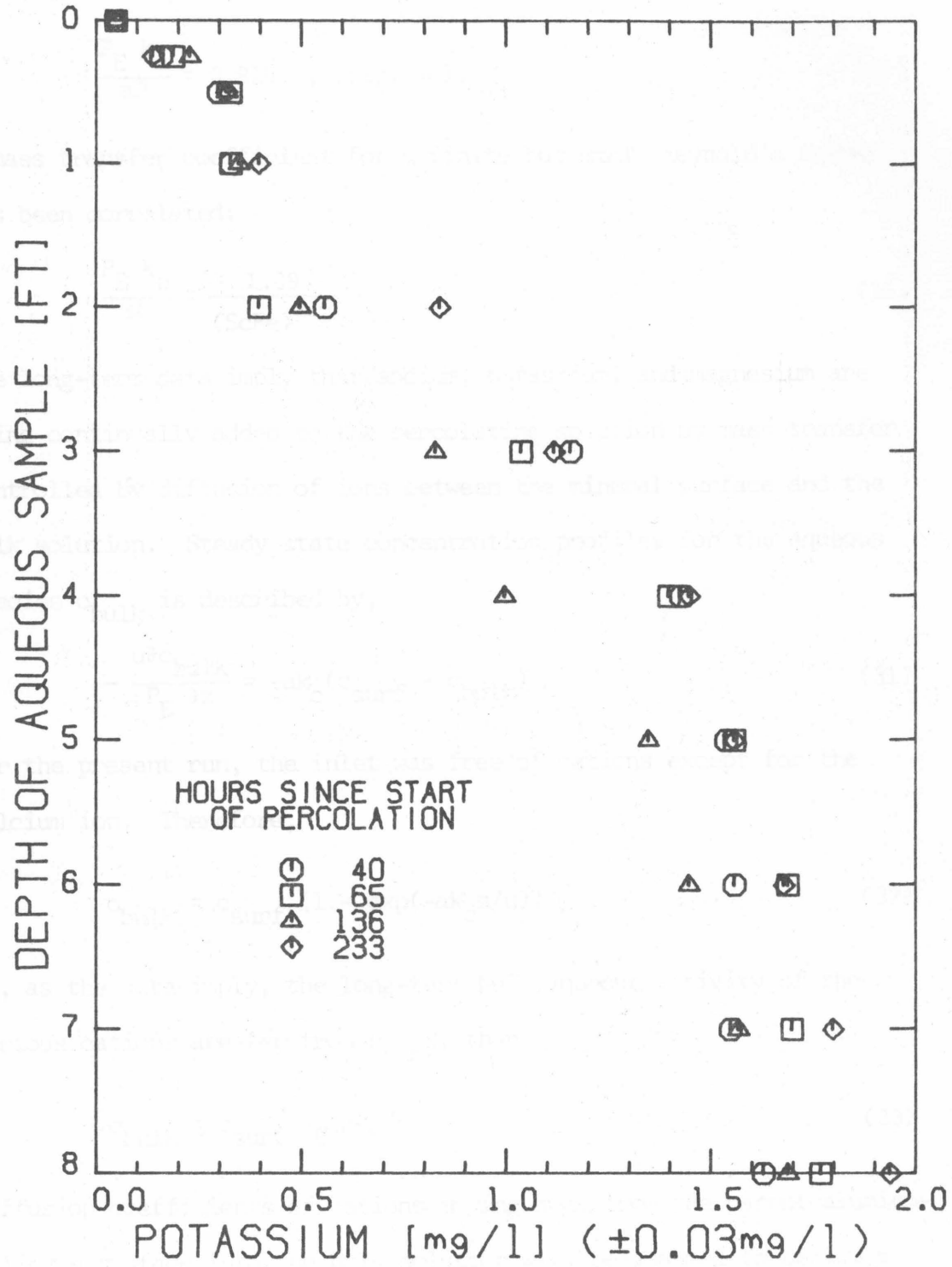

Figure 35: Aqueous Potassium Ion Content of a 40 mg Ca^{++}/ℓ Containing Inlet Solution Percolating at 36 ℓ/day through the Laboratory Column

$$\frac{P_E\, k_c}{aD} = 0.914 \quad , \text{(Yip, 40)}. \tag{29}$$

A mass transfer coefficient for a finite but small Reynold's number has been correlated;

$$\frac{P_E\, k_c}{aD} = \frac{1.09}{(ScRe)^{2/3}} \, . \tag{30}$$

The long-term data imply that sodium, potassium, and magnesium are being continually added to the percolating solution by mass transfer controlled by diffusion of ions between the mineral surface and the bulk solution. Steady state concentration profiles for the aqueous species c_{bulk} is described by,

$$-\frac{u\partial c_{bulk}}{P_E\, \partial z} = -ak_c(c_{surf} - c_{bulk}) \, . \tag{31}$$

For the present run, the inlet was free of cations except for the calcium ion. Therefore,

$$c_{bulk} = c_{surf}\,(1 - \exp(-ak_c z/u)) \, . \tag{32}$$

If, as the data imply, the long-term bulk aqueous activity of the various cations are far from c_{surf}, then

$$c_{bulk} = c_{surf}\, P_E\, ak_c/u \quad . \tag{33}$$

Diffusion coefficients of cations moving away from the parent aluminosilicate surface into the bulk solution will be assumed to be 1.5×10^{-5} cm^2/sec (Harned et al., 21,25,42). For the two flow rates 11.1 and 36 ℓ/day, the Peclet number (ScRe) is 2.4 and 7.1, respectively. The k_c values are then 4.5×10^{-3} and 6.4×10^{-3} $mg/(cm^2 \cdot hr \cdot mg/\ell)$,

respectively. If the minimum surface area is assumed as being one in which the particles are nonporous spheres, then ak_c/u will have a value greater than 20000 ft^{-1}. Therefore, external mass transfer by diffusion of chemical species from the bulk solution to the surface of the mineral is essentially infinitely fast and thus either reaction or internal diffusion control the overall rate of mass transfer.

Percolation of Lithium and Ammonium Salt-Containing Solutions

Particular attention must be directed at determining the rate at which aqueous calcium ions are released by the column's minerals in dissolution. For a period of one month the laboratory column was operated on an intermittent schedule with solution devoid of calcium salts. Magnesium chloride was used to adjust the solution's ionic strength back up to 11 mM. For a period of five months thereafter, a solution of the following composition was percolated intermittently:

2.43 mM LiCl

4.12 mM $LiHCO_3$

0.49 mM $(NH_4)_2SO_4$

Because the percolating solution was free of aqueous sodium, magnesium, potassium, and calcium, addition of small amounts of the same cations to the percolating solution was readily apparent. Solution samplings were taken periodically for five months. Final data collected showed the variation of aqueous calcium, magnesium, sodium, potassium, and silica in the percolating solution at different solution flow rates.

Throughout the study, magnesium content of the percolating solution dropped gradually from an outlet concentration of 3.5 to 1.5 mg/ℓ

(Figure 36). However, two years previously an effluent magnesium concentration of 0.2 mg/ℓ was attained after extensive percolation of 40 mg Ca^{++}/ℓ solution. Other aqueous cation profiles did not show sustained changes with time and are assumed to represent steady state situations. The outstanding phenomena observed was that despite a 150-fold variation of flow rate, the concentration profiles of all aqueous cations remained unchanged (Figures 37, 38, and 39) even though the level of aqueous silica dropped (Figure 40).

Considering the variation of solution composition in the top three feet of the column, the rate of release of any ion is controlled by chemical reaction or molecular diffusion inside the mineral structure. Aqueous silica was released from the minerals at the same rate no matter what the flow rate was. The variations of aqueous cations with depth are unchanged with flow rate changes. It would appear at first sight that the rate of release of cations from the minerals increases with increasing flow rate. The consistent constancy of concentration profiles, despite wide variations in flow rate, is a hint that a reversible reaction controls the aqueous cationic concentrations. Already it has been shown that ion exchange reactions occur in the column; however, large scale ion exchange reactions can be observed to die out with time (Figure 29). It is proposed that there is a secondary ion exchange reaction which is so fast that even when Reynold's Number of the flow is increased from 0.004 to 0.63, the extent of the ion exchange at each depth is unchanged. Because the concentrations of cations change with depth, the secondary ion exchange reaction must be in local equilibrium with the adsorbed

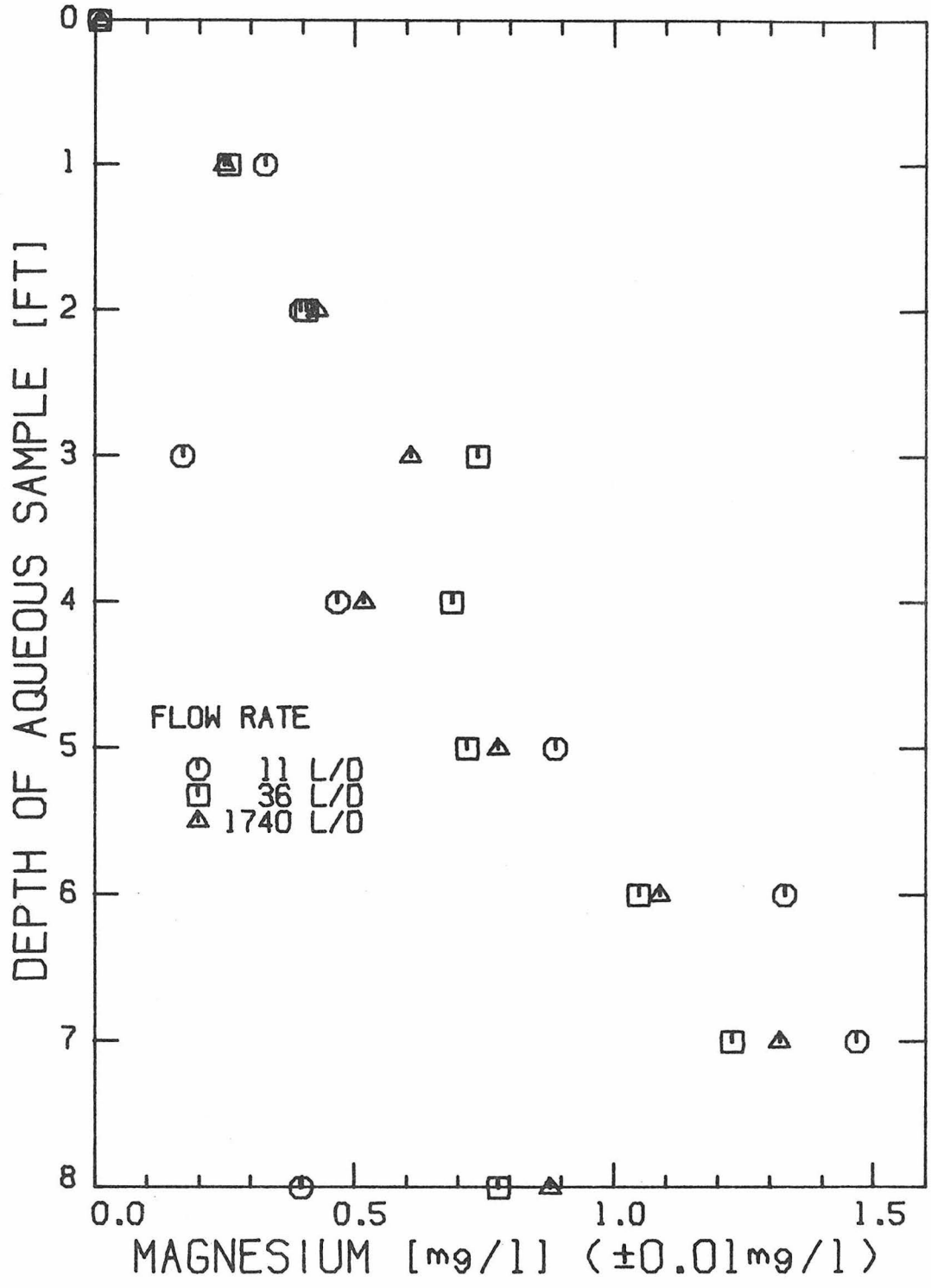

Figure 36: Aqueous Magnesium Ion Content of a Lithium and Ammonium Salt Containing Solution Percolating at Various Rates through the Laboratory Column

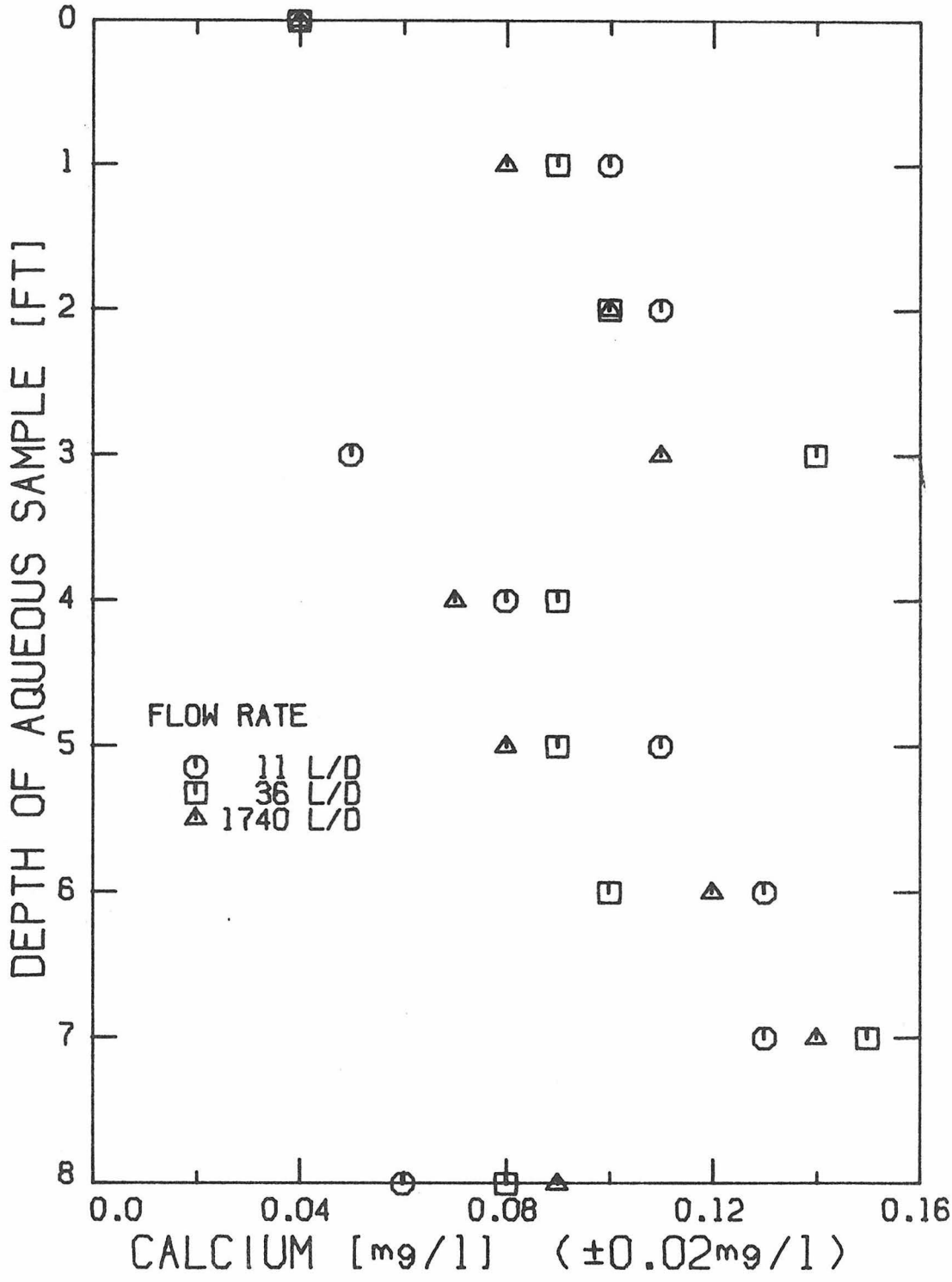

Figure 37: Aqueous Calcium Ion Content of a Lithium and Ammonium Salt Containing Solution Percolating at Various Rates through the Laboratory Column

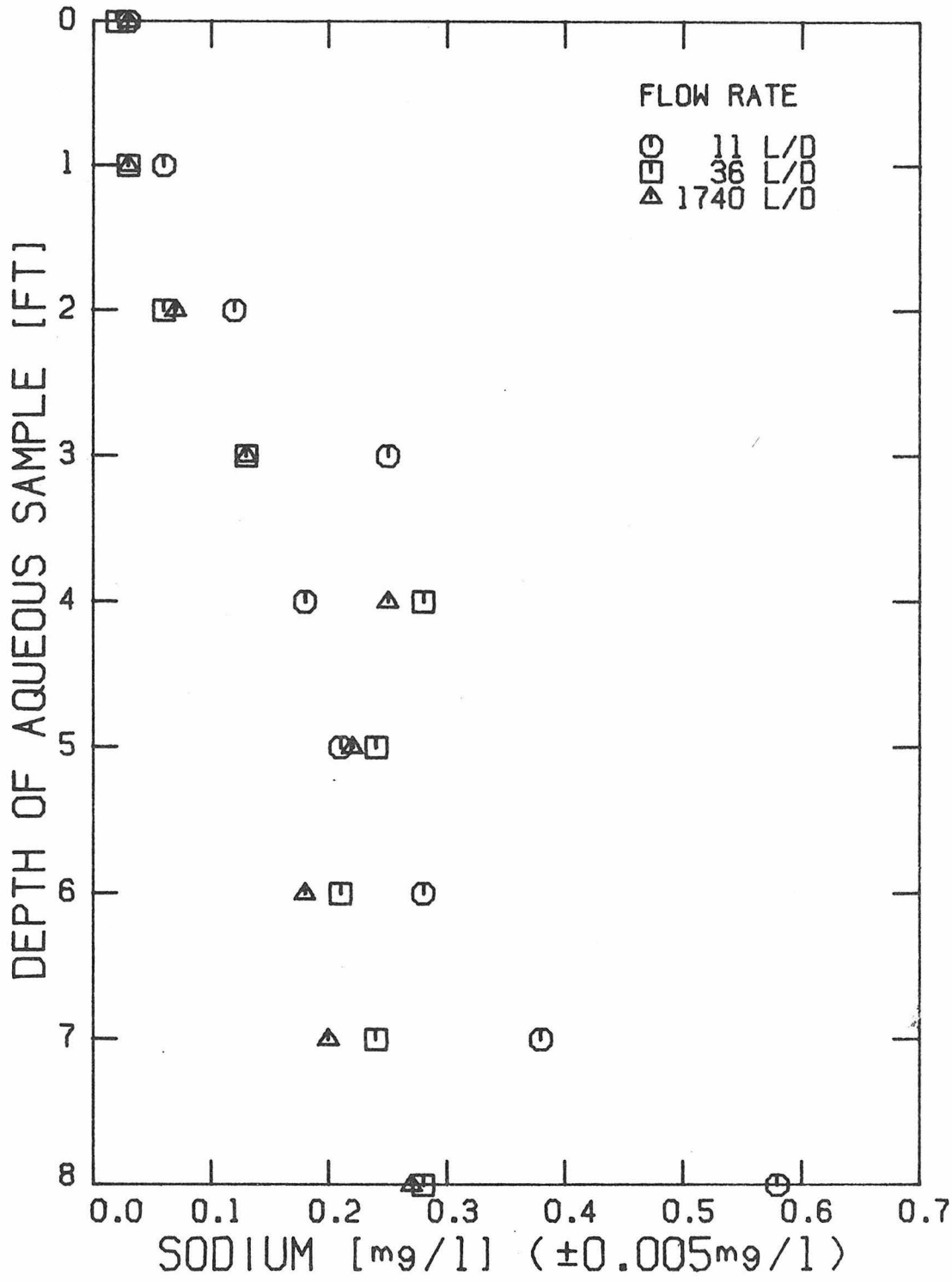

Figure 38: Aqueous Sodium Ion Content of a Lithium and Ammonium Salt Containing Solution Percolating at Various Rates through the Laboratory Column

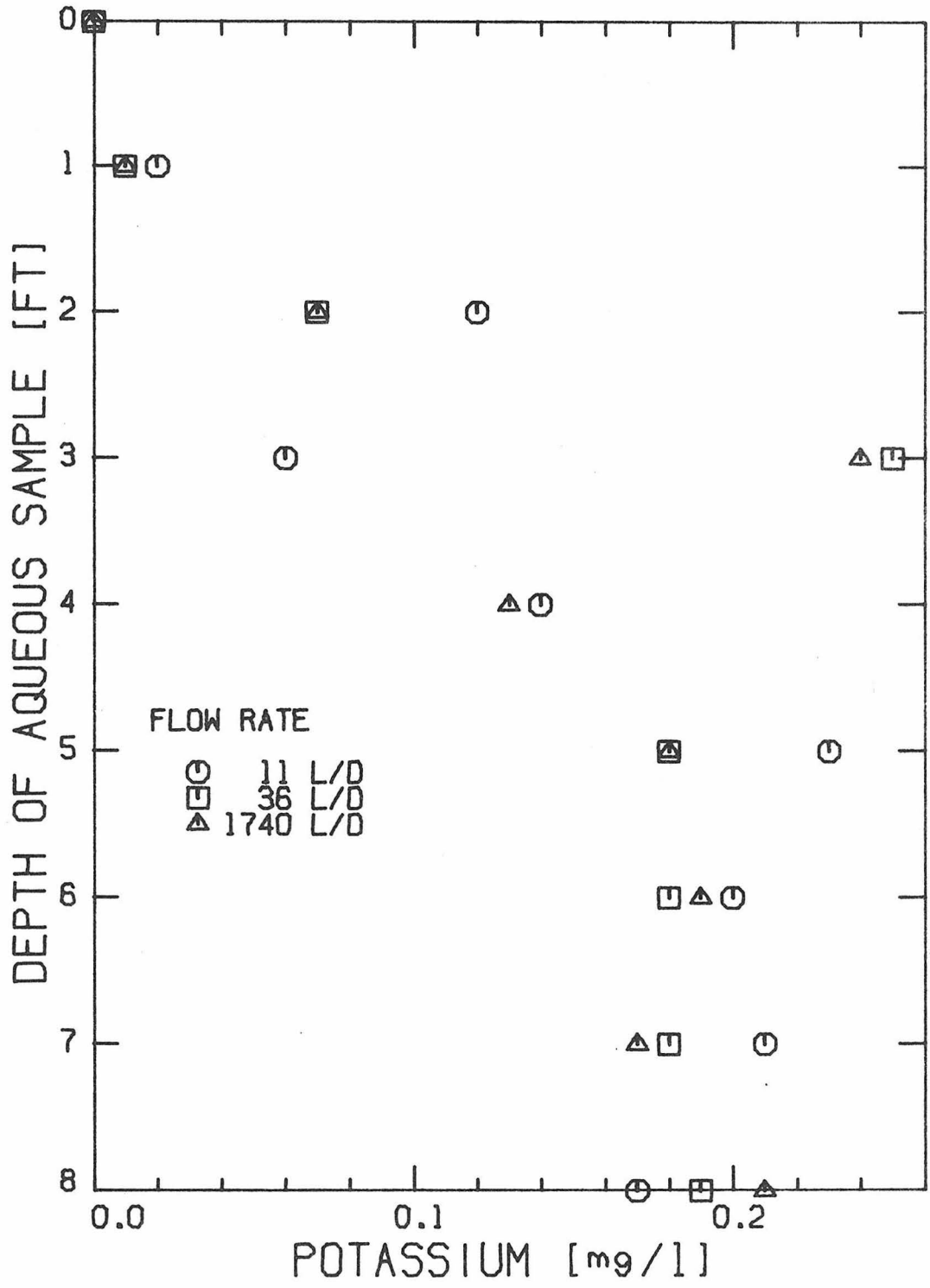

Figure 39: Aqueous Potassium Ion Content of a Lithium and Ammonium Salt Containing Solution Percolating at Various Rates through the Laboratory Column

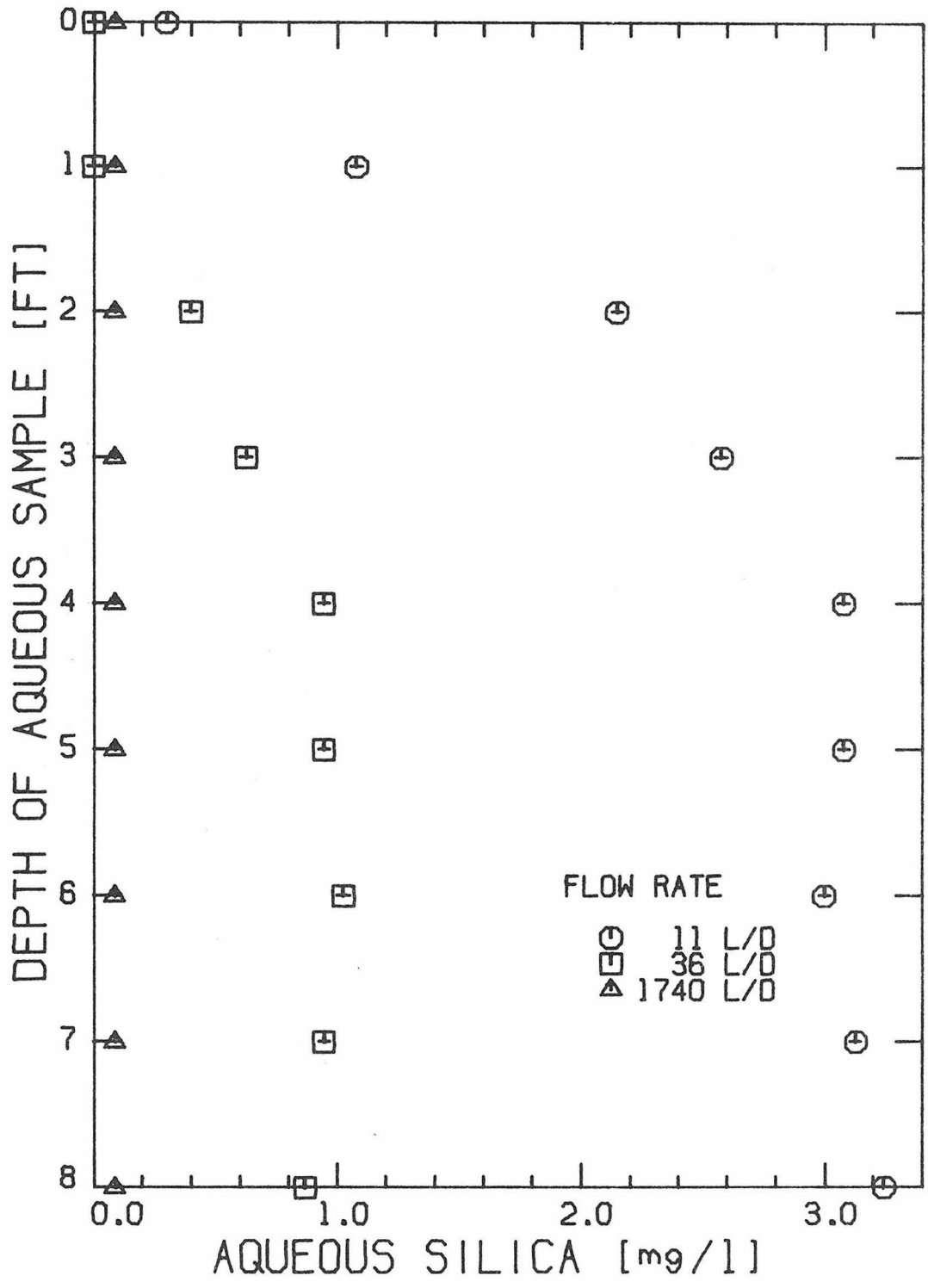

Figure 40: Aqueous Silica Content of a Lithium and Ammonium Salt Containing Solution Percolating at Various Rates through the Laboratory Column

chemical species on the sand at each depth. In general, the ion exchange reaction will be of the form

$$Li^+ + \bar{M} \rightleftharpoons M^+ + \overline{Li} \qquad (34)$$

where $\bar{M}$ is a chemisorbed cation. Primary ion exchange reactions involve electrostatically adsorbed cations. The chemisorbed cation must be part of the structure of the mineral, such as the calcium or sodium of plagioclase. Because, for all purposes, the concentration of the aqueous lithium ion is constant in the solution, the equilibrium expression for the reaction ideally is

$$K = M^+ (\overline{Li}/\bar{M}) \ . \qquad (35)$$

The particular variation of M^+ concentration with depth ideally is directly proportional to $(\bar{M}/\overline{Li})$. If the same percolating solution were sent through the column in the opposite direction, the cation concentrations would initially start at higher values and drop off to lower concentrations in reflection of the variation of $(\bar{M}/\overline{Li})$. The one stumbling block to the acceptance of a secondary ion exchange reaction is that it is always in equilibrium. Equilibrium of one ion exchange reaction would mean that the aqueous phase concentration of cations is always set by that reaction. To bring the theory in tune with all the known data, it must be assumed that when lithium is first brought into contact with the minerals of the column, it first ion exchanges with electrostatically adsorbed cations. During the electrostatic ion exchange reaction, the presence of aqueous lithium ions is unknown to chemisorbed cations until the lithium has exchanged with a majority of

the electrostatically adsorbed cations on the minerals' surfaces. Once the shielding effect of the electrostatically adsorbed cations is gone, lithium can carry on rapid reversible ion exchange with chemisorbed cations. Since the equilibrium coefficient for the exchange is small, and because the surface of the mineral is constantly being renewed, the chemisorbed cations are continually being added to the percolating salt solution.

Summary of Nonbiological Changes to a Percolating Solution

Investigations have been concentrated on nonbiological interactions between a percolating solution and a granitic sand matrix.

Minerals of the column were basically quartz and aluminosilicates. There had been chemical evidence (localized effervescence when a sand sample was acidified) of trace amounts of calcite ($CaCO_3$) in the sand but, after two years of percolations, trace amounts were no longer apparent. Forty per cent of the sand, quartz, dissolves at a negligible rate. The remaining 60 per cent is aluminosilicates which have molecular structures of silica and alumina interconnected by cations. Dissolution of the aluminosilicate will yield a cation but no anions.

Dissolution of the mixture of aluminosilicates in the column was evidenced by the release of aqueous silica to the percolating solutions. Aqueous silica was produced at the rate of 2.4 to 3.7 x 10^{-5} mg SiO_2/gm·hr aluminosilicate minerals at a pH between 8.5 and 5.5 irrespective of the ionic strength or flow rate of the solution. When the aqueous silica concentration climbs above 1.2 mg SiO_2/ℓ, the solution becomes supersaturated with respect to kaolinite ($Al_4Si_4O_{10}(OH)_8$).

Because some of the aqueous silica, dissolved from aluminosilicate minerals, potentially can be lost to kaolinite, or possibly some other clay mineral, the rate of appearance of aqueous silica is a lower bound on the estimate for the rate at which cations should be released by the aluminosilicate assemblage. Based on the ideal mineral formulas, the bulk composition of the aluminosilicates in the laboratory column suggests that the rate of release of calcium, magnesium, sodium, and potassium, respectively, should be 2.9 to 4.4 x 10^{-6}, 1.4 to 2.1 x 10^{-6}, 1.5 to 2.3 x 10^{-6}, and 1.6 to 2.5 x 10^{-6} mg/gm·hr aluminosilicate. The minimum rate of release of the respective cations experimentally was 1.4 x 10^{-6}, 2.2 x 10^{-6}, 3.6 x 10^{-6}, and 5.0 x 10^{-6} mg/gm·hr aluminosilicate.

Silica was released by the minerals at a rate that, contrary to the usual dissolution case, was not controlled by transfer of silica from the mineral surface to the bulk solution but rather by the dissolution reaction itself or by diffusion of silica inside the mineral. Variation of aqueous silica content of the percolating solution with depth Z can be modeled with the general equation

$$SiO_2(z) = SiO_2\Big]_0 (1 - \exp(-Az/u)) \qquad (36)$$

$SiO_2\Big]_0$ is an equilibrium, or quasiequilibrium concentration of aqueous silica and A is a constant that can be either the rate of the dissolution reaction or a diffusivity coefficient.

Release of cations from minerals can proceed by two ion exchange mechanisms. Primary ion exchange reactions are relatively short-lived, large scale exchanges of electrostatically held cations for cations in

the bulk solution. The capacity of the sand to hold such cations is on the order of 10 μeq/gm sand (it will later be shown to be 27 μeq/gm). Primary ion exchange reactions for a percolating solution are characteristically located in one band in the column above and below which the distribution of cations in the bulk solution is in equilibrium with the sand surface distribution of cations. Primary ion exchange reactions are the first and most prominent cation exchange reactions affecting a newly composed solution. The zone of the primary ion exchange reaction moves down and out the column as observed by the motion of an inflection in the concentration profile (Figures 26 and 27). Once the primary ion exchange reaction is gone, a secondary ion exchange reaction lingers on throughout the column for an indefinite duration of time. As long as the distribution of cations in the bulk solution does not sway too far from equilibrium with respect to primary ion exchange, the secondary exchange reactions are always in equilibrium so that any change in the flow rate of solution will not change the depth profiles of the concentrations of aqueous cations. The secondary reactions are believed to occur between the bulk solution and chemisorbed cations. Because the source of chemisorbed cations is in the structure of the aluminosilicates themselves, the capacity for chemisorbed cations is extremely large. Secondary ion exchange reactions are a first step in the overall mineral dissolution process whereby cations in the mineral structure are replaced by aqueous hydrogen ions or another cation. The replacement weakens the bonds of the alumina and silica superstructure which breaks up the mineral crystal, thereby exposing new chemisorbed cations ionically bonded in the crystal structure.

Nitrifying bacteria generate two aqueous hydrogen ions for every ammonium ion that is converted to nitrite. The hydrogen ion can exchange with electrostatically held cations or it can exchange with chemisorbed cations. Electrostatic cation exchange should be the major process redistributing the aqueous hydrogen ions between the solution and mineral phases. If the secondary ion exchange occurs, its effects would not be noticed due to the primary exchange reactions. Both cation exchange reactions are identical in their net effects to the cation concentration in the percolating solution; that is, an equivalent of hydrogen ions produced by the nitrifying bacteria will exchange an equivalent of calcium, magnesium, sodium, or potassium from the minerals.

CHEMICAL PROPERTIES OF THE LABORATORY COLUMN SAND

Mineral Dissolution

Positive proof was sought for three hypotheses. It was known that minerals were releasing cations at the rate of 10^{-5} to 10^{-6} mg/gm·hr, but the question was if the aluminosilicate structure of the mineral was actually disintegrating or if the observed aqueous silica was coming from some other source such as a clay (Siever et al., 46). Another question to be answered was concerned with the presence of a mass transfer hindering amorphous layer of mineral matter growing on the surface of a dissolving aluminosilicate mineral. Finally, positive proof of the release of aqueous calcium from aluminosilicates rather than from some trace mineral was sought. Answers to these questions were sought by observation of sand grain surfaces under a scanning electron microscope (SEM) before and after the grain was permitted to interact with various solutions.

Laboratory column sand was sampled and separated into feldspar, hornblende, and quartz fractions. Each fraction was mixed with epoxy. After drying, the epoxy was broken, thereby splitting in half individual sand grains. One half of each grain was kept as a specimen untreated with aqueous solution. The other face of each mineral was permitted to react for one to two months in one of three solutions. 0.16 M nitric acid was used to permit detection of actual breakup of the aluminosilicate structure in a strong acidic solution in a reasonably short time period. A solution to be used as a feed solution for the laboratory column (Table 3) was permitted to react with the mineral grains

so that the formation of an amorphous layer could be detected. The third solution was 1 M potassium fluoride and potassium phosphate for the detection of release of calcium ions from the aluminosilicate minerals. The mineral grains remained in the 1" x 1/8" x 1/8" epoxy support while they interacted with 30 mℓ of gently stirred solution.

Specimens treated with nitric acid showed signs that the epoxy itself had disintegrated slightly, possibly leaving some residue on the grain surfaces. Quartz showed no effects of the acid treatment either in low magnitude scanning electron micrographs or in higher magnitude pictures (Figure 41). The quartz surface was covered with sharp concoidal fractures characteristic of a freshly cleaved specimen. Pictures of freshly fractured plagioclase and hornblende mineral grains are compared to the upside-down reversed picture of the twin fragment that was treated for one month in 0.16 M nitric acid. The plagioclase crystal (Figure 43) did actually disintegrate in the acid (Figure 44) at approximately 4×10^{-4} mg/gm·hr. A closer look at the surface (Figure 42) does not reveal an amorphous layer formation to hinder dissolution of the parent mineral. Formation of an amorphous layer is theoretically doubtful in such an acidic environment. Hornblende (Figures 45 and 47) also actively dissolved in nitric acid (Figures 46 and 48) at approximately the same rate as the plagioclase. It is therefore seen that when the aluminosilicate ions exchange their cations with aqueous hydrogen ions, they also experience an actual disintegration of their structure in a measurable amount of time.

Plagioclase grains treated for two months in solution to be percolated through the laboratory column (Table 3) show clumps of matter on

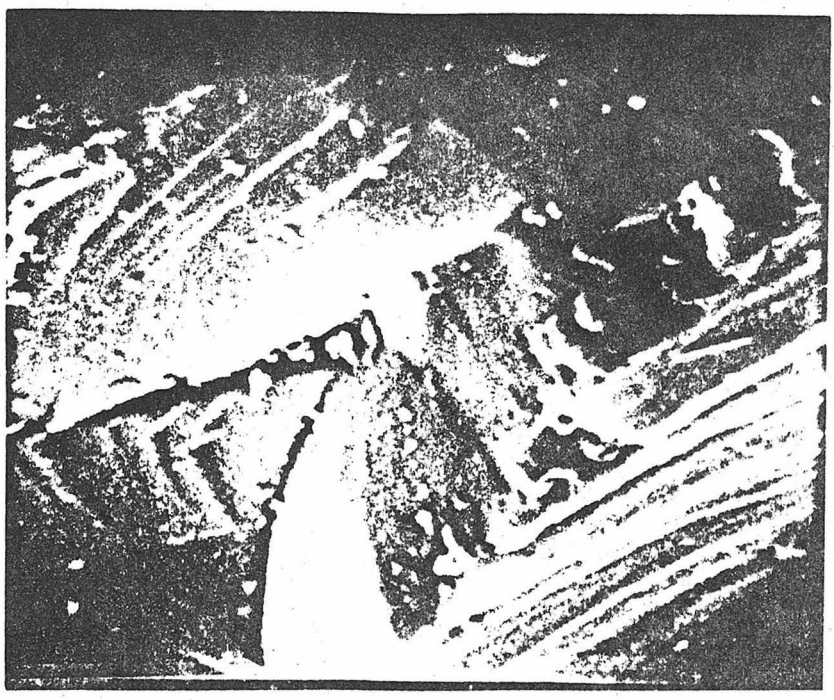

Figure 41: Quartz Surface after Two Month Treatment in 0.16 M Nitric Acid (7500 Magnification)

Figure 42: Plagioclase Surface after One Month Treatment in 0.16 M Nitric Acid (7800 Magnification)

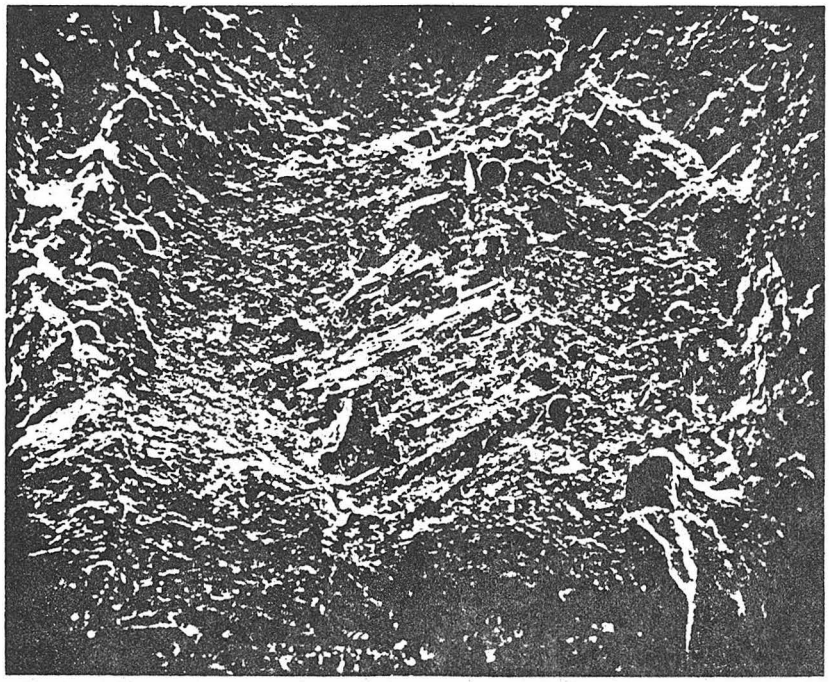

Figure 43: Freshly Fractured Plagioclase in Epoxy Support (79 Magnification)

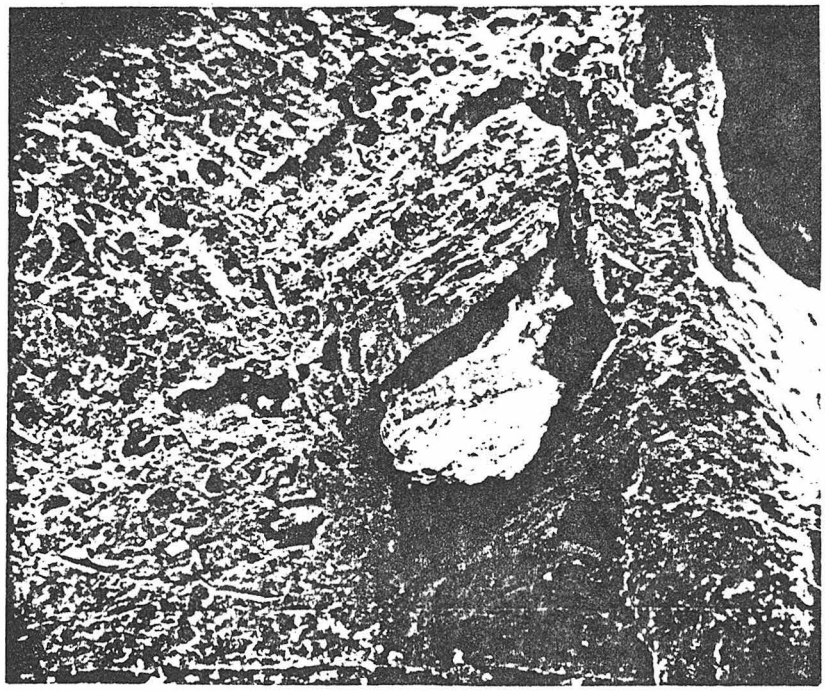

Figure 44: Twin Fragment of Freshly Fractured Plagioclase after One Month Treatment in 0.16 M Nitric Acid (79 Magnification)

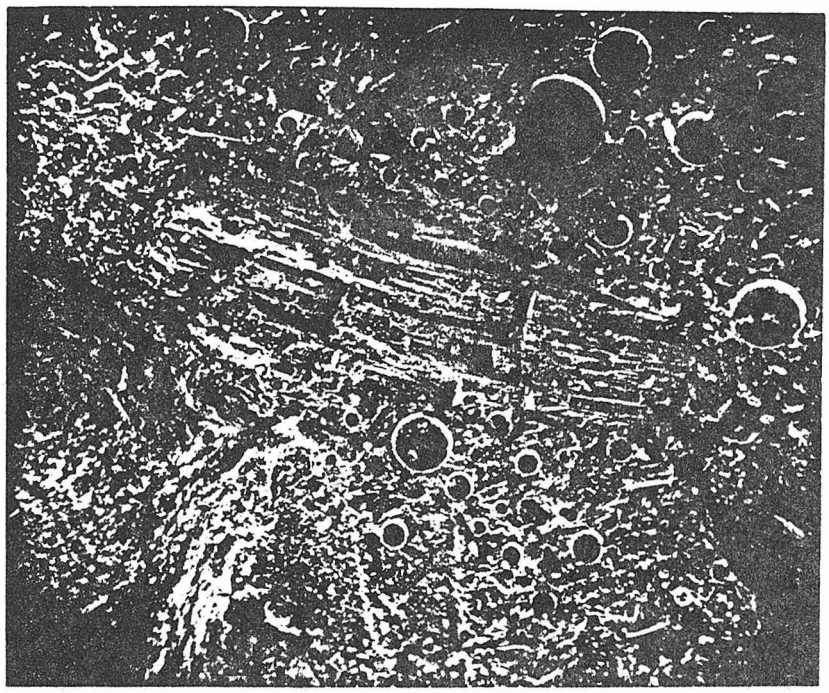

Figure 45: Freshly Fractured Hornblende in Epoxy Support (79 Magnification)

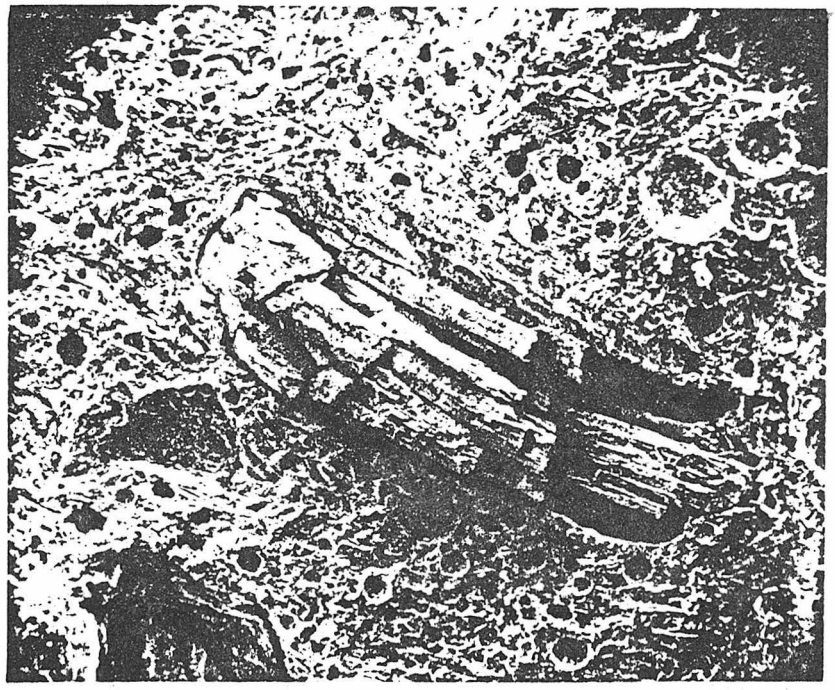

Figure 46: Twin Fragment of Freshly Fractured Hornblende after one Month Treatment in 0.16 M Nitric Acid (79 Magnification)

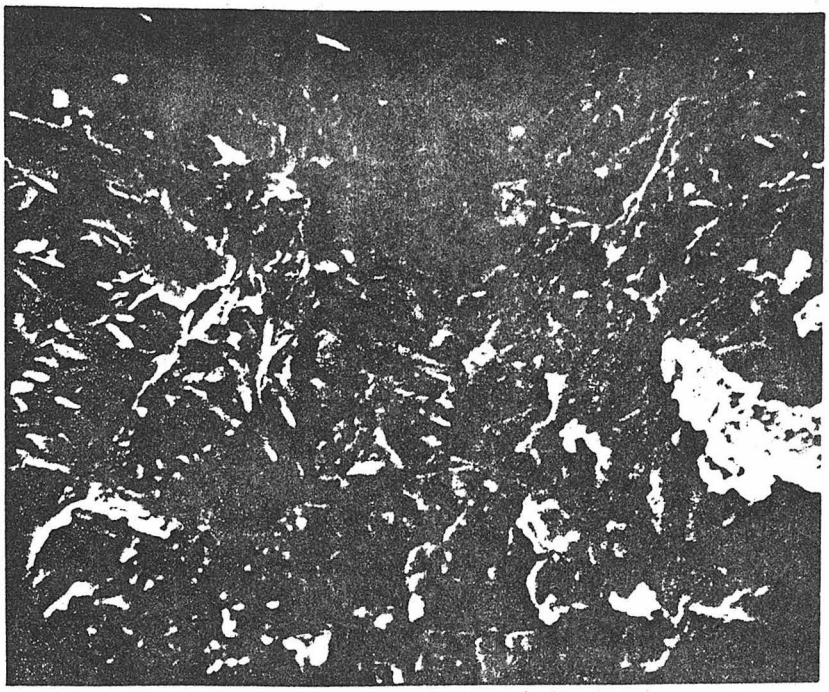

Figure 47: Freshly Fractured Hornblende (4000 Magnification)

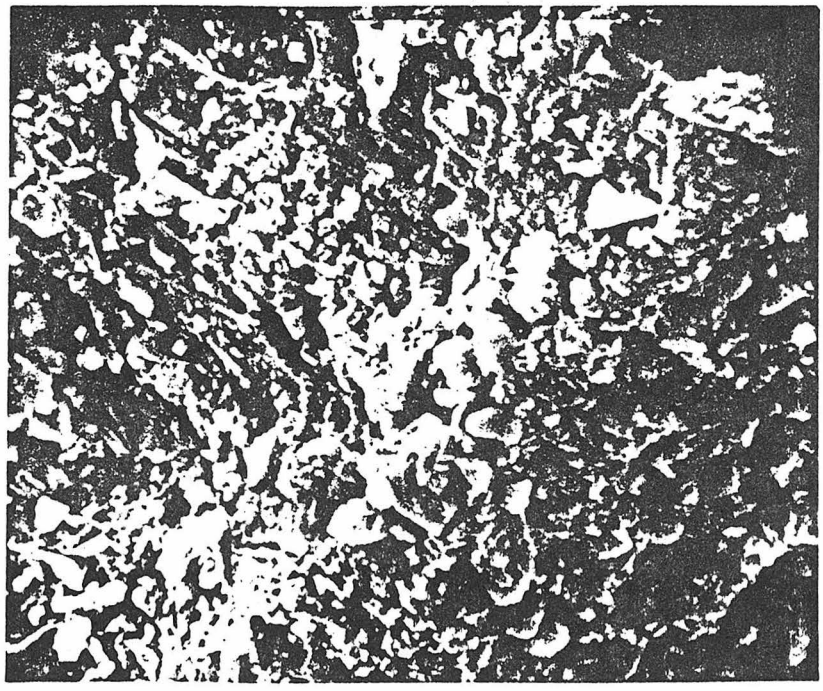

Figure 48: Twin Fragment of Freshly Fractured Hornblende after One Month Treatment in 0.16 M Nitric Acid (4000 Magnification)

the surface (Figure 49). The clumps are 1 to 0.1 micron in size. Because there was some clumpy material on the surface of the quartz grains treated in the same manner, the plagioclase debris cannot be assumed to have originated from the mineral itself. Hornblende grains also were coated with debris. The attempt to detect a surface coating must be judged inconclusive.

Quartz, plagioclase, and hornblende treated for two months in the potassium fluoride/phosphate solution were expected to show a coating of calcium fluoroapatite ($Ca_5(PO_4)_3F$) wherever calcium would be released from the crystal surface. Quartz was totally unchanged in the solution. Plagioclase (Figure 50), and especially hornblende (Figures 51 and 52), showed hexagonal crystals growing on the surfaces. The crystals were much stronger calcium emitters than the background mineral and are therefore assumed to be 0.2 to 0.5 micron crystals of calcium fluoroapatite. There was no preferential growth of crystals on any specific mineral cleavage plane; however, there was a conspicuous lack of crystals inside the mineral fissures (Figure 52). Presumably the calcium fluoroapatite crystals are present because of release of calcium from the interior of the aluminosilicate and subsequent reaction of the calcium ion with the fluoride and phosphate ions of the solution. The surfaces were freshly cleaved, calcium ions which had to have been desorbed from the mineral by the chemisorption of potassium ions from the solution. Judging from the coverage of crystals, calcium must have been released from the hornblende mineral at the rate of 5×10^{-3} mg Ca^{++}/gm·hr. The high concentration of aqueous potassium ions would tend to cause an ion exchange of calcium from the crystal

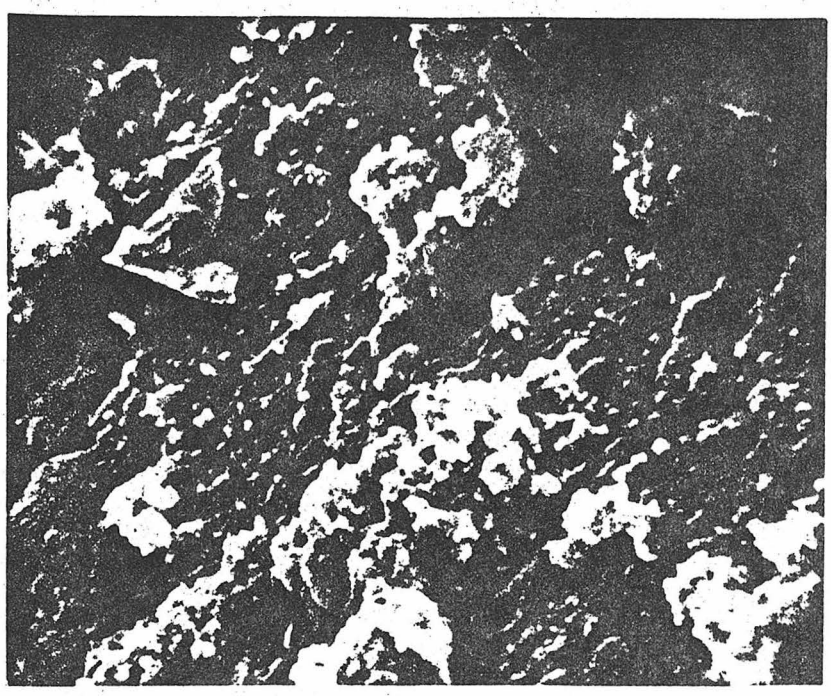

Figure 49: Plagioclase Surface after Two Month Treatment in Neutral Salt Solution (7750 Magnification)

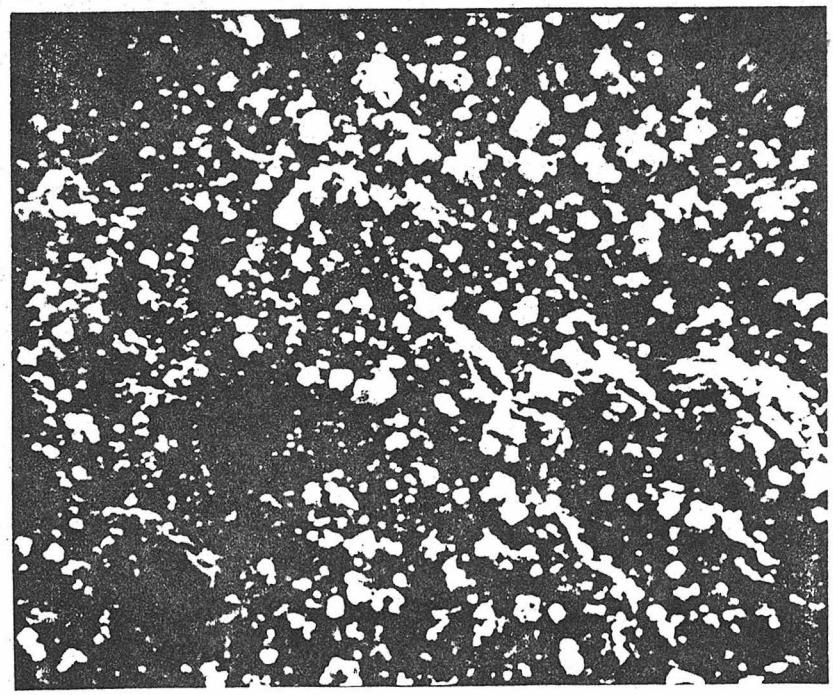

Figure 50: Plagioclase Surface after Two Month Treatment in Fluoride/Phosphate Solution (4000 Magnification)

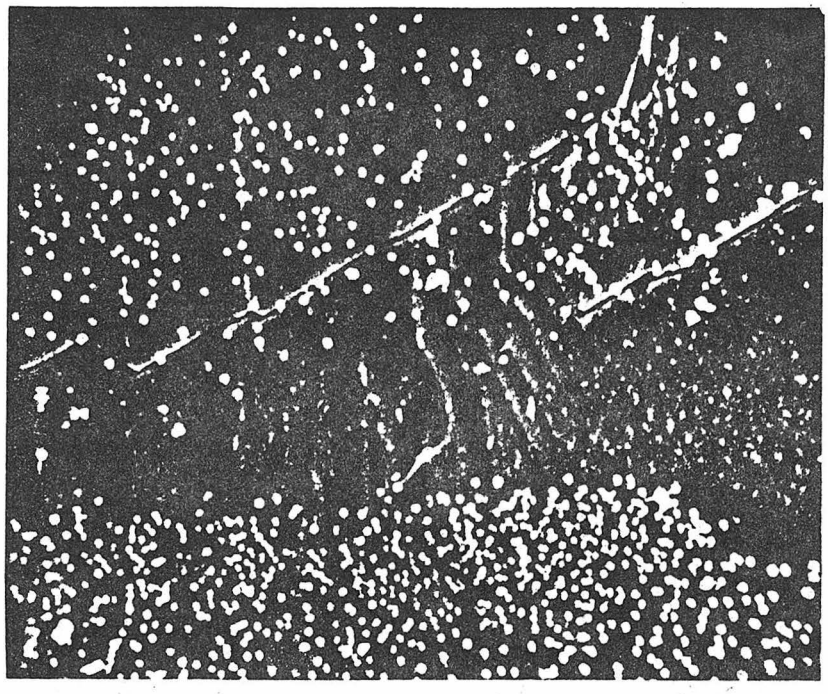

Figure 51: Hornblende Surface after Two Month Treatment in Fluoride/Phosphate Solution (3700 Magnification)

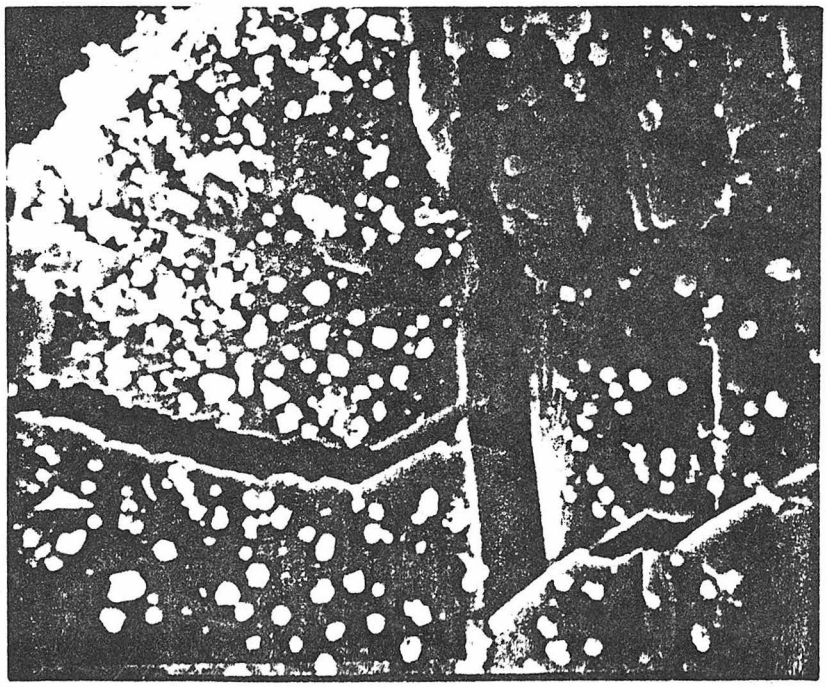

Figure 52: Hornblende Surface after Two Month Treatment in Fluoride/Phosphate Solution (7000 Magnification)

at a higher rate than lower strength solutions as used previously in percolation experiments through the column. Sharpness of crystal edges on the hornblende specimen suggests that this mineral did not experience disintegration of its structure during the two-month reaction with solution.

This present investigation has shown that plagioclase and hornblende do dissolve, in the manner of destruction of their crystalline structure, in a reasonable amount of time in an acidic solution. Disintegration of their structure could be neither confirmed nor disproven in neutral salt solutions. In a one molar potassium fluoride/phosphate solution, the destruction of the structure was not evident. Quartz was totally unaffected by any solution. Calcium ions were released from the interior of the aluminosilicate minerals with little or no alteration of the external appearance of the mineral. The reaction causing the release of calcium ions must be an ion exchange of aqueous potassium ions for chemisorbed calcium ions. Presence of a mass transfer hindering surface coating on the minerals was not observed in the acidic solution. In the 10 mM neutral salt solution, the coating's presence is inconclusive. Minerals interacting with the fluoride/phosphate solution showed no signs of a surface coating which follows from the observation that the mineral probably did not release silica in the destruction of its structure.

Determination of Ion Exchange Distribution Coefficients

Cationic exchange reactions have been demonstrated to be of importance for solutions percolating through a soil assemblage. An

empirical relationship was found to correlate the distribution of calcium, magnesium, ammonium, and the aqueous hydrogen ion on the column's sand surface to their respective concentrations in the aqueous solution. The potassium ion was not included in the study because this ion was found to be of minimal importance to solutions percolating through the laboratory column.

Experimental work was based on the assumption that equilibria between the distribution of the five cations on the sand and solution could be represented by determining the equilibrium distribution between calcium and each of the remaining cations. Sand samples that had previously been equilibrated with calcium salt solutions were re-equilibrated with four series of solutions containing varying concentrations of calcium, of ionic strength 11 nM, and one other cation salt buffered to pH 8.3 with bicarbonate (the hydrogen/calcium ion distribution was analyzed with nitric acid as the hydrogen ion "salt"). One dry gram of the sand was equilibrated with 25 mℓ of solution. After one week, solution was drained from the sand and analyzed for the concentrations of aqueous calcium and the other cation to give the distribution of ions in the aqueous phase. Weight of the moist sand gave the quantity of ions in the thick film of solution surrounding the sand. Ammonium acetate molar solution was used to leach the wet sand for four hours (in the case of calcium/ammonium distribution, barium chloride solution was used). Analysis of the leachate yielded the distribution of cations on the sand's surface (the hydrogen ion surface concentration was found by analysis of the pH of the 25 mℓ solution before and after the equilibration).

Binary ion exchange reactions, such as between calcium ions and an arbitrary cation M^+ follows the reaction

$$|Z_M|\overline{Ca} + 2M^+|Z_M| \rightleftharpoons |Z_M|Ca^{++} + 2\overline{M} \quad . \tag{37}$$

An equilibrium expression for the calcium/cation exchange can be defined as

$$K_M^{Ca} = \frac{x_{Ca}^{|Z_M|}}{x_M^{|Z_{Ca}|}} \frac{[M]^{|Z_{Ca}|}}{[Ca]^{|Z_M|}} \tag{38}$$

where $|Z_M|$ is the absolute value of the charge on the cation M, [M] is the activity of M in the aqueous phase, and x_M is the activity of M on the substrate. The equilibrium expression implies that a plot of $Ca^{|Z_M|}/M^{|Z_{Ca}|}$ versus $x_{Ca}^{|Z_M|}/x_M^{|Z_{Ca}|}$ would be a straight line. The experimental data did not plot linearly when the aqueous and surface activities were replaced respectively by molarity and surface equivalent fraction. If the surface species act like a regular solution (Garrels et al., 27), the activity coefficient of a surface species is

$$\lambda = \exp(Bx^2/RT) \tag{39}$$

where B is a constant, x is the surface concentration, R is a constant, and T is the temperature. For any distribution of the species

$$K_M^{Ca} = \frac{x_{Ca}^{|Z_M|}}{x_M^{|Z_{Ca}|}} \frac{[M]^{|Z_{Ca}|}}{[Ca]^{|Z_M|}} \exp(-B(x_{Ca} - x_M)/RT) \quad . \tag{40}$$

For surface distributions for which neither species dominates the

surface by more than 90 per cent

$$K^{Ca}_{1_M} = \left(\frac{x_{Ca}}{x_M} \frac{|Z_M|}{|Z_{Ca}|} \right) K^{Ca}_{2_M} \left(\frac{M}{Ca} \frac{|Z_{Ca}|}{|Z_M|} \right) . \qquad (41)$$

The data for the binary equilibrium reactions between calcium and four other cations all gave linear plots when plotted according to the above equation (Figure 53). Two constants, $K^{Ca}_{1_M}$ and $K^{Ca}_{2_M}$, are used to determine the distribution of calcium and another cation, M, in an ion exchange system.

Specific Role of the Aqueous Hydrogen Ion

The phenomenon of ion exchange of electrostatically held cations on an aluminosilicate is a result of charged sites on the crystal surface resulting from amphoteric dissociation of surface hydroxyl groups, SiOH and AlOH, giving positive or negative sites:

$$\underline{Si}OH \rightleftharpoons \underline{Si}O^- + H^+ \; ; \quad K_{eq} = 10^{-6} \text{ to } 10^{-8} \text{ (Stumm et al., 20; Dugger et al., 49)} \qquad (42)$$

$$\underline{Si}OH + H^+ \rightleftharpoons \underline{Si}OH_2^+ \; ; \quad K_{eq} = 10^{-2} \text{ to } 10^{-4}. \qquad (43)$$

Another origin of surface charge would result from isomorphic substitution of aluminum for silicon in a tetrahedral site in the structure of the mineral. The former mechanism of charge formation makes the aqueous hydrogen ion a potential-determining species.

The quantitative description of the surface charge for a mixture

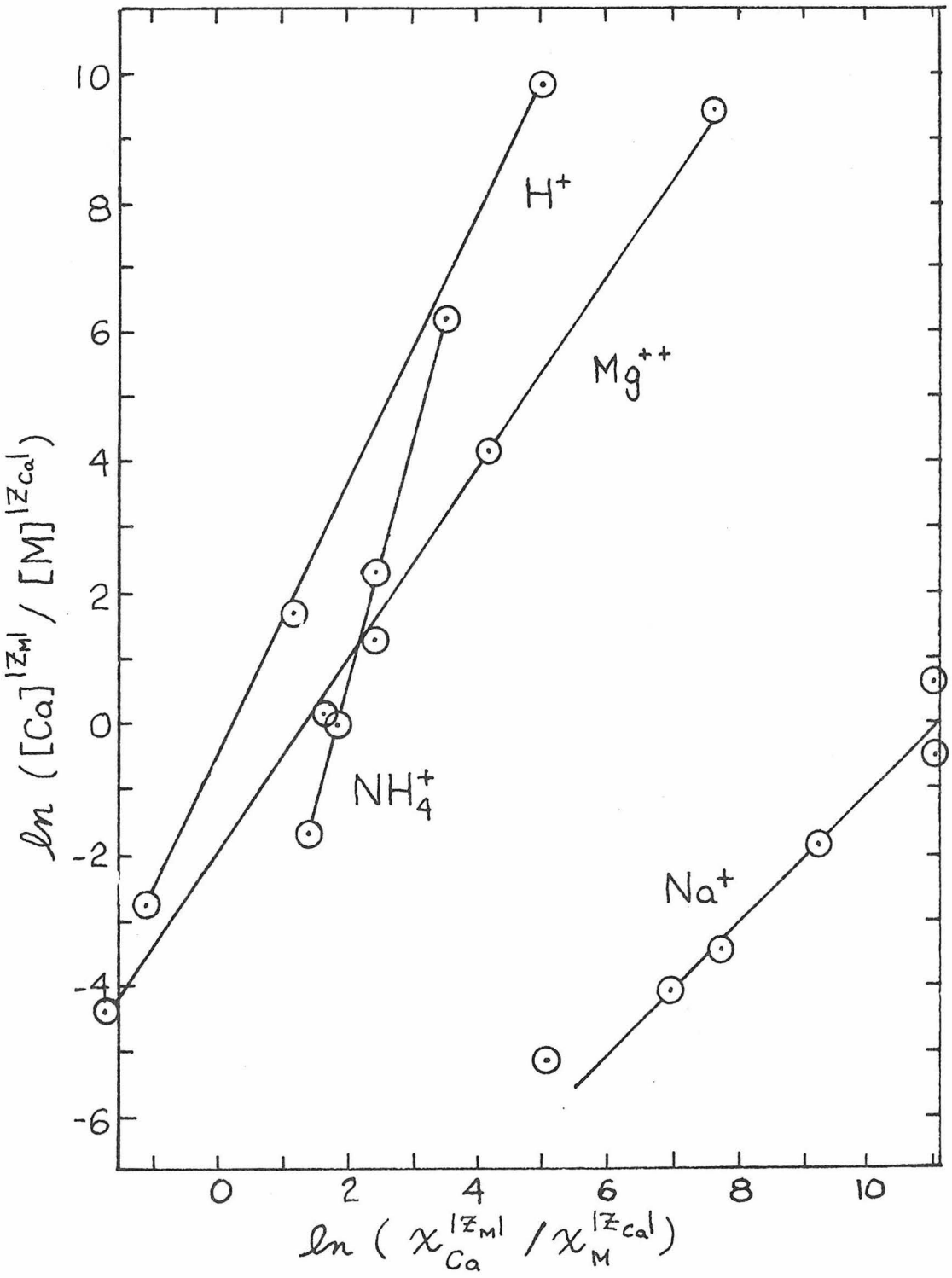

Figure 53: Ion Exchange Distributions for Calcium Ions and Four Other Cations

of minerals is complex. It would be expected that in a pH environment between 10 and 2, the hydroxylated silica surface would only act as neutral or negative sites. The hydroxylated alumina surface would be composed of negative and positive sites in the same pH range (Tanabe, 28). Kaolinite, a mixture of silica and alumina groups, has both negative and positive sites (Stumm et al., 20) over much of the pH range of an aqueous solution. Theoretically, the aqueous hydrogen ion can participate in any number of dissociation reactions on the column's mineral surfaces in the pH ranges found in the column's percolating solution. Such reactions are amphoteric dissociation reactions rather than common ion exchange of hydrogen ions.

Specific or selective ion exchange reactions are reactions involving cations attracted to the mineral surface by electrostatic forces augmented by chemical bonds. Ion exchange of cations bonded by chemical forces is a specific ion exchange reaction. Aluminosilicate minerals, of course, do have substantial capacity for chemisorbed cations. Even pure silica can hold an important quantity of chemisorbed calcium above pH 7 (Parks, 48). Both theory and experimental evidence suggest calcium, sodium, potassium, and magnesium are participants in specific ion exchange reactions with the minerals in the laboratory column, i.e., alkaline earths are ionically bound.

Aqueous cations attracted to the mineral surface by charged sites are positioned in a layer over the mineral surface so that they are balanced between the electrostatic force of the charged sites and the tendency of the cation to diffuse away from high concentration zones. Similarly, anions, repulsed by a surface charge (negatively adsorbed),

will be positioned in balance between their being repelled by a negative charge and diffusing back into a low concentration zone. The above two layers compose the Double Layer. A negatively charged mineral in an aqueous solution of ionic strength 10 mM should have a double layer thickness of approximately 30 A in which the cation concentrations could be thousands of times larger than in the surrounding solution (van Olphen, 24). If aqueous hydrogen ions are extensively being chemisorbed, then the interaction between sand surface and solution will be more complex than a simple ion exchange of the hydrogen ion for another cation. Chemisorption of an equivalent of hydrogen ions by the sand will not yield an equivalent release of other cations; instead, more equivalents of cations will be released (than hydrogen ions adsorbed) by virtue of the fact that less anions will be negatively adsorbed.

The equal equivalent exchange between the hydrogen ion and other cations was investigated. Column sand which had been equilibrated with sodium bicarbonate salt solution was permitted to react with a constant pH nitric acid solution. The sample was placed inside a 1/4-inch lucite tube through which approximately 35 mℓ of solution was circulated at 25 mℓ/min by a peristaltic pump (Figure 54). Circulation of the solution took it into a glass chamber where pH was monitored with a glass membrane/saturated rubidium chloride electrode system. A positive pressure was maintained above the chamber by helium to prevent acidification of the solution by atmospheric gases. Any deviation of the solution's pH was checked by addition of nitric acid from a titrator system. The quantity of hydrogen ions taken up by the sand

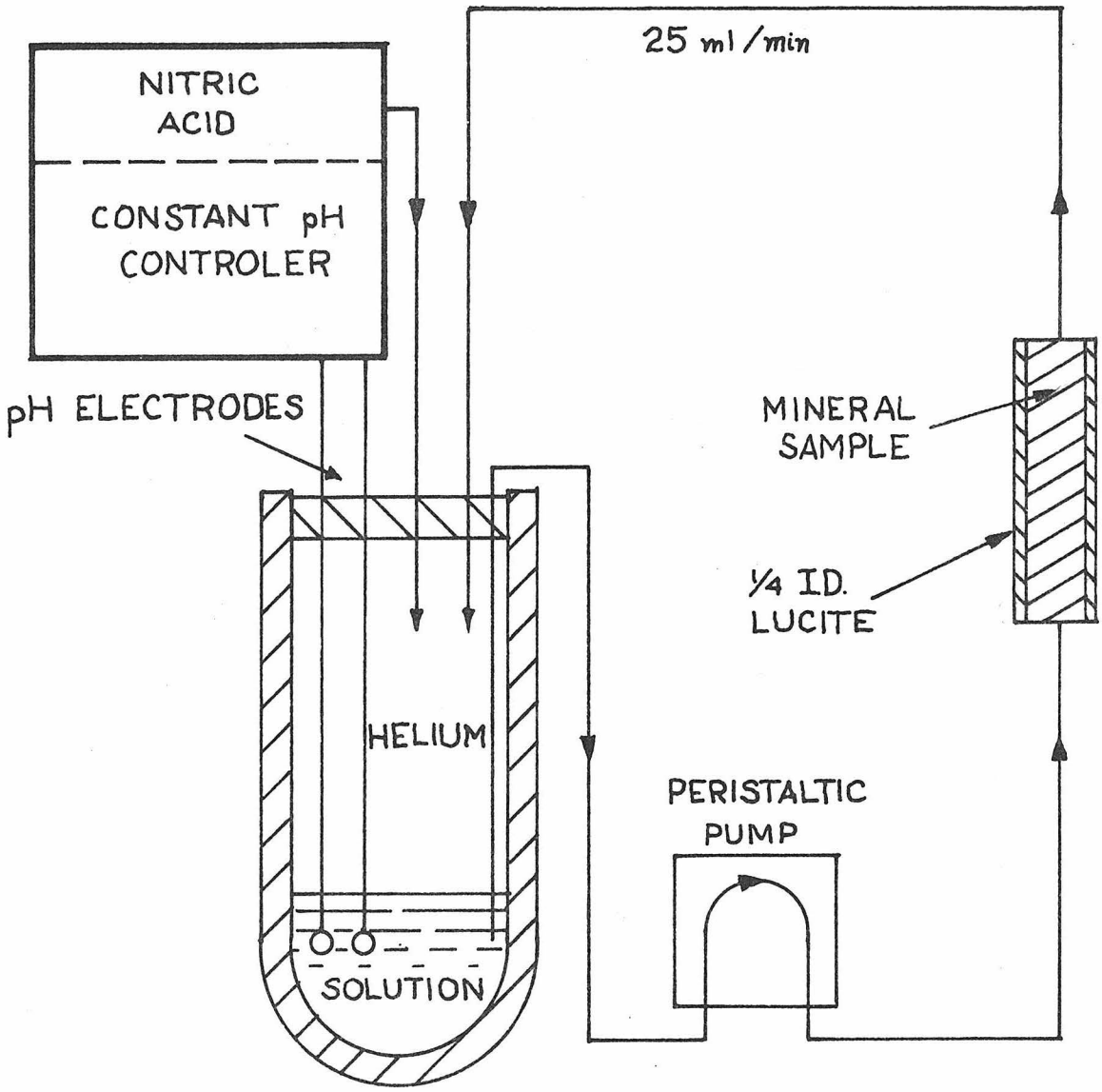

Figure 54: Apparatus for Long Duration, Constant pH Studies of Mineral/Solution Interactions

mixture was assumed to be equal to the quantity added to the solution to maintain a constant pH. The quantity of cations released by the sample was calculated from the analysis of the solution which had been circulated through the sample. Another method was used to determine if an equivalent adsorption of hydrogen ions would give an equivalent release of cations. A sand sample, previously equilibrated with calcium chloride solution, was permitted to react with a 11 mM solution of calcium chloride acidified to various pH's with nitric acid. The change of pH of the solution after a week gave the quantity of hydrogen ions adsorbed by the sample, and analysis of the quantity of calcium on the sand surface before and after the reaction gave a direct account of the quantity of calcium released from the sand surface. Results are plotted as quantity of hydrogen ions consumed against quantity of cations released (Figure 55). The points of largest uncertainty represent the results of the calcium chloride equilibrated sample. There was a tendency for more cations to be released than hydrogen ions to be adsorbed thereby suggesting that the aqueous hydrogen ion is being chemisorbed and changing the concentration of negatively charged sites on the sand surfaces. The effect is weak enough to warrant, as a first approximation, the assumption that, above pH 4, aqueous hydrogen ions exchange in a one-to-one equivalent ratio with other cations.

The capacity of a sand sample to hold cations by electrostatic forces must be known in order to model the distribution of cations between the sand surface and the percolating solution. When the binary ion exchange distribution coefficients between the calcium ion and four other cations was determined, the total cation exchange capacity

(Inserted numbers are the final solution pH.)

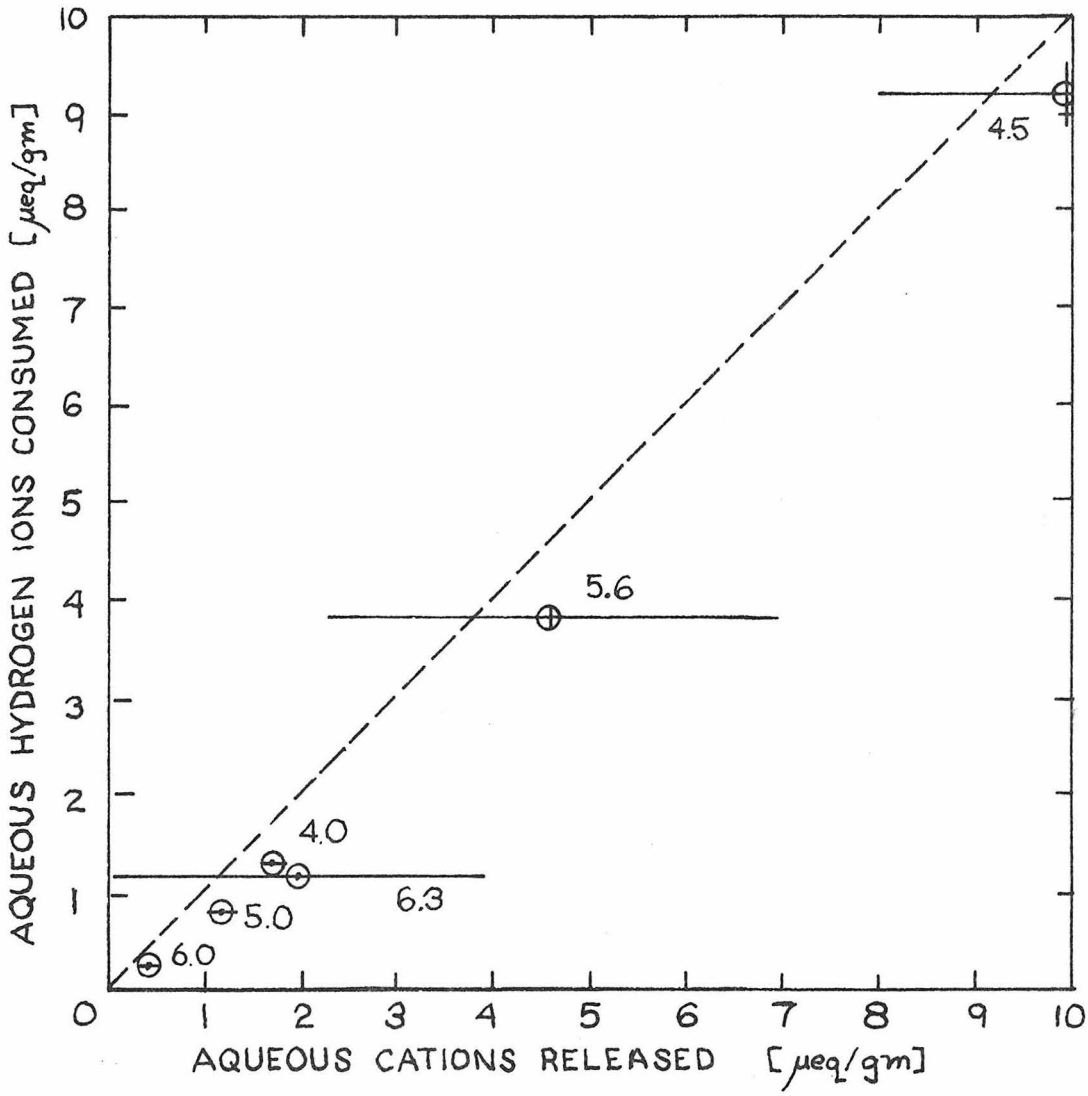

Figure 55: Test for an Equivalent Exchange of the Aqueous Hydrogen Ion with Cations Adsorbed to a Sand Sample

was found to be a function of the particular pair of cations. Cation exchange capacities for the binary pairs calcium/ammonium, calcium/magnesium, and calcium/sodium were, respectively, 15 ± 1, 11 ± 2, and 36 ± 3 microequivalents per gram of column sand at a pH of 8.3. The cation exchange capacity of the column sand mixture was determined in a solution of composition identical to the solution to be fed to the column (Table 3) but with a variable pH. The above capacity would be taken as the average for small changes of solution cationic composition around that of the percolating solution's inlet composition. A column sand sample that had been equilibrated with solution to be percolated through the column (Table 3) was permitted to react with the same solution at various pH's adjusted with nitric acid. After the equilibrium terminated, the adsorbed species were extracted from the sample with 200 mℓ of ammonium chloride for four hours. The total equivalents of calcium, sodium, potassium, and magnesium adsorbed to the samples at various solution acidities are plotted at the top of Figure 56. A similar experiment had been performed on a sand sample; however, a calcium chloride solution was used in place of the multi-salt containing solution. The results of the calcium adsorption investigation are plotted on the bottom of Figure 56. The cation exchange capacity of the sand mixture in the column feed solution varied from 23 to 29 μeq/gm in the pH range 4 to 8. The capacity to hold calcium remained approximately constant at 30 ± 5 μeq/gm over the same range of pH. Because there was no drastic change of the sand's capacity to adsorb cations in the wide range of pH from 4 to 8, it can be assumed that the hydrogen ion is not participating in chemisorption reactions in the same

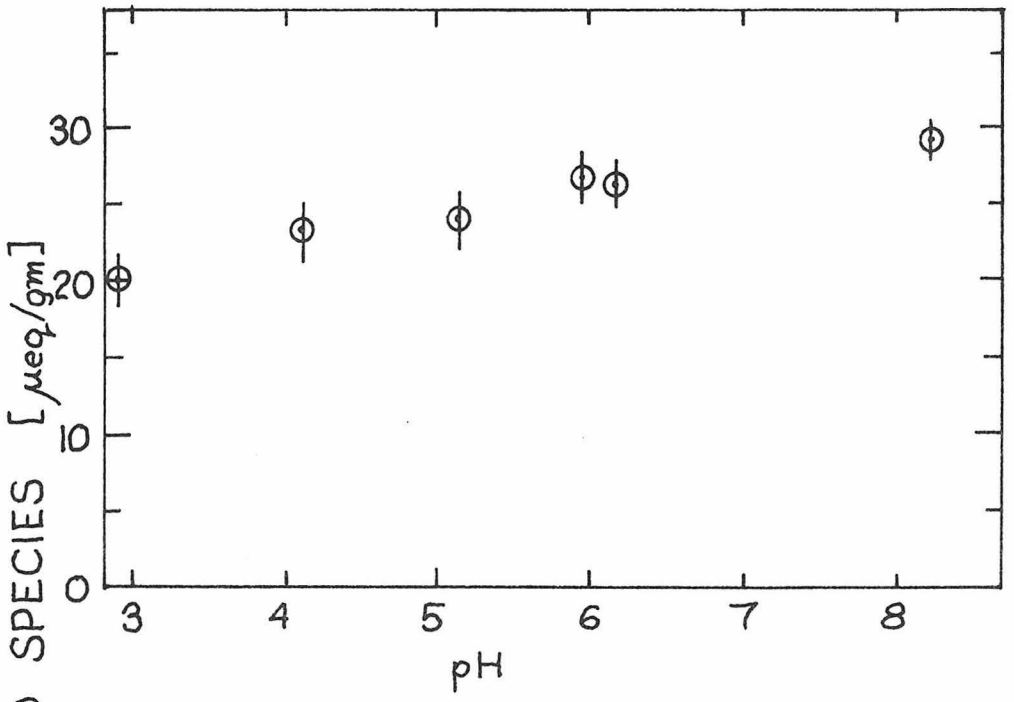

Quantity of Adsorbed Calcium, Magnesium, Sodium, and Potassium versus pH

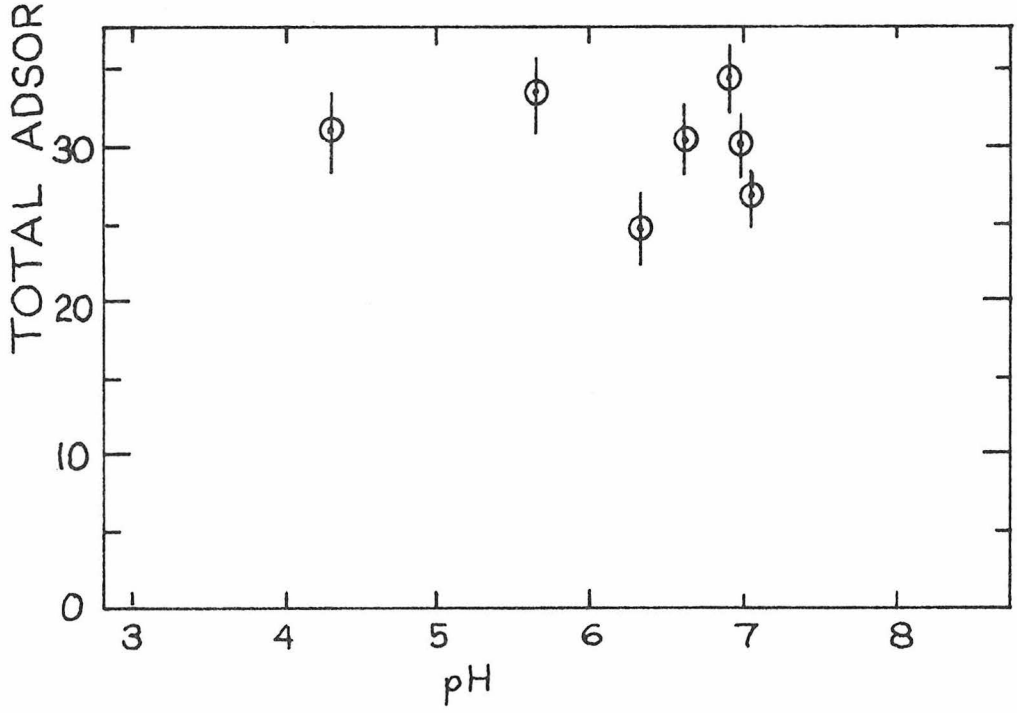

Quantity of Adsorbed Calcium versus pH

Figure 56: Cation Exchange Capacity of a Sand Mixture as a Function of pH

pH range. The total cation exchange capacity of sand will be assumed constant at 27 μeq/gm and changes of pH can be neglected. Even when the pH of the aqueous solution drops as low as 4, Figure 55 shows that the overall effect can still be treated as a simple ion exchange of cations between the sand surface and the aqueous solution.

Proof of the Rate Controlling Step of Ion Exchange

Data suggest that cations released by the column's sand particles originate within the mineral structure rather than on its surface or in a surrounding electric double layer. A more conclusive proof of the origin of cations was undertaken for the ion exchange between aqueous hydrogen ions and another cation in a continuous flow system.

One gram samples of column sand that had previously been equilibrated with a single salt solution were leached at 46 mℓ/hr with 22 mM hydrochloric acid. During the operation, the effluent was collected and analyzed for the cation of the salt with which the sand had been equilibrated with magnesium salt solution, the interruption was characterized by draining the sand and permitting it to rest for 3600 seconds. The calcium salt solution equilibrated sand was interrupted of leaching by its being drained, flushed with acetone, and dried followed by 4630 seconds of rest. The resumption of leaching was started and the effluent was constantly sampled. The accumulative quantity of cations released from the sand is plotted against the square root of time elapsed from the start of the leaching and also from the start of the resumption of leaching.

Time variation of accumulative quantities of cations released

from a sand sample can be determined for the condition that diffusion of reactants or products inside the crystal controls the overall rate. The time required for a species to diffuse a short distance L into a crystal is approximately L^2/D, where D is the effective diffusion coefficient. Suppose the crystal has S sites per crystal volume to be converted from one cationic form to another. The approximate time it would take to convert all the ion exchange sites a small depth, l, further into the crystal will be the number of sites, AlS (A is the area perpendicular to the direction of diffusion), divided by the rate of transport of cations into (or out of) the crystal, ADC/L (C is the concentration of the species diffusing). If the time to convert exchange sites 0.1L further into the crystal is much longer than the time required to transport cations between the sites and the surface of the crystal, then it is assured that the transport of cations through the crystal is approximately at steady state. The criterion of a steady state diffusion profile inside the mineral is

$$l << \frac{0.1\ S}{C} \quad .$$

If the number of exchange sites represents the number of chemisorbed cations in a mineral, then S is on the order of 10^4 μeq/ℓ. For the present investigation of exchanging a sand with a solution of 22.4 mM of hydrogen ions, the most stringent test of the criterion would be to assume that the diffusion of hydrogen ions into the minerals controls the release rate of other cations. Therefore C is 22.4 μeq/ℓ and the right hand side of the above criterion is 130 which is much larger than one. Under the further assumption that exchange reactions occur only

at sites at the furthest depth of penetration of cations inside the crystal, the rate of penetration of the reaction front into the mineral will be equal to the rate at which cations diffuse into or out of the crystal

$$DC/L = S \frac{dL}{dt} \tag{44}$$

or

$$L = \sqrt{DCt/S} \quad . \tag{45}$$

The accumulative release or consumption of cations for a crystal system of total area A is

$$Accum = A\sqrt{DSC/t} \quad . \tag{46}$$

A plot of accumulative release versus the square root of elapsed time should therefore yield a straight line if diffusion of cations inside the mineral structure controls the rate of release of cations.

The interruption test can eliminate external diffusion as the slowest step for the transport of cations between the bulk leaching solution and the inside of the crystal. If the diffusion of cations from the bulk solution to the mineral surface controls, then a sudden stoppage of flow of leachate and resumption will not change the rate of release of cations. On the other hand, if diffusion of cations inside the crystal (or the exchange reaction itself) controls, an interruption will permit internal diffusion (or reaction) to proceed such that when the leaching resumes the rate of release of cations would have suddenly increased. The latter was the case for the extraction of magnesium and calcium from the sand samples. At least for the secondary ion exchange

process, the rate of release of cations from the column's sand is not controlled by external diffusion.

Data are plotted against the square root of elapsed time to show an indication of the specific rate determining step (Figure 57). Initially when the acidified leachate reaches the sand sample, cations are released at a rate that does not indicate that internal diffusion controls. Presumably the initial release of cations is by the same primary ion exchange as presumed for percolating solutions in the laboratory column. The primary ion exchange reaction is exchange of cations in the mineral's double layer and must be controlled by the diffusion of cations between the bulk solution and the double layer. The curves of accumulative release become straight lines with time which implies that internal diffusion has taken over as the rate determining step. After the interruption (Figure 57), the curves tend to be linear. If the line is extended back to the origin, it does not intercept zero; therefore, during the interruption or immediately upon resumption of leaching, some cations have entered the double layer and disrupted its equilibrium with the leaching solution.

Summary of the Chemical Properties of the Column Sand

By direct observation, it was found that the aluminosilicate minerals dissolve in a reasonable amount of time with complete destruction of their structures. The steps leading to the final disintegration of their aluminosilicate superstructures can be traced. A solution coming in contact with the mineral will first redistribute cations in the double layer of the mineral. The redistribution comes about by

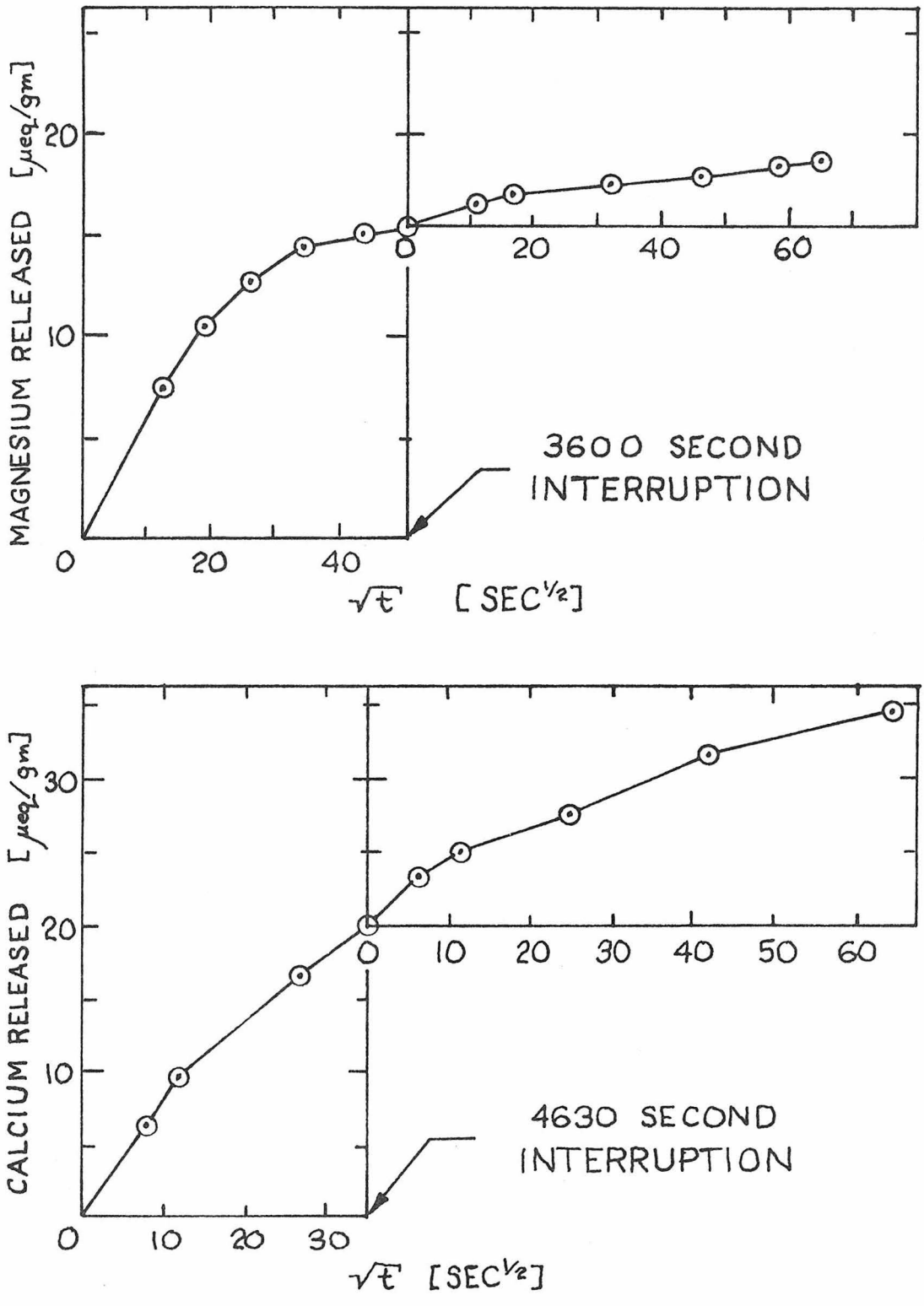

Figure 57: Accumulative Release of Cations from Sand Being Leached with Nitric Acid

cation exchange between the bulk solution and the double layer cations at a rate controlled by mass transfer of cations between the same two regions of cations. The double layer was found to be so thick, and the minerals' pores so small, that the cation exchange capacity of the column's sand is directly proportional to the external surface area of the sand. Once the double layer has reached equilibrium with the percolating solution, a continuing, but slower, exchange of cations from the interior of the mineral persists. Whereas the capacity of the sand for cations in the double layer was 27 μeq/gm, the cations being released from the interior of the mineral structure are chemisorbed cations and therefore, being part of the original structure of the crystal, have a capacity of 4000 μeq/gm. Electronmicrographic pictures of positions on the mineral structure of release of cations imply that chemisorbed cations are only released from the external surface of the mineral; therefore, the release rate is directly proportional to the external mineral surface area. The slowest step of the release of chemisorbed cations is the diffusion of cations inside the mineral structure. Apparently when the original cations of the mineral have been replaced by hydrogen ions, or some other cation, the aluminosilicate structure of the mineral breaks up at a fixed rate controlled by the disintegration reaction itself. Certainly in strongly acidic solutions the superstructure of the aluminosilicate mineral breaks up completely; however, in neutral solutions there is a thermodynamic possibility that the alumina and silica resolidify into a clay mineral and interfere with further mass transfer of cations to and from the parent mineral.

Ion exchange equilibria between calcium and each one of the cations magnesium, sodium, ammonium, and hydrogen was determined. Undoubtedly there was some specific ion exchange participating. Even though the aqueous hydrogen ion is a potential determining species for the column's sand, it can still be considered as an ordinary cation participating in nonspecific ion exchange reactions. Furthermore, as long as the solution pH is above 5.5, the cation exchange capacity of the column sand can be considered as constant at 27 μeq/gm. Because of specific cation exchange, the cation exchange capacity rigorously is a function of the cations participating in the ion exchange.

Consider a solution percolating through a soil matrix, cation exchange of cations in the double layer for cations in the bulk solution will be the most important first reaction to change the composition of the percolating solution. The extent of the cation exchange reactions of the solution's cations is dependent on the exchange distribution coefficients; however, the duration of the ion exchange process will be directly proportional to the surface area of the soil. A silty soil will change the composition of a percolating solution for a longer duration of time relative to a coarser soil. Once the solution has percolated past the zone of ion exchange, and thereby equilibrated itself with ions in the double layer of the soil's minerals, it will continue to show a slow change in its composition due to ion exchange with chemisorbed cations inside the structure of aluminosilicate minerals. For all intents and purposes, the aqueous hydrogen ion will participate in ion exchange in a manner similar to the other aqueous cations. As long as the mineral material of the soil is quartz or

aluminosilicates, the interactions of the percolating solution and the minerals will result in negligible change to the total dissolved cation content of the percolating solution. The hardness of the solution, of course, can be changed for the worse if a hard solution had previously been percolating through the soil or less so if the aluminosilicates are primarily calcium and magnesium containing. Again, the pH will be only as important as the concentration of any other cation in ion exchanging calcium or magnesium of a mineral. The concentration of hydrogen ions of the percolating solution becomes more important than the concentration of other cations when the percolating solution encounters a mineral such as calcite ($CaCO_3$) or dolomite ($CaMg(CO_3)_2$) which dissolves more rapidly in an acidic solution. Moderately soluble minerals such as calcite will dissolve to increase the total dissolved solids of the percolating solution as well as its hardness.

PERCOLATION OF SOLUTIONS THROUGH A NITRIFYING COMMUNITY

The last stage of experimental research focused on the variation of the aqueous chemical composition of solutions percolating through a nitrifying bacterial community. The nitrifying bacterial community alone was assumed responsible for the high dissolved solids content of percolating solution. The laboratory column had been purged for two months with solutions devoid of carbon-containing compounds and therefore of no value to any bacteria. It was necessary to encourage the growth of any bacteria which would survive in an inorganic solution of similar composition to that percolated at the Whittier Narrows test plot. Since it was the immediate goal of the research to approximate the Whittier Narrows data, the entire array of different autotrophic bacteria in the Whittier Narrows soil was permitted the opportunity to grow in the laboratory column. Approximately 50 grams of moist soil from the surface of the Whittier Narrows test basin was slurried with 250 mℓ of water and injected into the top segment of the column. The type of bacteria that would become dominant in the column's bacterial community should be similar to the bacteria of the test plot because the percolating solutions of both environments were similar except for a total lack of organic carbon in the laboratory solution.

Growth of the nitrifiers Nitrosomonas and Nitrobacter can occur only under a limited set of chemical conditions. Carbon dioxide is the carbon source of the nitrifying bacteria. The presence of organic carbon will encourage the growth of faster multiplying heterotrophic bacteria and may actually inhibit the growth of nitrifiers (Delwiche

et al., 60). Energy for the bacterial conversion of carbon dioxide to cellular material is from the reaction of ammonium and nitrite ions with oxygen to yield nitrite and nitrate ions, respectively. Composition of solution to be percolated intermittently through the laboratory column contained aqueous ammonium ions and dissolved oxygen and, in general, was very similar in composition to the solution spread on the Whittier Narrows test plot (Table 2). The final feed solution contained manganese and iron (Table 3) to satisfy the bacterial requirement for these aqueous species. Later in the study, ferric nitrate was not added to the feed solution because it was found that the iron would be lost from the feed solution as a precipitate in an aerobic environment. The laboratory column's feed solution contained aqueous ammonium ions, oxygen, and bicarbonate; theoretically the only type of bacteria that could be supported would be nitrifiers.

Many chemical species in the percolating solution were analyzed, but not all at the same time. Cation exchange reactions are important enough that all aqueous cations interact with one another; therefore, for a full understanding of one or two aqueous cation concentrations, all important cation concentrations (such as calcium, magnesium, sodium, potassium, ammonium, and the hydrogen ion) were determined. If nitrification was to be recognized during the one-week Wet Period, the primary reactants of nitrification, dissolved oxygen and aqueous ammonium ions, as well as the products, nitrite, nitrate, and the hydrogen ion, were determined. During the two-week Dry Period, oxygen carbon dioxide, and nitric oxide in the column's gaseous atmosphere were checked as indicators of nitrification (Yoshida et al., 22;

Table 2

Whittier Narrows Water Reclamation Plant
Effluent Quality

Aqueous Species	Concentration mg/ℓ
Calcium	51
Magnesium	12
Sodium	119
Potassium	11
Ammonium	18
Bicarbonate	251
Sulfate	114
Chloride	93
Nitrate	23
Phosphate	18
Total Dissolved Solids	703
Dissolved Oxygen	5.1
B.O.D.	4
C.O.D.	60

(Reid, 4)

Table 3

Composition of Solution Fed Intermittently to Column

Salt	Concentration mg/ℓ
Calcium Chloride $CaCl_2$	140.
Magnesium Sulfate $MgSO_4$	59.3
Manganese Chloride $MnCl_2 \cdot 4H_2O$	2.0
Potassium Phosphate $K_2HPO_4 \cdot 3H_2O$	16.3
Potassium Phosphate KH_2PO_4	14.9
Sodium Sulfate Na_2SO_4	28.5
Sodium Bicarbonate $NaHCO_3$	346.
Sodium Nitrate $NaNO_3$	28.9
Ammonium Sulfate $(NH_4)_2SO_4$	65.0
Ferric Nitrate $Fe(NO_3)_3 \cdot 9H_2O$	1.0

Verhoeven, 23). A quantitative measure of the bacterial populations of heterotrophic bacteria and the nitrifiers, Nitrosomonas and Nitrobacter, on the column sand was taken. All the important chemical compounds participating in nitrification reactions throughout the intermittent percolation schedule were monitored.

It was anticipated that as the feed solution percolated down through the column, nitrifying bacteria would consume aqueous ammonium ions and oxygen and generate sand-dissolving aqueous hydrogen ions, thereby releasing large quantities of aqueous calcium and magnesium ions. During the Dry Period of two weeks it was expected that nitrification would occur on the moist sand with consumption of gaseous oxygen and dissolution of the sand.

First Wet Period

Feed solution was percolated at 11 ℓ/day through the column for the typical one-week duration. Because the column would be experiencing a period of adjustment with respect to the distribution of bacteria throughout its length and with respect to the distribution of cations in the solution, only a few aqueous species were analyzed.

Up until the third day of percolation, aqueous oxygen content of the percolating solution hardly changed. By the last day, 5.6 mg O_2/ℓ of the inlet solution's 8 mg O_2/ℓ was consumed before the solution percolated to the 1/2-foot depth. Aqueous silica content increased linearly with depth from 0.25 of the inlet to 1.95 mg SiO_2/ℓ of the effluent. Analysis of the sand's adsorbed cations at the one-, four-, and eight-foot depths revealed that calcium was the most prominent

cation and that potassium and sodium comprised the remaining two per cent.

The variation of pH with depth is conspicuous because approximately 2 millimoles of acid would be required to lower the carbonate buffered solution's pH the amount observed. If the source of acidity is the first nitrification reaction

$$NH_4^+ (aq) + \frac{3}{2} O_2 \xrightarrow{\text{Nitrosomonas}} NO_2^- (aq) + 2H^+ + H_2O \ , \qquad (47)$$

$$NO_2^- (aq) + \frac{1}{2} O_2 \xrightarrow{\text{Nitrobacter}} NO_3^- (aq) \qquad (48)$$

then the consumption of 5.6 mg O_2/ℓ can account for only part of the total quantity of acid released to the percolating solution. Despite the solution's increased acidity, the quantity of silica released is the same as that of the deionized water and calcium salt solution percolation investigations. Because there were no chemical compounds capable of consuming large quantities of dissolved oxygen, it is assumed that oxygen is disappearing from the percolating solution due to the presence of bacteria.

First Dry Period

The first Dry Period was started by diverting solution away from the top of the column and permitting solution to continue exiting the bottom at 11 ℓ/day. It was later decided that such practice was causing unnecessarily complex initial and boundary conditions for later mathematical models of the column's gaseous atmosphere. The column, hereafter, was permitted to drain in as short a time as possible (approximately 30 minutes). Three gas samplings were taken from the

column and analyzed to detect aerobic bacterial activity during the two-week Dry Period.

No nitric oxide was detected at any depth of the column. However, nitrogen dioxide was detected as a trace gas but with a concentration no different from the ambient concentration. There was a noticeable decrease of gaseous oxygen with depth especially for the 48-hour profile (Figure 58). The 72- and 192-hour gas samplings showed less conspicuous changes of gaseous oxygen volume percentages with depth. Substantial quantities of carbon dioxide appeared in the gaseous atmosphere of the laboratory column. For the 72-hour gas samplings, carbon dioxide at the five-foot depth was 1.0 volume per cent whereas atmospheric carbon dioxide averages 0.033 volume per cent. Gas samplings below the seven-foot depth were not taken because of the interference by intermittently released interstitial water.

The first Dry Period showed that gaseous oxygen is consumed and carbon dioxide emitted very early in the period. Such behavior of the column's gaseous atmosphere implied that bacteria were consuming oxygen and producing acids to convert bicarbonate ions in the interstitially held water to carbon dioxide gas. Proof that nitrifying bacteria are responsible for the changes in the column's atmosphere will be presented further into this report.

Second Wet Period

Feed solution percolating into the column and displacing air out through the column's base terminated the previous Dry Period. Once solution reached the column's base, the flow was adjusted to 11.1 ℓ/day

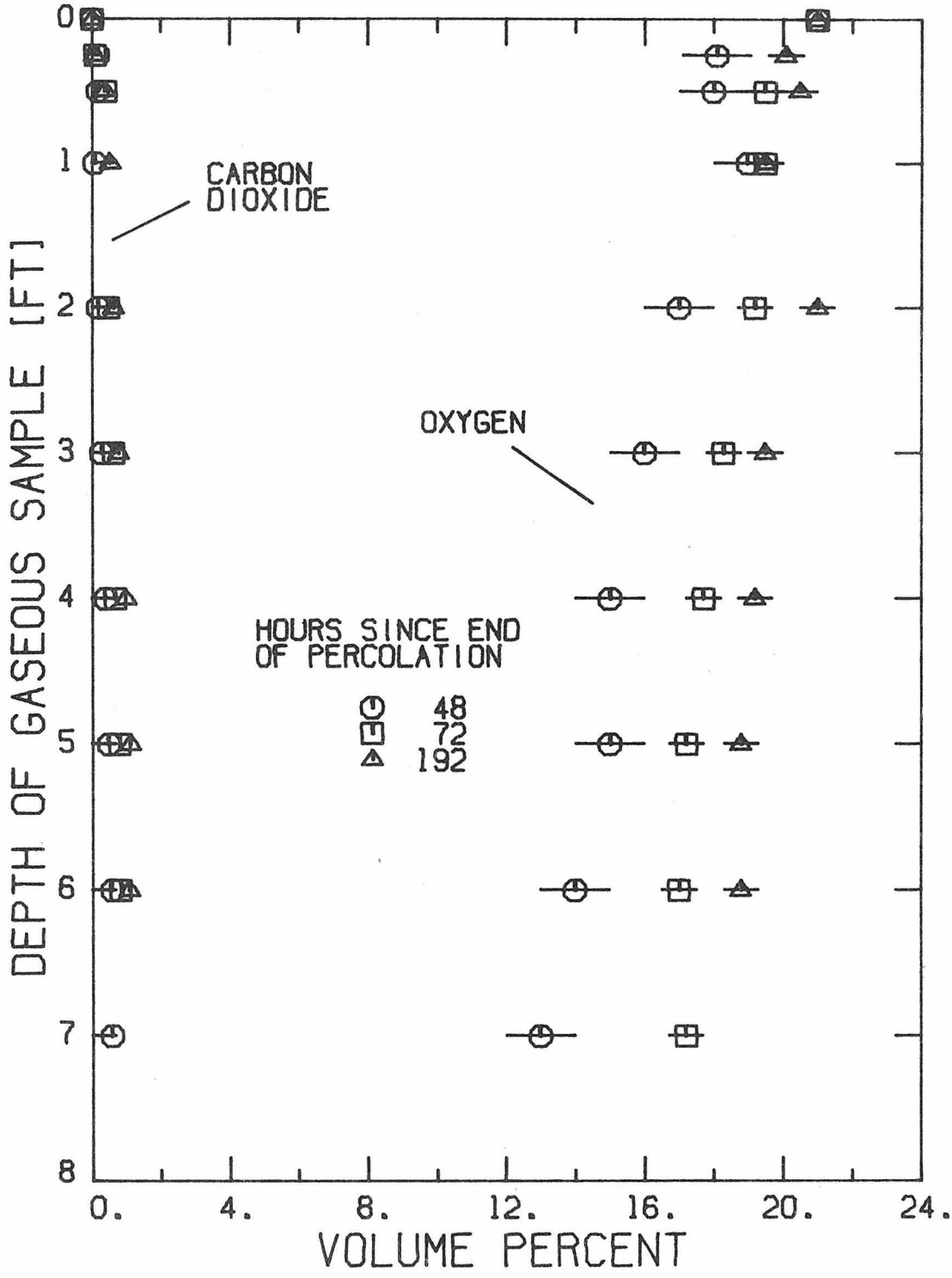

Figure 58: Carbon Dioxide and Oxygen Content of the Laboratory Column Atmosphere during the First Dry Period

for the duration of the one week Wet Period. Samples of solution were taken 42 and 85 hours after the run started. Sand samples from the column were analyzed just before the end of the Wet Period.

Except for aqueous sodium which did not sway from 120 mg/ℓ, all aqueous cationic concentrations in the percolating solution were time- and depth-dependent. Magnesium content of the solution exhibited typical ion exchange type profiles (Figure 59) with breakthrough curves taking the inlet magnesium concentration down to 0.3 mg/ℓ from 12.8 mg/ℓ. The rate at which the zone of magnesium ion exchange traveled down the column implied an addition of 1.6 μeq of magnesium per gram of sand. Potassium content of the percolating solution also changed in a manner suggestive of ion exchange with 0.24 μeq potassium added per gram of sand. The first hint of an increase of hardness of a percolating solution came from the aqueous calcium profiles which showed humps of calcium concentrations suggestive of ion exchange desorption of 0.9 μeq calcium/gram.

Acidity of the percolating solution increased as it traveled down the column (Figure 60). This increase represented a constant addition of acid to the percolating solution of 0.7 μeq/ℓ·ft down to the five-foot mark for the 43-hour profile and 0.6 μeq/ℓ·ft down to the seven-foot mark for the 85-hour profile. Therefore the appearance of aqueous hydrogen ions in the percolating solution did not occur at one particular zone in the column as typical of the other cationic concentration profiles.

The 85-hour profile of nitrogen compounds susceptible to nitrification is plotted (Figure 61). The most important feature is that

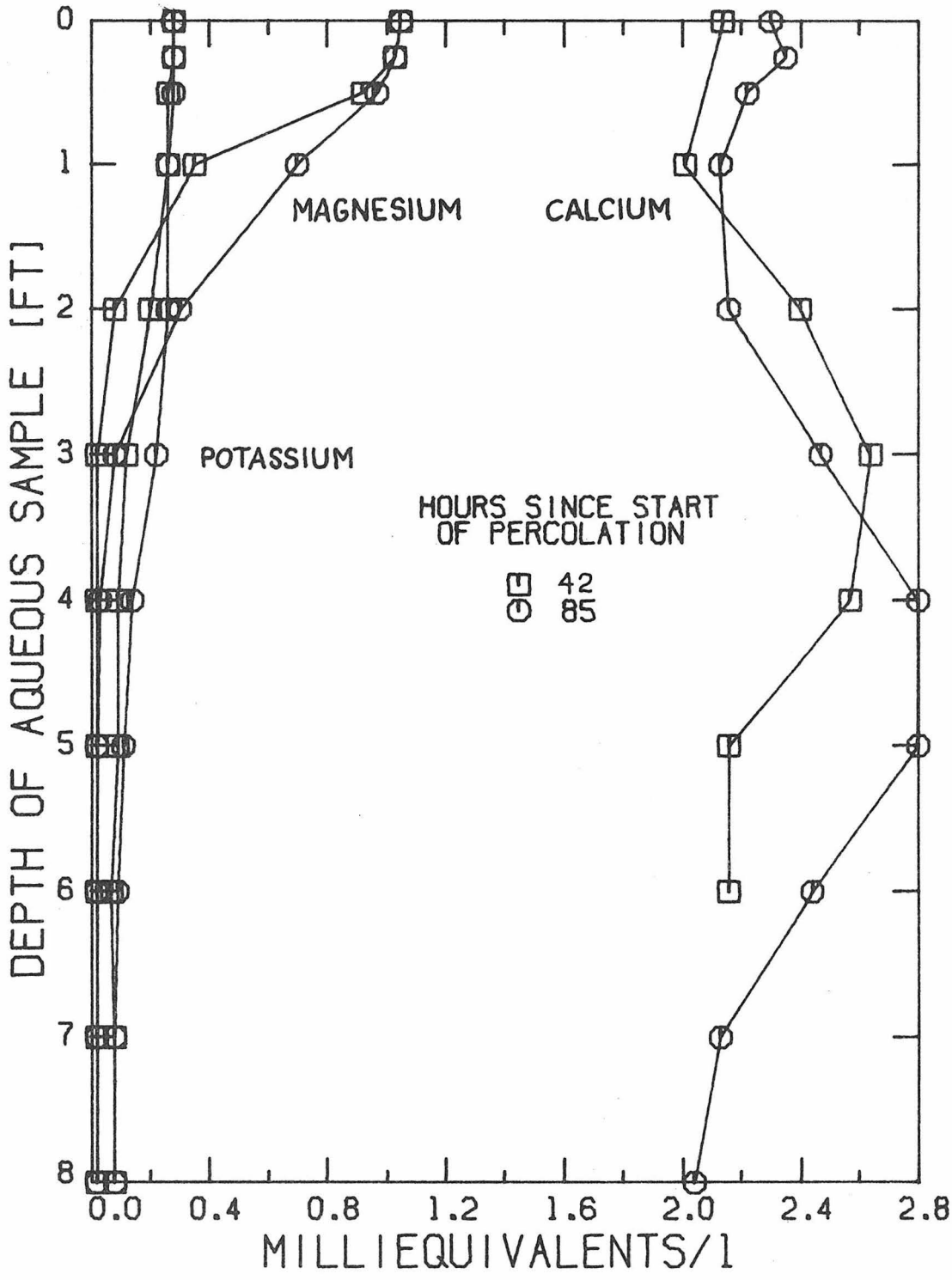

Figure 59: Aqueous Potassium, Magnesium, and Calcium Ion Content of Feed Solution Percolating through the Laboratory Column during the Second Wet Period

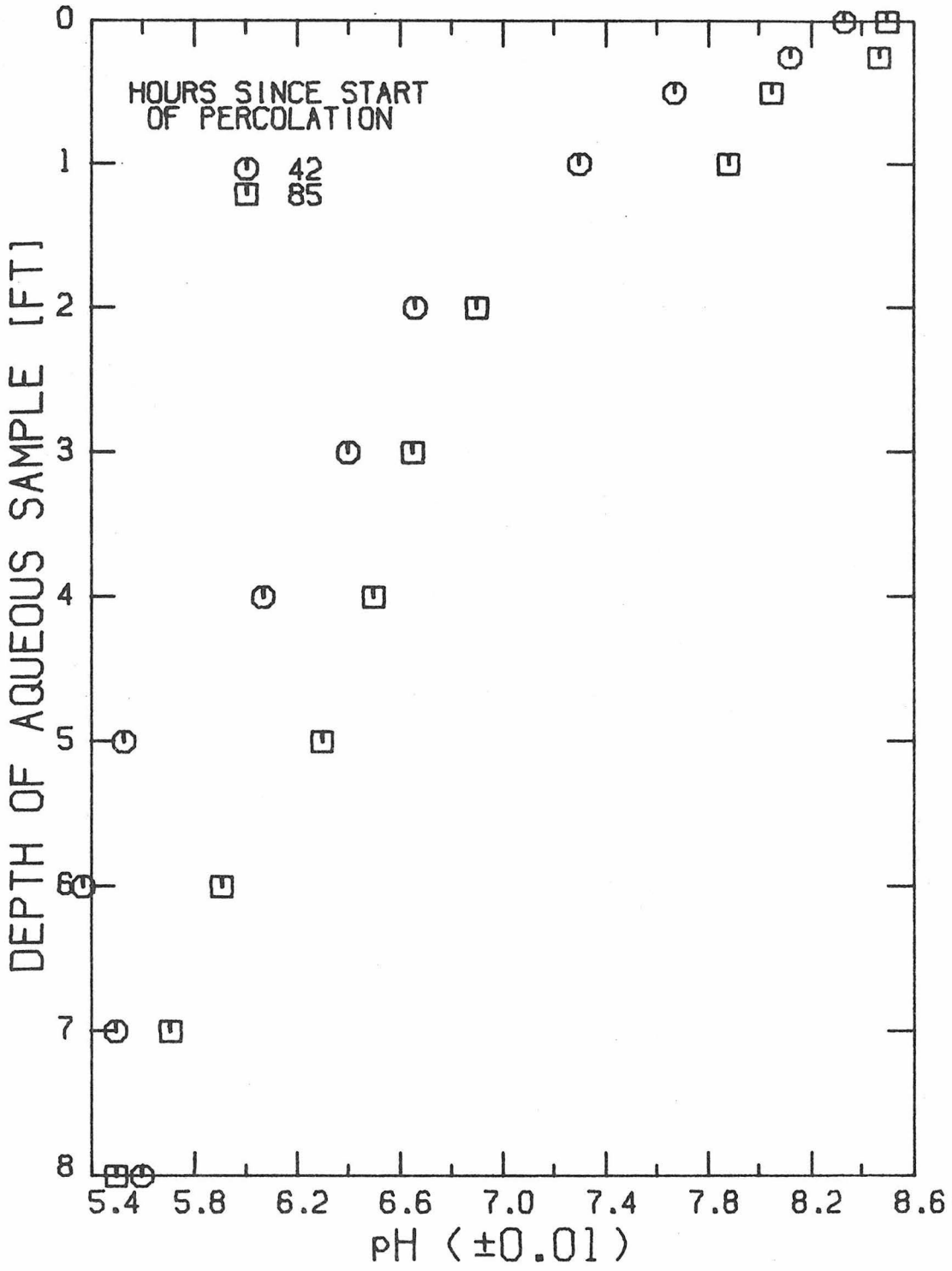

Figure 60: pH of Feed Solution Percolating through the Laboratory Column during the Second Wet Period

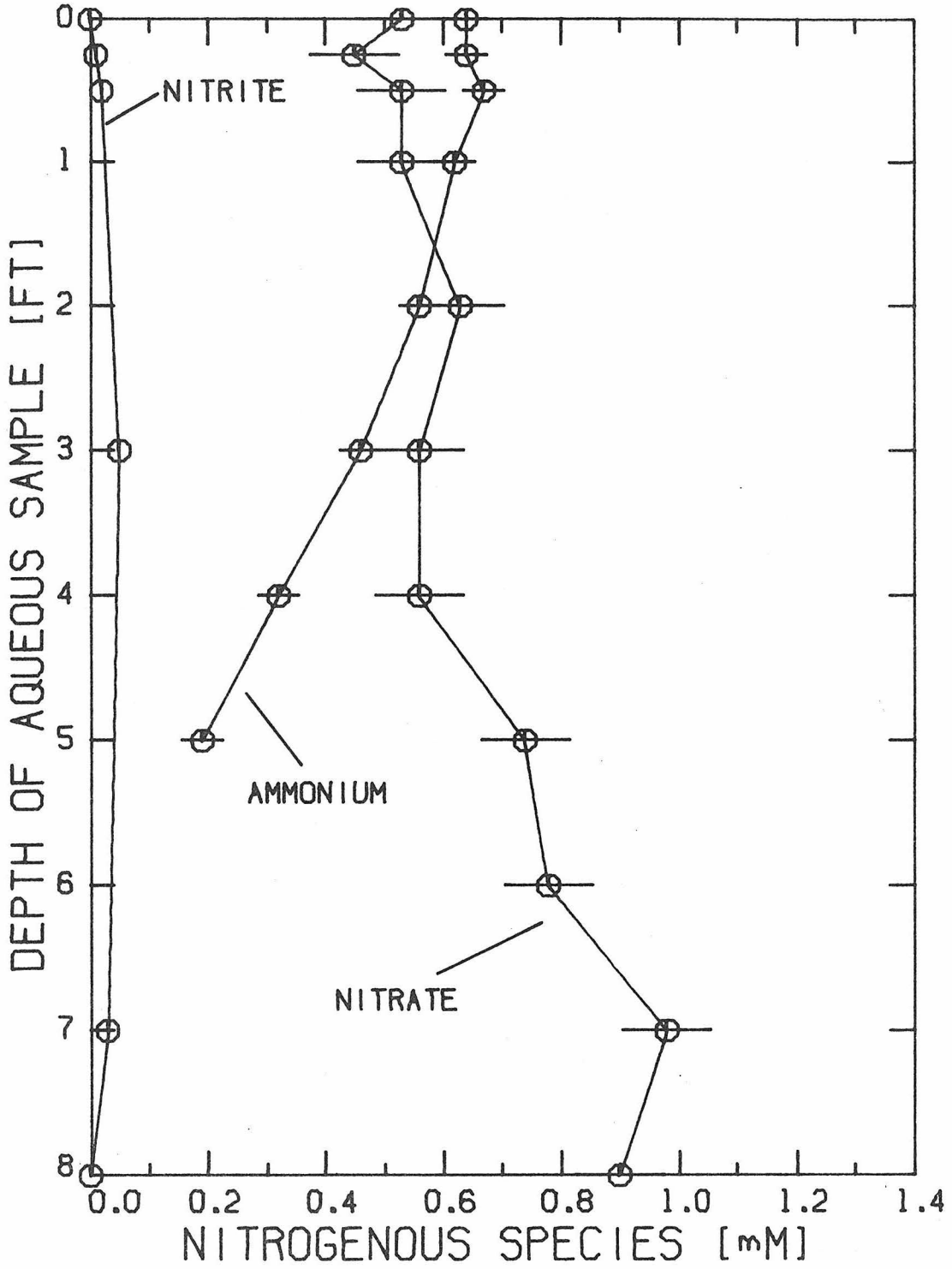

Figure 61: Aqueous Inorganic Nitrogenous Species Content of Feed Solution Percolating through the Laboratory Column during the Second Wet Period

aqueous ammonium ions were extracted from the percolating solution. There was an increase of aqueous nitrate ions and a lesser increase of aqueous nitrite ions. The maximum amount of ammonium ions that could be converted to nitrite ions, based on the quantity of dissolved oxygen, is 0.17 mM. The maximum concentration of nitrate ions that could result from nitrification, based on the dissolved oxygen content of the incoming solution, would be 0.13 mM. Despite the fact that dissolved ammonium ions and oxygen are disappearing from the solution and dissolved nitrate and hydrogen ions are appearing, it must be concluded that the bulk of the disappearance of aqueous ammonium ions is not due to bacterial nitrification of ammonium ions but rather due to adsorption of ammonium ions by the column's sand. The increase of nitrate ions at the base of the column is attributable to a lingering of high concentrations of nitrate ions from the previous Dry Period.

The oxygen profiles for the percolating solution show a drop of 6.5 mg O_2/ℓ (Figure 62) which presumably is due to bacteria; however, there was an increase of oxygen content of the solution further down the column. The increase is a result of oxygen-deficient solution percolating into regions of the laboratory column where oxygen-containing air is trapped in the interstices of the sand. Considering the rate at which the upward inflection of the aqueous oxygen profile moved down the column, exhausting interstitial air of oxygen, the volume fraction of interstitial air between the four- and six-foot depths should be 0.06--a reasonable result considering that the measured total porosity for solution in the column was 0.44 and the effective porosity was 0.35.

Sand samples removed from the column were leached at approximately

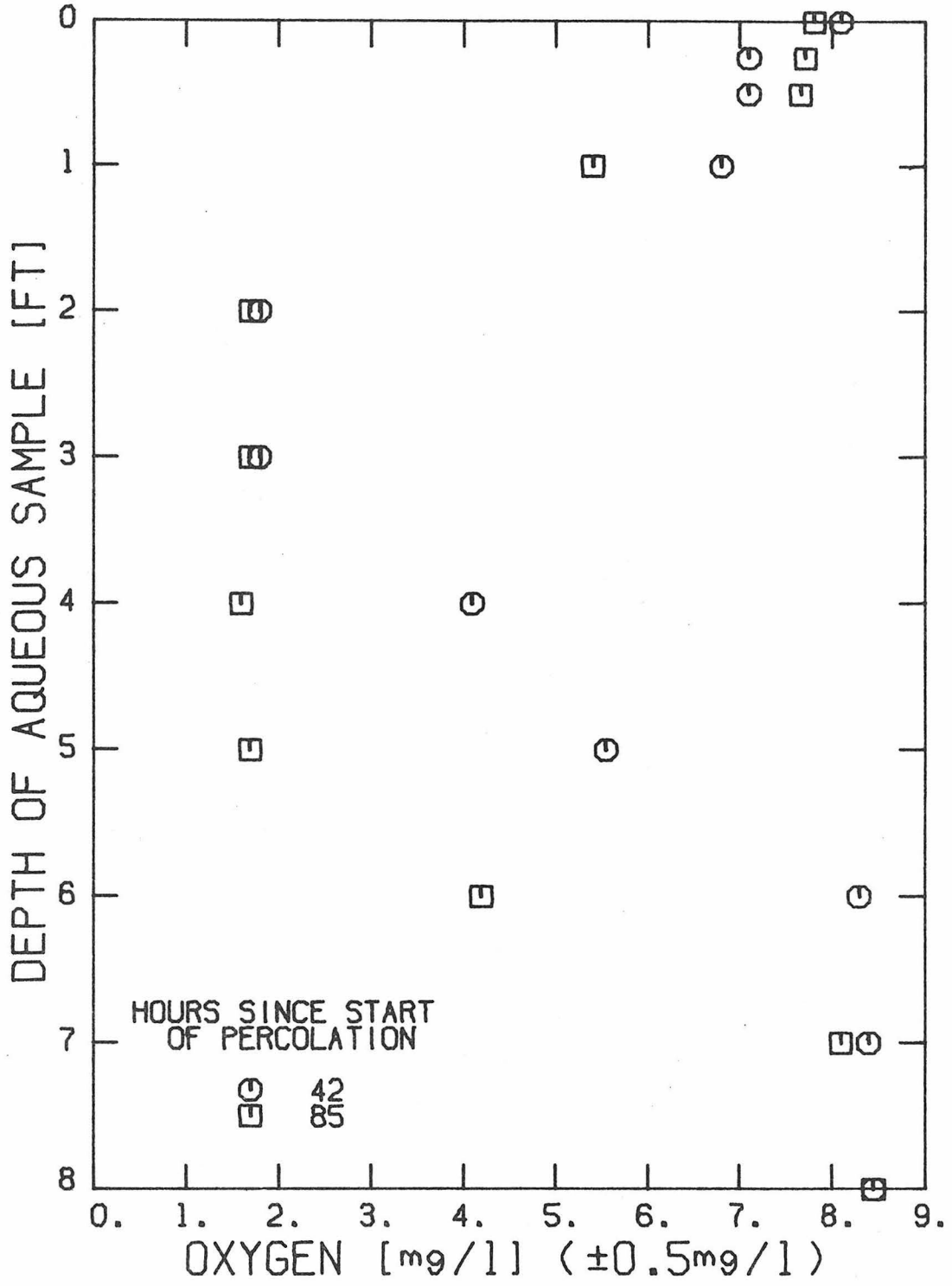

Figure 62: Dissolved Oxygen Content of Feed Solution Percolating through the Laboratory Column during the Second Wet Period

50 mℓ/hr for seven hours with 0.01 M barium chloride solution. The leachate was collected in one-hour batches and analyzed for magnesium, sodium, potassium, and calcium. The accumulative release rate of cations followed the trend previously observed with a rapid initial release of double layer cations and a slower final continuing release of chemisorbed cations. The chemisorbed desorption portion of the accumulative release curves was extrapolated back to the ordinate to determine the accumulative quantity of cations in the double layer. The results are plotted in Figure 63. Calcium is, by far, the most prominent adsorbed cation. Adsorbed magnesium tended to approach zero μeq/gm with depth, a fact which suggested that the magnesium ion exchange breakthrough curve had not traveled past the five-foot depth mark by the end of the second Wet Period. Adsorbed species on the sand prior to the second Wet Period did not include magnesium. The first and second Wet Periods were characterized by the column's sand adsorbing 1.6 μeq magnesium/gm thereby bringing the distribution of adsorbed cations on the sand in to closer equilibrium with the distribution of cations in the aqueous phase feed solution.

The second Wet Period has shown the percolating solution to lose its dissolved oxygen and ammonium ions and gain aqueous nitrate, calcium, and hydrogen ions. A close look at the quantitative data showed extensive nitrification was limited by the maximum aqueous oxygen concentration being 8 mg/ℓ. At least 80 per cent of the disappearing ammonium ions was adsorbed to the column's sand. Presumably the disappearance of dissolved oxygen was due to nitrification with production of 0.05 mM of nitrite ions and theoretically 0.08 mM of aqueous nitrate ions. No

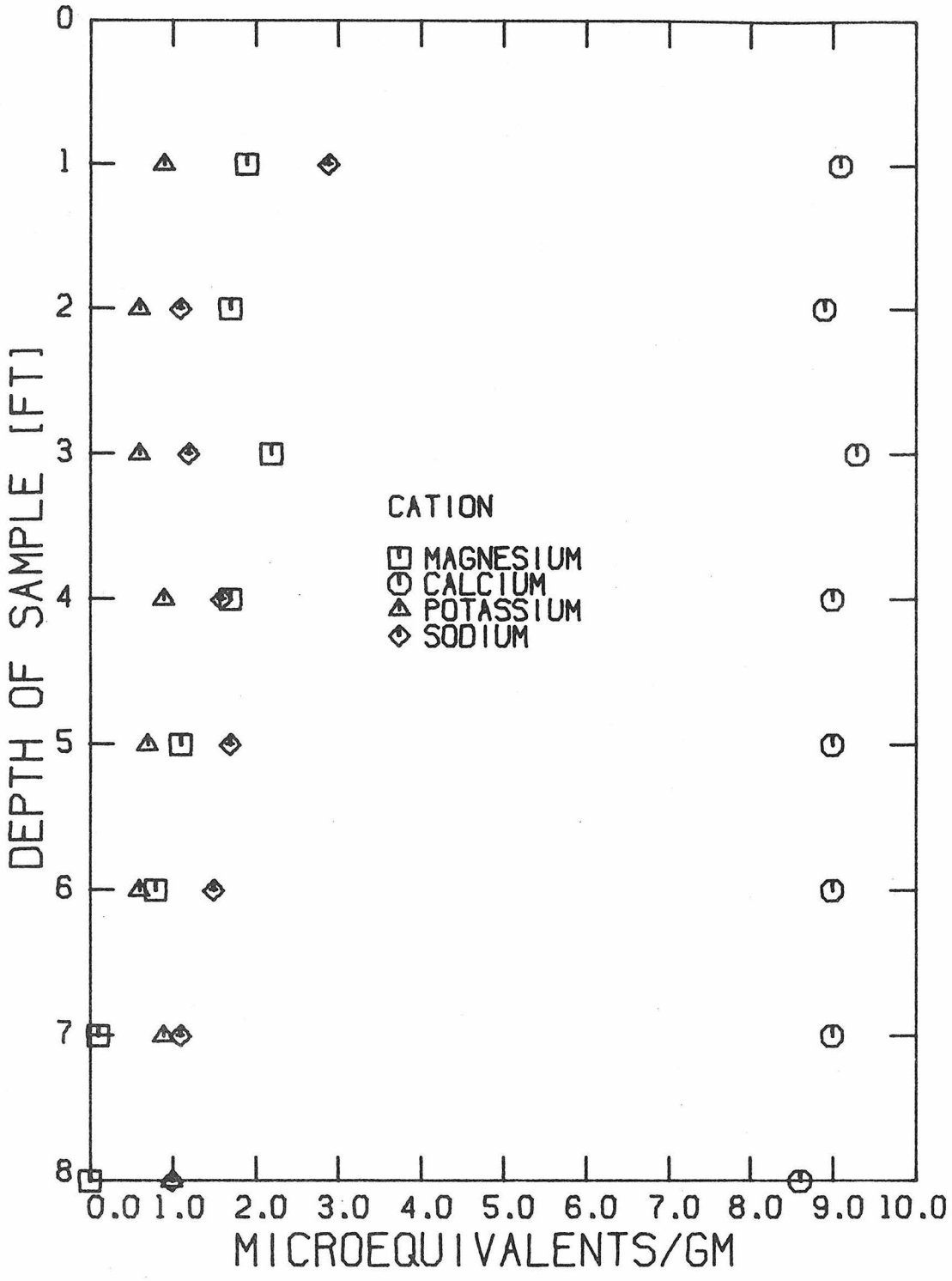

Figure 63: Quantity of Cations Extracted from Sand Samples Taken from the Laboratory Column at the End of the Second Wet Period

continuing large scale production of dissolved solids was observed.

Second Dry Period

The second Dry Period was initiated in the routine manner of permitting the column to drain of its solution in approximately 30 minutes and remain undisturbed for about two weeks with the top segment closure left open. Thirty-milliliter gas samples withdrawn from the 0.39 volume fraction of air in the column at three time intervals were analyzed for oxygen and carbon dioxide.

As previously observed, there was a consumption of gaseous oxygen and production of carbon dioxide (Figure 64). The total quantity of gas flowing through the top of the column would be the integral over time of the diffusivity (D) multiplied by the gas' concentration gradient at the entrance. The effective diffusivity of a gas in a porous media is approximately $0.69D$ (Edwards et al., 54). Because the diffusivity of oxygen in air is 0.69 ft^2/hr, approximately 9200 mg of oxygen were consumed in the laboratory column during the Dry Period. That amount of oxygen could be a potential reactant for nitrification of about 140 millimoles of ammonium ions. Because carbon dioxide diffusivity is 0.54 ft^2/hr, approximately 3000 mg of carbon dioxide were generated. Eleven millimoles of aqueous bicarbonate ions were consumed if the source of the carbon dioxide gas was the acidification of the interstitially held solution of 4 mM bicarbonate. The origin of the remaining carbon dioxide gas is not known.

Third Wet Period Start-Up

Consumption of gaseous oxygen and production of carbon dioxide

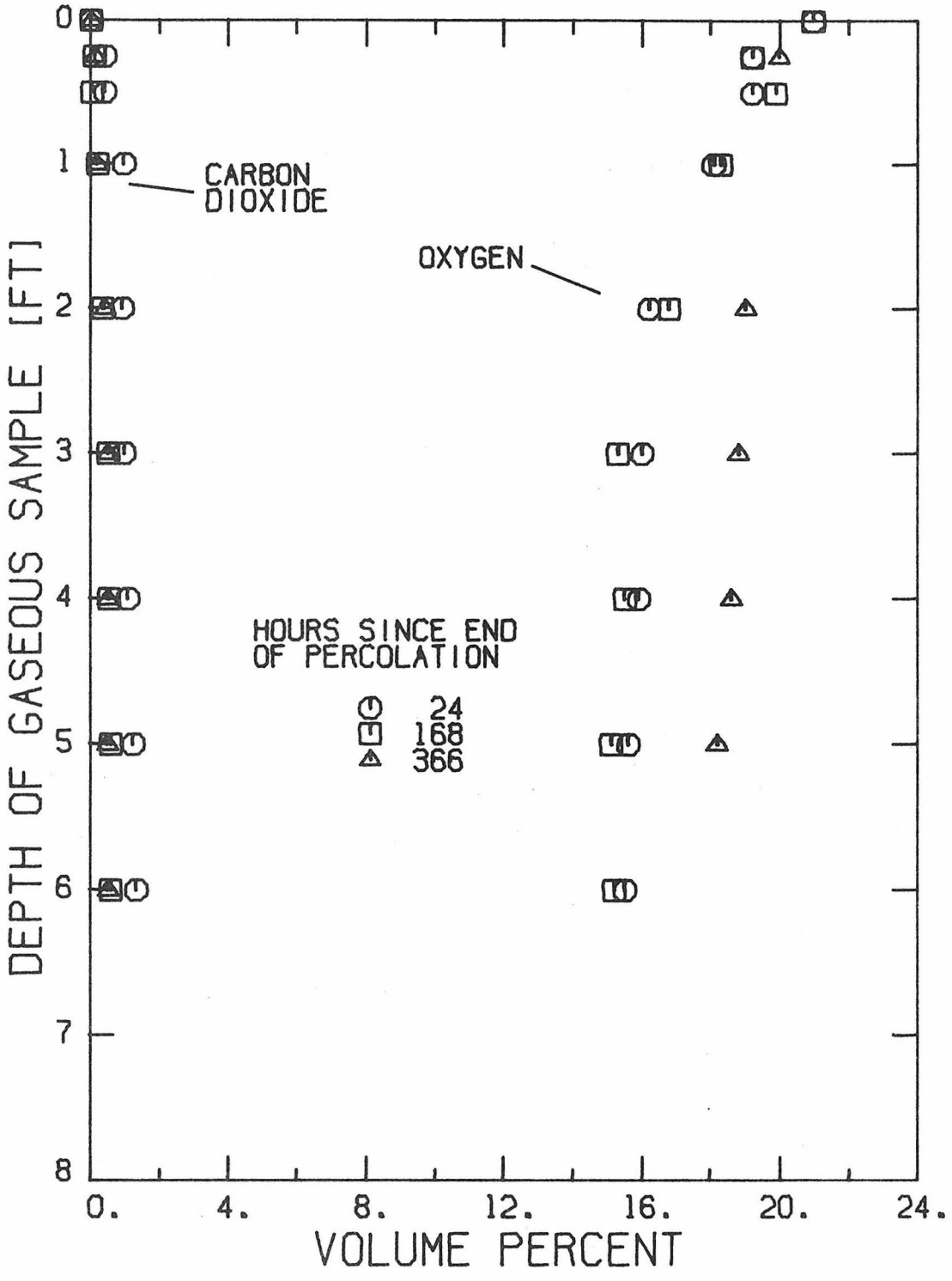

Figure 64: Carbon Dioxide and Oxygen Content of the Laboratory Column Atmosphere during the Second Dry Period

during the previous Dry Period implied the existence of a large amount of aerobic bacterial activity. To evaluate change in the composition of the 0.06 ± 0.02 volume fraction of interstitial solution surrounding the column sand during the Dry Period, the leading edge of solution initiating the third Wet Period was sampled as it reached progressively deeper down the column. Analysis of this leading edge would reflect on the actual constituency of the interstitial solution at the end of the previous Dry Period.

Exceptionally large quantities of dissolved cations were encountered by the leading edge (Figure 65). With an inlet calcium, magnesium, sodium, and potassium content of 48, 15.2, 113., and 11.2 mg/ℓ, the leading edge of the newly infiltrating solution peaked at 235, 52, 158, and 15 mg/ℓ for the same respective cations. The Whittier Narrows data of Reid (5) show that an inlet solution of aqueous calcium, magnesium, sodium, and potassium content respectively of 47 ± 2, 12 ± 1, 112 ± 2, and 10 ± 1 mg/ℓ would have acquired peak concentrations respectively of 135 ± 10, 40 ± 10, 178 ± 5, 16 ± 2 mg/ℓ at the four-foot mark. The ammonium ion content of the leading edge fell practically to zero by the first foot of travel. At Whittier Narrows the inlet aqueous ammonium ion content dropped from 20 ± 5 mg/ℓ to 3 ± 3 mg/ℓ by the second foot of percolation. Nitrate ion content, however, rose to 218 mg/ℓ (Figure 66), compared to 500 ± 50 mg/ℓ at Whittier Narrows. Lance (67) and Lance et al. (7) reported a 50 mg $NO_3^-(N)/ℓ$ move out of a soil column irrespective of the duration of their Dry Period. Pincince (6) measured a solution wave of 50 mg $NO_3^-(N)/ℓ$ in his soil column. The same author measured the concentration of nitrate

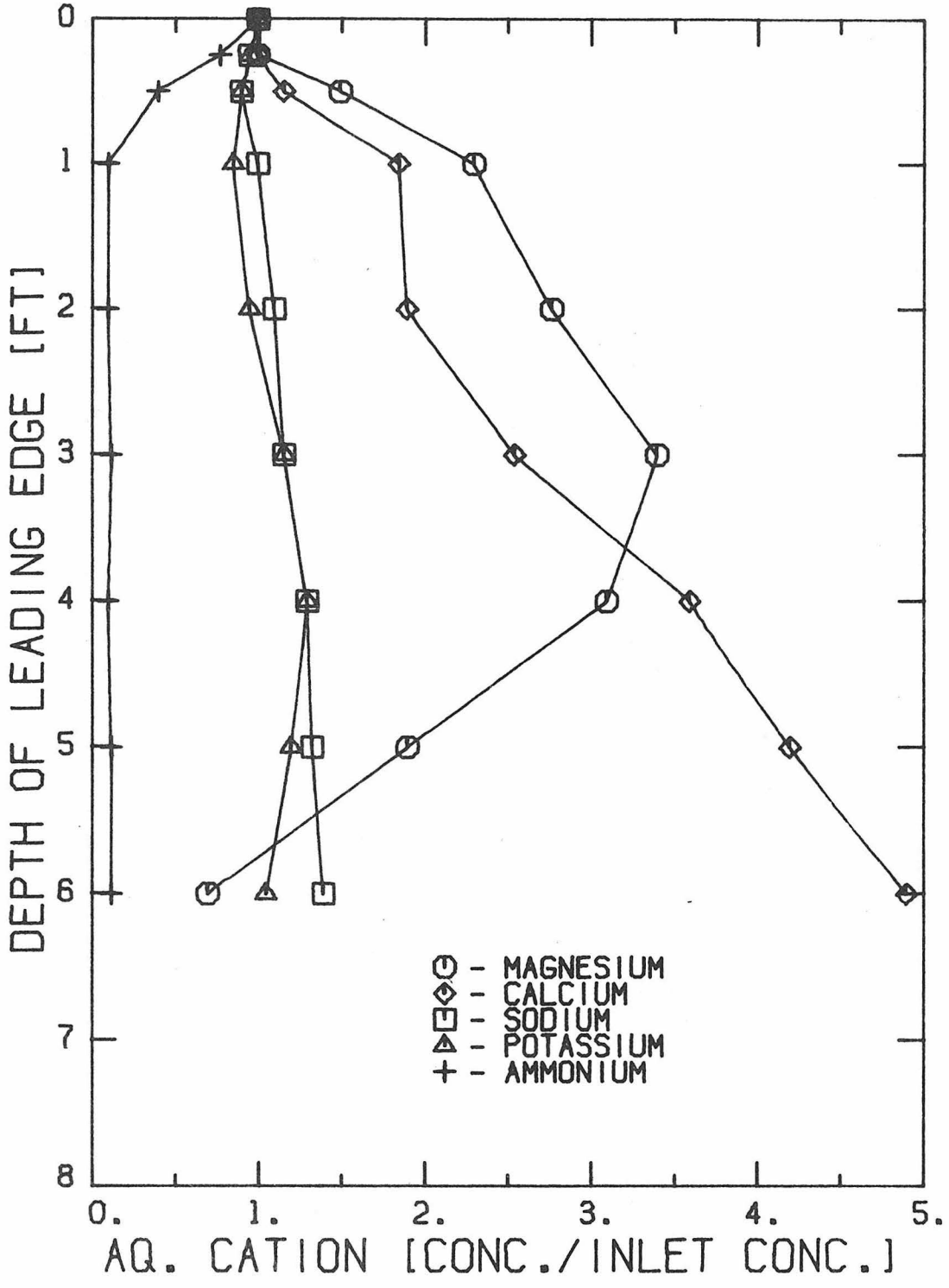

Figure 65: Aqueous Cation Concentrations in the Leading Edge Solution Starting the Third Wet Period

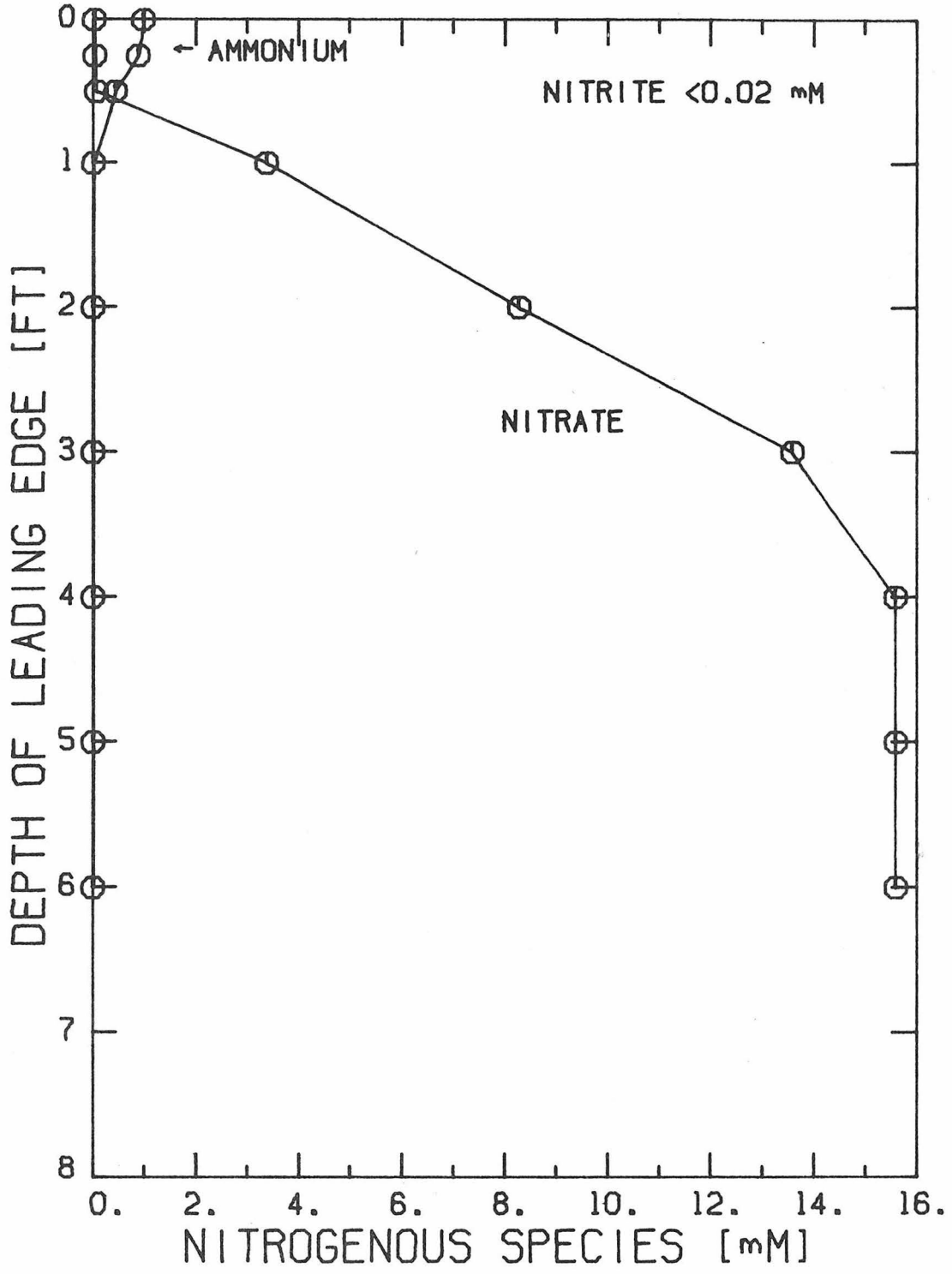

Figure 66: Aqueous Inorganic Nitrogen Species Concentrations in the Leading Edge Solution Starting the Third Wet Period

ions in the interstitial water at the Whittier Narrows test plot as 40 mg NO_3^-(N)/ℓ 14 hours into the Dry Period. The leading edge became more and more acidified as it increasingly gained the chemical characteristics of the column's interstitial solution (Figure 67). The pH of the leading edge at Whittier Narrows is, within experimental uncertainty, equal to that of the laboratory column. Silica content (Figure 68) rose to 6.9 mg/ℓ by the time the feed solution reached the six-foot mark.

During the first week, at least, of the Dry Period ammonium ions adsorbed to the minerals and contained in the 0.06 ± 0.02 volume fraction of solution surrounding the sand were nitrified by bacteria; hence, the consumption of gaseous oxygen during the Dry Period. Considering only the top six feet of the laboratory column, the total amount of nitrate ions produced was 31 millimoles. Because there were negligible quantities of aqueous nitrite ions generated, a total of 31 millimoles of ammonium ions must have been consumed during the Dry Period. The amount of ammonium ions in the interstitial solution at the start of the Dry Period was 1.2 millimoles based on the analysis of the ammonium ion content of the percolating solution at the end of the third Wet Period. The remaining ammonium ions have to have been adsorbed to the column's sand--0.62 μeq/gm of ammonium ions were therefore desorbed from the sand and nitrified. Note that the amount of gaseous oxygen consumed during the Dry Period could have been enough to convert a total of 140 millimoles of ammonium ions. Because 31 millimoles of nitrate ions were generated, then 62 millimoles of aqueous hydrogen ions must have been the byproduct of nitrification. Sixty-two

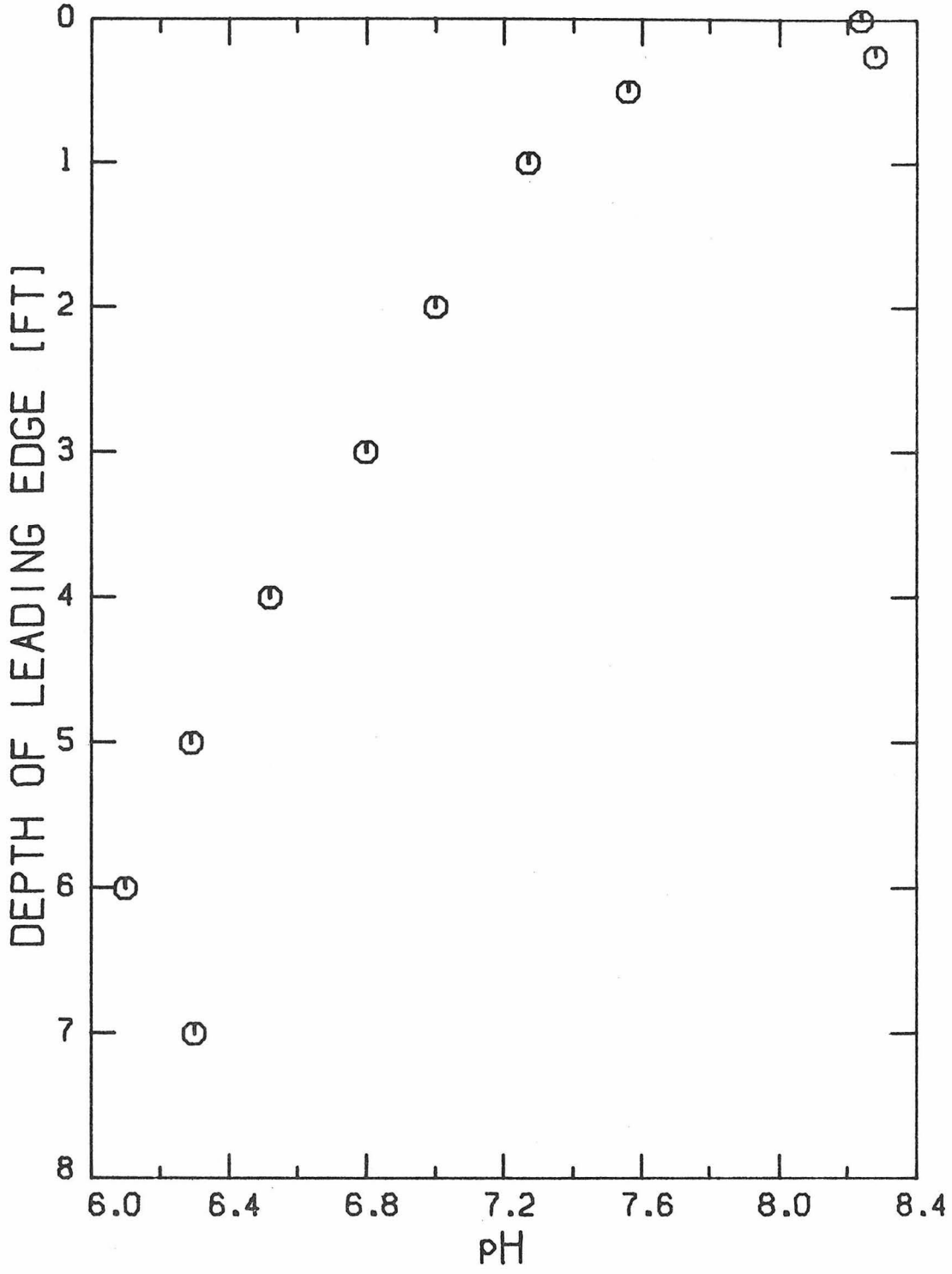

Figure 67: pH of the Leading Edge Solution Starting the Third Wet Period

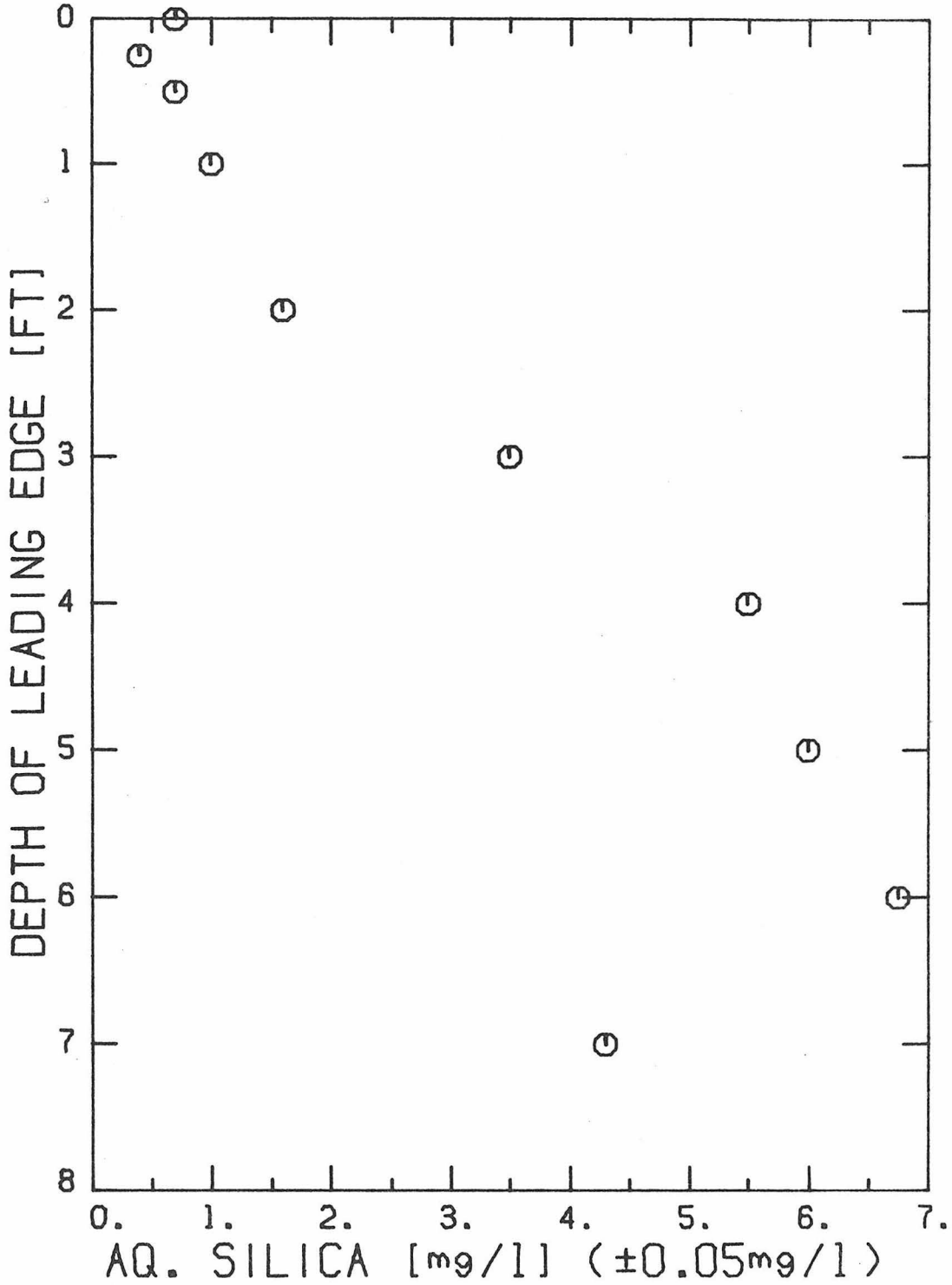

Figure 68: Aqueous Silica Content of the Leading Edge Solution Starting the Third Wet Period

millimoles of hydrogen ions is far and beyond the 8.3 millimole bicarbonate ion capacity to buffer the interstitial solution. The pH of the interstitial solution would have fallen to less than 2 during the Dry Period if it were not for the fact that hydrogen ions ion exchanged with cations on the sand. The average formula of the aluminosilicate minerals has 0.7 moles of calcium, magnesium, sodium, and potassium per mole of silica. The aqueous silica concentration of 0.11 mM implies essentially that only 0.08 mM of cations could have been released in the total destruction of the aluminosilicate minerals. The 31 milliequivalents of cations appearing in the interstitial solution were desorbed by 31 milliequivalents of aqueous hydrogen ions; the vacancy of 31 milliequivalents of adsorbed ammonium were taken up by the remaining aqueous hydrogen ions produced by bacterial nitrification. The net result was a near neutral solution of pH 6.2 and sand with 1.24 μeq/gm of its adsorbed ammonium, calcium, magnesium, sodium, and potassium replaced by hydrogen ions. The downward deflection of the concentration of aqueous magnesium ions in the leading edge profile is the strongest suggestion that the high concentration of aqueous magnesium ions in the interstitial solution originates not by dissolution of the column's minerals but by desorption of adsorbed cations from the mineral surfaces. Figure 63 has shown that below the three-foot mark in the column, sand was deficient of adsorbed magnesium ions; therefore, the interstitial solution in the same region of the column did not gain a large amount of magnesium ions during the Dry Period ion exchange of aqueous hydrogen ions (Figure 65). The 0.06 volume fraction of interstitial solution surrounding the sand at the beginning of the Dry

Period contained 7 mM of dissolved salts, half of which were in the form of bicarbonates and one-third were hardness salts; at the end of the Dry Period the same interstitial solution contained twice as much salts, most of which were nitrates and half were hardness salts. The newly infiltrating solution intercepted the interstitial solution and took on its characteristics. The above mechanism presumably is the mechanism for the major proportion of hardness and total dissolved solids appearing in the samples taken at Whittier Narrows. The aqueous nitrate ion content at Whittier Narrows, however, indicates that about four times more ammonium ions were nitrified than in the laboratory column.

Third Wet Period Continued

Once the leading edge of solution reached the column's base, the flow was set at 11.1 ℓ/day. During the one week of percolation, three solution sampling series were taken and analyzed. Because the sand had been forced to adsorb 1.2 μeq of hydrogen ions per gram sand from a solution of pH 6.2, it was natural that during the percolation of solution of pH 8.3 the sand would desorb hydrogen ions. Hydrogen ion desorption manifested itself as a pH change with depth of the percolating solution (Figure 69). pH at the Whittier Narrows test basin (Reid, 5) dropped from 7.1 to 6.5 after two feet of percolation 29 ± 9 hours after the start of the Wet Period. By the end of the Wet Period, the drop was only from 7.1 to 6.8. The change of pH reflected a rate of release of aqueous hydrogen ions into the bicarbonate buffered solution of 0.37, 0.25, and 0.11 millimoles of hydrogen ions per liter·foot

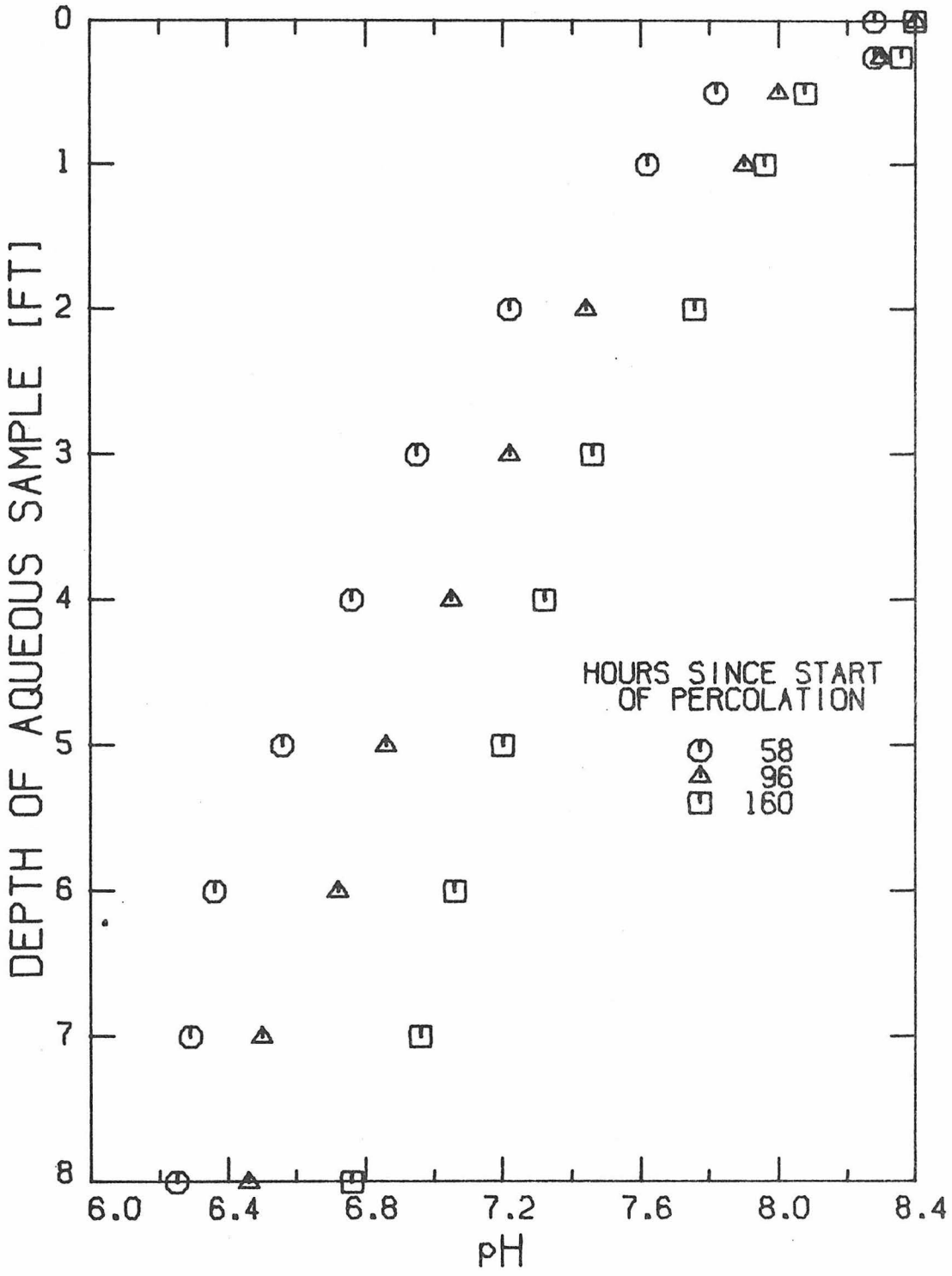

Figure 69: pH of Feed Solution Percolating through the Laboratory Column during the Third Wet Period

for the 58-, 96-, and 160-hour profiles, respectively, in the top six feet of the sand column. An average 2.5 ± 0.1 μeq/gm was desorbed throughout the six-foot length of the column during the seven days of the run. The desorption of aqueous hydrogen ions should be matched by an adsorption of an equivalent amount of other cations. Magnesium and potassium concentration profiles (Figure 70) contain breakthrough curves that represent an average adsorption of 0.5 μeq K^{+}/gm and 1.2 μeq Mg^{++}/gm. At Whittier Narrows there was no hint of ion exchange of incoming aqueous alkali ions for adsorbed hydrogen ions. The concentration of dissolved oxygen in the percolating solution (Figure 71), as at Whittier Narrows, limits the nitrification of aqueous ammonium ions to 0.1 mM; therefore, the minimum amount of ammonium ions that were adsorbed by the column's sand was 0.7 μeq/gm (Figure 72). At Whittier Narrows the percolating solution's ammonium ion content at the two-foot mark started at 3 ± 3 mg/ℓ at the start of the Wet Period but tended to rise to 6 ± 5 mg/ℓ after a week of percolation. Rather than having one breakthrough curve, the aqueous proton lost the trait of having a breakthrough curve due to its being desorbed at various zones in the column in response to the different locations of the breakthrough curves of three different cations.

The first quantitative measure of both Nitrosomonas and Nitrobacter was made on the last day of the third Wet Period. Sand samples were agitated in 40 mℓ of deionized water. The water was then plated on silica gel, and bacterial counts were made one month later. Cell population counts for both nitrifiers were approximately 2×10^{4} cells/gm sand throughout the column's length. Positive population counts

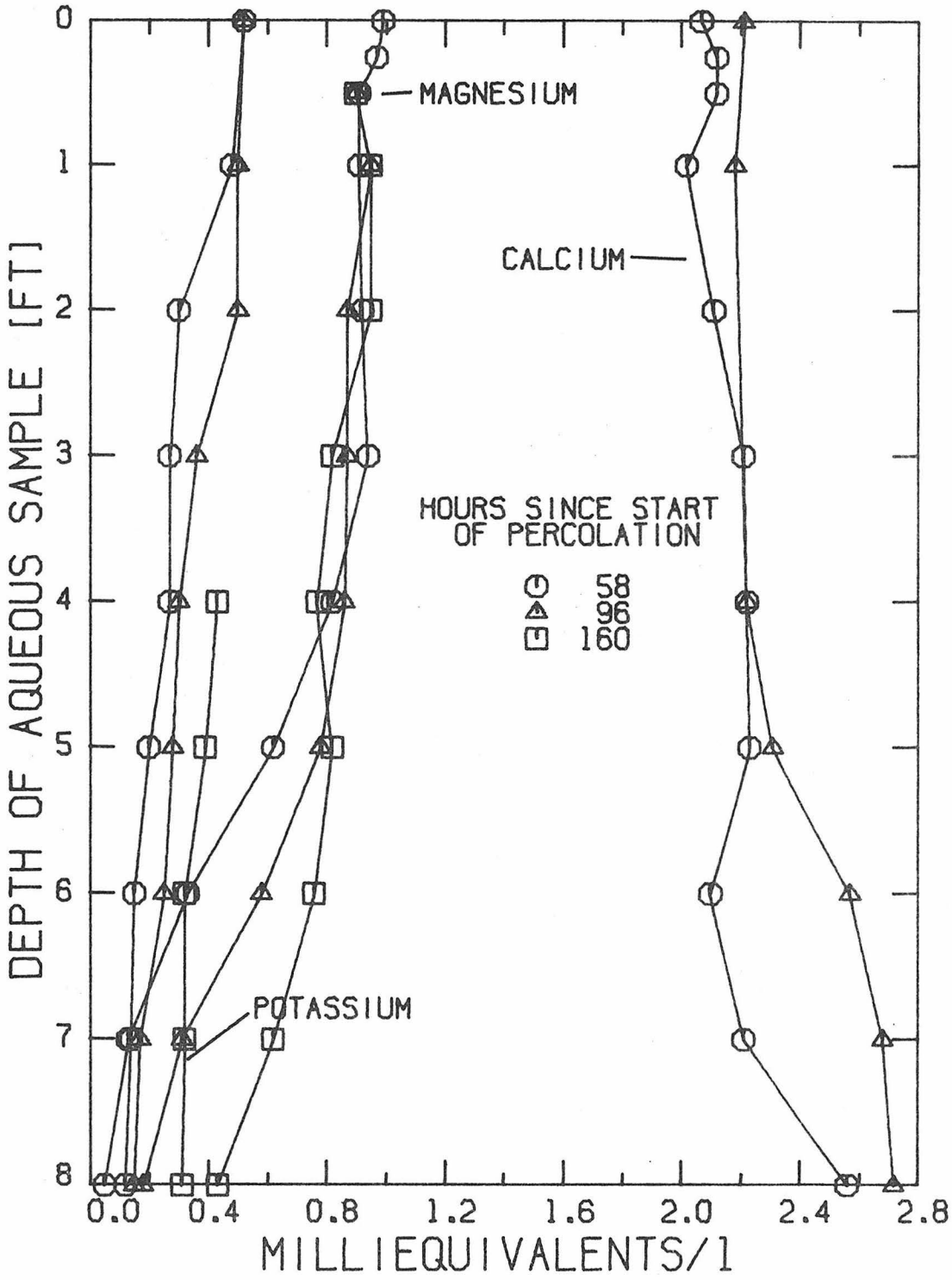

Figure 70: Aqueous Potassium, Magnesium, and Calcium Ion Content of Feed Solution Percolating through the Laboratory Column during the Third Wet Period

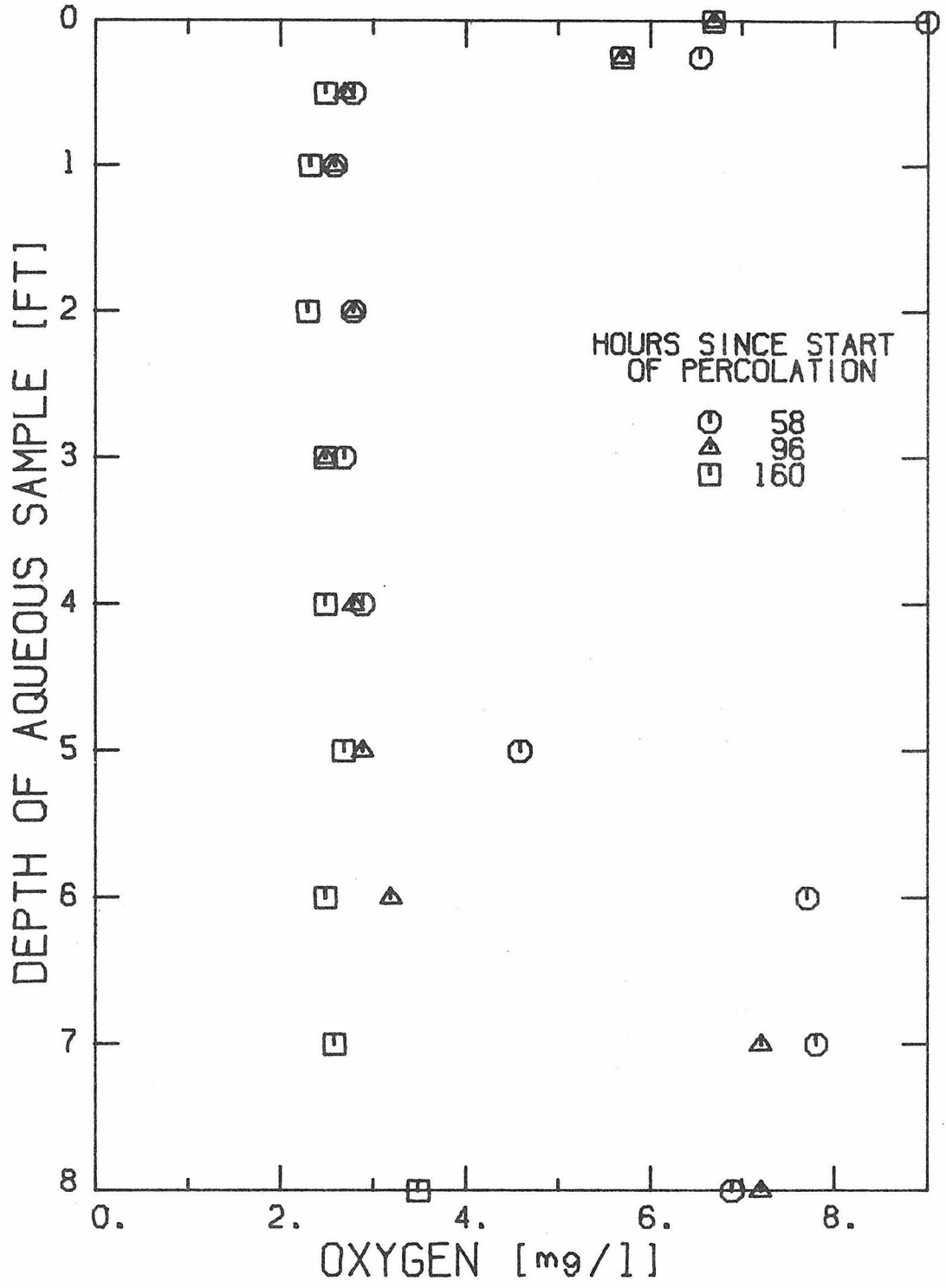

Figure 71: Dissolved Oxygen Content of Feed Solution Percolating through the Laboratory Column during the Third Wet Period

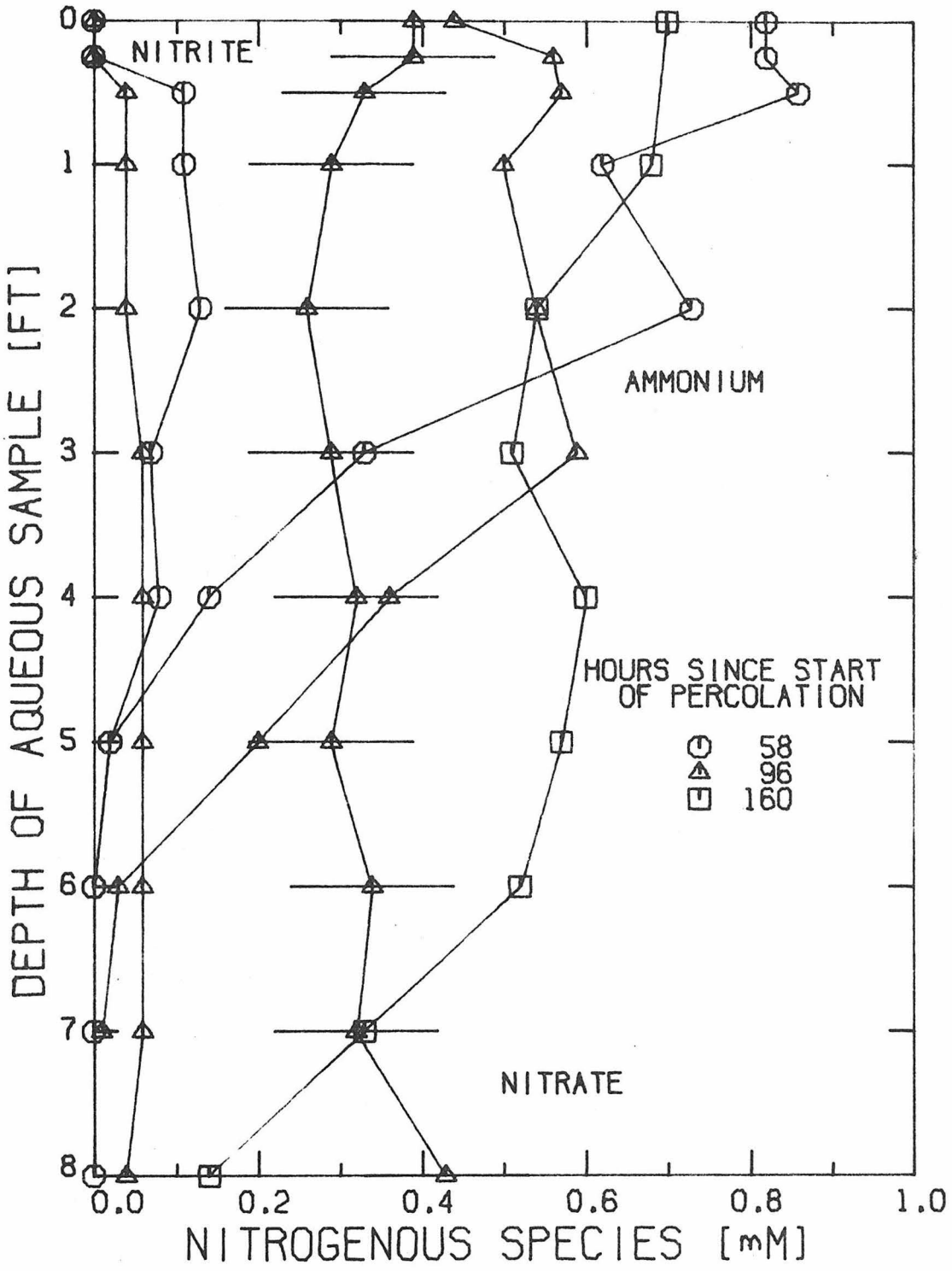

Figure 72: Aqueous Inorganic Nitrogenous Species Content of Feed Solution Percolating through the Laboratory Column during the Third Wet Period

of nitrifying bacteria reinforce the assumption of their being responsible for the nitrification of aqueous ammonium ions.

The third Wet Period permitted a theory that was held up in later tests to be presented. The column contains no relatively readily soluble minerals. A high Total Dissolved Solids content, however, was experienced. Nitrification of adsorbed ammonium ions on the sand during drying periods, when oxygen is readily available, causes a high concentration of nitrates in the interstitial solution. Aqueous hydrogen ions, produced by nitrification, exchange with other cations on the sand to yield an interstitial solution of concentrated nitrate salts. Newly infiltrating solutions displace the interstitial solution and acquire a temporarily high Total Dissolved Solids content. Subsequent percolation has only a slight increase, with depth, of Total Dissolved Solids; however, throughout the one week Wet Period aqueous hydrogen ions are desorbed from the sand and aqueous ammonium, magnesium, potassium, and possibly calcium and sodium are adsorbed, giving the appearance of extensive nitrification. If the Wet Period were extended in time, eventually ion exchange reactions would cease and the only change of the composition of the percolating solution would be the conversion of approximately 0.1 mM of aqueous ammonium ions to nitrate ions and 0.2 mM of hydrogen ions. A solution buffered with aqueous bicarbonate ions would show little change of pH.

Fourth Wet Period Leading Edge

A more accurate evaluation of the aqueous species in the column's interstitial Dry Period solution was accomplished. Previous

investigations used the chemical composition of the leading edge of the feed solution as an indicator of the chemical composition of the column's interstitial solution. There was no way to determine how much of the sample came from interstitial water and how much came from the percolating solution. To avoid this mixing problem, the present Dry Period was ended by percolating deionized water into the column and sampling its leading edge. The aqueous chloride ion content of the leading edge solution was used to determine how much of the leading edge solution originated from the invading solution and how much was interstitial water which already contained a known concentration of aqueous chloride ions from the previous Wet Period. In addition to cations and nitrate, bicarbonate ions were analyzed in the leading edge to confirm their having been acidified to carbon dioxide gas during the Dry Period. The known aqueous chloride ion content in the interstitial water and that of the infiltrating solution was used to correct for dilution of the dissolved salts in the interstitial water by the incoming solution so that the actual concentration of various aqueous species in the interstitial solution at the end of the Dry Period could be known.

Aqueous chloride content of the leading edge solution shows that three to four feet of travel was required for the chemical composition of the leading edge solution to represent the composition of the interstitial water. A depth error of ±1.5 feet should be placed on all data of the chemical composition of the interstitial solution. Data show (Figure 73) there to have been 160 mg Ca^{++}/ℓ in the interstitial water at the end of the Dry Period. This concentration increase over

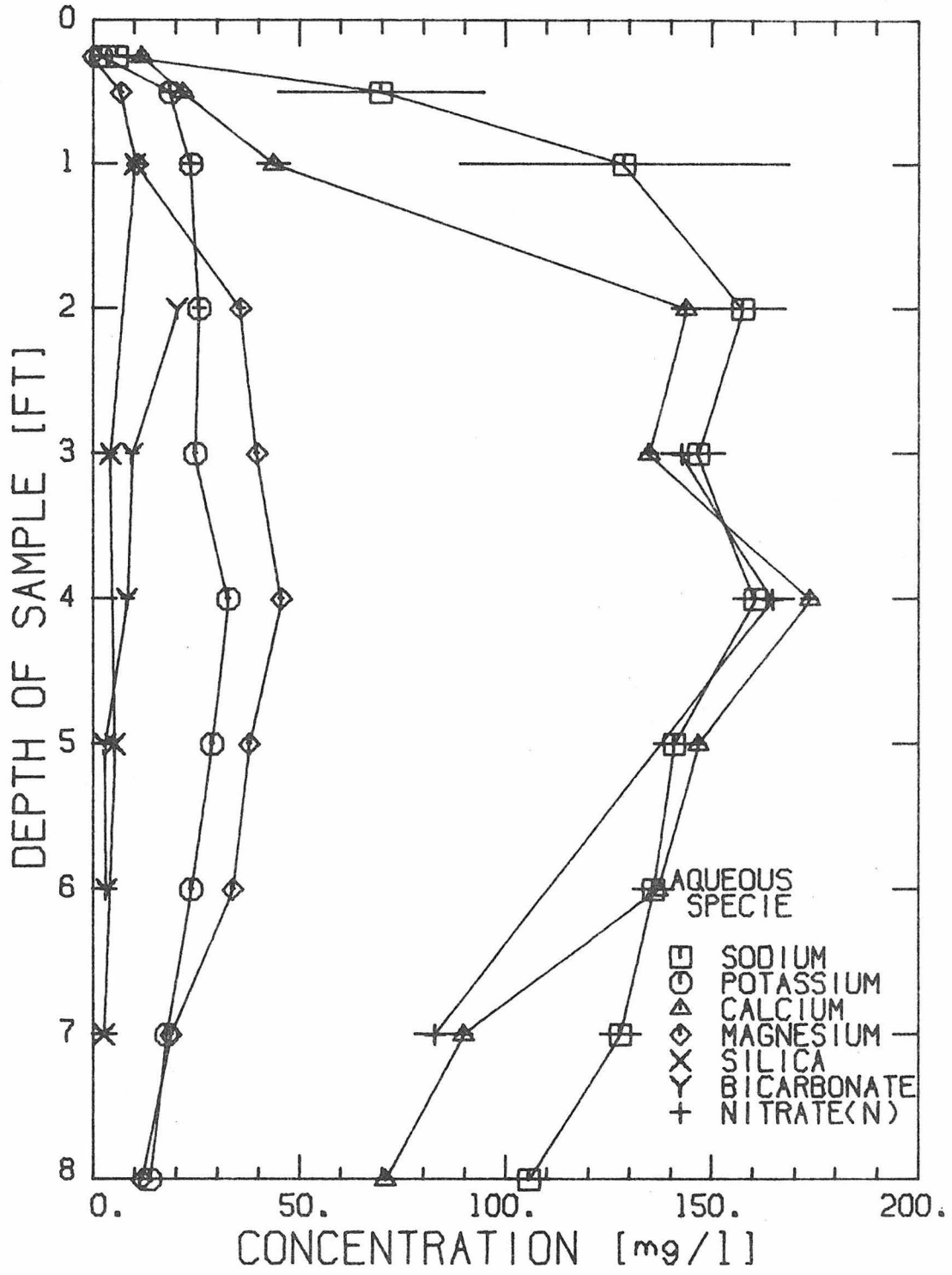

Figure 73: Aqueous Species Content of the Interstitial Solution of the Laboratory Column at the End of the Third Dry Period

40 mg Ca^{++}/ℓ represents a release of 0.23 μeq Ca^{++}/gm sand. Magnesium, sodium, and potassium ions were extracted from sand into the 0.06 volume fraction of interstitial water to the extent of 0.07, 0.06, and 0.02 μeq/gm, respectively. The aqueous silica concentration averaged to 0.15 millimoles SiO_2/ℓ; therefore, the 5.5 mM solution of cations is composed of very few cations from the actual destruction of aluminosilicate crystals. Appearance of aqueous nitrate ions implied that 0.42 μeq NH_4^+/gm had been consumed by nitrifying bacteria to generate a 21.4 mM hydrogen ion interstitial solution. The aqueous bicarbonate ion concentration, as expected, fell from 4.1 mM to 0.2 mM. Whittier Narrows data show that with an initial aqueous bicarbonate ion concentration of 235 ± 15 mg/ℓ, the approximate concentration of bicarbonate ions in the interstitial solution at the two-foot mark was approximately 184 ± 20 mg/ℓ. The bicarbonate ions were a sink for 3.9 millimoles H^+/ℓ. The remaining 17.5 millimoles H^+/ℓ were adsorbed to the sand as 0.8 μeq H^+/gm thereby leaving behind a near-neutral interstitial solution with 17.5 milliequivalents/ℓ of newly acquired cations.

Fifth Wet Period Bacterial Population Count

Before the end of the fifth Wet Period, a bacterial population count was made. Sand extracted from the laboratory column was agitated in 50 mℓ of deionized water. Ten mℓ of the water was diluted to 50 mℓ and 100 μℓ was plated. Plating was done on nitrite and ammonium ion containing silica gel. Also, nutrient agar plates were prepared to determine the population of heterotrophic bacteria. Final cell counting was made 12 days after the solutions were plated. The base ten

logarithm of the number of viable bacterial cells per gram of dry sand was:

Depth	Nitrobacter	Nitrosomonas	Heterotrophs
1	3.9	4.1	6.6
2	3.8	-	6.2
3	3.9	3.6	6.2
4	4.1	3.9	6.2
5	4.6	3.8	6.2
6	4.2	3.8	6.1
7	4.2	4.0	6.1

Despite the lack of organic carbon in the feed solution, there was still a large heterotrophic bacterial population in the column. Because they must have organic carbon as an energy and carbon source, these bacteria have been living off the carbon produced from the nitrifying bacteria.

Extensive Dry Period Analysis

A thorough study of the laboratory column's gaseous oxygen and carbon dioxide atmosphere was made with ten gas samplings during the 14-day Dry Period. Gas samples at the seven- and eight-foot depths could not be taken because solution had accumulated below the six-foot depth when the column's base was closed to prevent small amounts of air from entering. Gas sampling began just three hours after the column had its usual one-hour drainage. Sampling continued to within eight hours of the termination of the two-week Dry Period.

Just three hours after the start of the Dry Period there was noticeable change to the gaseous atmosphere (Figures 74 and 75). The maximum deflections in the depth profiles occurred 24 to 48 hours after the start. After 48 hours, the concentration profiles of oxygen and carbon dioxide relaxed toward their atmospheric levels. A much larger oxygen consumption was reported at Whittier Narrows by Pincince (6).

As a first order approximation for the Dry Period gaseous atmosphere, it was assumed that the chemical reaction causing changes to gaseous oxygen and carbon dioxide came only from the nitrification reaction. The equation governing the concentration profiles of oxygen and carbon dioxide is of the form

$$D \frac{\partial^2 c}{\partial z^2} = \frac{\partial c}{\partial t} + r \tag{49}$$

where r is a constant reaction rate term. In the top six feet of the column, approximately 32 millimoles of aqueous nitrate ions were produced; therefore, 64 millimoles of oxygen were consumed and 64 millimoles of carbon dioxide were generated. The data show that after approximately two days the profiles of both gases relaxed, an indication that nitrification reactions ended. For the first mathematical approximation it is assumed that nitrification proceeds at a constant rate throughout the column for a specific period of time. The steady state solution for the above equation is

$$c(z) = c_{atm} + \frac{r}{D}\left(\frac{z^2}{2} - Lz\right) \tag{50}$$

where c_{atm} is the atmospheric concentration of the gas and L is the length of the column. A plot of $c(z) - c_{atm}$ versus $z^2/2 - Lz$ will

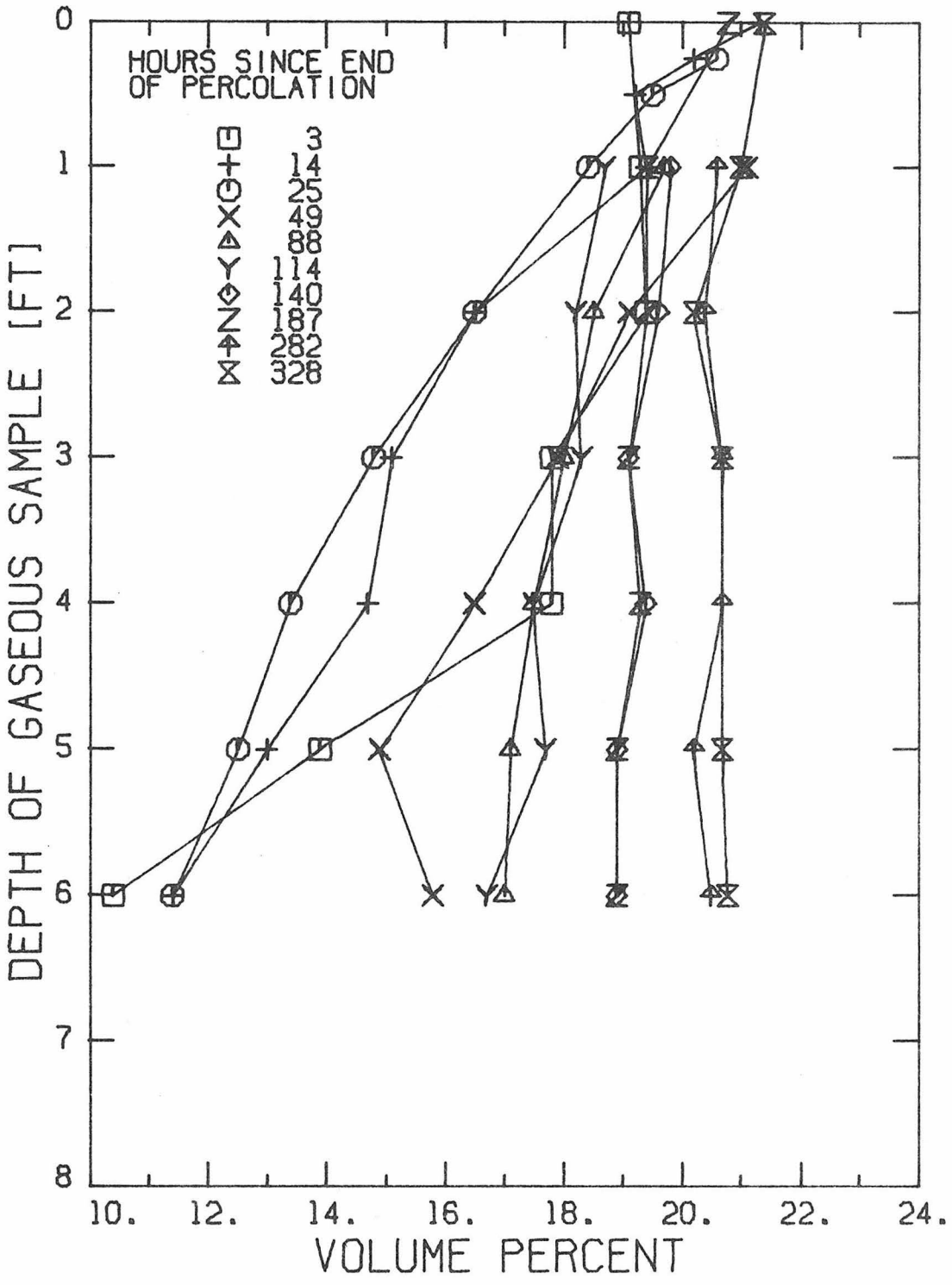

Figure 74: Oxygen Content of the Laboratory Column Atmosphere during a Fourteen Day Duration Dry Period

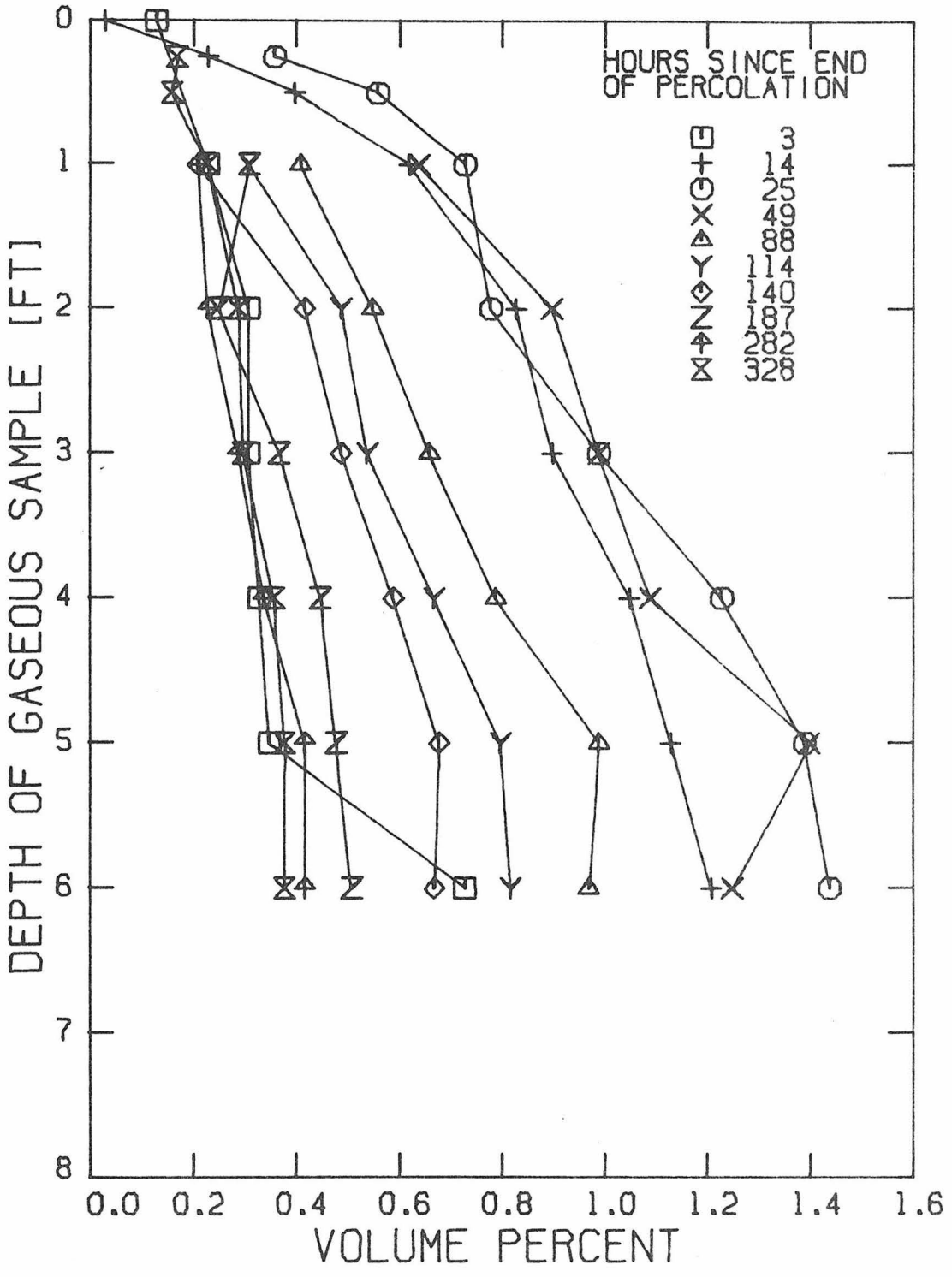

Figure 75: Carbon Dioxide Content of the Laboratory Column Atmosphere during a Fourteen Day Duration Dry Period

produce a straight line of slope, r/D, if the concentration profile, c(z), depicts a gaseous system at steady state. Data for the 25-hour concentration profiles were plotted according to the steady state equation and, within a five percentage concentration uncertainty, gave a straight line. The rate constants were -82 mg $O_2/ft^3 \cdot hr$ and 14 mg $CO_2/ft^3 \cdot hr$. Considering the total change of oxygen and carbon dioxide in the column, the reaction period would have to be 55 hours. The unsteady state diffusion equation was solved numerically and is plotted with the appropriate elapsed time (hours) labels (Figure 76).

A boundary condition of the column's gaseous atmosphere required that the gaseous concentration gradient be zero at the base of the column. The experimental data show that the slope of the gaseous concentration gradients are not zero at six feet; the base of the column's gaseous atmosphere must be below six feet but above seven feet (solution filled the column up to at least the seven-foot mark). The initial condition for the mathematical model is a gaseous concentration equal to that of the atmosphere throughout the column's length. A completely different initial condition exists at the start of the Dry Period. The three-hour profile showed that the gaseous concentration gradients at depths in the column became increasingly more disturbed by the bacterial activity. Apparently very fast bacterial reactions changed the gaseous composition even as it was being pulled into the column by the downward draining solution. Very rapid bacterial activity was observed by Pincince (55) when he found that substantial nitrification had occurred in just 30 minutes. The unsteady state gaseous profiles are typified by a zero concentration gradient of gases deep

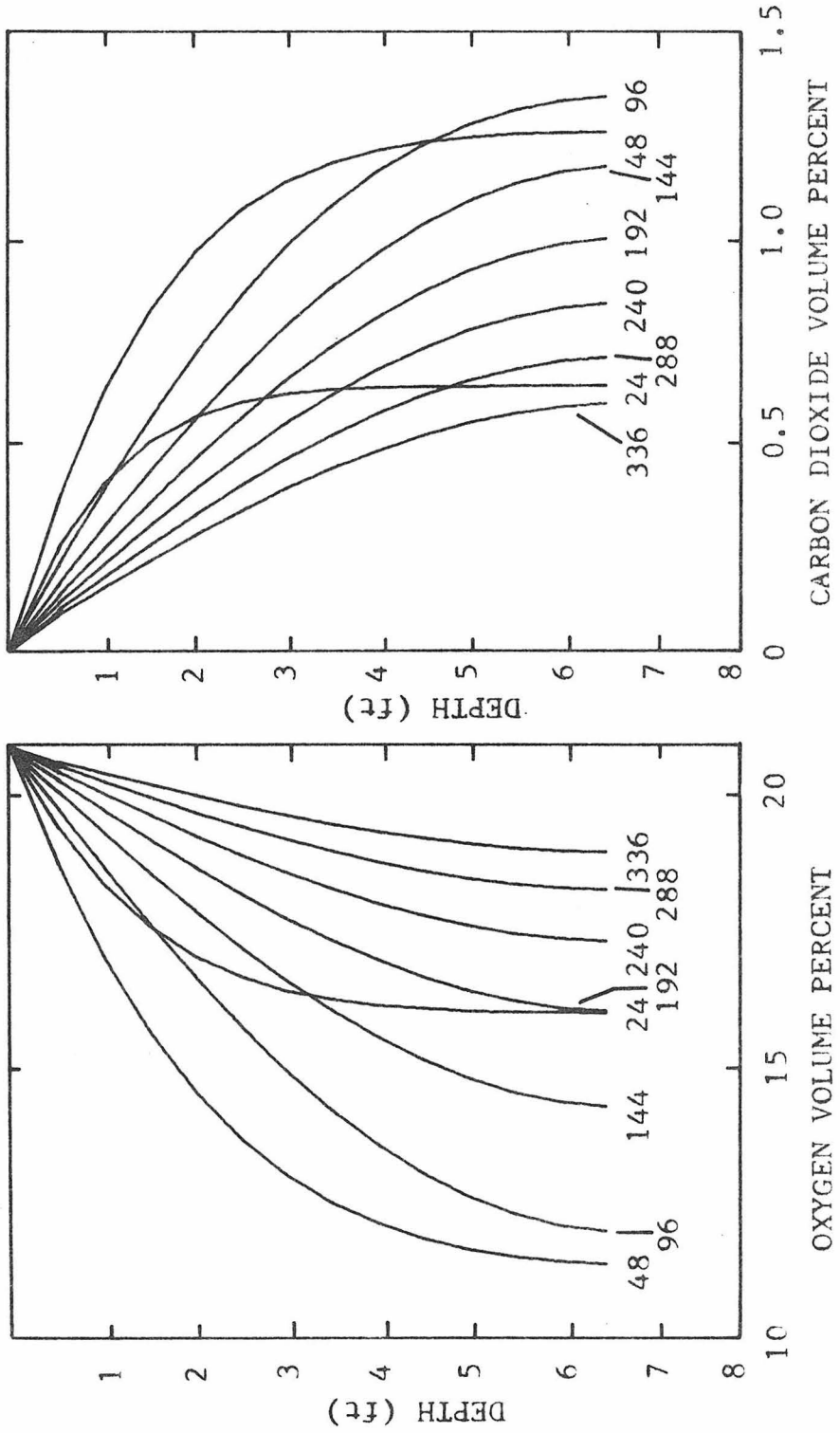

Figure 76: Theoretical Oxygen and Carbon Dioxide Contents of the Laboratory Column Atmosphere during a Dry Period

in the column where $r >> D\partial^2 c/\partial z^2$. Experimental concentrations do not show a zero concentration gradient zone; apparently the initial gaseous composition of the column had obliterated it. The graphical evaluation of

$$\int_{t=0}^{t=328} D \left.\frac{\partial c}{\partial z}\right|_{z = 1 \text{ foot}}$$

for the experimental gaseous data gives the quantity of gas passing through the column's one-foot depth mark. Throughout the Dry Period, 6000 ± 500 mg O_2 diffused into the column and 960 ± 90 mg CO_2 diffused out. The maximum quantity of nitrate ions generated during the Dry Period would require only 2050 mg of oxygen. The quantity of bicarbonate ions in the interstitial solution could release only 360 mg of carbon dioxide gas. The excess 4000 mg of oxygen and 600 mg of carbon dioxide is attributed to the millions of heterotrophic bacteria per gram of sand consuming the organic carbon byproducts of the nitrifiers (Lance et al., 7).

Consistency Check

A check was made to insure that a high cation content of a newly infiltrating solution was a consistently occurring phenomenon. The column was permitted two Wet Periods and two Dry Periods. Solution samplings were taken from the leading edge of newly infiltrating solutions for both Wet Periods. Both samplings were analyzed for aqueous calcium, magnesium, sodium, and potassium ions.

The results are plotted (Figure 77) in dimensionless form by dividing the concentration of a given aqueous species by its

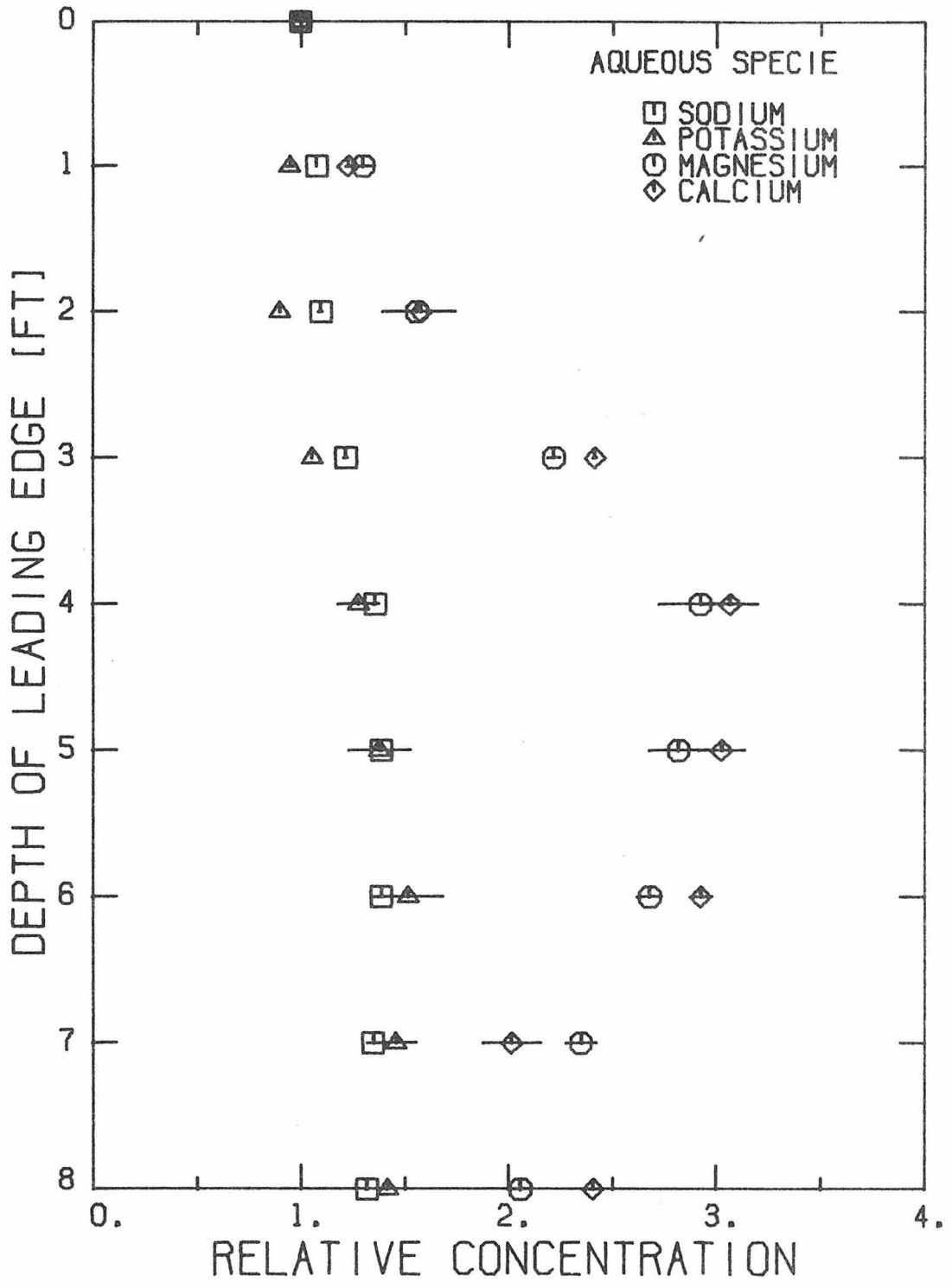

Figure 77: Aqueous Cation Content of Leading Edge Solutions Starting Two Separate Wet Periods

concentration in the feed solution. The feed solution concentration of calcium, magnesium, sodium, and potassium ions was 40 ± 2, 12 ± 1, 120 ± 10, and 6 ± 1 mg/ℓ, respectively. Calcium ions were consistently the most prominent additive to the leading edge solution. There was an increasingly larger addition of aqueous calcium ions to the infiltrating solution until the four- to six-foot depths were reached whereafter the calcium ion content of the solution dropped off. Aqueous sodium and magnesium ions were the next most conspicuous additives. Their additions reach a maximum also at the four- to six-foot mark. The drop of cation concentrations in interstitial water below the six-foot depth in the column is attributed to a lack of nitrification due to a lack of oxygen there caused by flooding.

Total Quantity of Aqueous Species in Interstitial Solution

Estimates of the total quantity of aqueous species in the column's interstitial solution at the end of the Dry Period have been determined by multiplying the concentration of the various aqueous species in the solution by the quantity of interstitial solution. The uncertainty of the quantity of interstitial solution is 33 per cent. This run will determine the total quantity of dissolved species in the interstitial solution more accurately than 33 per cent. A Dry Period was terminated by percolating a feed solution through the column at 1680 ℓ/day until the effluent held at a steady composition. The effluent was analyzed periodically so that an accumulative quantity of dissolved solids released from the column could be determined.

After two hours of percolation, the high concentration of aqueous

species leveled off to some constant value. Aqueous potassium concentrations did not level off at the same value as the inlet solution; with an inlet solution of 5.9 mg K^+/ℓ, the effluent leveled off at 7.4 mg K^+/ℓ despite the relatively high rate of percolation of the solution. Integration, with respect to time, of the effluent's excess dissolved species concentrations (above the inlet concentrations) showed that the total quantity of calcium, magnesium, sodium, potassium, and silica released into the interstitial water during the Dry Period was 350 ± 14, 92 ± 4, 194 ± 7, 68 ± 3, and 7.6 ± 0.3 milligrams, respectively. The presumed source mechanism of the excess aqueous cations is desorption from the column's sand; therefore, the quantity of cations released from the sand was 0.34 ± 0.01 μeq Ca^{++}/gm, 0.14 ± 0.01 μeq Mg^{++}/gm, 0.17 ± 0.01 μeq Na^+/gm, and 0.03 ± 0.001 μeq K^+/gm. The total quantity of the cations distributed on sand in equilibrium with feed solution is 22 μeq Ca^{++}/gm, 3.4 μeq Mg^{++}/gm, 2.4 μeq Na^+/gm, and 0.5 μeq K^+/gm. The change in the total quantity of adsorbed cations is therefore approximately ten per cent. Because the total quantity of cations released by the sand was 0.68 μeq/gm, the quantity of hydrogen ions adsorbed by the sand following the nitrification reaction was 1.34 μeq H^+/gm.

Bacterial Population Counts

Six months after the original bacterial seeding of the laboratory column and two months after the previous bacterial population census, heterotrophic and nitrifying bacterial population counts were made for the column's sand and solution. Approximately one gram of sand

extracted from the column was agitated with 40 mℓ of deionized water. Procedure for the heterotrophic bacterial population count was to dilute 0.1 mℓ of the 40 mℓ of water to 10 mℓ and plate 100 μℓ on nutrient agar. For the nitrogen microorganism population count, 1 mℓ of the deionized water slurry was diluted to 40 mℓ and 100 μℓ was plated on the appropriate silica gel medium to cultivate Nitrosomonas or Nitrobacter. Final counting of the colonies was made 11 days later. The logarithm of the number of bacterial cells per dry gram of sand was:

Depth	Nitrobacter	Nitrosomonas	Heterotrophs
1	6.6	5.1	6.4
2	6.6	5.0	6.3
3	6.6	4.5	6.2
4	6.6	-	6.3
5	6.6	4.9	6.3
6	6.6	4.7	6.5
7	6.6	5.0	6.4
8	6.6	4.2	6.2

A conspicuously lower population of Nitrosomonas than Nitrobacter exists. A tenfold smaller population of Nitrosomonas than Nitrobacter was observed in natural soils by Ardakani et al. (65). The same authors' data show there to be little depth dependence of bacteria population in the soil down to 20 inches except possibly for a larger quantity of Nitrobacter near the soil surface. The heterotrophic microorganism population had remained stable since the last time the bacteria were counted. The ability of heterotrophic cells to grow with autotrophic

cells in a medium otherwise free of organic material is well known. Pan et al. (66) reported that certain heterotrophs actually grow in mutual stimulation with Nitrobacter.

A bacterial population count was made for the leading edge solution starting a new Wet Period. Because the most intense bacterial activity occurred during the Dry Period, it was assumed that bacterial populations grew substantially during the same period. A newly infiltrating solution encountering an overly populated bacterial community should redistribute bacteria down through the column. Ten microliters of the leading edge solution w

logarithm of the number of cells per milliliter of solution are:

Depth	Nitrobacter	Nitrosomonas	Heterotrophs
0	4.5	2.6	4.6
1	4.6	2.6	4.7
2	4.4	2.8	4.5
3	4.4	2.3	4.5
4	4.0	2.5	4.4
5	3.8	2.4	4.3
6	3.9	2.3	4.4
7	3.0	1.8	4.2
8	3.6	-	4.5

Bacteria not only existed in the column's percolating solution but also in the feed solution for the column. The holding and constant head tanks were hereafter cleaned with deionized water before and after each Dry Period.

Proof of the Nitrification Mechanism

Nitrification is of course an aerobic process requiring ammonium ions. If nitrification was the sole reason that calcium, magnesium, sodium, and potassium were released by the sand into the interstitial solution, then a lack of oxygen or ammonium ions during the Dry Period should prevent such cation release. A Dry Period with an initial low oxygen containing atmosphere was investigated. As soon as a Wet Period ended, approximately 10 mℓ/sec of helium was pumped for eight hours up the length of the laboratory column. As a result, the Dry Period proceeded with a gaseous atmosphere composed of only four volume per cent of oxygen. A different Dry Period was initiated which followed two ammonium ion-free Wet Periods. Both investigations were analyzed by studying the aqueous composition of the leading edge feed solution terminating the Dry Period. Both Dry Period investigations were expected to show no increase of aqueous calcium, magnesium, sodium, or potassium in the interstitial water.

Leading edge analyses of aqueous cations are presented in dimensionless form based on the inlet constituency for the respective cation (Figure 78). There was no great addition of cations to the interstitial solution during the oxygen deficient Dry Period. Both aqueous sodium and potassium content of the leading edge solution showed very little change of concentration. There actually was a decrease of calcium and magnesium ion content of 12 and 4 mg/ℓ, respectively, as the leading edge of feed solution percolated beyond the five-foot mark. Dissolved silica is presented with comparative aqueous silica contents after normal well aerated Dry Periods (Figure 79). Well aerated Dry Periods

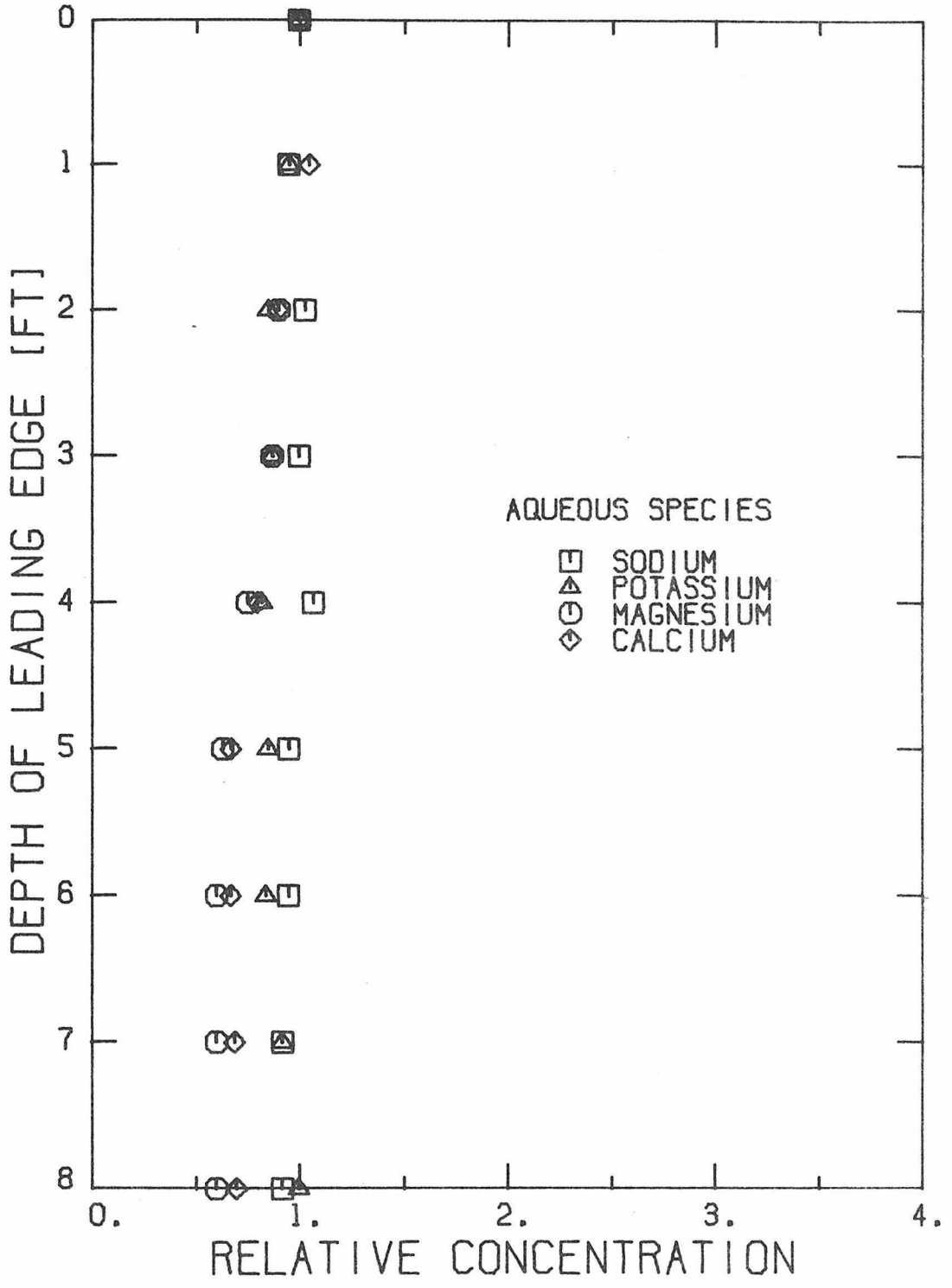

Figure 78: Aqueous Cation Content of the Leading Edge Solution Terminating an Oxygen Deficient Laboratory Column Dry Period

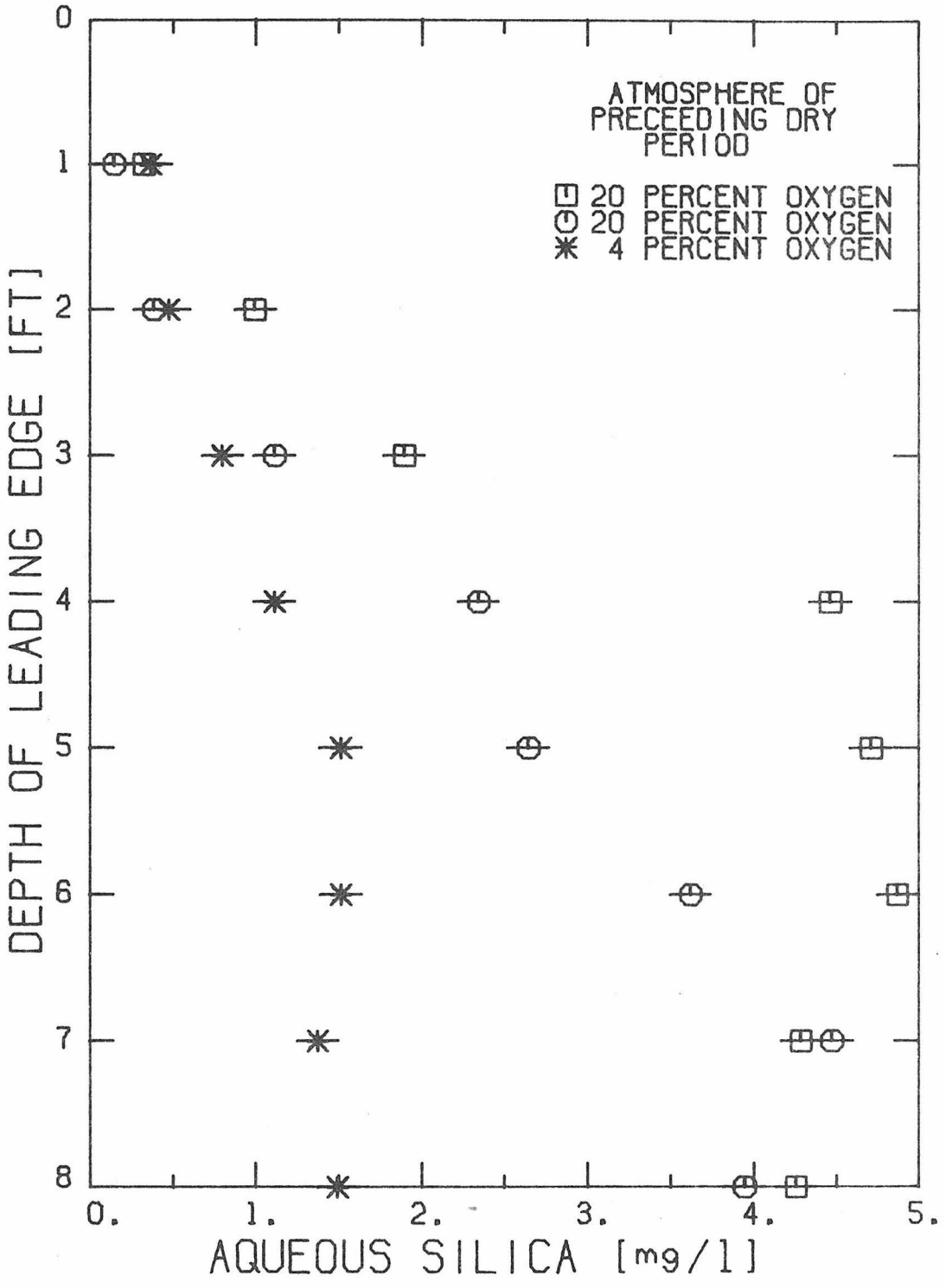

Figure 79: Aqueous Silica Content of the Leading Edge Solution Terminating an Oxygen Deficient Laboratory Column Dry Period

lead to an interstitial solution of silica content up to 4 or 5 mg SiO_2/ℓ. The oxygen starved Dry Period yielded an interstitial solution of dissolved silica content of only 1.7 mg SiO_2/ℓ. The well aerated Dry Period led to a 16 to 20 mM nitrate ion interstitial solution. A Dry Period with a gaseous atmosphere with only four volume per cent oxygen totally prevented nitrification (Figure 80). Gas analysis of the soil at Whittier Narrows by Pincince (55) showed that, at least up to 52 hours into the Dry Period, oxygen content fell to near zero down to the two-foot mark; nitrification, therefore, would be inhibited below the two-foot depth by lack of oxygen. Newly infiltrating solution entering soil below the two-foot mark, as seen in the Whittier Narrows data (Reid, 5), has a leading edge nitrate ion content that reflects the low concentration of the nitrate ion in the interstitial water.

Two ammonium ion-free Wet Periods in a row were conducted. By the end of the second Wet Period, the aqueous concentration of calcium, magnesium, and sodium were constant of depth. There was, however, still a disappearance of 5 mg O_2/ℓ from the percolating solution by the three-foot depth. Dry period data were collected after the second Wet Period. Despite the resumed lack of ammonium ions, oxygen was still consumed and carbon dioxide was produced during the Dry Period (Figure 81 and 82). The total quantity of oxygen consumed was 3000 mg, and 3564 mg of carbon dioxide was produced. The initial quantity of bicarbonate ions in the interstitial solution was 11 millimoles (484 mg of carbon dioxide). Obviously most of the carbon dioxide could not have been caused by the acidification of the bicarbonate to carbon dioxide; in fact, four times more carbon dioxide was produced in the absence of adsorbed ammonium

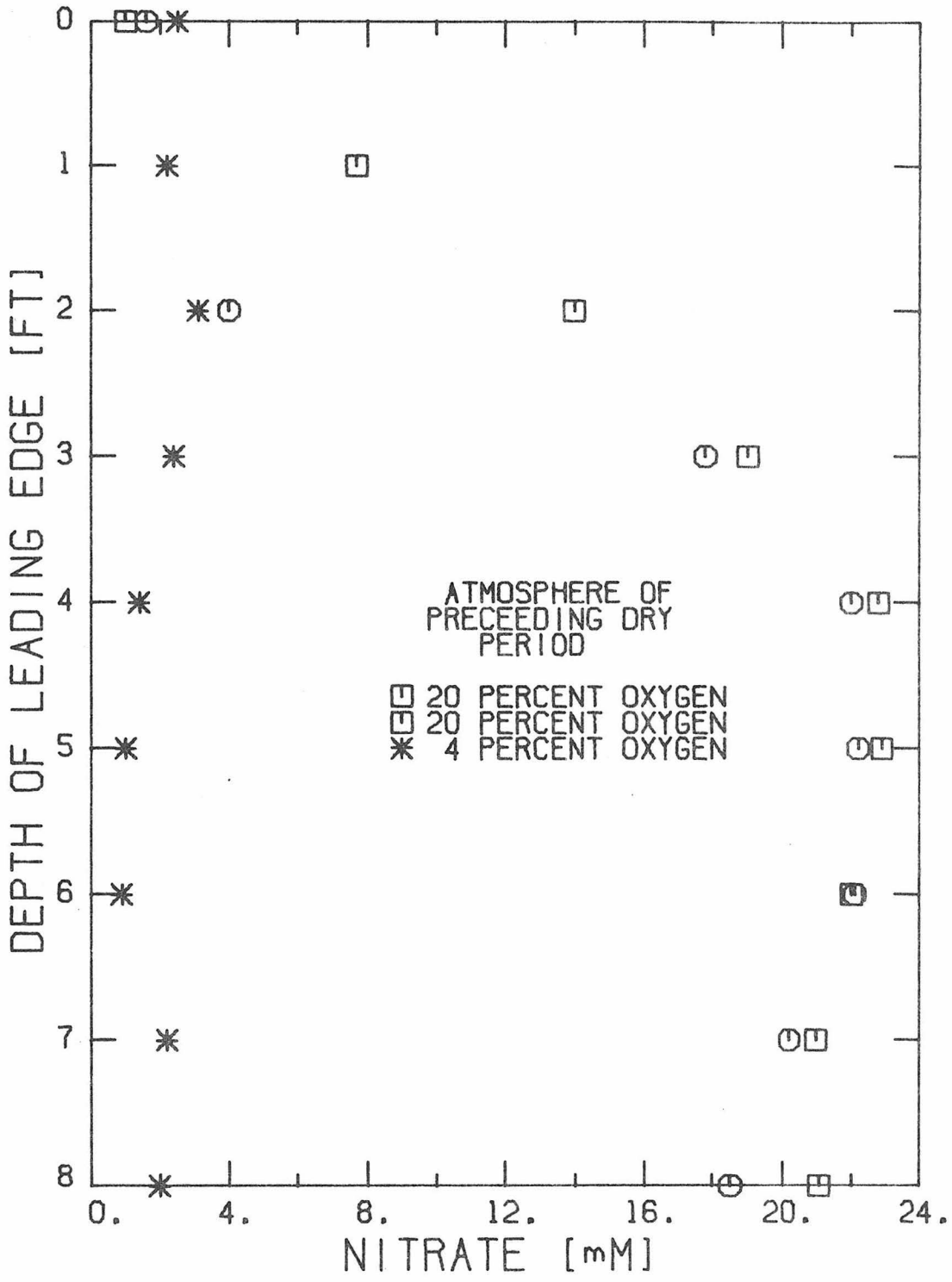

Figure 80: Aqueous Nitrate Ion Content of the Leading Edge Solution Terminating Oxygen Deficient and Oxygen Sufficient Laboratory Column Dry Periods

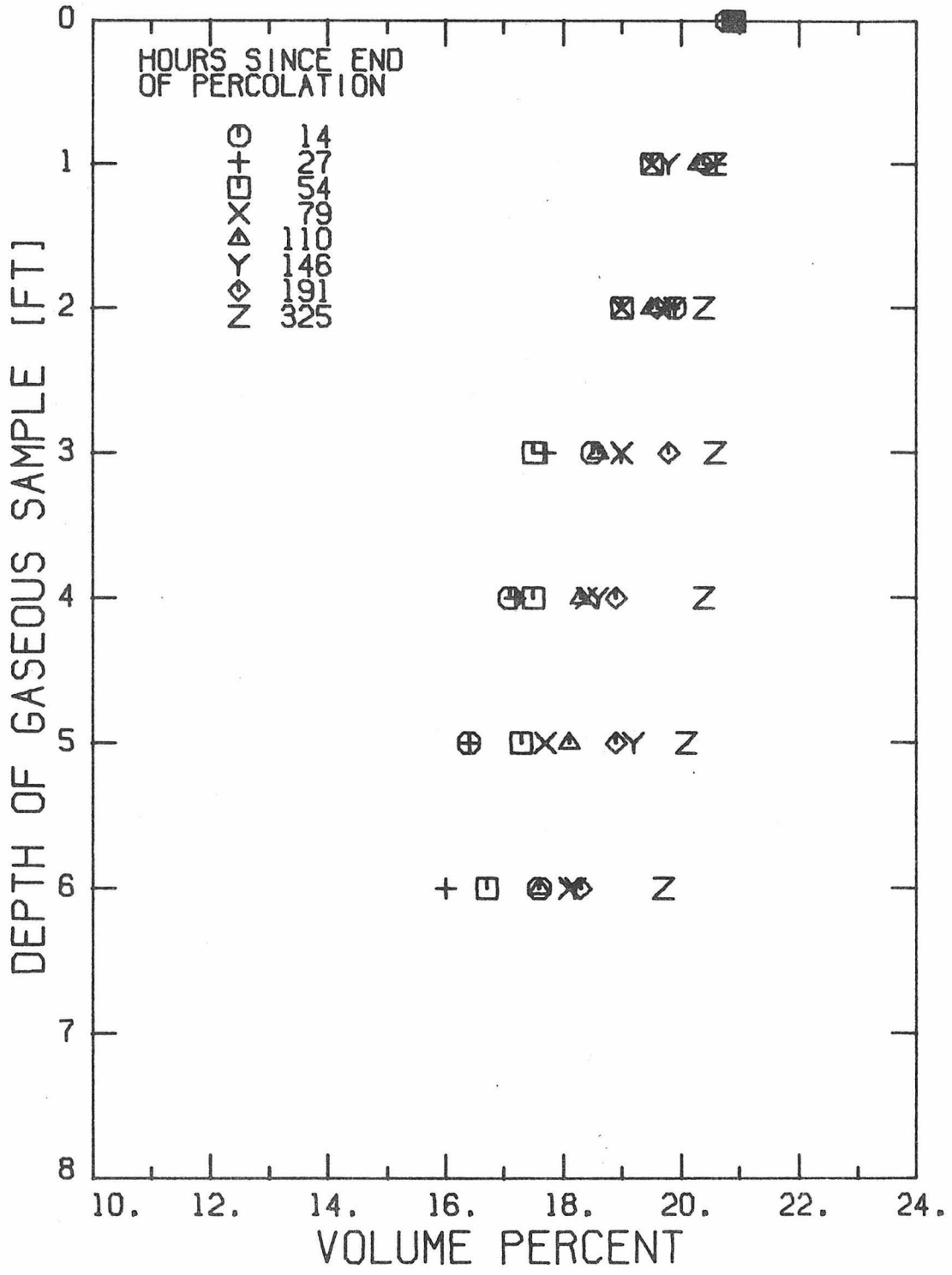

Figure 81: Oxygen Content of the Laboratory Column Atmosphere during a Dry Period following Two Ammonium Ion Free Wet Periods

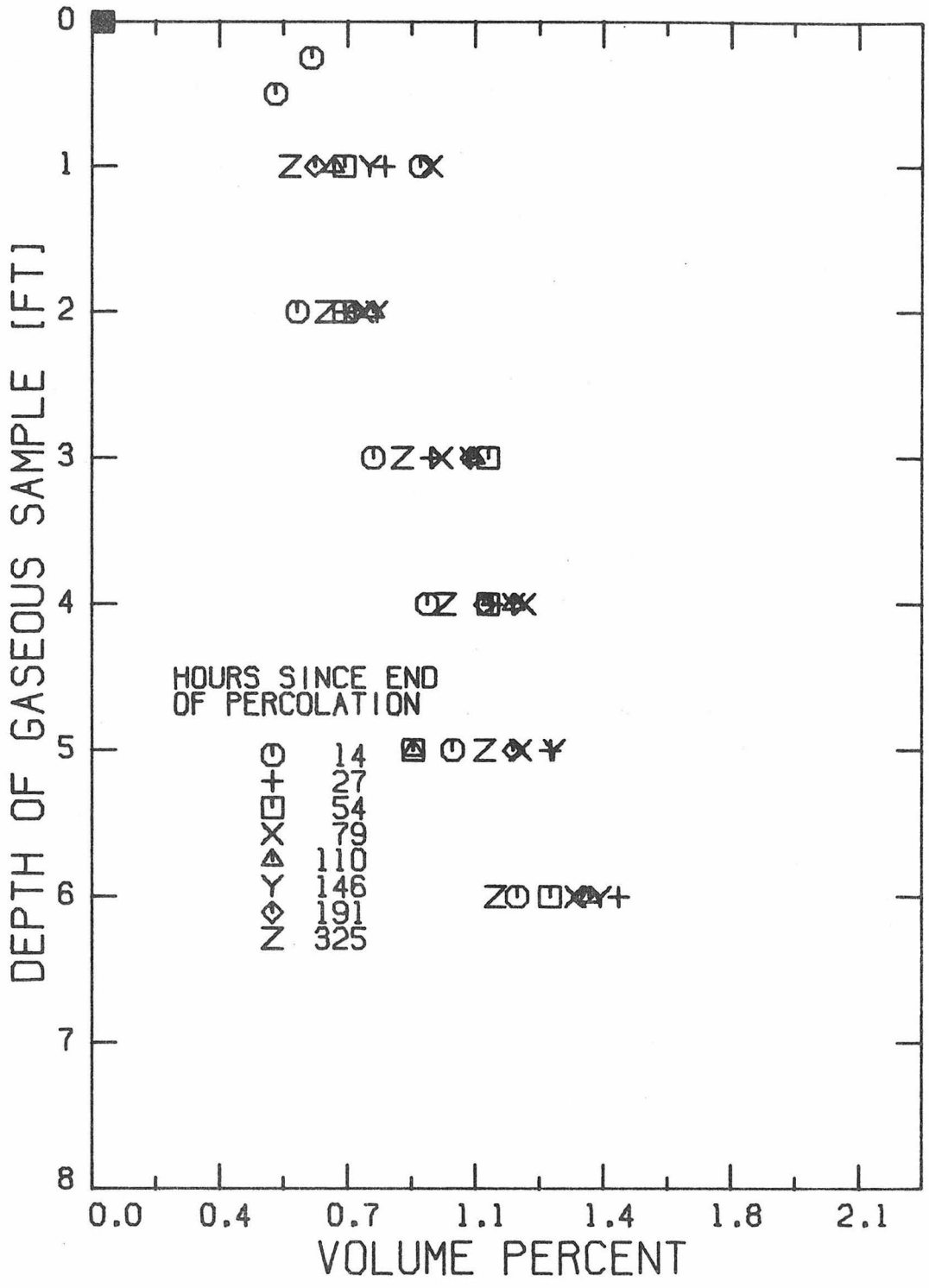

Figure 82: Carbon Dioxide Content of the Laboratory Column Atmosphere during a Dry Period following Two Ammonium Ion Free Wet Periods

ions. Furthermore, it should be noted that the carbon dioxide concentration profiles do not relax throughout the Dry Period as they had previously been observed to do when ammonium ions were present at the start of the Dry Period (Figure 75).

The leading edge of solution following the ammonium ion-free Dry Period showed very little change of pH (Figure 83). The lack of ammonium ions did stop the acidification of the interstitial solution. The concentration of bicarbonate ions in the interstitial solution did fall, but only 0.5 millimoles/ℓ, as compared to 3 millimoles/ℓ for a Dry Period run with aqueous ammonium ions. The concentration of alkali cations was unchanged or decreased in the interstitial solution (Figure 84).

The above investigations and analyses prove that the cause for the Dry Period release of alkali cations to the interstitial solution is the aerobic nitrification of aqueous ammonium ions by Nitrosomonas. The bacteria consume ammonium ions, the source of which is 95 per cent in the form of adsorbed ammonium ions. Oxygen from the 0.39 volume fraction of atmosphere in the column is used for the nitrification of ammonium ions and nitrite ions. Bacterial acidification of the solution surrounding the aluminosilicate minerals did cause an increased destructive dissolution of these minerals. Mineral dissolution, however, is a negligible source of alkali cations for the Dry Period's interstitial solution. When the nitrification reactants are lacking during the Dry Period, nitrifying bacteria cannot reproduce or maintain themselves; as a result, the nitrifying bacteria presumably deteriorate by spontaneous oxidation or decomposition by oxidation by heterotrophic

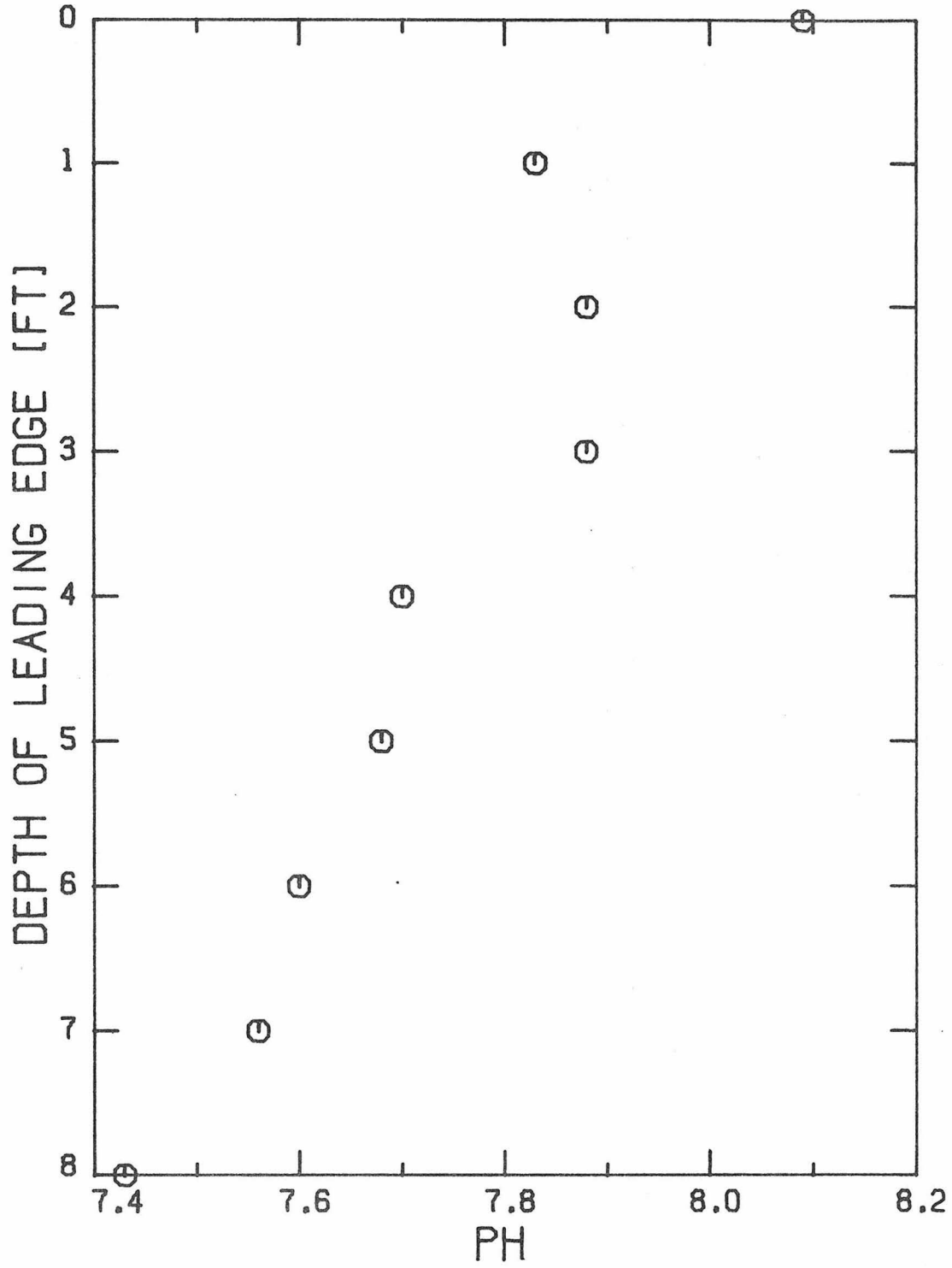

Figure 83: pH of the Leading Edge Solution Terminating an Ammonium Ion Free Laboratory Column Dry Period

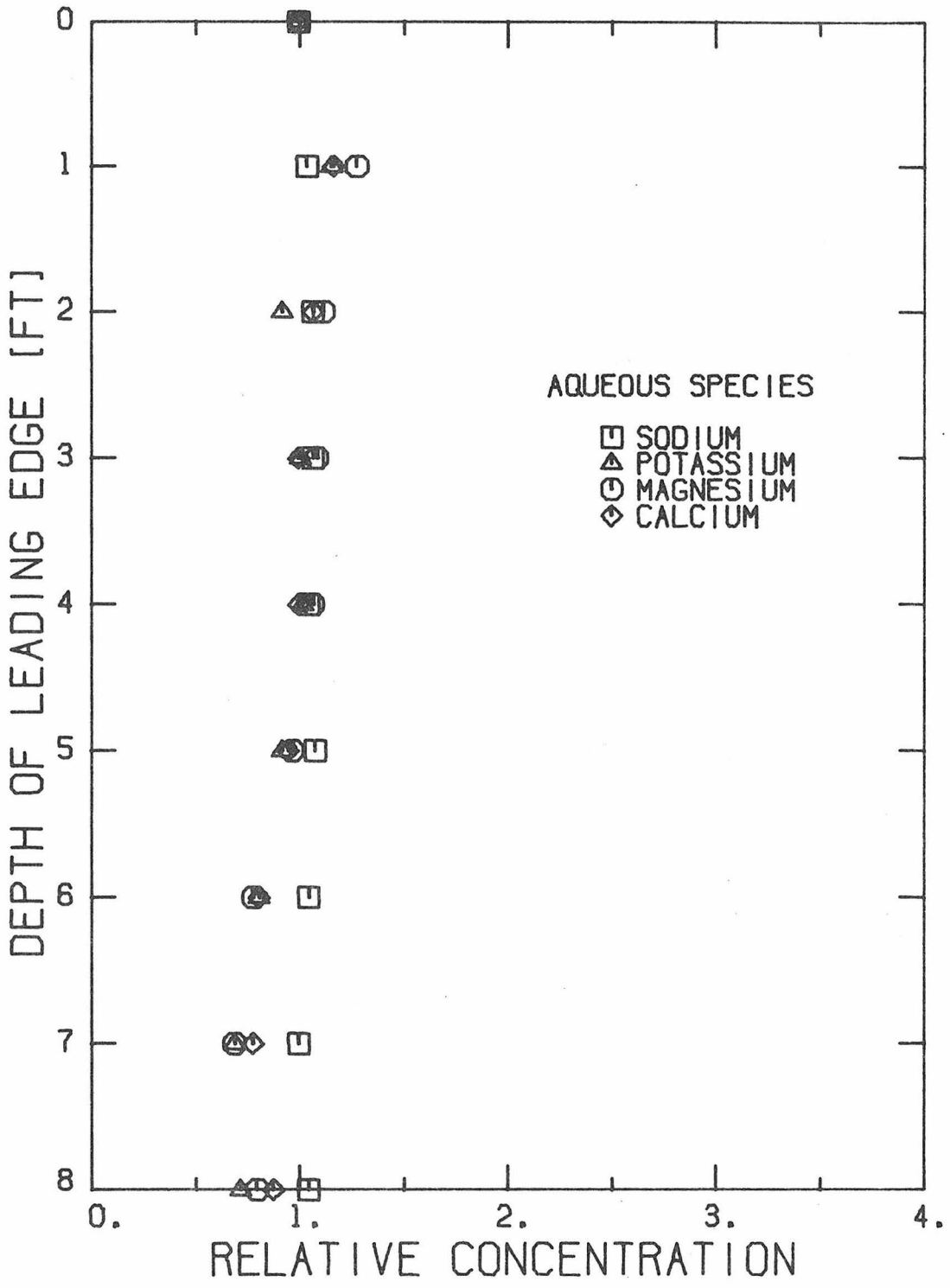

Figure 84: Aqueous Cation Contents of the Leading Edge Solution Terminating an Ammonium Ion Free Laboratory Column Dry Period

bacteria. The decomposition reaction does not change the interstitial solution's pH.

Effects of Variations in the Duration of the Dry Period

Fourteen days was the standard duration of the Dry Period based on the schedule used at the Whittier Narrows test basin. Gaseous concentration profiles show that bacterial activity is at a maximum 24 to 48 hours after the start of the Dry Period and stops thereafter. This investigation centers on Dry Periods of duration 14, 5, 2.2, and 1 day. Such durations should confirm the gaseous profiles that bacterial activity is confined to the very beginning of the Dry Period.

The Dry Periods were ended by percolating deionized water through the column. Chloride content of the leading edge was analyzed and used to correct the dissolved species concentrations for various mixing ratios of the infiltrating and interstitial solutions.

The change from the 14 to 5 day duration showed little improvement in the alkali content of the interstitial solution (Figures 85 and 86). Even the 2.2 day Dry Period (Figure 87) showed little improvement. The largest change came when the Dry Period lasted only 1 day (Figure 88). Calcium ion content of the interstitial solution increased only 1.9 times instead of the usual triple increase. Aqueous sodium content did not increase. The bicarbonate ion content, however, did drop substantially.

This investigation showed that practically all the nitrification of adsorbed ammonium ions occurs just one day after air is allowed to enter the laboratory column. Apparently the first sink for bacterially

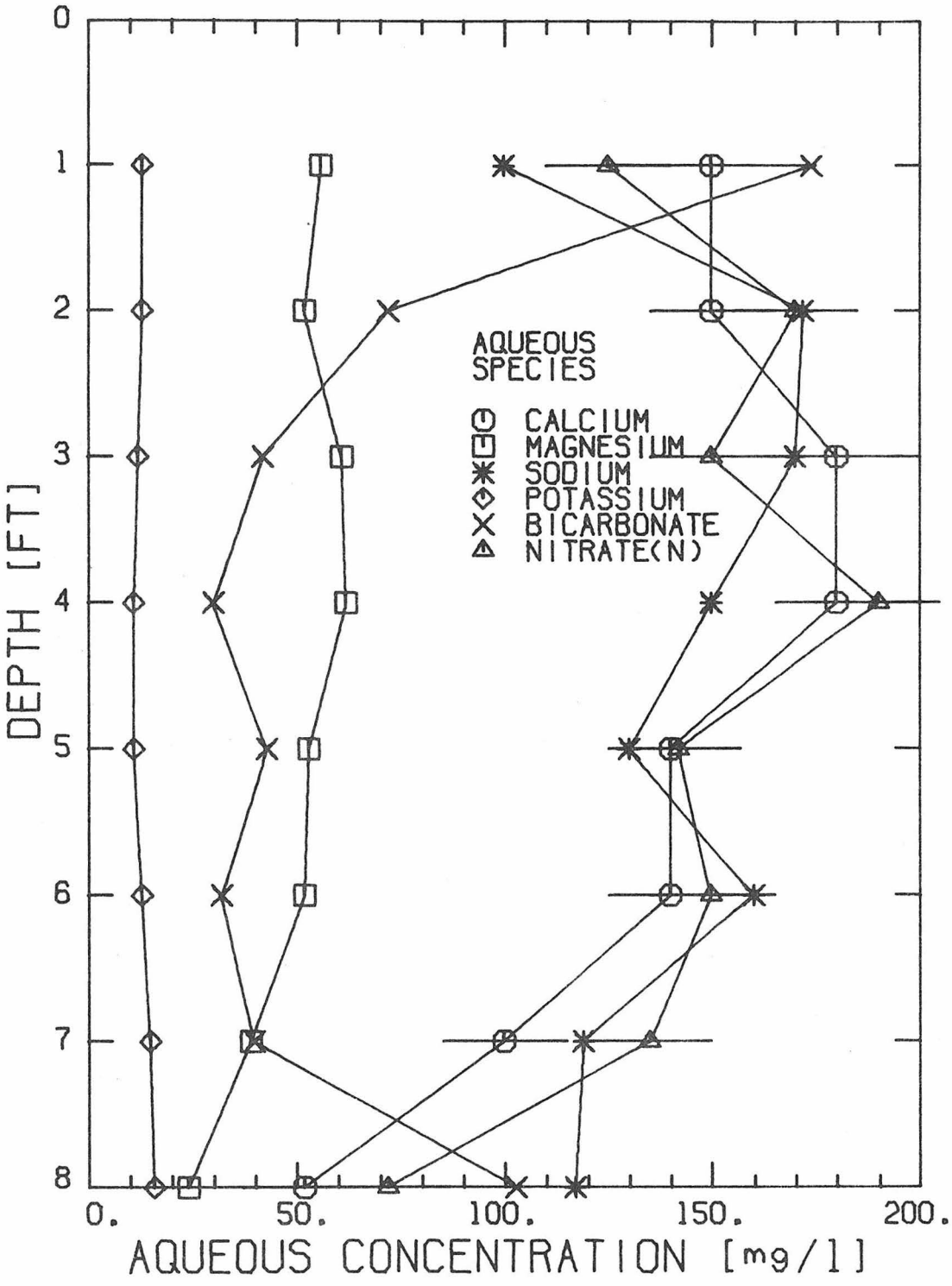

Figure 85: Aqueous Species Contents of the Interstitial Solution of the Laboratory Column at the End of a Fourteen Day Dry Period

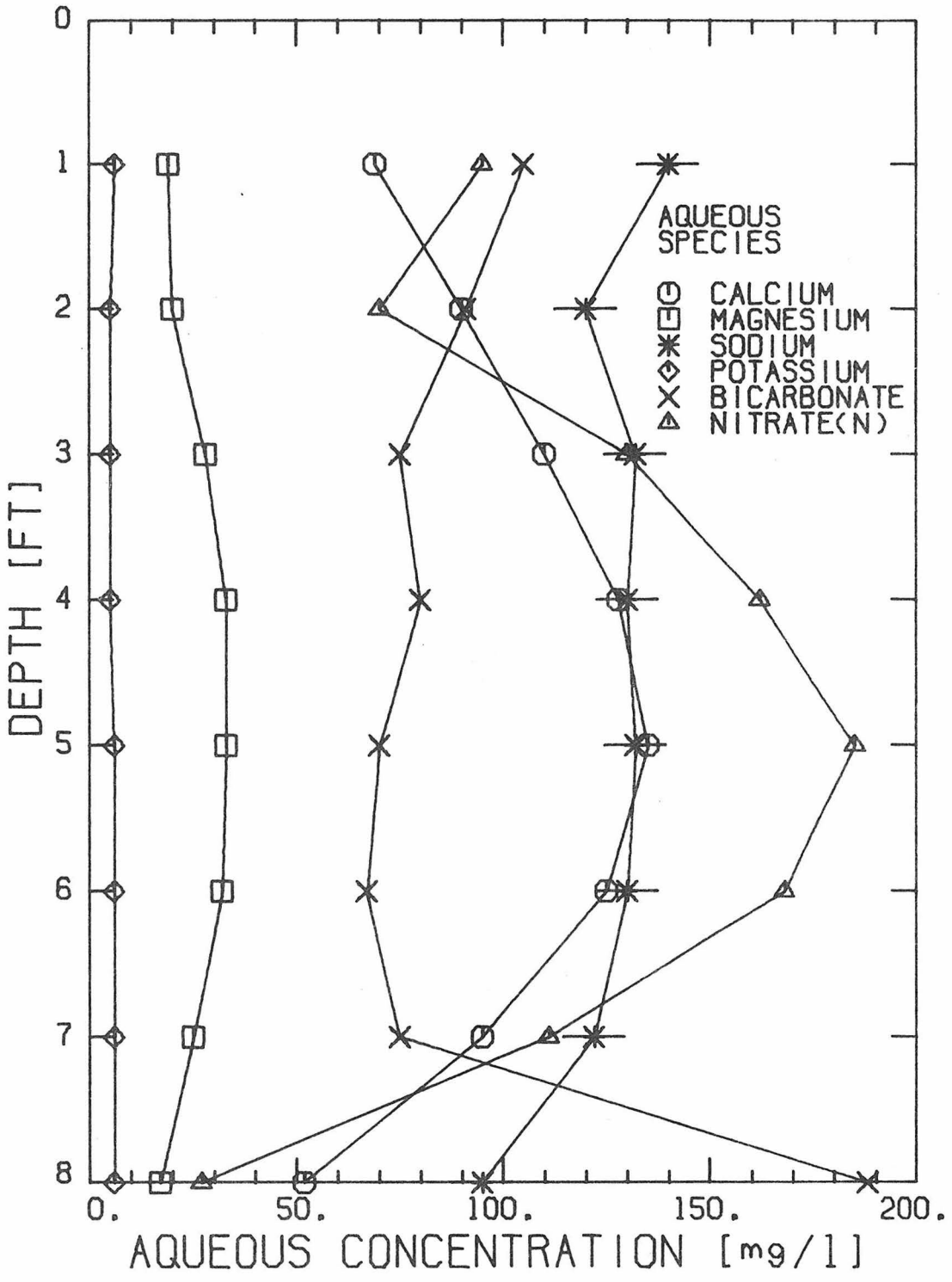

Figure 86: Aqueous Species Contents of the Interstitial Solution of the Laboratory Column at the End of a Five Day Dry Period

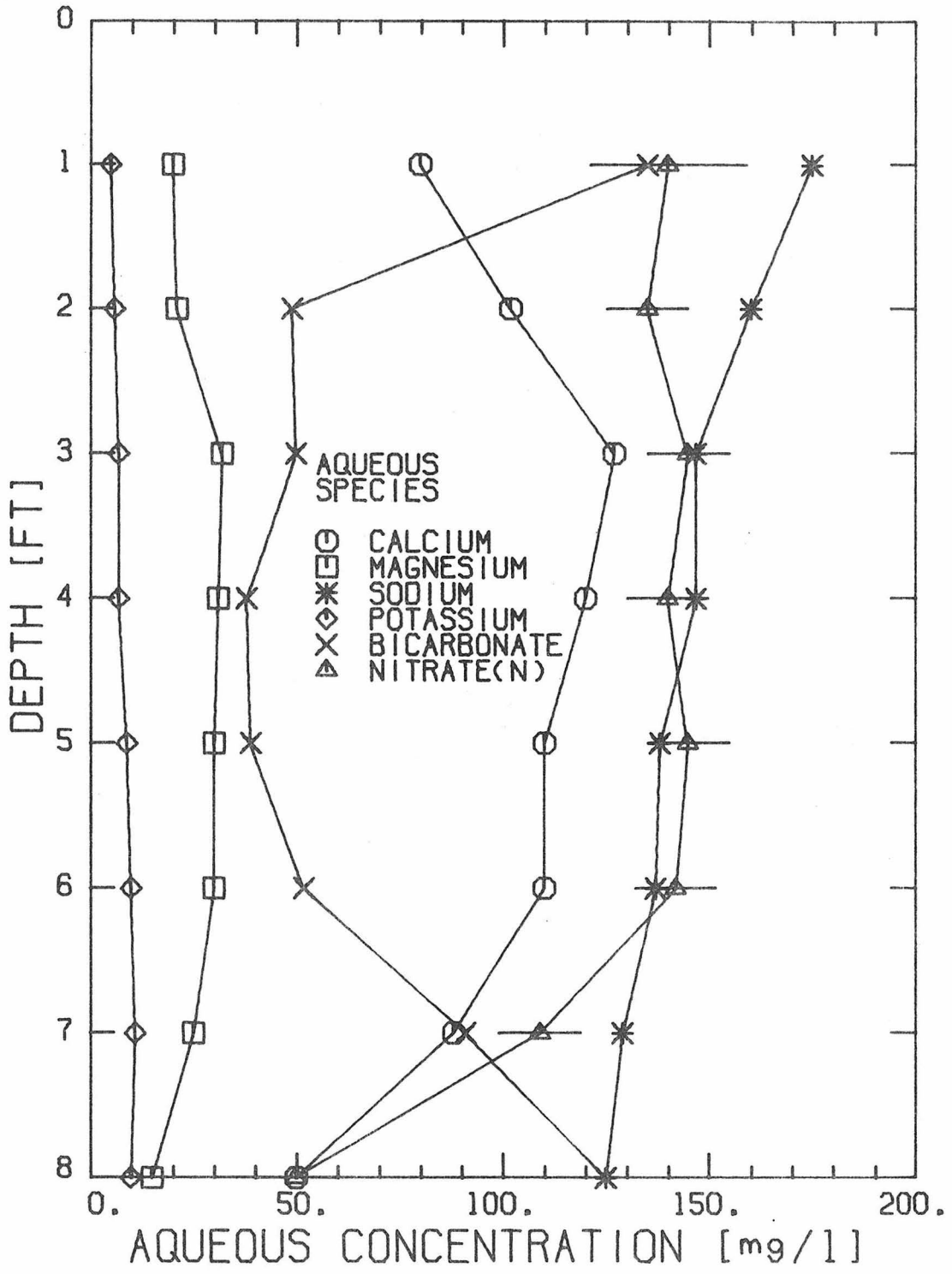

Figure 87: Aqueous Species Contents of the Interstitial Solution of the Laboratory Column at the End of a 2.2 Day Dry Period

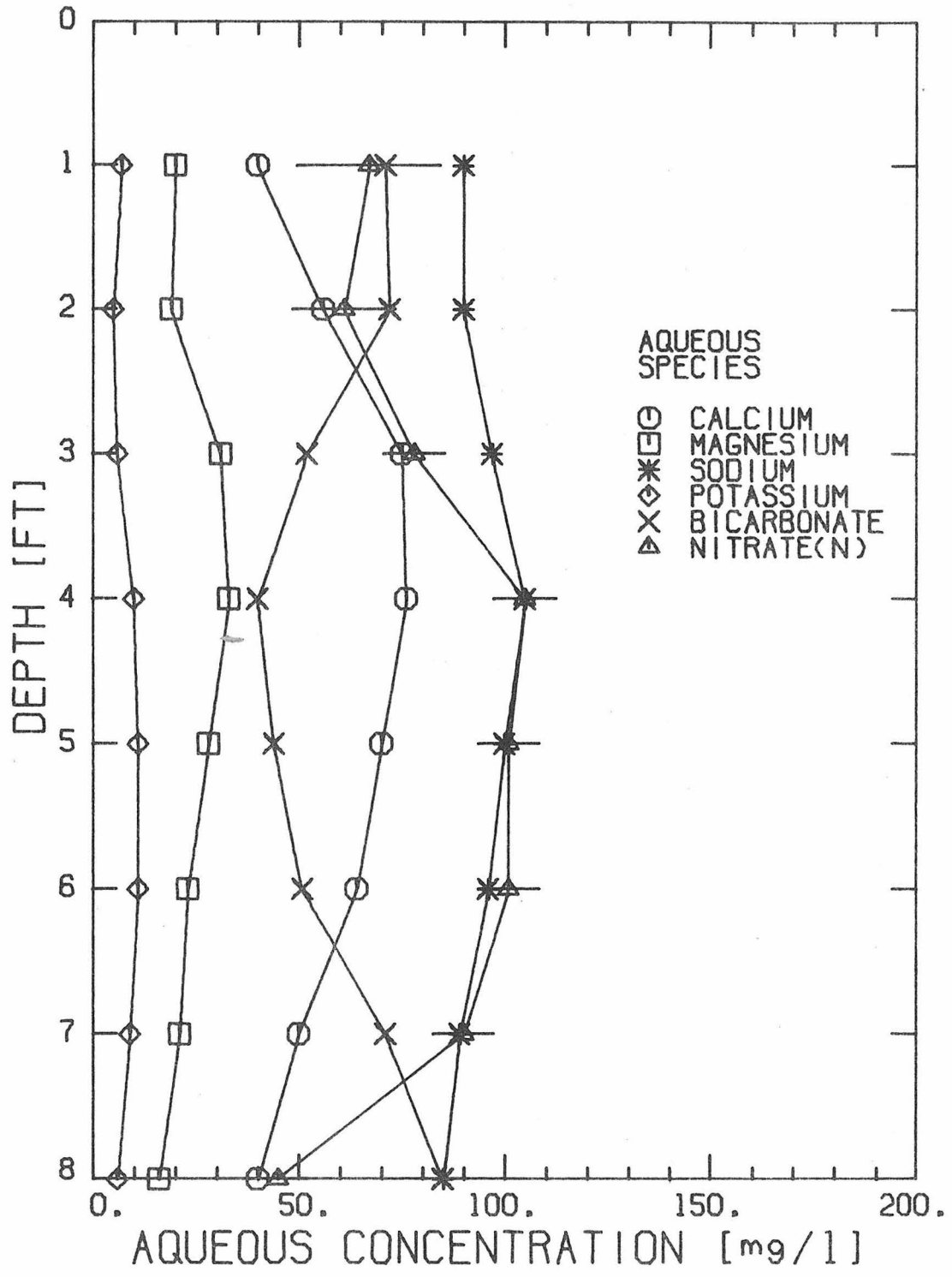

Figure 88: Aqueous Species Contents of the Interstitial Solution of the Laboratory Column at the End of a One Day Dry Period

generated hydrogen ions is the bicarbonate ion. Once the aqueous bicarbonate is utilized, aqueous hydrogen ions exchange alkali ions off the sand. Two days after the start of the Dry Period, the nitrifying bacteria end their reactions and the gaseous atmospheres relax back toward their atmospheric concentrations. Dry Periods of extreme duration would start to show increases of carbon dioxide gas again as nitrifying bacteria, having comsumed all the ammonium ions, start to decompose. The duration of the nitrification reactions is, of course, dependent on the bacterial populations and the amount of ammonium ions adsorbed to the soil. Soil of low bacterial concentrations or soils with high capacities for adsorbing aqueous ammonium ions would have long duration nitrification periods, perhaps lasting the entire Dry Period.

Source of Dry Period Aqueous Cations

Cations are released to the interstitial water during a period of dryness by reaction with aqueous hydrogen ions generated by bacterial nitrification of aqueous ammonium ions. It has been observed that sand deficient in adsorbed magnesium ions (Figure 63) will produce an interstitial solution also deficient in magnesium ions (Figure 65). It is apparent that adsorbed cations, rather than cations from salts, are released by aqueous hydrogen ions to interstitial water.

Aqueous calcium ions in the percolating solution have been the most prominent additives both in the laboratory column and at the Whittier Narrows test plot. If the source of high concentrations of calcium in the laboratory column is adsorbed calcium, then removal of

the adsorbed calcium should prevent the transient wave of dissolved calcium salts at the start of each Wet Period. Feed solution was formulated in a manner similar to all the previous feed solutions (Table 3) with the exception that it was free of calcium salts. The loss of calcium salts was compensated by the addition of an equimolar quantity of the same magnesium salt. The calcium-free feed solution was percolated through the column intermittently for over one month until the effluent aqueous calcium ion concentration was less than 5 mg/ℓ. Two wet/dry cycles were run and the last Dry Period's interstitial solution was studied for data by analyzing the dissolved species in the leading edge of deionized water as it terminated the Dry Period.

The data show that only 5 mg Ca^{++}/ℓ was added to the interstitial solution during the two week Dry Period (Figure 89). An average 9.3 ± 0.5 mM nitrate interstitial solution was generated; therefore, 19.0 ± 1.0 μeq hydrogen ions/ℓ were also generated. 9.3 ± 0.5 μeq/ℓ of those hydrogen ions replaced the ammonium ions that were nitrified. Because the aqueous bicarbonate content of the interstitial solution dropped from 250 to 60 mg/ℓ, 3.2 μeq H^{+}/ℓ went to convert bicarbonate ions to carbon dioxide gas. The remaining 6.2 ± 0.5 μeq H^{+}/gm had to have exchanged with the same equivalent of alkali ions to leave only a slightly acidified interstitial solution. The concentration of aqueous calcium, magnesium, sodium, and potassium ions in the interstitial solution at the start of the Dry Period was 0, 37, 113, and 6 mg/ℓ, respectively. At the end of the Dry Period, the average respective concentrations were 3, 105 ± 10, 133 ± 10, and 8 ± 3 mg/ℓ. The excess μeq/ℓ of the respective aqueous cations was 0.15, 5.6 ± 0.8, 0.9 ± 0.5,

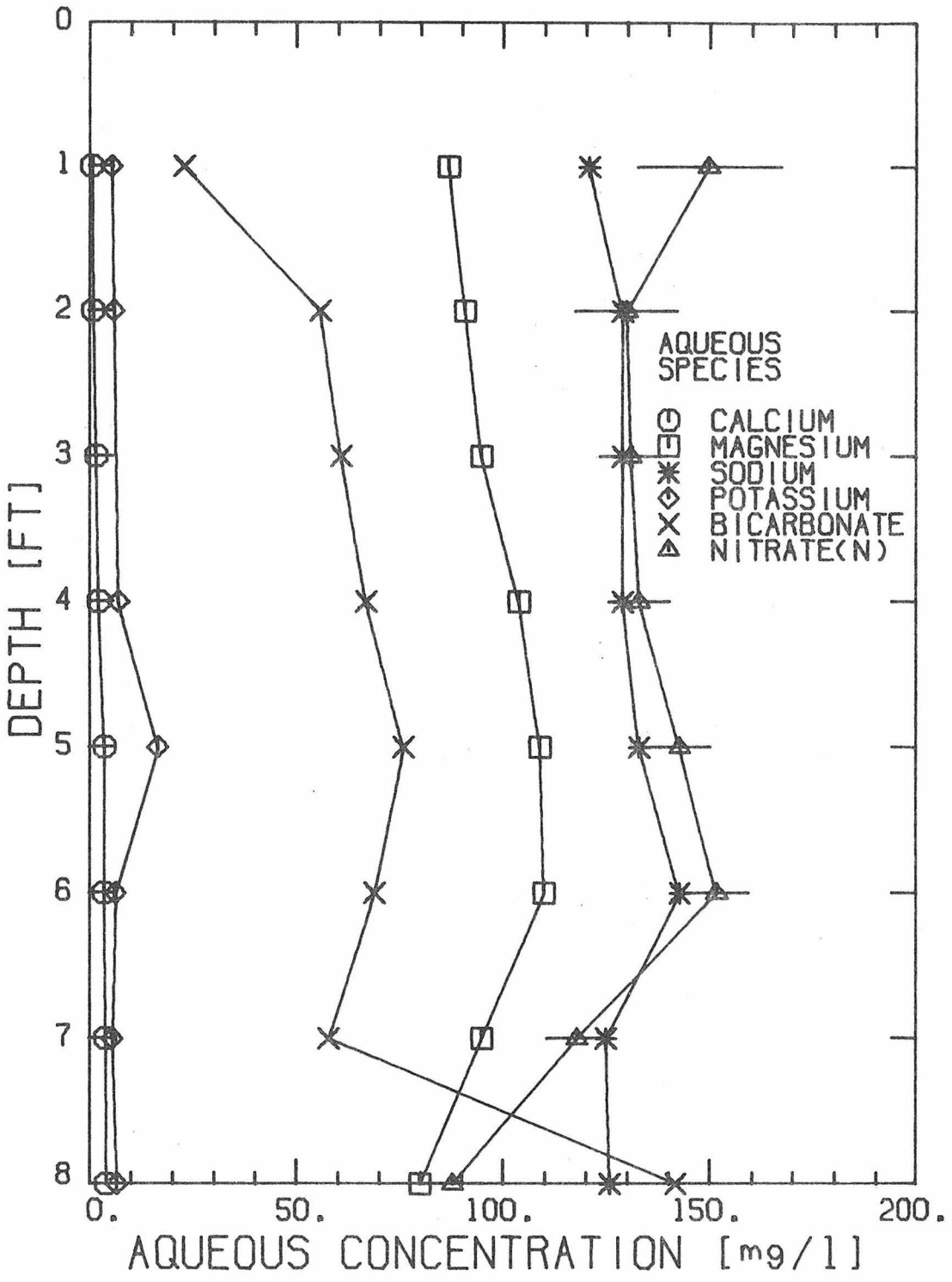

Figure 89: Aqueous Species Contents of the Interstitial Solution of the Laboratory Column at the End of a Dry Period following Calcium Ion Free Wet Periods

and 0.5 ± 0.2--a total of 6.7 ± 1.2 μeq/ℓ, the same quantity of hydrogen ions that would have had to have been consumed.

The source of high concentrations of calcium salts dissolved in the solutions starting the laboratory column's Wet Period is calcium ions adsorbed to the sand from previous percolating solutions. It should follow that all high concentrations of aqueous cations in the leading edge of newly infiltrating solutions should have originated from adsorbed cations rather than a naturally occurring salt. No aqueous lithium ions have been detected in the column; therefore, a feed solution was prepared only with lithium and ammonium salts to test the theory that the constituency of previous feed solutions determines what aqueous cations appear in the column's Dry Period interstitial solution. The feed solution had the following formulation:

2.43 mM LiCl

4.12 mM $LiHCO_3$

0.49 mM $(NH_4)_2SO_4$

For one and a half months, the feed solution was percolated intermittently through the column. Bacterial nitrification was sustained during the Wet Period (Appendix B). It was very difficult to remove magnesium ions adsorbed to the column's sand. The final effluent from the column contained 0.2 mg $Na^+/ℓ$, 0.16 mg $Ca^{++}/ℓ$, and 3.5 mg $Mg^{++}/ℓ$. Previous data show it possible to bring the magnesium content down much further (Figure 27); appreciable quantities were still adsorbed to the sand at the start of the Dry Period. The composition of the interstitial solution of the two-week Dry Period was studied by analyzing the composition of the leading edge of solution as deionized water

infiltrated the column.

As the leading edge of the infiltrating solution pushed down through the column, it forced ahead of it interstitial solution which had a minimum pH of 4.4 (Figure 90). The most important finding, however, was that the interstitial solution at the end of the Dry Period had a maximum aqueous cation content of 10 mg Ca^{++}/ℓ, 100 mg Mg^{++}/ℓ, 6 mg Na^{+}/ℓ, and 150-300 mg Li^{+}/ℓ (Figure 91). There was a vast amount of nitrification especially nearer the top of the column where 400-630 mg $NO_3^-(N)/\ell$ was generated. The aqueous silica content was unusually high in the one-foot through eight-foot depths of 40, 25, 20, 16, 10, 3, 2.4, and 2.4 (± 2%) mg SiO_2/ℓ.

Calcium and sodium ions had previously been leached from the sand; when nitrification occurred, negligible quantities of calcium and sodium ions were released to the interstitial solution. The sand originally contained no lithium ions; however, when lithium ions were exchanged into the sand during a Wet Period, a Dry Period nitrification released vast quantities of lithium ions to the interstitial solution. In a soil of sparsely soluble minerals such as feldspar, the predominant source of a high concentration of alkali ions in the leading edge of a newly infiltrating solution is the alkali ions in previously infiltrated solutions. If previously percolated solutions are devoid of cation "x", then the future percolated solutions starting Wet Periods will show no cation "x" in their leading edges providing readily soluble minerals such as calcite are absent.

The concentration of aqueous nitrate ions in the interstitial solution at the one-foot mark was 45 μeq/ℓ. The reason for such a

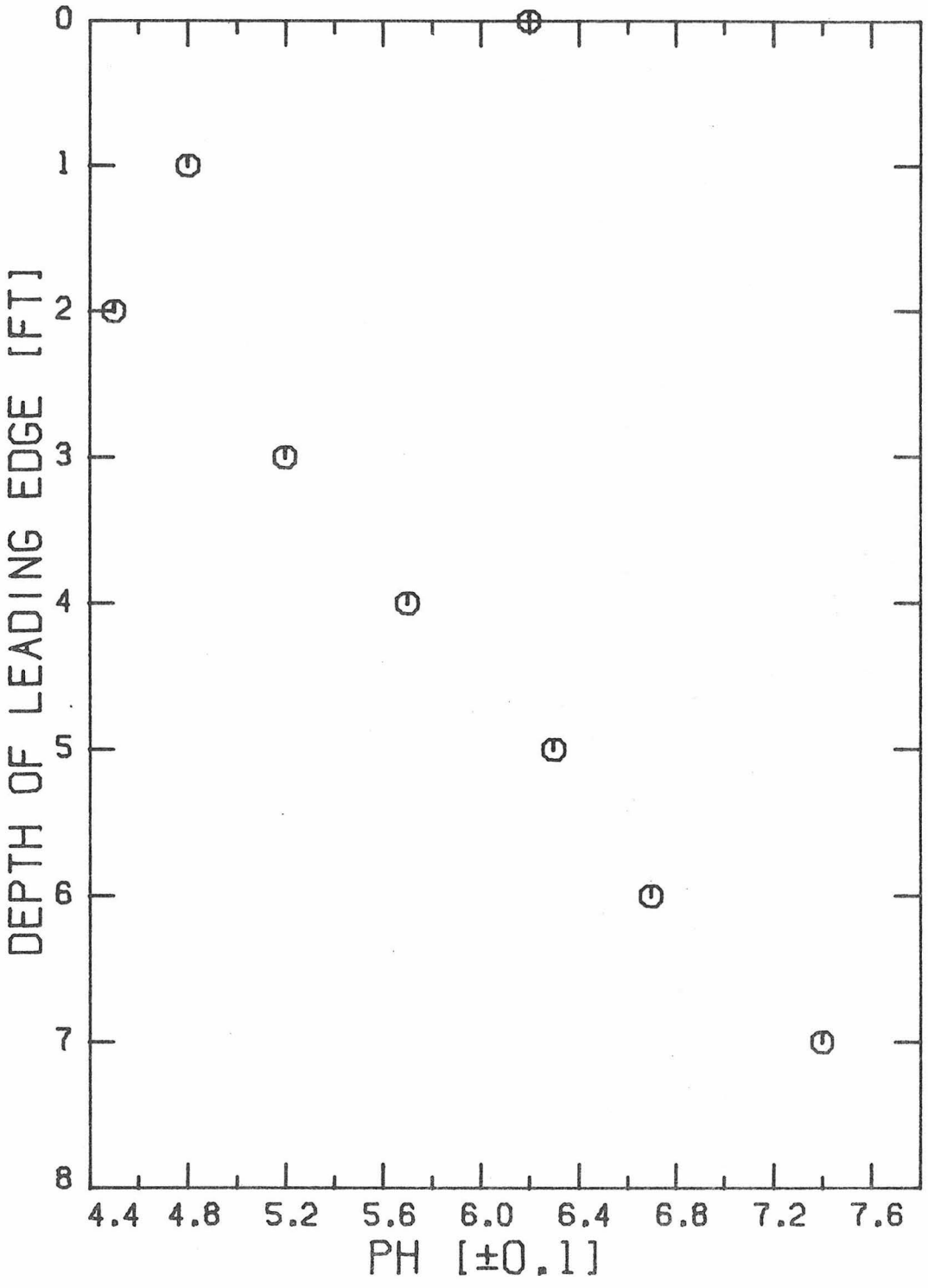

Figure 90: pH of the Leading Edge Solution Terminating a Dry Period following Lithium Ion Rich Wet Periods

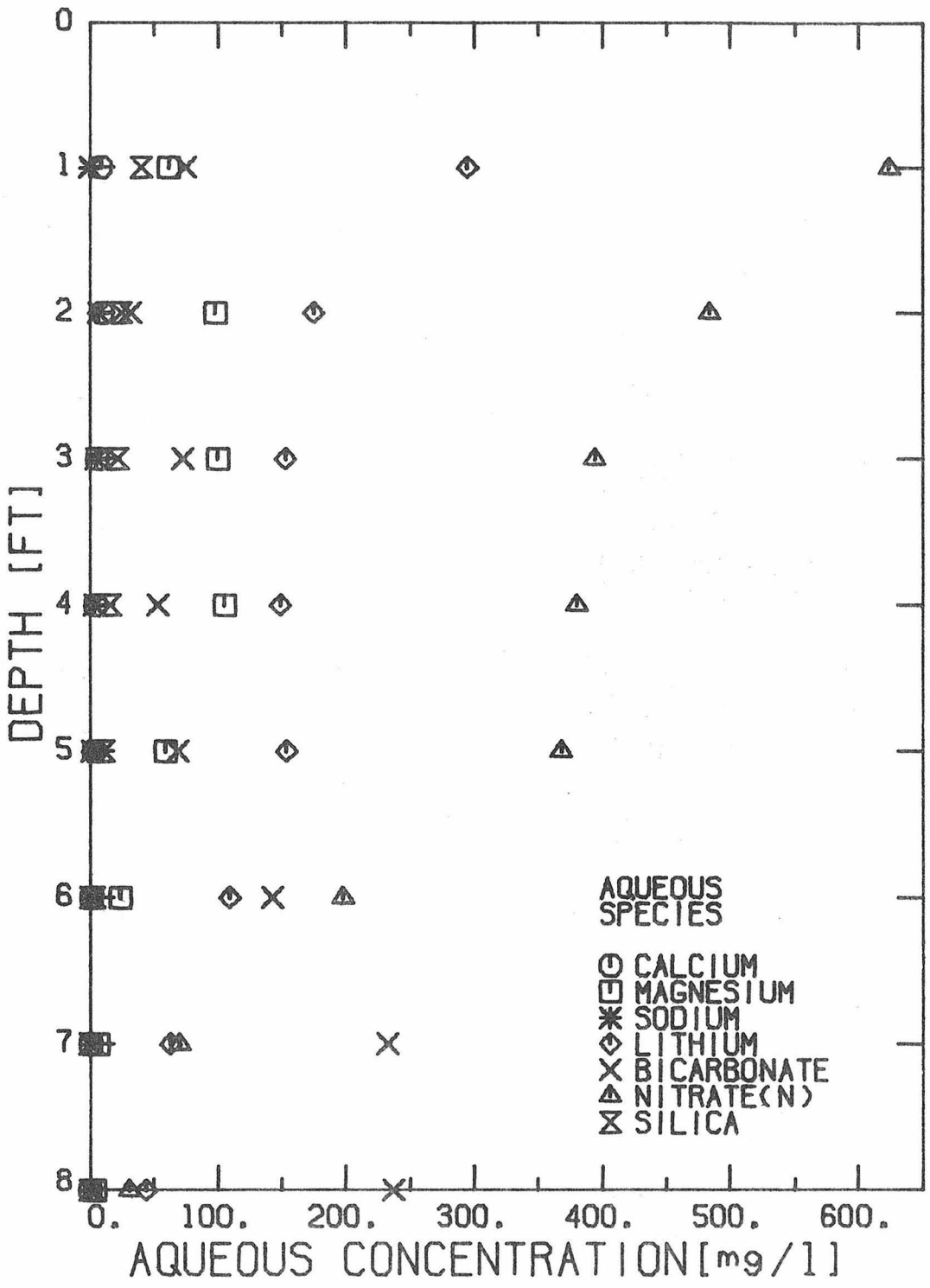

Figure 91: Aqueous Species Contents of the Interstitial Solution of the Laboratory Column at the End of Dry Period following Lithium Ion Rich Wet Periods

large quantity of aqueous nitrate ions is assumed due to a large quantity of adsorbed ammonium ions--1.9 μeq/gm. Ammonium ions are expected to adsorb more readily to the sand when they have to compete with a univalent lithium ion rather than a bivalent calcium or magnesium ion. The production of 45 μeq NO_3^-/ℓ must be accompanied by 90 μeq H^+/ℓ. 45 μeq H^+/ℓ replaced the nitrified adsorbed ammonium ions and 3.5 μeq H^+/ℓ converted aqueous bicarbonate ions to carbon dioxide gas. The balance of aqueous hydrogen ions exchanged with adsorbed cations to give 36 μeq Li^+/ℓ and 8 μeq Mg^{++}/ℓ.

The appearance of 40 mg SiO_2/ℓ in the leading edge solution at the one-foot depth reflected on the massive amount of nitrification that occurred. It is again observed that acidification of the sand's interstitial solution did cause destructive dissolution of aluminosilicate minerals. The transient wave of high total dissolved solids content of the percolating solution still is primarily due to ion exchange rather than mineral dissolution.

MATHEMATICAL MODEL

Aqueous constituency of the percolating solution of the intermittent groundwater recharge process was modeled mathematically by two separate processes--the Wet Period and the Dry Period. Final chemical conditions of one period were the initial chemical conditions of the other. The Wet Period system consisted of a solution percolating through a packed bed of minerals interdispersed with air. Gas-liquid chemical exchange, bacterial nitrification, ion exchange, and mineral dissolution acted to alter the composition of the dissolved chemical species in the percolating solution. The Dry Period system was composed of a gas phase diffusing into the packed bed of minerals interdispersed with solution. The same processes that affected the aqueous phase of the Wet Period affected the solution phase of the Dry Period. Center of focus of both the Wet and Dry Periods was on the aqueous phase composition. Other phases were considered as sources or sinks of chemical species for the solution phase.

The mathematical system forming the Wet Period model consisted of a fixed bed of uniformly sized and composed granules acting as the reservoir for the release or consumption aqueous chemical species. The model recognized the presence of interstitially held air in the packed bed. The percolating solution of the mathematical model flowed axially with no radial component. Concentrations of dissolved species in the solution were assumed to be radially averaged values. Concentrations of aqueous calcium, magnesium, and sodium ions were followed because of their being important constituents of the Total Dissolved

Solids content of percolating solution. Aqueous ammonium, nitrite, nitrate, and hydrogen ions were included in the mathematical model of the Wet Period because of their proven importance to the cause of a Total Dissolved Solids wave in newly percolating solutions. The bicarbonate ion was modeled as a component in the percolating solution as a buffer against extreme pH levels in the solution. Acid producing nitrification reactions require dissolved oxygen as a reactant; therefore, aqueous oxygen content of the percolating solution was modeled. Oxidation of aqueous ammonium ions is thermodynamically favored in a well-oxidized environment at a rate that is dependent on the population density of Nitrosomonas; similarly, the rate of oxidation of aqueous nitrite ions to nitrate ions is increased by the presence of Nitrobacter. Both nitrifying bacterial population densities were monitored in the mathematical model for the Wet Period. Because the experimental work revealed that the primary ion exchange reaction between the percolating solution and the electric double layer was an important process affecting the percolating solution, cation exchange reactions of the aqueous ammonium, hydrogen, calcium, magnesium, and sodium ions were considered as part of the mass balance equations.

Solution percolating through a packed bed during the Wet Period was assumed to move with an interstitial linear velocity, u, defined by the superficial linear velocity, v, divided by the effective porosity for the solution phase, P_E. An effective diffusivity coefficient, D_E, was used to account for both molecular diffusion of dissolved compounds and hydrodynamic dispersion of the solution. If the average radial concentration of dissolved chemical species, i, is c_i, then the

unsteady state variation of c_i in the percolating solution with depth, z, is

$$-u \frac{\partial c_i}{\partial z} + D_E \frac{\partial^2 c_i}{\partial z^2} = \frac{\partial c_i}{\partial t} - \sum_j R_{ij} \qquad (51)$$

where R_{ij} is the change to chemical species, i, due to reaction, j. Aqueous oxygen concentration was affected by exchange reactions between the percolating solution and the interstitial gas and by bacterially induced oxidation of the aqueous ammonium and nitrite ion. Aqueous cations were affected by bacterial ion exchange, or dissolution reactions. The total carbonate ions (H_2CO_3, HCO_3^-, and CO_3^-), early in the modeling study, were found to be negligibly affected by bacterial consumption or by conversion to carbon dioxide gas; therefore, later models neglected a reaction term, R_{ij}, for the differential mass balance of the aqueous carbonate ion. The aqueous potassium ion was not included in the mathematical model because experimental work showed it to compose less than three per cent of the aqueous cation content of the percolating solution at any one time. The mathematical model did not permit the formation of organic carbon compounds in the percolating solution; therefore, there was no provision for denitrification reactions. Heterotrophic bacteria were known to exist in the laboratory column; however, the mathematical model did not include their possible effect on the dissolved oxygen. The mathematical model for the Wet Period also did not allow for the decomposition of dead nitrifying bacteria.

The system comprising the mathematic model for the Dry Period consisted of a packed bed of homogeneous granules of mineral matter

acting as a support for a nitrifying bacterial community. The voids between granules were occupied by interstitial solution and a gas phase that was free to diffuse throughout the packed bed. Nitrosomonas and Nitrobacter were modeled to consume aqueous ammonium, nitrite, and oxygen chemical compounds and generate aqueous nitrite, nitrate, and hydrogen ions. As with the mathematical model for the Wet Period, the Dry Period model permitted cation exchange reactions. The gas phase acted as a source or sink for both oxygen and carbon dioxide; the total carbonate content of the aqueous phase during the Dry Period was permitted to change. The differential mass balance for chemical species in the gas phase would follow equation (51) without the convective term; the chemical species in the aqueous phase would have neither the convective nor the diffusive terms.

Gases of the mathematical model acted as sources or sinks for aqueous oxygen or carbon dioxide. It was assumed that the oxygen content of the aqueous phase, c_{O_2}, was in local equilibrium with the oxygen content of the gas phase, g_{O_2}, therefore,

$$c_{O_2} = \frac{Keq_{O_2}\, g_{O_2}}{g_{O_2} + 791} \tag{52}$$

where g_{O_2} is in mg/ℓ, and Keq_{O_2} is the equilibrium constant for the distribution of oxygen between the gas and aqueous phase. The overall transfer of carbon dioxide between the bulk gas phase and the bicarbonate ion dissolved in the interstitial solution was assumed to be in local equilibrium; therefore,

$$c_{H_2CO_3(aq)} + c_{CO_2(aq)} = Keq_{CO_2}\, g_{CO_2} \tag{53}$$

where g_{CO_2} is the gaseous concentration of carbon dioxide in mg/ℓ and Keq_{CO_2} is the distribution coefficient.

Nitrifying bacteria were assumed affixed to the mineral granules. In the presence of adequate space and chemical reactants, and in the absence of inhibiting chemical compounds, bacteria will divide regularly. The growth of a bacterial population, m_i, is

$$\frac{\partial m_i}{\partial t} = Kg_i \cdot m_i$$

where Kg_i is the maximum growth rate constant of the bacterial species, i. Extreme environmental conditions stop both bacterial growth and maintenance causing a decline of the bacterial population, m_i, according to

$$\frac{\partial m_i}{\partial t} = Kd_i \cdot m_i \tag{55}$$

where Kd_i is the death rate constant of the bacterial species, i. As specific chemicals necessary to the bacteria are consumed, the cell population gradually stops growing. The classical method for mathematically accounting for modification of bacterial growth due to deficiency of a chemical species of concentration, c_j, is to use the Michaelis expression to modify the bacterial growth rate constant,

$$Kg_i = Kg_{max,i} \prod_{j=1} \frac{c_j}{s_j + c_j} \tag{56}$$

$Kg_{max,i}$ is the largest growth rate constant for bacterial species, i, in the presence of sufficient chemical species and space for growth. s_j, the saturation constant for dissolved chemical species, c_j, is

the concentration of j for which the growth rate of the bacteria is just halved due to an insufficient concentration of c_j. Dissolved oxygen experimentally tends to be consumed, from the solution, to a low enough concentration that the Michaelis expression of oxygen was used to modify both nitrifying bacteria's growth rate constants. Michaelis expressions for aqueous ammonium and nitrite ion concentrations were used to modify the growth rate constants respectively of Nitrosomonas and Nitrobacter. Experimentally and theoretically it was found that the concentration of dissolved carbonate ions did not come close enough to a zero value to warrant its use in a Michaelis expression. Aqueous nitrite ions act a biostatic agents. Boon et al. (61) have concluded that the aqueous nitrous acid species inhibits the metabolism of Nitrobacter such that the growth rate constant can be described mathematically as

$$Kg_b = Kg_{max,b}/(1 + c_{NO_2}\, c_H\, 22000). \qquad (57)$$

c_{NO_2} and c_H are the aqueous concentrations of the nitrite ion (mg (N)/ℓ) and hydrogen ion (moles/ℓ). Equation (57) also mathematically allows for the decreased metabolism of the bacteria in increasingly acidic environments. Nitrosomonas is also inhibited by the presence of aqueous nitrite ions; however, there was little quantitative data to formulate an expression for the effect. The mathematical model for the Wet and Dry Period uses the same expression (57) to modify the growth rate constant of Nitrosomonas. Both nitrifying bacteria show an optimal growth in a solution of pH 8 (Boon et al., 61; Engel et al., 15; Hofman et al., 62; and Loveless, 11). Inhibition by aqueous

hydroxide was not included in the model. Nitrobacter was found to be inhibited by the aqueous nitrate ion (Boon et al., 61) above at least 300 mg NO_3^-(N)/ℓ. Nitrosomonas metabolism was hindered by aqueous ammonium concentrations above 700 mg NH_4^+(N)/ℓ (Hofman et al., 62). Inhibition effects by the aqueous nitrate and ammonium ions were neglected in the mathematical model because the maximum respective concentrations of the ions were found experimentally to be only 400 and 13 mg (N)/ℓ. Bacterial population densities are limited, at least by the physical size of space, if not by mass transfer limitations between the bacterial cell and the bulk of the aqueous medium. A maximum bacterial population density, m_{max}, was supplied to the mathematical model. If the maximum density is m_{max}, then the model modified the bacterial growth rate constant according to

$$Kg = Kg_{max} \left(1 - \frac{m}{m_{max}}\right) \tag{58}$$

It was assumed that in a given bacterial community bacteria are dying according to equation (55), irrespective of the environmental conditions, and growing according to equation (54). The net change to the Nitrosomonas population density, m_s, will be

$$\frac{\partial m_s}{\partial t} = \left[Kg_s \frac{c_{NH_4}\, c_{O_2}}{(s_{NH_4} + c_{NH_4})(s_{O_2} + c_{O_2})(1 + 22000\, c_{NO_2}\, c_H)} \left(1 - \frac{m_s}{m_{max}}\right) - Kd_s \right] m_s \tag{59}$$

The Nitrobacter population density, m_b, will change with time according to

$$\frac{\partial m_b}{\partial t} = \left[Kg_b \frac{c_{NO_2}\, c_{O_2}}{(s_{NO_2} + c_{NO_2})(s_{O_2} + c_{O_2})(1 + 22000\, c_{NO_2}\, c_H)} \left(1 - \frac{m_b}{m_{max}}\right) - Kd_b \right] m_b \qquad (60)$$

McLaren (63) equated the change of an aqueous substrate, c_i, due to a bacterial population, m, as

$$-\frac{dc_i}{dt} = \alpha \frac{dm}{dt} + \beta m + \gamma \frac{c_i}{K_m + c_i} m \qquad (61)$$

Here α, β, γ, and K_m are constants. The first term represents the consumption of substrate for cell growth, the second term accounts for substrate utilization for cell maintenance, and the third term expresses wastage of chemical substrate. McLaren reported the wastage term to be dominant over the other terms. Other data (Laudelout et al., 14) confirm McLaren's report that only 10 to 50 per cent of the energy extracted from the nitrification reactions goes to the production of cell material. The consumption of aqueous substrate by nitrifiers will be assumed to be of the form

$$-\frac{dc_i}{dt} = A_{ij}\, B_j m_j \qquad (62)$$

where A_{ij} represents the rate constant for the amount of substrate, c_i, consumed by a bacterial population, m_j, and B_j represents the modification of the rate constant, A_{ij}, due to deficiency of a necessary substrate or to inhibition of the bacterial metabolism due to a dissolved aqueous species. The formulation of B_j is identical to the formulation used to modify the growth rate constants. The B_j for Nitrosomonas is

$$B_s = \frac{c_{NH_4}\, c_{O_2}}{(s_{NH_4} + c_{NH_4})(s_{O_2} + c_{O_2})(1 + 22000\, c_{NO_2}\, c_H)} \qquad (63)$$

and for Nitrobacter the expression is

$$B_b = \frac{c_{NO_2}\, c_{O_2}}{(s_{NO_2} + c_{NO_2})(s_{O_2} + c_{O_2})(1 + 22000\, c_{NO_2}\, c_H)} \qquad (64)$$

Cation exchange reactions are included in the mathematical model for the aqueous species NH_4^+, H^+, Na^+, Mg^{++}, and Ca^{++}. The exchange reactions were considered to be in local equilibrium with the equilibrium expressions of the form equation (41). The total cation exchange capacity is assumed constant.

Constants used in the numerical solution of equations (51) through (64) are discussed in Appendix E. The numerical solutions themselves are also discussed in Appendix F.

Results of the Wet Period portion of the mathematical model are plotted in 24 hour intervals for a total of one week. The mathematical initial conditions for the Wet Period were set by assuming the soil was suddenly purged with solution thereby displacing the high dissolved solids containing solution of the Dry Period. As typified by experimental data, the initial aqueous ammonium ion concentration was close to zero whereas other aqueous species concentrations were identical to the concentration of the inlet solution.

Bacterial populations, in general, decreased in the soil of the mathematical model. Nitrosomonas bacterial populations were set between $10^{6.2}$ and $10^{5.6}$ cells per gram of soil at the start of the Wet Period in accordance with experimental bacterial population counts. The population of Nitrosomonas dropped as aqueous oxygen became depleted. Deep in the mathematical column where aqueous oxygen was still replenished by interstitial gaseous oxygen, Nitrosomonas populations grew in numbers only to decline when anoxic solution finally penetrated to the column's base. Nitrobacter population initially was set to $10^{6.6}$ cells per gram throughout the column. Due to a lack of both aqueous oxygen and nitrite ions, Nitrobacter populations decreased throughout most of the column. Only in the top six inches of the mathematical column did both bacterial population densities increase. Nitrosomonas populations at the top of the column were limited by the maximum population density set at $10^{7.3}$. Limitations of aqueous nitrite and oxygen leveled the the Nitrobacter population off at $10^{6.6}$ at the top of the column.

Aqueous oxygen initially was between 8.3 and 9.2 milligrams per liter but was soon pulled downward by bacterial metabolism, especially at the top of the column. In accordance with experimental findings, as oxygen deficient solution penetrated the depths of the mathematically modeled column, the solution was recharged with oxygen from interstitially held air. Eventually the interstitial air became devoid of oxygen and the percolating solution remained in an anaerobic state. In the top six inches of the column, aqueous ammonium ions of the inlet solution were nitrified in accordance with the quantity of aqueous oxygen available. Large inflections in the aqueous ammonium ion curve from 12 to 0 milligrams per liter were due to recharge of the soil surface with adsorbed ammonium ions. Eventually the inflection, or breakthrough curve, moved down and out of the column confining any change in aqueous ammonium ions to the top of the column. Wet Period aqueous ammonium ion concentrations of the model simulated the data taken from the laboratory column. Aqueous nitrite ion content for the modeled Wet Period solution generated by Nitrosomonas bacteria eventually appeared only in the top six inches of the column. The mathematical model's inlet solution contained 4.76 milligrams $NO_3^-(N)$ per liter. With available oxygen and nitrite ions, Nitrobacter produced increasingly more aqueous nitrate ions until approximately 11 milligrams $NO_3^-(N)$ per liter existed in the modeled percolating solution at the 7-foot depth. Production of aqueous nitrate ions was eventually held down to only one milligram $NO_3^-(N)$ per liter when aqueous oxygen was limited to the top of the mathematically

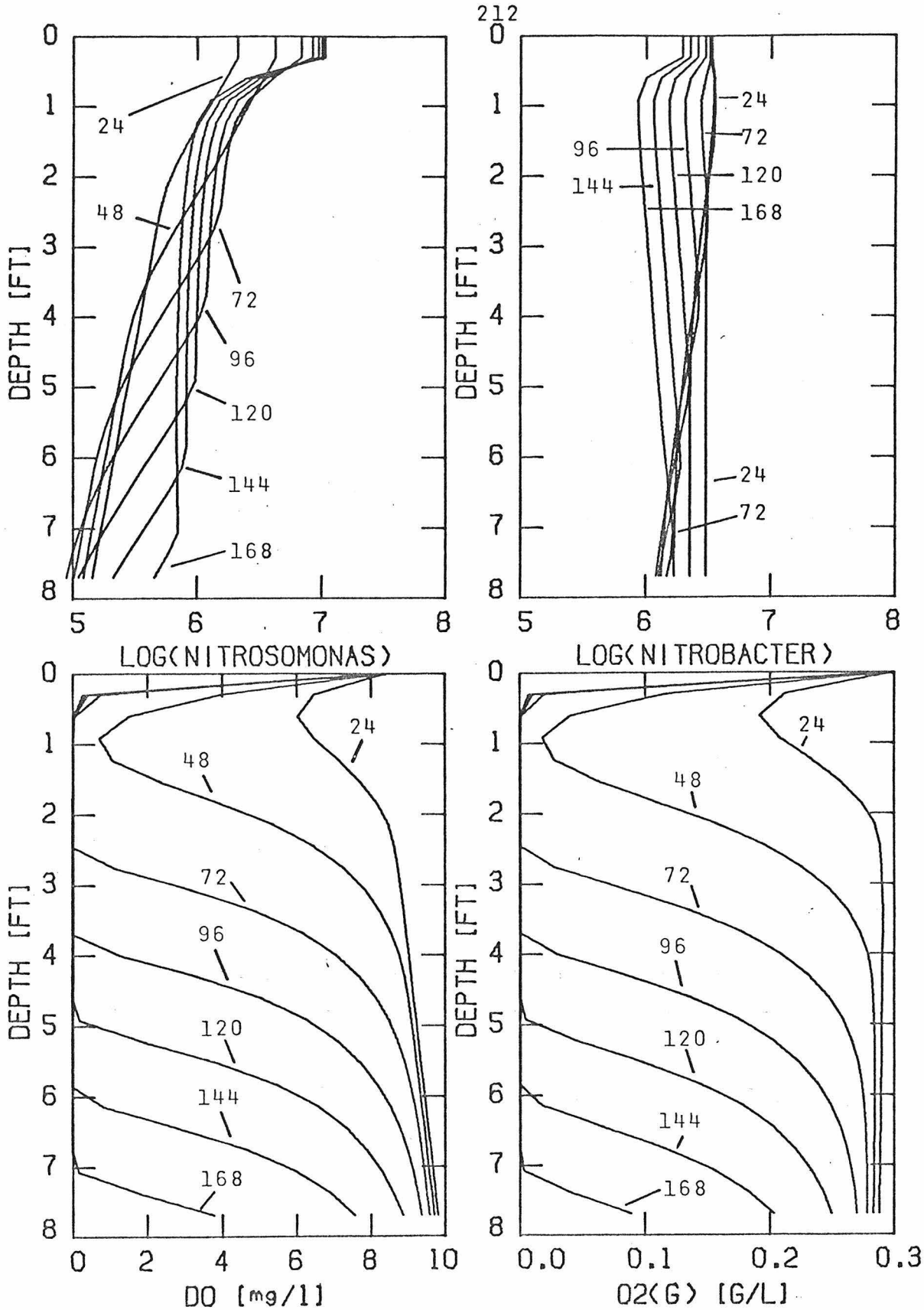

Figure 92: Theoretical Population Densities of Nitrosomonas and Nitrobacter and Concentrations of Dissolved Oxygen and Gaseous Oxygen During Seven Day Wet Period

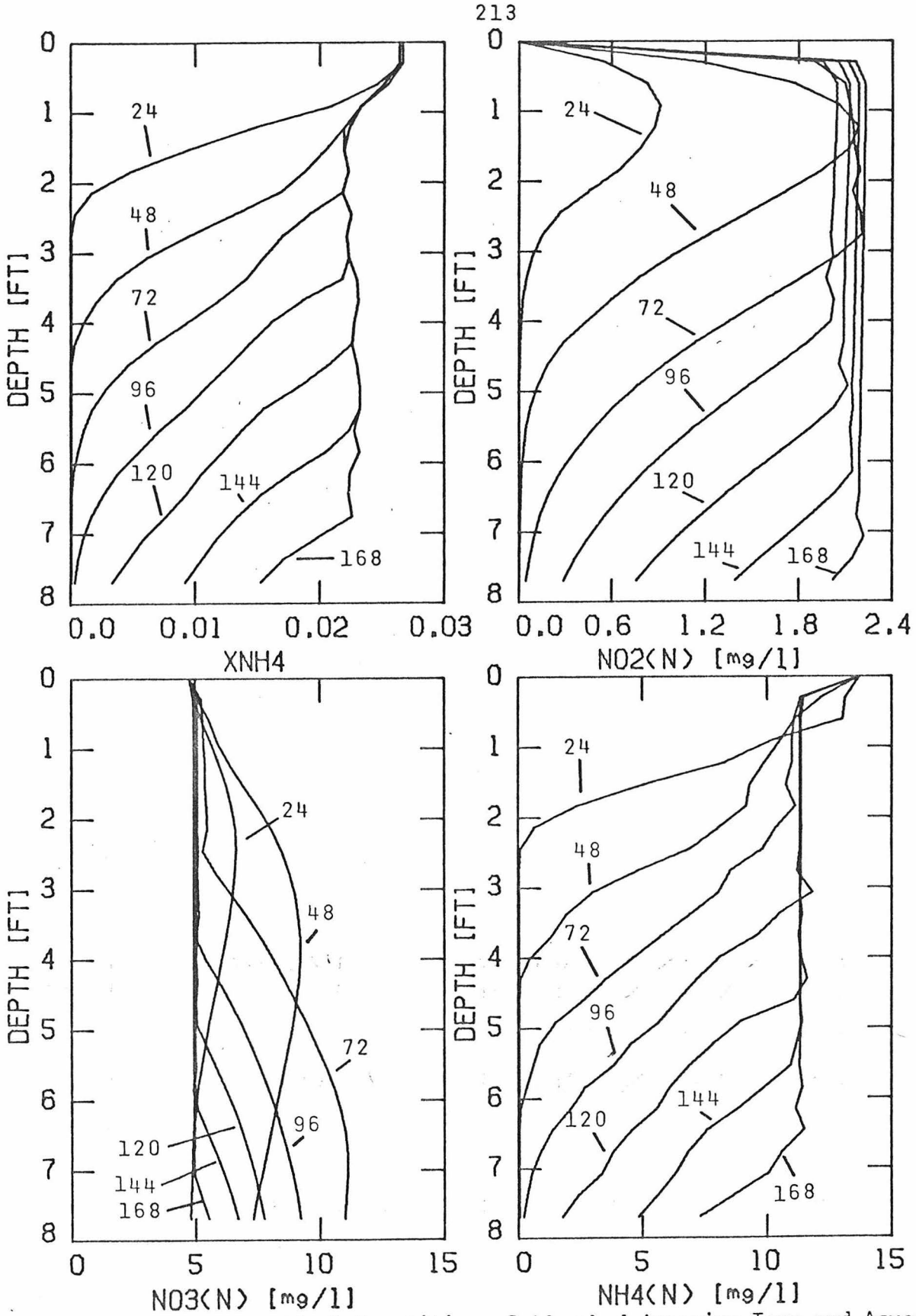

Figure 93: Theoretical Quantities of Adsorbed Ammonium Ions and Aqueous Nitrite, Nitrate, and Ammonium Ions During Seven Day Wet Period

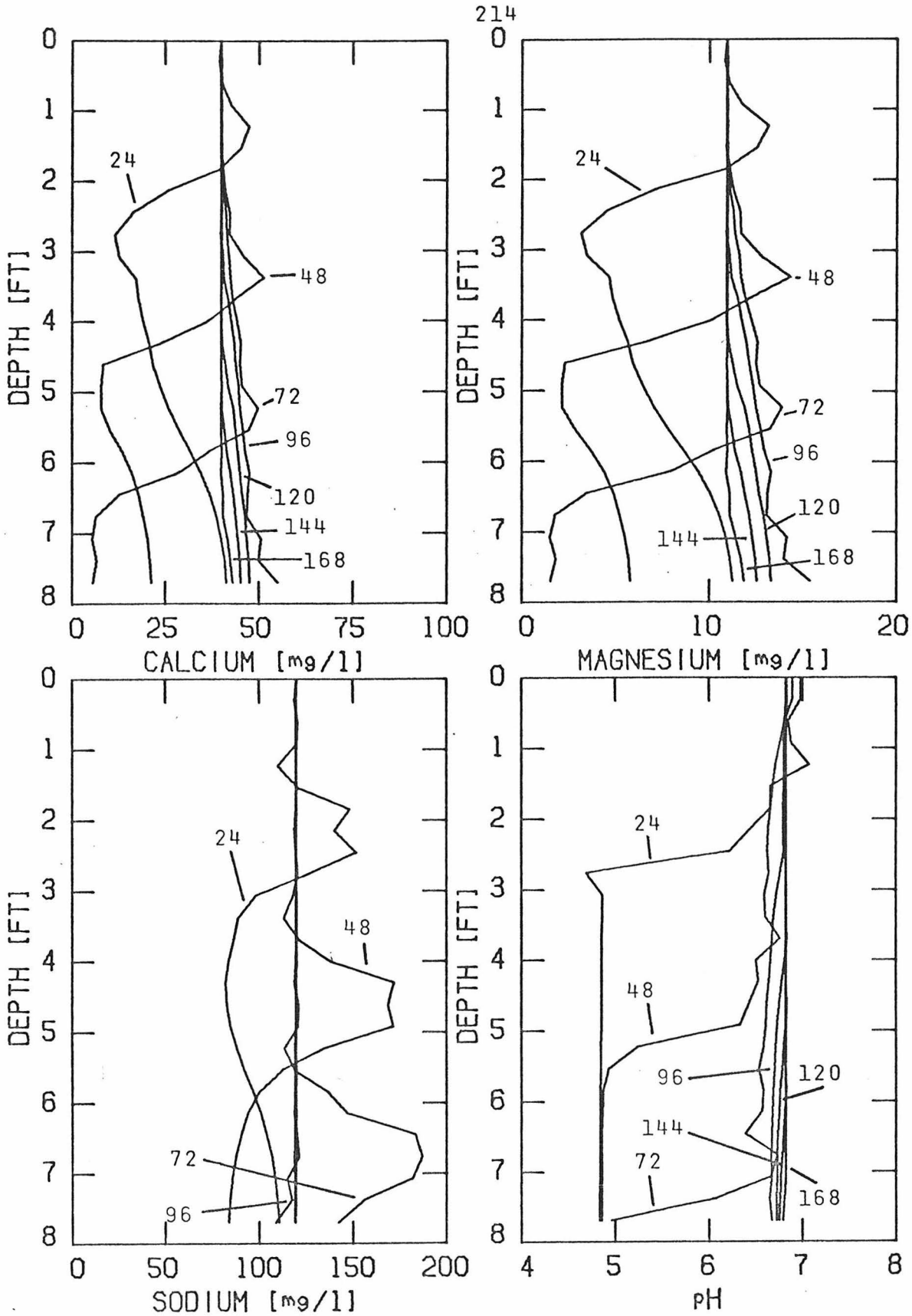

Figure 94: Theoretical Quantities of Aqueous Calcium, Magnesium, Sodium, and Acidity During Seven Day Wet Period

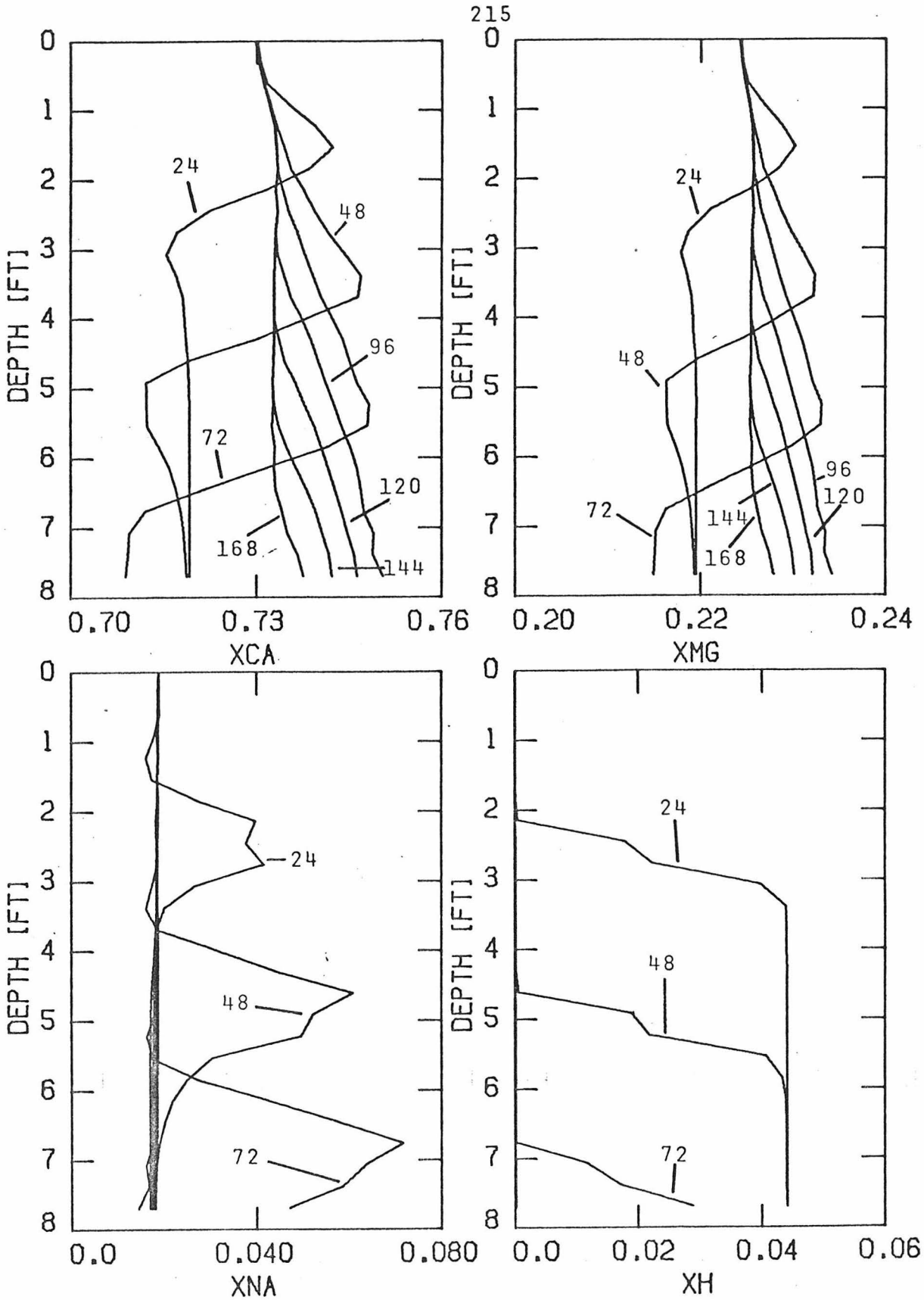

Figure 95: Theoretical Quantities of Adsorbed Calcium, Magnesium, Sodium, and Hydrogen Ions During Seven Day Wet Period

modeled column. The Wet Period mathematical model for the nitrogenous aqueous species is in good correspondence with the actual laboratory data.

The particular initial conditions of the Wet Period model caused a slight adsorption of aqueous alkaline earth cations onto the sand throughout the column at the first onset of the percolation. As percolation progressed the same alkaline earth cations were desorbed into the solution. The position of the cation desorption reaction is located at the breakthrough curve of the respective cation. The aqueous hydrogen ion breakthrough curve moved down through the mathematically modeled column with the fastest rate of eight feet in 72 hours. The aqueous ammonium ion breakthrough curve moved at the much slower rate of eight feet in 144 hours. Interaction of the breakthrough curves caused a multiplicity of inflections in the concentration profiles of the aqueous cations. The lingering aqueous ammonium ion breakthrough curve resulted in inflecting the aqueous calcium and magnesium concentrations upward slightly in response to adsorption of ammonium ions. The transient depth profiles of the aqueous concentrations of the alkaline earth cations were not verified experimentally; however, the modeled aqueous ammonium ion profiles compare well with the experimental data (Figures 61 and 72). Experimental pH profiles tend to be much broader than the model predicted.

Results of the Dry Period mathematical model are presented with 12 hour intervals for a total of four days. The effective porosity of the top foot of the mathematically modeled column was set to increase

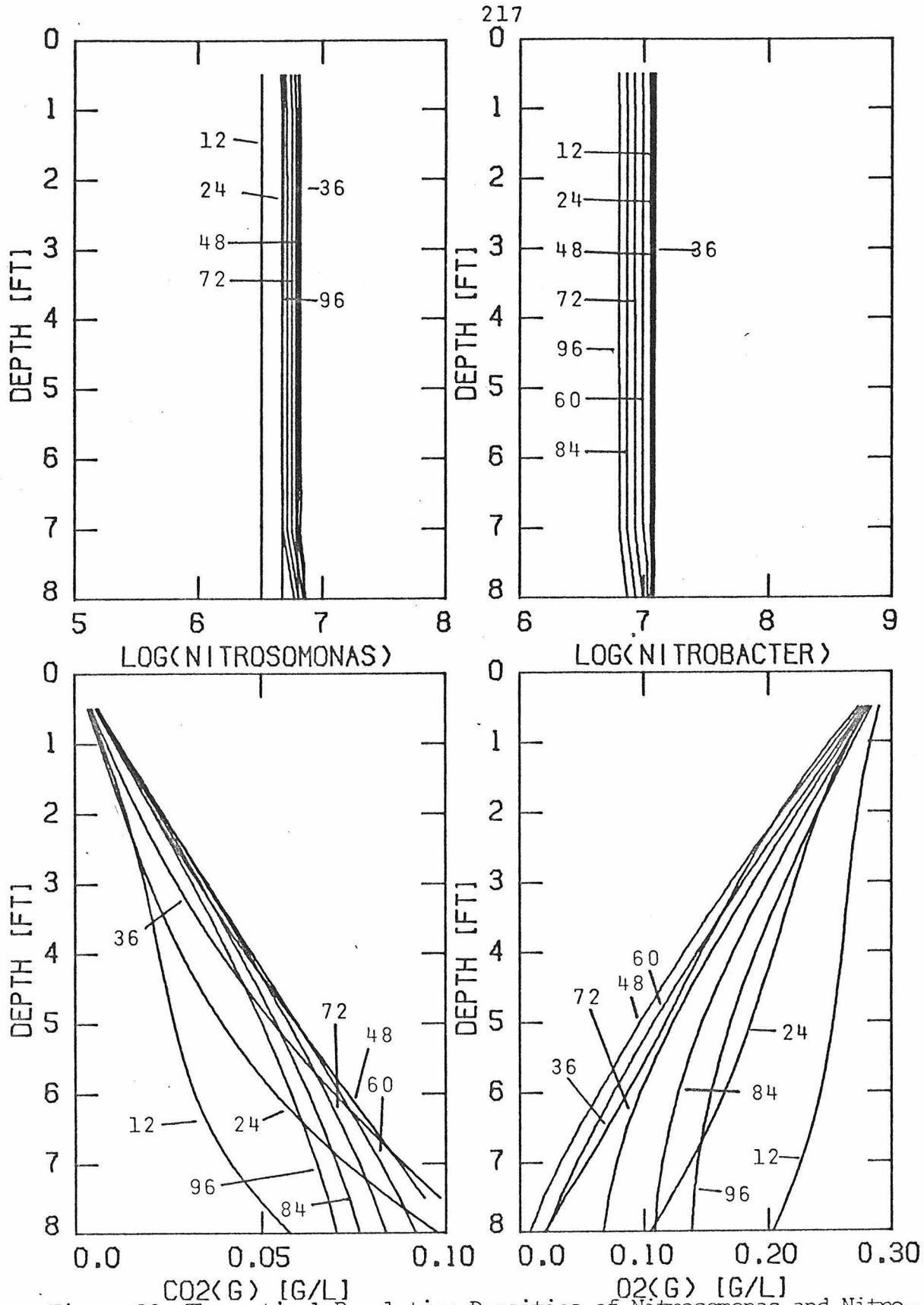

Figure 96: Theoretical Population Densities of Nitrosomonas and Nitrobacter and Concentrations of Gaseous Carbon Dioxide and Oxygen During First Four Days of Dry Period

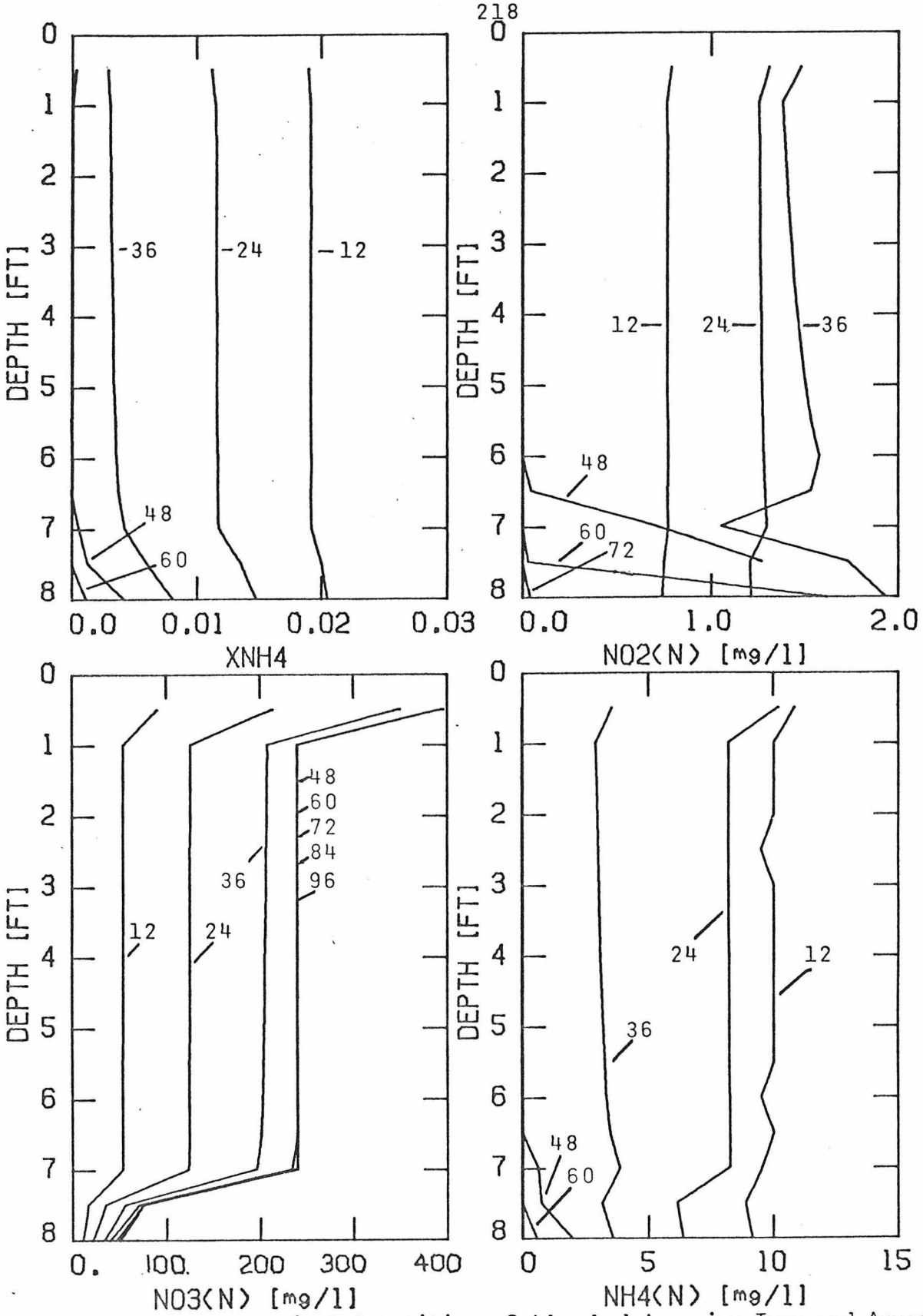

Figure 97: Theoretical Quantities of Adsorbed Ammonium Ions and Aqueous Nitrite, Nitrate, and Ammonium Ions During First Four Days of Dry Period

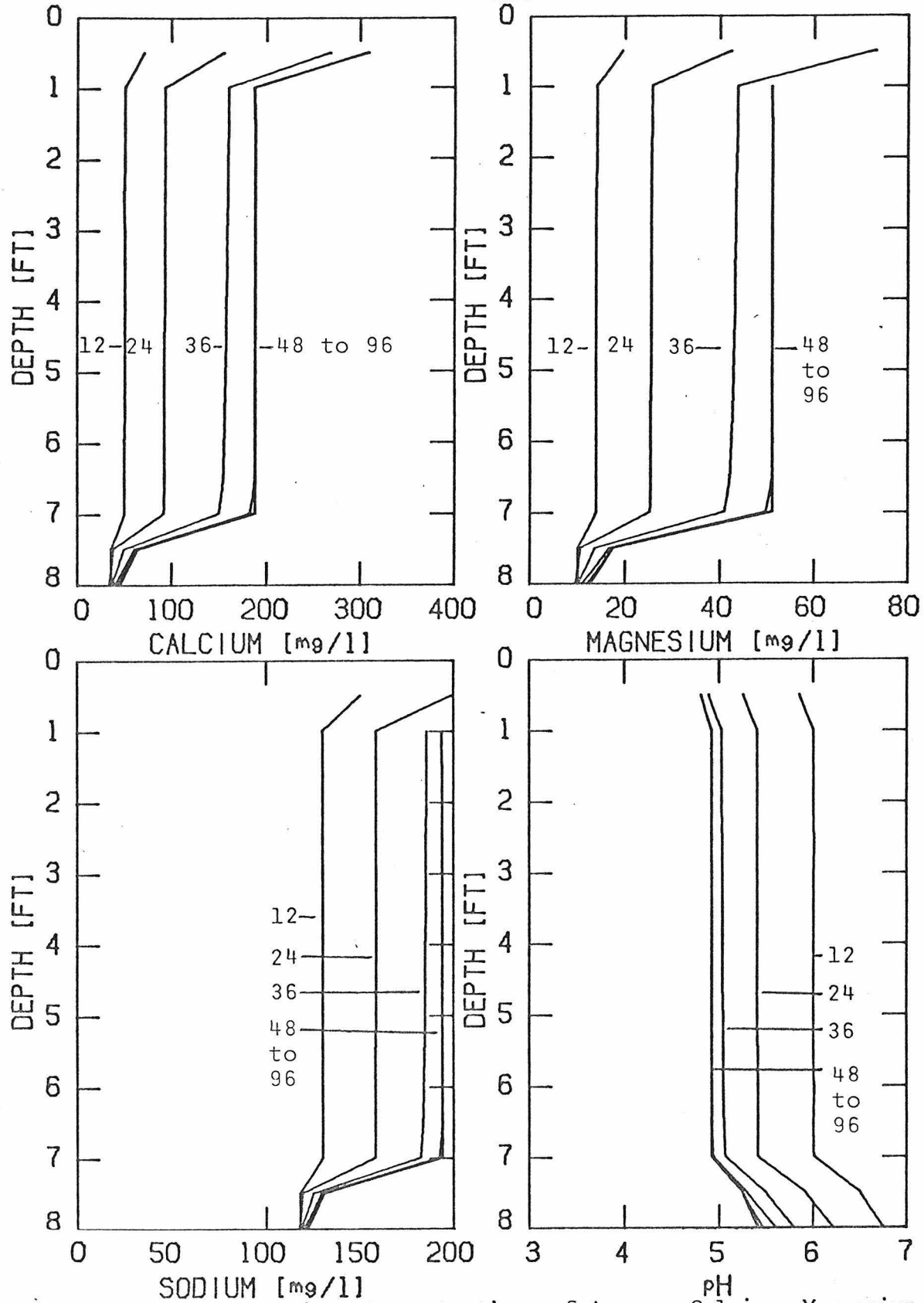

Figure 98: Theoretical Concentrations of Aqueous Calcium, Magnesium, Sodium, and Hydrogen Ions During First Four Days of Dry Period

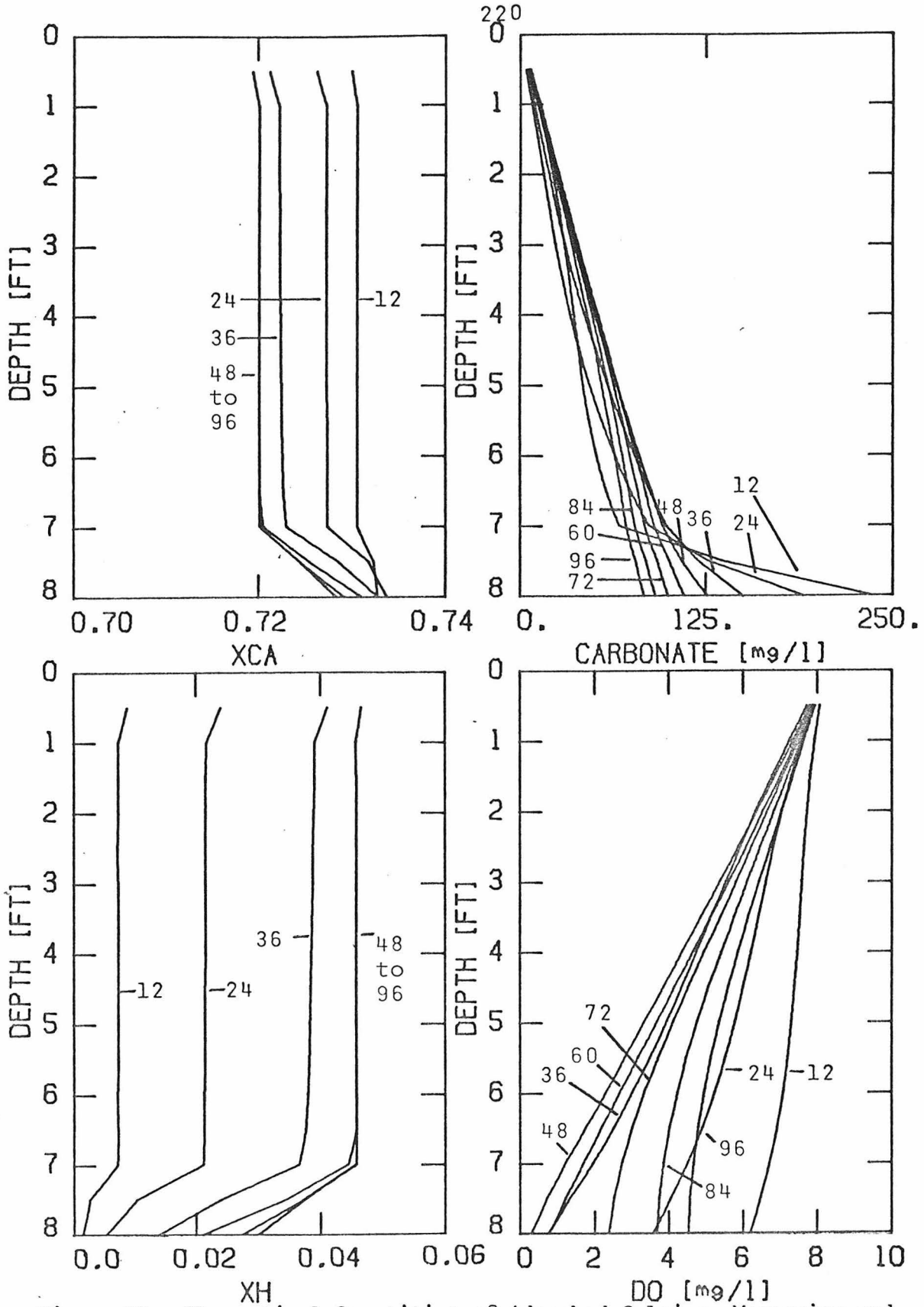

Figure 99: Theoretical Quantities of Adsorbed Calcium, Magnesium and Hydrogen Ions and Aqueous Oxygen During First Four Days of Dry Period

from 0.03 to 0.06 volume fraction. Between the one-foot depth and the seven-foot depth the effective porosity was 0.06 volume fraction. Below the seven-foot depth the porosity increased linearly from 0.06 to 0.39. The initial population density of Nitrobacter bacteria in the model was set at twice the number at the end of the previous Wet Period. Both nitrifying bacteria grew in numbers throughout most of the period up to 36 hours since the start. Their growth stopped as aqueous ammonium and nitrite ion concentrations became deficient. Carbon dioxide gas was generated in the gaseous atmosphere of the modeled column due to conversion of bicarbonate ions with generated aqueous hydrogen ions. The largest total aqueous carbonate ion decline occurred in the first 12 hours of the Dry Period. Eventually the total carbonate content of solution at the base of the column was 100 milligrams per liter and that near the top was 0 milligrams per liter. Gaseous oxygen profiles show the most extensive consumption of the gas was at the start of the Dry Period. As nitrification proceeded, aqueous ammonium ion content of the interstitial solution steadily decreased to zero. A corresponding increase of aqueous nitrate ion levels in the interstitial solution of the mathematical model to 250 milligrams per liter was predicted. Aqueous nitrite content of the solution remained below 2 milligrams per liter. Aqueous calcium, magnesium, and to a lesser extent sodium were desorbed from the modeled sand into the interstitial solution and their adsorbed counterparts showed drops in value. The computed dissolved oxygen contents of the solution film were depressed toward zero.

The Wet Period mathematical model qualitatively predicted the

the transient behavior of aqueous species in a percolating solution. The bacterial population density of Nitrobacter was experimentally found to be larger than that of Nitrosomonas. The mathemtical model predicted the Nitrobacter population to drop below the population of Nitrosomonas. Eventually, with successive Wet/Dry Periods, the Nitrosomonas population would exceed that of Nitrobacter thereby causing aqueous nitrite ion concentrations to build up over aqueous nitrate ion concentrations. The aqueous oxygen and nitrogenous species concentrations of the model were in good agreement with experimental results. The width of the zone of sand desorbing aqueous hydrogen ions for the model was much narrower than experimental findings.

The Dry Period model was also in good qualitative agreement with the experimental results. The bottom one to two feet of the laboratory column was saturated with solution throughout the duration of the Dry Period. The modeled column was given a low effective porosity at the bottom. The low porosity caused the observed inflections in the oxygen and carbon dioxide gas profiles at the column's base to become more prominent. There was a much larger quantity of carbon dioxide generated at the start of the modeled Dry Period than experimentally found; furthermore, a lesser concentration of total aqueous carbonate ions persisted in the modeled column than in the experimental column. Twice as much aqueous sodium was added to the interstitial solution than experimentally observed. Less drastic addition of salts to the interstitial solution at the column's bottom was correctly

predicted. The experimental column showed lesser additions of salts to the interstitial solution at the column's top than elsewhere; however, the model predicted more of an addition.

SUMMARY,RECOMMENDATIONS,ENGINEERING SUGGESTIONS

In consideration of the Dry Period portion of the intermittent groundwater recharge process, it will be assumed that the soil has attained an equilibrium between cations in its electric double layer and the percolating secondary treated sewage effluent of the Wet Period. Ideally the Dry Period is initiated by a sudden withdrawal of solution from the soil, thereby leaving behind mineral grains coated with a solution film and surrounded by air. The film is well-aerated by gaseous oxygen diffusion into the soil matrix. Conversion of aqueous ammonium ions to nitrate ions is catalyzed by colonies of Nitrosomonas and Nitrobacter (other species of nitrifying bacteria are possible). The Nitrosomonas bacteria acquire energy by converting aqueous ammonium ions to aqueous nitrite ions. A larger population of Nitrobacter bacteria consumes the biostatic nitrite ion to give the nitrate ion. Hydrogen ions generated by Nitrosomonas first are consumed in converting some of the solution's bicarbonate ions to carbon dioxide gas which diffuses out from the soil. As aqueous ammonium ions are continuously converted to nitrite ions, adsorbed ammonium ions are desorbed off the mineral surfaces. Concurrently aqueous hydrogen ions fill the vacancy left by the ammonium ions. As nitrification continues and the aqueous hydrogen ion content climbs, calcium, magnesium, sodium, and potassium ions are ion exchanged by the aqueous hydrogen ion into the interstitially held solution. Because the solution's pH does not drop substantially, the net effect is a conversion of adsorbed ammonium and alkaline earths into dissolved alkaline earth nitrate salts.

Degradation of soil minerals as a result of the acidification of the interstitial solution occurs as a secondary source of aqueous cations. For a granitic sand, aluminosilicate minerals are responsible for sources of aqueous silica. Based on the quantity of silica released, approximately one per cent of the cations added to the interstitial solution originated from dissolution of the minerals. All adsorbed ammonium ions are converted to nitrate ions in two days with little accumulation of ammonia or nitric oxide gases or nitrite ions. Close to the soil surface nitrification is hindered possibly due to drying of the soil. Once the aqueous ammonium ions are depleted, metabolism by Nitrosomonas and Nitrobacter ends and cell population densities begin to decline. Spontaneous degradation of the cellular matter, or degradation catalyzed by heterotrophic bacteria, causes a renewed production of gaseous carbon dioxide. The overall result of the Dry Period is that cations adsorbed to the soil minerals are replaced slightly by hydrogen ions and the solution film surrounding the minerals acquires a huge concentration of dissolved nitrate salts.

Lack of aqueous ammonium ions in the percolating solution would prevent Dry Period nitrification reactions; furthermore, organics would encourage the growth of aerobic heterotrophic bacteria in the soil and result in their competing with nitrifying bacteria for oxygen. Limited quantities of aqueous bicarbonate ions in the percolating solution would result in the generation of more cations in the interstitial solution. Because most of the ammonium ions nitrified originally were adsorbed to the soil minerals, addition of competing aqueous

cations with plus three or four valences will reduce the extent of nitrification in the soil during the Dry Period. Only a small fraction of the adsorbed alkaline earth cations are desorbed during the Dry Period; once the soil has adsorbed a particular cation, it will appear over and over again in successive Dry Period interstitial solutions.

The source of cations in samplings taken at the Whittier Narrows test plot follows the same pattern shown with the laboratory column and with the mathematical model. Nitrification at Whittier Narrows is limited to the top three to four feet of the soil due to the siltiness of the soil limiting diffusion of oxygen. The leading edge of solution traveling down through the soil matrix is high in aqueous nitrate, calcium, magnesium, and sodium. Aqueous bicarbonate ion concentration does not drop due to a three to five per cent occurrence of carbonates in the soil and aerobic heterotrophic bacterial activity acting on native organic compounds. The source of aqueous calcium and magnesium in the Whittier Narrows test basin aqueous solution is primarily due to the desorption of adsorbed calcium and magnesium. Dissolution of calcites or dolomites is not important judging from the lack of a substantial increase of aqueous bicarbonate ions with the hardness increase. The total dissolved solids increase at the Whittier Narrows test plot is a result of cation exchange reactions during the first day of the Dry Period in the top four feet of the soil. Hardness in the percolating solution is a result of calcium and magnesium ions being extracted from previously percolating solutions and adsorbing to

the soil. The net result over many successive periods is but a slight increase of Total Dissolved Solids added to the groundwater reservoirs. Prevention of the transient wave of dissolved solids would be possible by conversion of the aqueous ammonium ions to nitrate ions before the solution percolates into the soil. After a period of adjustment with respect to cation exchange reactions, which would tend to momentarily add aqueous cations to the percolating solution throughout the Wet Period, no change of Total Dissolved Solid content of the percolating solution would be apparent in the top four feet of the soil.

Cation exchange equilibrium distributions for the mathematical model were forced to correspond to the experimental data by adjustment of the cation exchange equilibrium coefficients to values different from those derived from Figure 53. The cation exchange mechanism must be determined in more detail. There is a specific adsorption of the aqueous ammonium and hydrogen ions to the granitic sand causing more ammonium and hydrogen ions to be adsorbed to the sand than sodium ions (Figure 53). Specific adsorption is further suggested by the apparent variation of the cation exchange capacity of the mineral mixture (page 121). A quantitative mathematical model of the variation of cationic species throughout the intermittent groundwater recharge process would require the determination of the amount of cations in the electric double layer and bonded to the mineral surface.

Several aspects of the biological system of the soil must be clarified. Aerobic heterotrophic bacteria compete for oxygen with the nitrifiers. Despite the lack of organic carbon in the inputs to the

laboratory column, heterotrophic bacteria populated the sand surfaces. A mathematical model should include the presence of heterotrophic bacteria. The model's Dry Period bacterial population densities had to be adjusted upward to permit the nitrification reactions to be completed in 2 days. The quantitative analysis of bacteria on the soil required the assumption that all bacteria could be forced off the soil and into a solution by vibrating the soil in a solution. The validity of the assumption should be tested. The mathematical model for the bacterial population densities should be changed to show the lag phase typical of bacterial population variations; furthermore, the inhibition of bacterial growth to acid should be refined. The diminished bacterial activity at the top of the laboratory column during the Dry Period should be investigated as possibly due to insufficient moisture.

Mineral dissolution was only a slight contributor of dissolved solids to the Dry Period solution film of the laboratory column. Research is needed to determine if, when large quantities of ammonium ions are adsorbed to the sand, the resulting larger concentration of acid resulting from the nitrification reaction could cause more extensive mineral dissolution. Investigation of the influence of carbonate minerals on the solution is needed because of the widespread occurrence of carbonate minerals in the soils.

An eight foot thick layer of granitic sand, of grainsize 0.5 mm, could be spread over the existing percolation site. Solution would be percolated through the layer until the aqueous ammonium ion content of the effluent from the layer showed a non-zero value. A three day

Dry Period would be long enough for all the adsorbed ammonium ions to be nitrified. Aqueous hydrogen ions produced by the reaction would desorb alkaline earth cations from the mineral surfaces into the interstitially held solution film. To terminate the Dry Period secondary treated sewage effluent would be pumped at a rate greater than 2 ft/day into the bottom of the eight foot thick layer of sand. Coarseness of the overlying layer, compared to the subsurface sand, would result in solution percolating upward carrying the solution film of salts up and out of the sand layer. Once the solution film was discarded flow of the sewage effluent would start from the top again. The removal of the solution film (4-5 percent of the total percolated solution) would reduce the net quantities of ammonium, calcium, and magnesium ions added to the groundwater reservoirs by 80, 25, and 30 percent respectively.

Several nonideal situations are possible that would harm the percentage reduction of ammonium and alkaline earth cations. If the sand became clogged or was silty by nature, oxygen diffusion hindrance would diminish nitrification reaction the percentage of ammonium removal. Nitrification would also be hindered by excessive quantities of adsorbed ammonium ions which would yield bacterially inhibitive concentrations of aqueous nitrate ions in the solution film. Too coarse of a sand would permit so much aeration that moisture levels would drop so as to be inhibitive for bacterial nitrification reactions. Ideal operation would result in a beneficial reduction of dissolved salts added to the groundwater reservoirs.

REFERENCES

1. Mitchelson, A. T. 1937. Spreading Water for Storage Underground, U.S.D.A. Technical Bulletin 578.

2. Leonard, R. L. 1964. Integrated Management of Ground and Surface Water in Relation to Water Importation. University of California, Division of Agricultural Science (California Agricultural Experiment Station, Gianini Foundation Research Report #279).

3. McMichael, F. C. and McKee, J. E. 1965. Report of Research on Wastewater Reclamation at Whittier Narrows. W. M. Keck Laboratory of Environmental Engineering, California Institute of Technology.

4. Reid, D. M. 1972. Surface Spreading of Reclaimed Water. California State Polytechnic College Kellog-Voorhis.

5. Reid, D. M. 1973. Whittier Narrows Test Basin Progress Report. Los Angeles County Flood Control District.

6. Pincince, A. B. 1968. Oxygen Relationships in Intermittent Sand Filtration of Wastewaters. Ph.D. thesis, California Institute of Technology.

7. Lance, J. C. and Whisler, F. D. 1972. Nitrogen Balance in Soil Columns Intermittently Flooded with Secondary Sewage Effluent. Journal of Environmental Quality 1:180-185.

8. Bouwer, H. 1969. Waste Water Renovation by Ground-Water Recharge through Surface Spreading in the Salt River Bed, Phoenix, Arizona. The Flushing Meadows Project Annual Report, U.S. Water Conservation Laboratory Agricultural Research Service, U.S.D.A., Phoenix, Arizona.

9. Bouwer, H. 1970. Water Quality Aspects of Intermittent Systems using Secondary Sewage Effluent. Artificial Groundwater Recharge Conference, University of Reading, England.

10. Bouwer, H. 1971. Waste-Water Renovation by Spreading Treated Sewage for Ground-Water Recharge. U.S. Water Conservation Laboratory Annual Report abstraction. Phoenix, Arizona.

11. Loveless, J. E. and Painter, H. A. 1968. The Influence of Metal Ion Concentrations and pH Value on the Growth of a Nitrosomonas Strain from Activated Sludge. Journal of General Microbiology. 52:1-14.

12. Lees, H. 1952. The Biochemistry of the Nitrifying Organisms. Biochemistry of the Nitrifying Organisms. Biochemistry Journal. 52:134-139.

13. Dessers, A., Chiang, A. D., and Laudelout, H. 1970. Calorimetric Determination of the Free Energy Efficiency in Nitrobacter Winogradskyi. Journal of General Microbiology. 64:71-76.

14. Laudelout, H., Simonart, P-C., and van Droogenbroeck, R. 1968. Calorimetric Measurement of Free Energy Utilization by Nitrosomonas and Nitrobacter. Archiv für Mikrobiologie. 63:256-277.

15. Engel, M. S. and Alexander, M. 1958. Growth and Autotrophic Metabolism of Nitrosomonas Europea. Journal of Bacteriology. 76:217-222.

16. Stanier, R. Y. 1963. The Microbial World. Prentice-Hall, Englewood Cliffs.

17. Breed, R. S. 1957. Bergey's Manual of Determinative Bacteriology. Williams and Wilkins, Baltimore.

18. Barber, R. G. and Rowell, D. L. 1972. Charge Distribution and the Cation Exchange Capacity of an Iron-Rich Kaolinitic Soil. Journal of Soil Science. 23:134-146.

19. Sivasubramaniam, S. and Talibudeen, O. 1972. Potassium-Aluminum Exchange in Acid Soils I. Kinetics. Journal of Soil Science. 23:162-175.

20. Stumm, W. and Morgan, J. M. 1970. Aquatic Chemistry. Wiley-Interscience, New York.

21. Harned, H. S. and Nuttal, R. L. 1949. The Differential Diffusion Coefficient of Potassium Chloride in Aqueous Solutions. Journal of the American Chemical Society. 71:1460-1463.

22. Yoshida, T. and Alexander, M. 1970. Nitrous Oxide Formation by Nitrosomonas Europaea and Heterotrophic Microorganisms. Soil Science Society of America Proceedings. 34:880-883.

23. Verhoeven, W. 1956. Some Remarks on Nitrate and Nitrite Metabolism in Microorganisms. Johns Hopkins University, McCollum-Pratt Institute Contribution Number 125:61-87.

24. van Olphen, H. 1963. An Introduction to Clay Colloid Chemistry. Interscience Publications.

25. Harned, H. S. and Parker, H. W. 1955. The Diffusion Coefficient of Calcium Chloride in Dilute and Moderately Dilute Solutions at 25^{o}. Journal of the American Chemical Society. 77:265-266.

26. Miyauchi, T. and Kikuchi, T. 1975. Axial Dispersion in Packed Beds. Chemical Engineering Science. 30:343-348.

27. Garrels, R. M. and Christ, C. L. 1965. Solutions, Minerals, and Equilibria. Harper and Row, New York.

28. Tanabe, K. 1970. Solid Acids and Bases. Academic Press, Tokyo.

29. Wollast, R. 1967. Kinetics of the Alteration of K-feldspar in Buffered Solutions at Low Temperature. Geochimica et Cosmochimica Acta. 31:635-648.

30. Lagerström, G. 1959. Equilibrium Studies of Polyanions. Acta Chemica Scandinavica. 13:722-736.

31. van Lier, J. A., de Bruyn, P. L., and Overbeck, J. T. G. 1960. The Solubility of Quartz. Journal of Physical Chemistry. 64:1675-1682.

32. Henderson, J. H., Syers, J. K., and Jackson, M. L. 1970. Quartz Dissolution as Influenced by pH and the Presence of a Disturbed Surface Layer. Israel Journal of Chemistry. 8:357-372.

33. Helgeson, H. C. 1972. Kinetics of Mass Transfer among Silicates and Aqueous Solutions: Correction and Clarification. Geochimica et Cosmochimica Acta. 36:1067-1077.

34. Amphlett, C. B. 1964. Inorganic Ion Exchangers. Elsevier Publishing Co., Amsterdam.

35. Helgeson, H. C., Garrels, R. M., and MacKenzie, F. T. 1969. Evaluation of Irreversible Reactions in Geochemical Processes Involving Minerals and Aqueous Solutions II. Geochimica et Cosmochimica Acta. 33:455-481.

36. Gardner, L. R. 1970. A Chemical Model for the Origin of Gibbsite from Kaolinite. American Mineralogist. 55:1380-1389.

37. Garrels, R. M. 1957. Some Free Energy Values from Geologic Relations. American Mineralogist. 42:780-791.

38. Weaver, C. E. 1967. The Significance of Clay Minerals in Sediments;

in Fundamental Aspects of Petroleum Geochemistry. (ed.) Bartholomew Nagy, Amsterdam.

39. Reed, M. G. and Scott, A. D. 1962. Kinetics for Potassium Release from Biotite and Muscovite in Sodium Tetraphenylboron Solutions. Soil Science Society of America Proceedings. 26:437-439.

40. Yip, H. 1973. Mass Transfer Coefficients in Packed Beds at Low Reynolds Numbers. University of California, Berkeley. Lawrence Berkeley Lab. LBL-1831.

41. Wilson, E. J. and Geankoplis, C. J. 1966. Mass Transfer at Very Low Reynolds Numbers in Packed Beds. I & EC Fundamentals. 5:9-14.

42. Harned, H. S. and Hildreth, C. J. 1951. The Differential Diffusion of Lithium and Sodium Chlorides in Dilute Aqueous Solutions at 25°. Journal of the American Chemical Society. 73:650-652.

43. Helfferich, F. 1962. Ion Exchange. McGraw-Hill, New York.

44. Frye, K. 1974. Modern Mineralogy. Prentice-Hall, New Jersey.

45. Deju, R. A. 1971. A Model of Chemical Weathering of Silicate Minerals. Geological Society of America Bulletin. 82:1055-1062.

46. Siever, R. and Woodfard, N. 1973. Sorption of Silica by Clay Minerals. Geochimica et Cosmochimica Acta. 37:1851-1880.

47. Kerr, P. F. 1959. Optical Mineralogy. McGraw-Hill, New York.

48. Parks, G. A. 1967. Aqueous Surface Chemistry of Oxides and Complex Oxide Minerals, in Equilibrium Concepts in Natural Water Systems, Advances in Chemistry Series, number 67, Washington D. C.

49. Dugger, D. L., Stanton, J. H., Irby, B. N., McConnell, B. L., Cunnings, W. W., and Maatman, R. W. 1964. The Exchange of Twenty Metal Ions with the Weakly Acidic Silanol Group of Silica Gel.

Journal of Physical Chemistry. 68:757-760.

50. Hodgman, C. D. (ed.). 1963. Handbook of Chemistry and Physics. Chemical Rubber Co., Cleveland.

51. Knowles, G., Downing, A. L., and Barrett, M. J. 1965. Determination of Kinetic Constants for Nitrifying Bacteria in Mixed Culture, with the Aid of an Electronic Computer. Journal of General Microbiology. 38:263-278.

52. Lijklema, L. 1973. Model for Nitrification in Activated Sludge Process. Environmental Science and Technology. 7:428-433.

53. Moore, G. S. M. and Rose, H. E. 1975. Dissolution of Powdered Quartz. Nature. 253:525-527.

54. Edwards, M. F. and Richardson, J. F. 1968. Gas Dispersion in Packed Beds. Chemical Engineering Science. 23:109-123.

55. Pincince, A. B. 1968. Oxygen Relationships in Intermittent Sand Filtration of Wastewaters. Ph.D. Thesis, California Institute of Technology.

56. Taras, M. J. (ed.). 1971. Standard Methods. American Public Health Association, Washington D. C.

57. Pramer, D. 1957. The Influence of Physical and Chemical Factors on the Preparation of Silica Gel Media. Applied Microbiology. 5:392-395.

58. Collins, R. E. 1961. Flow of Fluids through Porous Materials. Reinhold, New York.

59. Lewis, R. F. and Pramer, D. 1958. Isolation of Nitrosomonas in Pure Culture. J. Bacteriology. 76:524-528.

60. Delwiche, C. C. and Finstein, M. S. 1965. Carbon and Energy

Sources for the Nitrifying Autotroph Nitrobacter. J. Bacteriology. 90:102-107.

61. Boon, B. and Laudelout, H. 1962. Kinetics of Nitrite Oxidation by Nitrobacter Winogradskyi. Biochemistry Journal. 85:440-447.

62. Hofman, T. and Lees, H. 1952. The Biochemistry of the Nitrifying Organisms. 4. The Respiration and Intermediary Metabolism of Nitrosomonas. Biochemistry Journal (London). 54:579-583.

63. McLaren, A. D. 1971. Kinetics of Nitrification in Soil: Growth of the Nitrifiers. Soil Science Society of America Proceedings. 35:91-95.

64. van Gool, A. P., Tobback, P. P., and Fischer, I. 1971. Autotrophic Growth and Synthesis of Reserve Polymers in Nitrobacter Winogradskyi. Archiv für Mikrobiologie. 76:252-264.

65. Ardakani, M. S., Schulz, R. K., and McLaren, A. D. 1974. A Kinetic Study of Ammonium and Nitrite Oxidation in a Soil Field Plot. Soil Science Society of America Proceedings. 38:273-277.

66. Pan, P. and Umbreit, W. W. 1972. Growth of Mixed Cultures of Autotrophic and Heterotrophic Organisms. Canadian Journal of Microbiology. 18:153-156.

67. Lance, J. C. 1972. Nitrogen Removal by Soil Mechanisms. Journal Water Pollution Control Federation. 44:1352-1361.

68. Tefflemire, T. J. and van Alstyne, F. E. 1974. Land Disposal of Wastewater. Journal Water Pollution Control Federation. 46:1201-1208.

69. Fetter, C. W. and Holzmacher. 1974. Groundwater Recharge with Treated Wastewater. Journal Water Pollution Control Federation.

46:260-270.

70. Finstein, M. S. and Bitzky, M. R. 1972. Relationships of Autotrophic Ammonium-Oxidizing Bacteria to Marine Salts. Water Research. 6:31-40.

71. Dowell, M. and Jarratt, P. 1971. A Modified Regula Falsi Method for Computing the Root of an Equation. BIT. 11:168-174.

APPENDIX A

Artificial Soil

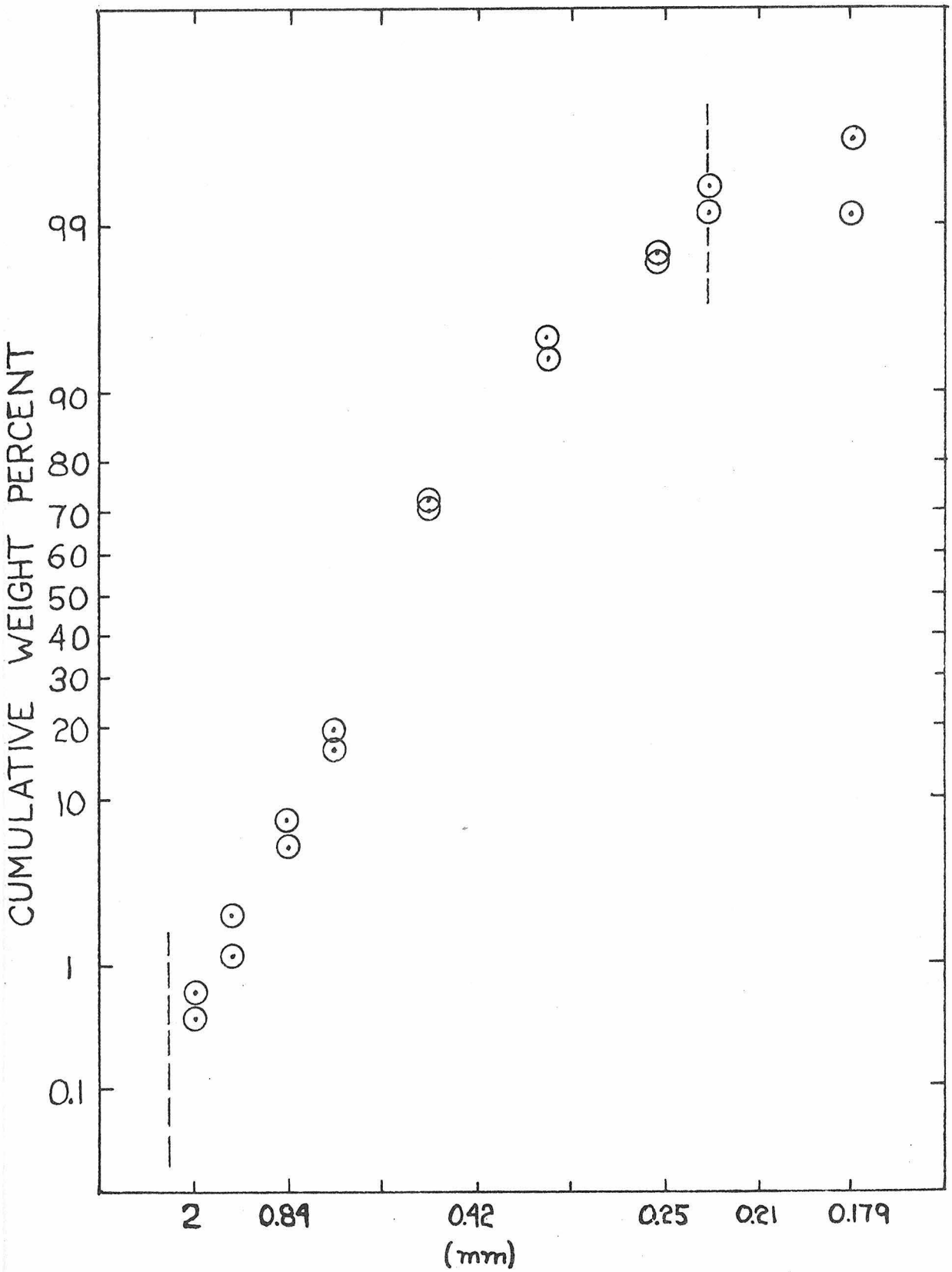

Figure A1: Grain Size Distribution of Artificial Soil

APPENDIX B

Percolating Solution Analyses

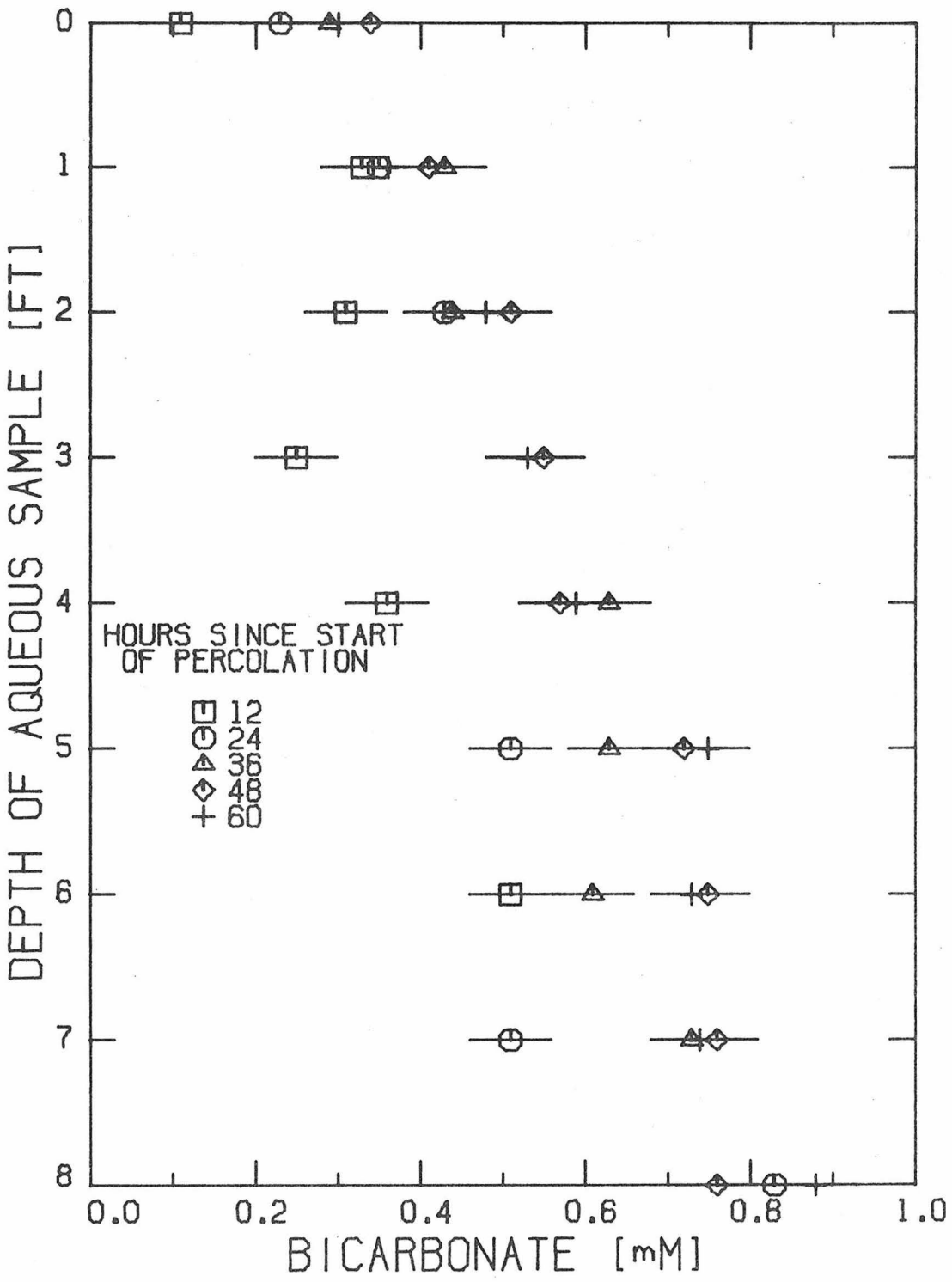

Figure B1: Aqueous Bicarbonate Ion Content of a 38 mg Ca^{++}/ℓ Solution Percolating at 3.7 ℓ/day through the Laboratory Column Displacing a Deionized Water Solution

TABLE B1

Aqueous Nitrate and Ammonium Ion Content
of a Lithium and Ammonium Salt Solution
Percolating through the Laboratory
Column at 11.1 ℓ/day

36 hours since the start of the percolation:

Depth	Nitrate (mM)	Ammonium (mM)
0	0.00	0.78
1	0.22	0.03
2	0.32	0.00
3	0.32	0.17
4	0.32	0.38
5	0.28	0.31
6	0.46	0.22
7	0.46	0.12

100 hours since the start of the percolation:

Depth	Nitrate (mM)	Ammonium (mM)
0	0.00	0.85
1	0.1	0.70
2	0.1	0.00
3	0.1	0.00
4	0.1	0.05
5	0.1	0.1
6	0.1	0.1
7	0.1	0.2
8	0.1	0.3

APPENDIX C

Method of the Numerical Solution of the Unsteady State Variation of Aqueous Calcium and Magnesium Content of a Solution Percolating through a Packed Bed of Ion Exchange Medium.

The full system of differential mass balance equations for prediction of the aqueous calcium and magnesium content of a solution percolating through an ion exchange medium such as the sand column is:

$$-\frac{u}{P_E}\frac{\partial Ca}{\partial x} + D_E\frac{\partial^2 Ca}{\partial z^2} = \frac{\partial Ca}{\partial t} - \frac{1-P_L}{P_E}S_s\, d_{Ca} - \frac{1-P_L}{P_E}\ \text{sites}$$

$$\cdot K(1.65 Mg\, x_{Ca} - Keq\ Ca\, x_{Mg}) \ .$$

$$-\frac{u}{P_E}\frac{\partial Mg}{\partial z} + D_E\frac{\partial^2 Mg}{\partial z^2} = \frac{\partial Mg}{\partial t} - \frac{1-P_L}{P_E}S_s\, d_{Mg} - \frac{1-P_L}{P_E}\ \text{sites}$$

$$\cdot K(Mg\, x_{Ca} - Keq\ 0.608\ Ca\, x_{Mg}) \ .$$

$$\frac{\partial x_{Ca}}{\partial t} = K(Keq\ Ca\, x_{Mg} - 1.65\ Mg\, x_{Ca}) \ .$$

$$\frac{\partial x_{Mg}}{\partial t} = K(Mg\, x_{Ca} - Keq\ 0.608\ Ca\, x_{Mg}) \ .$$

where

$$Keq \equiv \frac{Mg\, x_{Ca}}{Ca\, x_{Mg}}$$

and K is the ion exchange rate constant. The differential equations are subject to the initial aqueous cation concentration depth profiles,

$$Ca(z,0) = Ca_I + \frac{1-P_L \cdot S_s \cdot d_{Ca}}{u}\ z \ ,$$

$$Mg(z,0) = Mg_I + \frac{1-P_L \cdot S_s \cdot d_{Mg}}{u}\ z \ .$$

Ca_I and Mg_I are the aqueous calcium and magnesium ion content of the inlet solution to the laboratory column that previously brought the

adsorbed distribution of calcium (x_{Ca}) and magnesium (x_{Mg}) on the column's sand to the steady state values

$$x_{Mg}(z,0) = 1/(x_{Ca}/x_{Mg}]_0 + 1)$$

$$x_{Ca}(z,0) = 1 - x_{Mg}(z,0) \quad .$$

$x_{Ca}/x_{Mg}]_0$ is defined by equation (20). The boundary conditions on the differential equations are

$$Ca(0,t) = Ca_{II}$$

$$Mg(0,t) = Mg_{II}$$

$$\left.\frac{\partial Ca}{\partial z}\right|_{\infty} = 0$$

$$\left.\frac{\partial Mg}{\partial z}\right|_{\infty} = 0 \quad .$$

The differential equation derivatives were replaced by the difference equations

$$\frac{\partial c}{\partial z} = \frac{c(z - 1,T) - 1 - c(z + 1,T)}{\Delta z}$$

$$\frac{\partial^2 c}{\partial z^2} = \frac{c(z + 1,T) - 2c(z,T) + c(z - 1,T)}{\Delta z^2} \quad .$$

$$\frac{\partial c}{\partial T} = \frac{c(z,T + 1) - c(z,T)}{\Delta T} \quad .$$

A time step of 0.1 hours and a spatial step of 0.05 feet were used to avoid instabilities in the numerical solutions caused by the reaction and diffusion terms. The plotted results (Figure 28) are based on the

following constants:

$P_E = 0.35$

$P_L = 0.44$

$u = 0.0645$ ft/hr

sites = 14.34 μeq/ℓ

$S_s d_{Ca} = 0.0594$ mg/ℓ·hr

$S_s d_{Mg} = 0.0171$ mg/ℓ·hr

$K = 0.45\ hr^{-1}$

$k_{eq} = 1$

$D_E = 0.003\ ft^2/hr$

$Ca_I = 0$ mg/ℓ

$Mg_I = 0$ mg/ℓ

$Ca_{II} = 39$ mg/ℓ

$Mg_{II} = 0$ mg/ℓ

APPENDIX D

Chronology of the Operation of the Laboratory Column and Analyses of Data

STARTING DATE	OPERATION OF LABORATORY COLUMN*	FIGURE NUMBER OF DATA
June '73	Deionized water percolation (720 ft/day).	
30 June '73	Deionized water (2 ft/day).	
11 July '73		15 through 20
13 July '73	60 ℓ of 40 mg Ca^{++}/ℓ water percolated at the rate of 11 ℓ/day.	
14 July '73		21 through 27
21 July '73	40 mg Ca^{++}/ℓ solution percolated through column at 36 ℓ/day.	
22 July '73		29 through 35
31 July '73	40 mg Ca^{++}/ℓ solution percolated through column at 11 ℓ/day.	
10 August '73	Column purged with air.	
19 August '73	First Wet Period.	
27 August '73	First Dry Period.	58
12 September '73	Second Wet Period.	
12 September '73	Oil contamination of percolating solution.	
12 September '73	40 mg Ca^{++}/ℓ solution percolated. Reseeding of column with bacteria.	
24 September '73	Second Wet Period restarted.	59 through 63
1 October	Second Dry Period.	64
15 October '73	Third Wet Period.	65 through 72
22 October '73	Third Dry Period.	
21 November '73	Purge of column with deionized water. Wet Period started.	73

* Between August 1972 and June 1973 inorganic solutions had been percolated intermittently through the laboratory column.

STARTING DATE	OPERATION OF LABORATORY COLUMN	FIGURE NUMBER OF DATA
27 November '73	Dry Period.	
9 December '73	Feed solution purge. Bacterial population count made for nitrifying and heterotrophic bacteria.	
10 December '73	Column drained of solution.	
10 January '74	Wet Period.	
16 January '74	Dry Period.	74 and 75
30 January '74	Wet Period started with deionized water purge to determine the total quantity of dissolved species in the interstitial solution at the end of a Dry Period.	
7 February	Dry Period.	
15 February '74	Wet Period.	77
23 February '74	An aerobic Dry Period.	
2 March '74	Wet Period.	78 through 80
9 March '74	Dry Period.	
12 March '74	Wet Period.	
17 March '74	Dry Period.	
3 April '74	Deionized solution used to start Wet Period. Bacterial population counted.	85
10 April '74	Dry Period.	
24 April '74	Wet Period without dissolved ammonium ions.	
1 May '74	Dry Period.	81 and 82
15 May '74	Wet Period with deionized water purge. Wet Period was continued with the regular feed solution.	83 and 84

STARTING DATE	OPERATION OF LABORATORY COLUMN	FIGURE NUMBER OF DATA
23 May '74	Dry Period of five days.	
28 May '74	Wet Period with deionized water purge.	86
3 June '74	Dry Period.	
19 June '74	Wet Period.	
26 June '74	Dry Period of 2.2 days.	
28 June '74	Wet Period with deionized water purge.	87
2 July '74	Dry Period of one day.	
3 July '74	Wet Period with deionized water purge.	88
11 July '74	Dry Period.	
25 July '74	Calcium ion free Wet Period.	
1 August '74	Dry Period.	
13 August '74	Calcium ion free Wet Period.	
19 August '74	Dry Period.	
30 August '74	Calcium ion free Wet Period.	
27 September '74	Dry Period.	
11 October '74	Calcium ion free Wet Period.	89
24 October '74	Lithium/Ammonium solution used for a Wet Period.	
31 October '74	Dry Period.	
3 November '74	Wet Period with Lithium/Ammonium solution.	
10 November '74	Dry Period.	
12 November '74	Wet Period with Lithium/Ammonium solution.	

STARTING DATE	OPERATION OF LABORATORY COLUMN	FIGURE NUMBER OF DATA
19 November '74	36 ℓ/day purge with Lithium/Ammonium containing solution.	
2 December '74	Dry Period.	
9 December '74	Wet Period with Lithium/Ammonium solution.	Table B1
16 December '74	Dry Period.	
21 January '75 through February '75	One week Wet Periods of Lithium/ Ammonium containing solutions and two week Dry Periods were run.	
25 February '75	Dry Period ended by purging column with deionized water.	90
25 February '75 through 25 March '75	Lithium/Ammonium solutions percolated through the laboratory column.	91

APPENDIX E

Numerical Solutions

$$-u \frac{\partial c}{\partial z} + D \frac{\partial^2 c}{\partial z^2} = \frac{\partial c}{\partial t} - \sum R \qquad \text{(E1)}$$

was converted into a difference equation by considering concentration at three spatial positions to approximate the first and second derivative of concentration with respect to position. The first derivative of concentration with respect to time was replaced by two concentrations in time. A weighting constant, H, was used to evaluate the gradient of concentration. The gradient of aqueous concentration at some depth, z, in the packed bed was approximated by

$$\left.\frac{\partial c}{\partial z}\right|_{t,z} \simeq \frac{H\left(\frac{c_{t,z+\Delta z} - c_{t,z}}{\Delta z}\right) + \left(\frac{c_{t,z} - c_{t,z-z}}{\Delta z}\right)}{(H+1)} \qquad \text{(E2)}$$

where Δz is the spatial step size or interval for the packed bed model and $c_{t,z+\Delta z}$ is the concentration at some time, t, and some depth, $z+\Delta z$. The second derivative with respect to position was approximated with

$$\left.\frac{\partial^2 c}{\partial z^2}\right|_{t,z} \simeq \frac{c_{t,z+\Delta z} - 2c_{t,z} + c_{t,z-\Delta z}}{\Delta z^2} \qquad \text{(E3)}$$

The time derivative of concentration was approximated by

$$\frac{\partial c}{\partial t} \simeq \frac{c_{t+\Delta t,z} - c_{t,z}}{\Delta t} \ . \qquad \text{(E4)}$$

The completed difference equation was

$$c_{t+\Delta t,z} = c_{t,z+\Delta z}\left(\frac{D\Delta t}{\Delta z^2} - \frac{u\Delta t}{(H+1)\Delta z}\right) + c_{t,z}\left(1 - \frac{2D\Delta t}{\Delta z^2} - \frac{(H-1)u\Delta t}{(H+1)\Delta z}\right) \qquad \text{(E5)}$$

$$+ c_{t,z-\Delta z}\left(\frac{Hu\Delta t}{(H+1)\Delta z} + \frac{D\Delta t}{\Delta z^2}\right) + \sum R\, t \ . \qquad \text{(E6)}$$

For utilization of the difference equation, the initial concentrations of aqueous species, bacterial populations, and gaseous compositions were known at each depth. The concentrations at each depth were computed simultaneously for each spatial position at a new time one Δt into the future. Concentration of aqueous species in the inlet solution set the concentrations at the zeroth position. In the case of the Dry Period mathematical model, the atmospheric concentrations of oxygen and carbon dioxode set the zeroth position concentration of the respective gases. The packed bed was treated mathematically as an infinitely long bed for the Wet Period by computing concentrations 20 spatial steps beyond the length of the laboratory column (eight feet). A mathematical boundary condition for the Wet Period model was that the concentration gradient of dissolved species should be zero at an "infinite" depth; therefore, the concentrations of dissolved chemical species at the last two spatial positions are equated to one another. The zero gradient boundary condition for the Wet Period mathematical model was useful in preventing concentration instabilities from traveling up the mathematically modeled column. The Dry Period mathematical model also had a zero gradient for the gaseous component at the base of the packed bed. The zero concentration gradient in this case was due to a lack of chemical reactions, affecting the gas compositions, beyond the bed's base. The step size used for the numerical solutions had to meet two criteria to minimize the possibility of numerical instabilities in the solutions. The time step, Δt, and the spatial step size, Δz, must be of such values that

$$\frac{2\ D\Delta t}{\Delta z^2} \leq 1 \qquad \text{(E7)}$$

where D is the diffusivity coefficient used in the dispersive term, $D\partial^2 c/\partial z^2$, of the differential mass balance for the dissolved species, c, or for the gaseous species, c. The other criterion that tends to limit the maximum value for the time step is a result of the chemical reaction terms. The reaction term limits the size of the time step to a value small enough to prevent any chemical reactant from reaching a negative value as a result of the time step. The time and spatial steps for the Dry Period mathematical model were 0.2 hour and 0.5 feet, respectively. For the Wet Period model the time step was 0.05 hour and the spatial step was 0.3 feet.

The most time consuming computation for the mathematical model was the determination of the distribution of cations between the aqueous phase and the double layer of the sand. The most effort went into optimizing the ion exchange distribution computation routine. Cation exchange processes are assumed to be in a state of local equilibrium. The general rationale for the computation of the cation exchange equilibrium distribution, as well as any other equilibrium distribution, was that the packed bed was essentially mathematically broken up into a number of well-mixed tanks of volume $A\Delta z$, where A is the area of the packed bed available for gas or solution flow. For a particular differential volume, time is permitted to advance one time step. The concentrations of chemical species will change due to convection, diffusion, and biological reactions to new values Ca_i, Mg_i, Na_i, NH_{4i}, and A_i (acidity). The sand in contact with the solution in the differential

volume element will still have surface distributions (in equivalent fraction units) x_{Ca_i}, x_{Mg_i}, $x_{NH_{4i}}$, and x_{A_i}. The determination of the new distribution of species is accomplished by using the distribution coefficients of ion exchange and a mass balance for each chemical species around the differential well-mixed "tank".

Iteration for the distribution takes place on x_{Ca_f}, the final surface equivalent fraction of calcium. The value of x_{Ca_f} is between 0.0 and either 1.0 or $x_{Ca_f max}$,

$$x_{Ca_f max} = \frac{Ca_i}{s\ 20.04} + x_{Ca_i} \tag{E8}$$

s is a conversion factor for converting aqueous concentrations to surface equivalent fractions and Ca_i has the unit of mg/ℓ. $x_{Ca_f max}$ is an upper bound on x_{Ca_f} caused by the requirement that the final calcium concentration be nonnegative. x_{Ca_f} is varied until f equals zero,

$$f \equiv x_{Ca_f} + x_{Mg_f} + x_{Na_f} + x_{NH_{4f}} + x_{A_f} - 1.0 \quad . \tag{E9}$$

As x_{Ca_f} is varied from zero to one, f starts at -1.0 and increases linearly. As x_{Ca_f} approaches x_{Ca_f} (the x_{Ca_f} that causes f to be zero), f acquires a more positive first derivative. Finally x_{Ca_f} hits $x_{Ca_f max}$ where

$$f(x_{Ca_f max}) = \left[\frac{Ca_i}{20} + \frac{Mg_i}{12.2} + \frac{Na_i}{23} + A_i\right]/s \quad . \tag{E10}$$

The actual iteration on x_{Ca_f} is started at $x_{Ca_f max}$. A step is made toward a lower x_{Ca_f}. f is evaluated at that new x_{Ca_f} by use of the following:

calcium mass balance - $Ca_f = Ca_i + (x_{Ca_i} - x_{Ca_f})$ s 20.04 , (E11)

magnesium mass balance - $Mg_i + x_{Mg_i}$ s 12.16 = $Mg_f + x_{Mg_f}$ s 12.16 (E12)

distribution expression - $KCM1 = \frac{Mg_f}{Ca_f}\left(\frac{x_{Ca_f}}{x_{Mg_f}}\right)^{KCM2}$. (E13)

then

$$0 = x_{Mg_f}^{KCM2} + x_{Mg_f}\left(\frac{x_{Ca_f}^{KCM2} \text{ s } 12.16}{KCM1\ 0.608\ Ca_f}\right) + \left(\frac{x_{Ca}^{KCM2}\ (-Mg_i - x_{Mg_i} \text{ s } 12.16)}{KCM1\ 0.608\ Ca_f}\right) \quad \text{(E14)}$$

or

$$g_{Mg} = 0 = x_{Mg_f}^{KCM2} + A_{Mg}\, x_{Mg} + B_{Mg} \quad . \quad \text{(E15)}$$

Similar equations are derivable for the sodium and ammonium ion. The function, g, is monotonic, increasing over the range of its independent variable, x_{Mg_f}. The initial equivalent fraction, x_{Mg_i}, permits the formulation of an approximate solution for equation (E15) by a linear interpolation between the x_{Mg_f} values of 0.0 and x_{Mg_i} ($g(0)$ is less than zero and $g(x_{Mg_i})$ is greater than zero):

$$x_{Mg_f guess} = \frac{-B_{Mg}}{x_{Mg_i}^{KCM2-1} + A_{Mg}}$$

A_{Mg} and B_{Mg} are constants of x_{Mg_f} for equation (E15). The initial guess, $x_{Mg_f guess}$, is used in the Newton Raphson scheme to compute the x_{Mg_f} that causes $g(x_{Mg_f})$ to vanish. A similar procedure is used to compute x_{Na_f} and $x_{NH_{4f}}$. Two iterations were necessary for x_{Mg_f} and one iteration was necessary for x_{Na_f} and $x_{NH_{4f}}$ to obtain their values to within 10^{-5} of the values that caused the respective g function to

go to zero.

The determination of x_{A_f} is complicated by the fact that the aqueous hydrogen ion participates in three reversible reactions

$$H^+ + HCO_3^- = H_2CO_3$$

$$HCO_3^- = H^+ + CO_3^=$$

$$H^+ + OH^- = H_2O \quad .$$

The mass balance for the aqueous hydrogen ion is replaced by the electroneutrality condition

$$A_i + x_{Ca_i} s = H_f - \frac{K_w}{H_f} - HCO_{3f}^- - 2\, CO_{3f}^= - ELEK + x_{A_f} s \quad . \qquad (E17)$$

A_i is the initial aqueous acidity concentration in the differential volume, H_f is the final concentration of aqueous hydrogen ions, and K_w is the equilibrium constant for the water dissociation reaction, Also

$$ELEK = H_o - OH_o^- - HCO_{3\,o}^- - 2\, CO_{3\,o}^=$$

where the subscripted variables represent the respective aqueous concentrations of the chemical species at spatial position zero, that is, at the inlet to the packed bed (in the case of the Dry Period model, ELEK is defined according to the concentrations at the start of the Dry Period). Other variables used in the electroneutrality condition are

$$HCO_{3f}^- = \frac{C_T}{61\left[\frac{H_f}{KC1} + 1 + \frac{KC2}{H_f}\right]} \qquad (E18)$$

where C_T is the total dissolved carbonate species in the aqueous phase and KC1 and KC2 are the first and second dissociation constants for the bicarbonate ion. The concentration of the carbonate ion is

$$CO_{3f}^{=} = \frac{2\ C_T}{61\left(\frac{H_f^2}{KC1\ KC2} + 1 + \frac{H_f}{KC2}\right)} \qquad \text{(E19)}$$

the electroneutraiity expressions simplify to an expression, F. F is a linear equation of terms $H_f^{\alpha}\beta$ where α is a real power and β is a real coefficient. F at some H_f^* is zero and that H_f^* is the final concentration of aqueous hydrogen ions in the differential volume element. Newton Raphson iterations on F do not converge unless the initially guessed H_f is extremely close to H_f^*. As pH_f changes from large values toward zero, F starts out slightly less than zero and reaches a minimum value. As pH_f becomes smaller, F suddenly increases to large values. A binary search coupled with linear interpolation (Dowell et al., 71) was used to determine the final pH to within ± 0.001 unit. Approximately four iterations were needed to arrive at the final pH of the differential volume element when the initial pH of the solution was used as the initial guess for the iteration scheme. With the computation of x_{Mg_f}, x_{Na_f}, $x_{NH_{4f}}$, and x_{A_f}, f (E9) can be computed. A modified Reguli Falsi search was used to determine the x_{Ca_f} that causes f to vanish. An average of four iterations were necessary to find the correct x_{Ca_f}.

For the Dry Period, mathematical model x_{Ca_f} was computed to within ± 0.01. The Wet Period model computed x_{Ca_f} to within ± 0.0005. The greater accuracy of the Wet Period computation was necessary to prevent instabilities from growing in the concentration profiles. To

save computation time, several modifications were made to avoid entering an ion exchange distribution iteration. For the Dry Period model, if the change of aqueous ammonium ion concentration due to bacterial reactions was less than 0.01 mg $NH_4^+(N)/\ell$, then the ion exchange computation was not performed. It was recognized that it was the biological change of the aqueous ammonium ion concentration and aqueous hydrogen ion concentration that caused the redistribution of ion exchanging species. For the Wet Period mathematical model, if the change of aqueous ammonium ion concentration at some depth, and before the ion exchange process was computed, was less than seven per cent and if the pH was greater than 5 , then the ion exchange computation was skipped. It was assumed that the ion exchange breakthrough curves for aqueous ammonium ions were in phase with the same curves for aqueous calcium, magnesium, sodium, and the hydrogen ion; however, it was realized that there was biological conversion of aqueous ammonium ions deep in the column even before the aqueous ammonium ion breakthrough curve had traveled the full column length. Another computation saving decision was that if the pH was greater than 7, then the iteration for x_{A_f} was not performed; rather, x_{A_f} was assumed equal to x_{A_i} and pH_f equal to pH_i.

APPENDIX F

Evaluation of Constants Used in the Mathematical Model for the Intermittent Percolation Process

Porosities used in the mathematical model were those experimentally evaluated. Molecular diffusivity coefficients of cations in solution were all assumed equal to 5.8×10^{-5} ft^2/hr (Harned et al., 21, 25, 42). The data of Miyauchi et al. (26) shows that the effective diffusivity for a solution percolating through a packed bed at a Reynold's number of 0.004 is 3×10^{-4} ft^2hr. Assuming that a bacterial population was not diminishing the porosity of the column for gas diffusion, then the diffusivity coefficient for oxygen and carbon dioxide were assumed to be 0.39 ft^2/hr. The solubility of oxygen in water (Hodgman, 50) was correlated to temperature. The ionic strength of the model's percolating solution was not enough to appreciably affect the solubility. Assuming Henry's law is valid for oxygen, the equilibrium coefficient relating the concentration of oxygen in the aqueous phase (mg O_2/ℓ) to the weight fraction of oxygen in the gaseous atmosphere is

$$Keq_{O_2} = 10000 \exp (17.52/T-11.41)(1 + 0.0295\ z)$$

where T is the centigrade temperature and z is the depth in the column to which the solution has percolated. For the Dry Period expression, the term "1 + 0.0295 z" is not needed in the expression for Keq_{O_2} to correct for an increased gaseous pressure due to a hydrostatic loading. The distribution of carbon dioxide between the gaseous and the aqueous phase is expressed mathematically by

$$0.0339 = (H_2CO_3(aq) + CO_2(aq))/P_{CO_2}$$

where P_{CO_2} is the pressure of carbon dioxide in the atmosphere (atm). $(H_2CO_3(aq) + CO_2(aq))$ (M) is given by

$$(H_2CO_3(aq) + CO_2(aq)) = C_T / \left(1 + \frac{5.01 \times 10^{-7}}{c_H} + \frac{2.82 \times 10^{-17}}{c_H^2}\right)$$

where C_T is the total concentration of carbonate ions dissolved in the solution and c_H is the molar concentration of hydrogen ions in solution.

According to Knowles et al. (51), the growth rate constants for Nitrosomonas and Nitrobacter are temperature sensitive. The authors gave the logarithms of the constants (day^{-1}) as

$$Log_{10}(Kg_s) = 0.0413\ T - 0.944$$

$$Log_{10}(Kg_b) = 0.0255\ T - 0.492\ .$$

The death rate constants were derived from the data of Laudelout et al. (14) who studied the decline of populations of nitrifying bacteria in a chemically starved medium. The rate constant for the death of a population of Nitrosomonas and Nitrobacter, respectively, were 0.00721 and 0.0121 hr^{-1}. Knowles et al. (51) have given the Nitrosomonas saturation constant, as a function of temperature T (centigrade), for aqueous ammonium ions as

$$Log_{10}(s_{NH_4}) = 0.051\ T - 1.158\ .$$

The same authors gave the Nitrobacter saturation constant for aqueous nitrite ions as

$$Log_{10}(s_{NO_2}) = 0.063\ T - 1.149\ .$$

Nitrobacter saturation constant for dissolved oxygen was reported by

Boon et al. (61) to be 0.5 mg O_2/ℓ, and by Laudelout et al. (14) to be 2.0 mg O_2/ℓ. The data of Knowles et al. (51) showed that the saturation constant of dissolved oxygen for Nitrobacter would be approximately 1.0 mg O_2/ℓ and for Nitrosomonas the value would be less than 0.5 mg O_2/ℓ. The mathematical model uses a saturation constant of oxygen for Nitrobacter and Nitrosomonas as 0.8 and 0.4 mg O_2/ℓ, respectively.

Engel et al. (15) present data of the accumulative number of Nitrosomonas cells and nitrite ions in solution over a period of time. Because bacteria grow according to

$$\frac{dm_s}{dt} = Kg_s \, m_s$$

and aqueous nitrite ions are produced according to

$$\frac{dc_{NO_2^-}}{dt} = A_{NO_2} \, m_s$$

(in the absence of growth inhibiting circumstances), then a plot of m_s versus c_{NO_2} produces a straight line of slope A_{NO_2}/Kg_s. The A_{NO_2} value for Nitrosomonas was found to be $4.4 \times 10^{-9}/Kg_s$ mg $NO_2^-(N)$/cell Nitrosomonas. The data of Dessers et al. (13) for the quantity of aqueous nitrite ions consumed to produce a given population of Nitrobacter cells gave $A_{NO_2^-}$ for Nitrobacter as $4(\pm 0.5) \times 10^{-9}/Kg_b$ mg $NO_2^-(N)$/cell Nitrobacter. The data of Laudelout et al. (14) gave $A_{NO_2^-}$ for Nitrobacter as $5.4 \times 10^{-9}/Kg_b$ mg $NO_2^-(N)$/cell; van Gool et al. (64) gave the value $2.3 \times 10^{-9}/Kg_b$ mg $NO_2^-(N)$/cell; and Knowles et al. (51) gave $3.5 \times 10^{-9}/Kg_b$ mg $NO_2^-(N)$/cell Nitrobacter. The consumption and production rates of aqueous oxygen, ammonium, hydrogen and nitrate ions are based on the rate changes of the aqueous nitrite ion according to

the nitrifying reactions

$$NH_4^+(aq) + \frac{3}{2}\,O_2(aq) \xrightarrow{\text{Nitrosomonas}} NO_2^-(aq) + 2H^+(aq) + H_2O$$

$$NO_2^-(aq) + \frac{1}{2}\,O_2(aq) \xrightarrow{\text{Nitrobacter}} NO_3^-(aq)\ .$$

Should the environmental conditions of the mathematical model allow it, the bacterial populations will grow to the bound delimiting their population densities. The average population of nitrifying bacteria in the soil is between 1×10^6 and 1×10^8 cells per mℓ soil. Loveless (11) reported the maximum population density of 1×10^8 cells per gm soil. The maximum nitrifying bacterial population density found in the laboratory column was 4×10^6 cells per gm sand. The mathematical model used maximum bacterial populations in a range from 10^6 to 10^7 cells per mℓ sand.

APPENDIX G

Fortran Listing of Dry and Wet Period Mathematical Models

```
      IMPLICIT REAL*4 (A-Z)
C     **** WET PERIOD ****
      COMMON /WETDRY/
     -     TMP  ,KGS  ,KGB  ,KDS  ,KCB  ,KLS  ,KMS  ,KLB  ,KMB  ,DCMBO2
     -     ,DCMSO2,DCMSI2,DCMBI2,DCMBA3,DCMSA,DCMSAM,ALPHA,BETA ,DELTA
     -     ,ETA  ,KAPPA,                    LAMBDA,CMICRN,MBMX ,MSMX,CVRPPS
     -     ,OVRPPB,CSNH4,CSC2S,CSC2B,CSNO2
     -     ,KC1  ,KC2  ,KOX  ,KEQCX,CNSNO,HIST,DELX,CENH4(100)
     -     ,         CNO3O,CNC3(100),CNH4O,CNH4(100), CNO2O,CNC2(100)
     -     ,CCAO,CCA(100),CMGO,CMG(100),CNAO,CNA(100),MB (100), MS (100)
     -     ,          CCO2O,CCC2(100),CO2O,CO2(100),CAO,CA(100),PH(100)
C     'COMMON' FORCES CNO3(0)=CNC3O,CCA(0)=CCAO, ETC
      COMMON /IONEX /
     -      CCAN,XCA(100),SITES,CMGN ,XMG(100)       ,CNH4N ,XNH4(100)
     -     ,      CNAN ,XNA(100),CAN,  GCCA,PL  ,PE  ,ZMG,ZNH4,ZNA
     -     ,KCM1,KCM2,KCN1,KCN2,KCA1,KCA2,KCH1,KCH2,ZH,XH(100),ELEK,STPV
      COMMON /CNSTNT/ KCH2O,KCH14O,KCH2OH
      COMMON /BLOCK1/ PPH,DMY1,DELPH,CT   ,ORDER,X    ,HSKIP
      COMMON /SLAVE /
     -     U1(100),U2(100),U3(100),U4(100),U5(100),U6(100),U7(100)
     -     ,U8(100),U9(100),UA(100),UB(100),UC(100),UD(100),UE(100)
C     'SLAVE' BLOCK - TEMPORARY STORAGE OF RESULTS OF SPATIAL STEPS
      DIMENSION        DEPTH(100),LGS(100),LGB(100),CGC2(100)
     -     ,LPR1(10,10),LPR2(10,10),LPRTCN(10,40),LPR3(10,10),LPR4(10,10)
C
C
      INTEGER*4  XMAX,I4   ,DUM ,ISW,JSW
      INTEGER*2
     -     XSTRT,XEND ,XSTEP,HSKIP,TMAX ,J    ,I    ,DUMMY,N
     -    ,      KNT ,LMTD1,LMTD2  ,PSEUDO      ,X   ,PLOTSW,INDEX1
     -     ,INDEX2,LIMITD, CNT, ORDER,HSKP(100)
      EQUIVALENCE (LPR1(1,1),LPRTCN(1,1)),
     -            (LPR2(1,1),LPRTCN(1,11)),
     -            (LPR3(1,1),LPRTCN(1,21)),
     -            (LPR4(1,1),LPRTCN(1,31))
C     LPRTCN(I,J) = CONC. PROTON (MOLE/L) AT:
C       (254.-I) MG TOT. CARBONATE/L (I MAX=10)
C            (-0.0051+J/10000.) MOLES ACID+ELEK/L (J MAX=20)
C       AT=17.6 PPM,PT=17.1 PPM
      DATA LPR1/
     - 8.79, 8.83, 8.88, 8.91, 8.96, 8.99, 9.02, 9.05, 9.08, 9.12,
     - 8.44, 8.51, 8.58, 8.63, 8.69, 8.74, 8.80, 8.85, 8.88, 8.93,
     - 8.04, 8.10, 8.16, 8.23, 8.30, 8.37, 8.44, 8.51, 8.58, 8.65,
     - 7.74, 7.79, 7.82, 7.87, 7.91, 7.96, 8.02, 8.08, 8.15, 8.23,
     - 7.55, 7.57, 7.60, 7.63, 7.66, 7.69, 7.73, 7.77, 7.82, 7.85,
     - 7.40, 7.43, 7.44, 7.46, 7.49, 7.51, 7.54, 7.57, 7.58, 7.62,
     - 7.29, 7.30, 7.32, 7.33, 7.35, 7.37, 7.40, 7.41, 7.43, 7.46,
     - 7.18, 7.19, 7.21, 7.23, 7.24, 7.26, 7.27, 7.29, 7.30, 7.32,
```

```
     - 7.10, 7.12, 7.12, 7.13, 7.15, 7.16, 7.18, 7.19, 7.19, 7.21,
     - 7.02, 7.04, 7.04, 7.05, 7.07, 7.08, 7.08, 7.10, 7.12, 7.12/
      DATA LPR2/
     - 6.96, 6.96, 6.98, 6.99, 6.99, 7.01, 7.01, 7.02, 7.04, 7.04,
     - 6.90, 6.90, 6.91, 6.91, 6.93, 6.93, 6.94, 6.96, 6.96, 6.98,
     - 6.83, 6.85, 6.85, 6.85, 6.87, 6.87, 6.88, 6.88, 6.90, 6.90,
     - 6.79, 6.79, 6.79, 6.80, 6.80, 6.82, 6.82, 6.83, 6.83, 6.85,
     - 6.73, 6.74, 6.74, 6.74, 6.76, 6.76, 6.77, 6.77, 6.79, 6.79,
     - 6.68, 6.68, 6.69, 6.69, 6.71, 6.71, 6.71, 6.73, 6.73, 6.73,
     - 6.63, 6.63, 6.65, 6.65, 6.65, 6.66, 6.66, 6.66, 6.68, 6.68,
     - 6.58, 6.58, 6.60, 6.60, 6.60, 6.62, 6.62, 6.62, 6.63, 6.63,
     - 6.54, 6.55, 6.55, 6.55, 6.57, 6.57, 6.57, 6.57, 6.58, 6.58,
     - 6.51, 6.51, 6.51, 6.51, 6.52, 6.52, 6.52, 6.54, 6.54, 6.54/
      DATA LPR3/
     - 6.46, 6.46, 6.46, 6.48, 6.48, 6.48, 6.48, 6.49, 6.49, 6.49,
     - 6.41, 6.41, 6.43, 6.43, 6.43, 6.43, 6.44, 6.44, 6.44, 6.44,
     - 6.38, 6.38, 6.38, 6.38, 6.38, 6.40, 6.40, 6.40, 6.40, 6.41,
     - 6.33, 6.33, 6.33, 6.35, 6.35, 6.35, 6.35, 6.35, 6.37, 6.37,
     - 6.29, 6.29, 6.30, 6.30, 6.30, 6.30, 6.32, 6.32, 6.32, 6.32,
     - 6.26, 6.26, 6.26, 6.26, 6.26, 6.27, 6.27, 6.27, 6.27, 6.27,
     - 6.21, 6.21, 6.21, 6.23, 6.23, 6.23, 6.23, 6.23, 6.24, 6.24,
     - 6.16, 6.16, 6.18, 6.18, 6.18, 6.18, 6.18, 6.19, 6.19, 6.19,
     - 6.13, 6.13, 6.13, 6.13, 6.13, 6.13, 6.15, 6.15, 6.15, 6.15,
     - 6.08, 6.08, 6.08, 6.08, 6.08, 6.10, 6.10, 6.10, 6.10, 6.10/
      DATA LPR4/
     - 6.04, 6.04, 6.04, 6.04, 6.05, 6.05, 6.05, 6.05, 6.05, 6.05,
     - 5.99, 5.99, 5.99, 5.99, 6.01, 6.01, 6.01, 6.01, 6.01, 6.01,
     - 5.94, 5.94, 5.94, 5.94, 5.94, 5.96, 5.96, 5.96, 5.96, 5.96,
     - 5.90, 5.90, 5.90, 5.90, 5.90, 5.90, 5.90, 5.90, 5.91, 5.91,
     - 5.83, 5.83, 5.83, 5.85, 5.85, 5.85, 5.85, 5.85, 5.85, 5.85,
     - 5.79, 5.79, 5.79, 5.79, 5.79, 5.79, 5.79, 5.80, 5.80, 5.80,
     - 5.73, 5.73, 5.73, 5.73, 5.73, 5.73, 5.73, 5.74, 5.74, 5.74,
     - 5.65, 5.65, 5.66, 5.66, 5.66, 5.66, 5.66, 5.66, 5.66, 5.68,
     - 5.58, 5.58, 5.58, 5.58, 5.58, 5.58, 5.58, 5.60, 5.60, 5.60,
     - 5.49, 5.49, 5.51, 5.51, 5.51, 5.51, 5.51, 5.51, 5.51, 5.51/
C     CCAO = INLET CALCIUM ION CONCENTRATION (MG/L)
C     ELEK = ELECTRONEUTRALITY CONDITION OF FEED TO COLUMN (MM)
C     ASSUME CONSTANT SURFACE AREA,VALID HENRY'S LAW,T=25,NO EFFECT
C         BY IONIC STRENGTH
C     KEQOX = EQUILIBIUM CONSTANT FOR O2/H2O SYSTEM  AT SURFACE
C           (MG O2/L) 17AG73,25AP74
C     CGO2 = CONCENTRATION OF O2 IN TRAPPED GAS (MG/L GAS)
C     CGN2 = CONCENTRATION OF N2 IN TRAPPED GAS (MG/L)
C     CGCO2 = CONCENTRATION OF CO2 IN TRAPPED GAS (MG/L)
C     PE = EFFECTIVE POROSITY OF COLUMN
C     PL = TOTAL POROSITY OF COLUMN
C     PHO = INLET PH
C     ASSUME:
C        NO VARIATION OF CELLUAR EFFICEINCY THAT IS A FCN OF ION CONC
C        NO VARIATION OF DIFFUSION WITH ION SIZE
```

```
C        NO CELLUAR LAG PHASE
      A=1.
C     PSTRT = DEPTH AT WHICH FIRST PRINTING IS DESIRED (FT)
C     PRNTX = DEPTH INTERVALS FOR PRINT (FT)
C     XFNL  = DEPTH AT WHICH LAST PRINTING IS DESIRED (FT)
C     DELT  = TIME INTERVAL IN DIFFERENCE EQUATION (HRS)
C     DELX  = DEPTH INTERVAL IN DIFFERENCE EQUATION (FT)
C     TFNL  = TIME AT WHICH COMPUTATIONS WILL  STOP (HRS)
C     PRNTT = TIME INTERVALS FOR PRINTOUT (HRS)
C     AR    = CROSS SECTIONAL AREA OF COLUMN (FT**2)
C     D     = EFFECTIVE DIFFUSIVITY (FT**2/HR)
C     CNH4 = AQUEOUS AMMONIUM (N) (MG/L)
C     CNO2 = AQUEOUS NO2(N) (MG/L)
C     CNO3 = AQUEOUS NO3(N) (MG/L)
C     MB   = NITROBACTER COUNT IN MATERIAL  (CELLS/ML SAND)
C     MS    = NITROSOMONAS COUNT IN MATERIAL (CELLS/ ML DRY SAND)
C     KGS = GROWTH CONSTANT FOR NITROSOMONAS (1/HR)
C     CSNH4 = SATURATION CONSTANT FOR NH4 AND NITROSOMONAS (MG(N)/L)
C     ALPHA= CONSUMPTION RATE OF NH4(N) BY NITROSOMONAS DURING GROWTH
C        (MG NH4(N)/CELL)
C     CNH40 = INLET NH4(N) (MG/L)
C     KGB = GROWTH CONSTANT FOR NITROBACTER (1/HR)
C     CSNO2 = SATURATION CONSTANT FOR NO2 AND NITROBACTER (MG(N)/L)
C     BETA = CONSUMPTION RATE OF NO2 BY NITROBACTER DURING GROWTH
C     DELTA = PRODUCTION RATE OF NO2 BY NITROSOMONAS DURING GROWTH
C     CNO20 = INLET NO2(N) (MG/L)
C     ETA = PRODUCTION RATE OF NO3 (N) BY NITROBACTER
C      CNO30 = INLET NO3(N) (MG/L)
C     MBMX = MAXIMUM COUNT ALLOWABLE FOR NITROBACTER
C     MSMX = MAXIMUM COUNT ALLOWABLE FOR NITROSOMONAS
C     TMP   = TEMPERATURE (C)
C     CSO2S = SATURATION CONSTANT FOR OXYGEN/NITROSOMONAS (MG/L)
C     CSO2B = SATURATION CONSTANT FOR OXYGEN/NITROBACTER (MG/LE
C     KAPPA = CONSUMPTION RATE OF OXYGEN BY NITROSOMONAS
C     LAMBDA = CONSUMPTION RATE OF OXYGEN BY NITROBACTER
      A=0.
C     CCO20 = INLET CARBONATE CONCENTRATION (MG(CO3-)/L)
C     CO20  = INLET OXYGEN CONCENTRATION (MG/L)
C     CMICRN = PRODUCTION CONSTANT OF ACIDITY BY NITROSOMONAS
C     PI    = PRODUCTION CONSTANT OF ACIDITY BY NITROBACTER
C     CA0   = INLET ACIDITY CONCENTRATION (MG/L)
C     KDB   = DEATH RATE OF NITROBACTER (1/HR)
C     KDS   = DEATH RATE OF NITROSOMONAS (1/HR)
C     SITES = MEQ/L ON SAND
      A=0.
C     CCA = CALCIUM ION CONCENTRATION (MG/L)
C     ONSND = RHO OF COLUMN MATERIAL (G/ML)
C     HSKIP       = SET AS SUCH TO INDICATE IF PH IS NECESSARY
C                   FOR ION EXCHANGE COMPUTATION
C
```

```
C
C
C     ***** PROGRAM PARMS
C
      XFNL=8.
      PRNTX=0.3
      PSTRT=0.3
      PRNTT=24.
      TFNL=168.
      DELT=0.05
      DELX=0.3
      TMAX =(TFNL/DELT+1.E-5)
      XSTRT =(PSTRT/DELX+1.E-5)
      XEND =(XFNL/DELX+1.E-5)
      XSTEP = (PRNTX/DELX+0.1)
      XMAX =(XFNL/DELX+1.E-5)
C     WILL COMPUTE CONCENTRATIONS 6/ SPATIAL STEPS BEYOND THE
C     ACTUAL COLUMN LENGTH
      DUMMY=XMAX+6
      DO 8 J=1,XMAX
          DEPTH(J)=DELX*J
8     CONTINUE
      DUM=PRNTT/DELT
      PSEUDO=XMAX+4
      LIMITD=PSEUDO-2
      HIST=2.
C
C
C
C     ***** DYNAMIC AND PHYSICAL PARMS
C
      PE = 0.35
      PL = 0.44
C     25JL74 PL=PL(Z)
      U = 2./24.
C     U IS SUPERFICIAL VELOCITY
      V = U/PE
C     V IS NOW INTERSTITIAL VELOCITY
      D=0.0003
      DNSND=2.5
C     ***
      SITES = 70.2
      MIP=2.E-07
C
C
C
C     ***** BIOLOGICAL PARAMETERS
C
      TMP = 25.0
C     **
```

```
      CSC2S = 0.4
      CSC2B = 0.8
      KGS = (10.**(0.0413*TMP-0.944))/24.
      CSNH4=(10.**(0.051*TMP-1.158))
      KGB=(10.**(0.0255*TMP-0.492))/24.
      KLS=0.00721
      KMS=KLS/10.
      KLB=0.0121
      KMB=KLB/10.
C     ABOVE ARE ASSUMED PROGS OF 14JAN74,22OCT4
      CSNO2=10.**(0.063*TMP-1.149)
      BETA=4.E-9*KGB
      KDB = 0.0121
      KDS = 0.00721
      DELTA=4.E-9*KGS
      CMICRN=5.71E-10*KGS
      KAPPA=1.37E-8*KGS
      ETA=BETA
      ALPHA=  DELTA
      LAMBDA=4.57E-9*KGB
C     11OCT74
C     BETWEEN ** AND THIS CARD ALL ARE 5-4-73; 26MY74
      MBMX=2.E7
      MSMX=2.E7
C     LIMITED BY HYDRODYNAMIC DRAG
C     CONVERT 'PER ML SAND' TO 'PER L SOLUTION'
      ALPHA =ALPHA *((1.-PL)/PE)*1000.
      BETA  =BETA  *((1.-PL)/PE)*1000.
      DELTA =DELTA *((1.-PL)/PE)*1000.
      ETA   =ETA   *((1.-PL)/PE)*1000.
      KAPPA =KAPPA * ((1.-PL)/PE)*1000.
      CMICRN=CMICRN* ((1.-PL)/PE)*1000.
      LAMBDA=LAMBDA* ((1.-PL)/PE)*1000.
C
C
C
C     ***** CHEMICAL PARAMETERS
C
      KC1=10.**(-6.3)
      KC2=10.**(-10.25)
      KCX = 0.25
      KEQCX= 6990.*EXP(-11.41+1752./(TMP+273.2))
C     KCX,KEQCX 6OCT73,14NOV73,25AP74
C     CATION EXCHANGE EQUILIBRIUM PARAMETERS
      KCM1= EXP(0.8)
      KCM2=1.35
      KCN1=55950.
      KCN2=1.
      KCA1=800.
      KCA2=1.
```

```
      KCH1=1.
      KCH2=1.
      KCH2C=1./KCH2
      KCH140=40.08/KCH1
      KCH2CH=0.5*KCH2O
C       30AG74
C
C
C
C     ***** BOUNDARY CONDITIONS
C
      CNAO=120.
      CNH4O = 0.98*14.
      CGO2O=299.
      CNO2O =      0.
      CNO3O = 0.34*14.
      CCAO = 40.0
      CCO2O = 250.
      CO2O = 8.4
      CAO=0.
C     GCCA = INITIAL GUESS AT THE CALCIUM ION CONCENTRATION
      GCCA=CCAO+1.E-30
C     CP4-30-73
      ELEK=-CCO2O/61.
C     FLEK= -HCO3          ACTUALLY ADDED TTHE SOLUTION (MM)
C     5-23-73
      CMGO=11.
      WRITE(6,97793) CCAO,CMGO,CNAO,CNH4O,CNO3O,CNO2O,CGO2O,CO2O,
     -     PHOSO,SULFO,CAO
97793 FORMAT(' INLET CHEMICAL CONSTITUENTS (MG/L):'/
     -     '    CALCIUM = ',F7.2/'    MAGNESIUM = ',F7.2/
     -     '    SODIUM = ',F7.2/'   AMMONIUM (N) = ',F7.2/
     -     '    NITRATE (N) = ',F7.2/'    NITRITE ( N) = ',F7.2/
     -     '    TOTAL CARBONATE = ',F7.2/'    OXYGEN = ',F7.2/
     -     '    PHOSPHATE = ',F7.2/'    SULFATE = ',F7.2/
     -     '    ACIDITY = ',F7.2/)
C     OTHER BOUNDARY CONDITION IS THE GRADIENT AT INFINITY IS ZERO
C
C
C
C     ***** INITIAL CONDITIONS
C
C     SOLUTION IS SUDDENLY INTRODUCED TO THE COLUMN
      DO 2 J=1,DUMMY
          CNO2(J)=1.E-5
          CNO3(J)=0.34*14.
          CCO2(J)=250.
          CGO2(J)=299.
          CO2(J)=8.4
          CGN2=301.
```

```
          CGCO2=0.6482
C     BACTERIAL POPULATIONS ARE EXPERIMENTALLY DETERMINED
          MB (J)=4.E6
          MS (J)=10.**(6.+(J-1)/(1.-DUMMY))
          CENH4(J)=0.0
          PH(J)=8.3
          XNA(J)=0.013972
          XH(J)=0.045EC46
          XNH4(J)=0.4609E-4
          XMG(J)=0.21999
          XCA(J)=0.7203
          CNA(J)=120.
          CA(J)=3.932
          CNH4(J)=1.E-5
          CMG(J)=11.
          CCA(J)=40.
2     CONTINUE
      ZCA=XCA(1)
      WRITE(6,97794) XCA(1),XMG(1),XNH4(1),XNA(1),XH(1),MS(1),MB(1)
97794 FORMAT(' INITIAL COLUMN PARAMETERS (AT TOP):'/
     -     ' EXCHANGABLE SPECIES (EQUV FRACTION):'/
     -     '    CALCIUM = ',F9.4/'    MAGNESIUM = ',F9.4/
     -     '    AMMONIUM = ',F9.4/'    SODIUM = ',F9.4/
     -     '    PROTON = ',F9.7/
     -     ' BACTERIAL POPULATION (CELLS/CC DRY SAND):'/
     -     '    NITROSOMONAS (+) =',E14.7/'    NITROBACTER  (+) =',E14.7/
     -     )
C
C
      DELX2=DELX*DELX
      COEF1=(D*DELT/DELX2-U*DELT/(DELX*(HIST+1.)))
      COEF2=(1.-2.*D*DELT/DELX2-(HIST-1.)*U*DELT/((HIST+1.)*DELX))
      COEF3=(HIST*U*DELT/((HIST+1.)*DELX)+D*DELT/DELX2)
C     DELTA PE IS IGNORED 15FB74
      STPV=SITES*(1-PL)/PE
C     NEGLECT CO2 LOSS INTO VOIDS AND CO2 BICONVERSION
C
C
C
C
C     **** 'I' - ELAPSED TIME ****
      DO 1 I=1,TMAX
C
C
C     **** 'X' - SPATIAL POSITION IN COLUMN ****
          DO 9 X=1,PSEUDO
              EQOX=KEQOX*(1+X*DELX)*0.0295)
C     HAVE JUST ACCOUNTED FOR HYDROSTATIC PRESSURE AFFECTS
C
C               BIOLOGICAL COMPUTATIONS
```

```
C
              MSV=MS(X)
              MBV=MB(X)
              VIVESC=0.
              VIVEBC=0.
              CO2X=CO2(X)
              CGC2X=CGC2(X)
              IF(CO2X  .LT.0.01) GC TO 600
C             DANGER OF VIVESP OR ...BP GOING NEGATIVE
              VIVESP=0.
              IF(MSV.GT.MSMX) GO TC 610
              VIVESP=1.-MSV/MSMX
610           VIVEBP=0.
              IF(MBV.GT.MBMX) GO TC 620
              VIVEBP=1.-MBV/MBMX
620           CONTINUE
              INHIB=1./(1.+CNO2(X)*8710.*10.**(-PH(X)))
C             INHIB 27CC74
              VIVESC=CNH4(X)*CC2X  /((CNH4(X)+CSNH4)*(CO2X  +CSC2S))
              VIVEBC=CNO2(X)*CC2X  /((CNC2(X)+CSNC2)*(CO2X  +CSC2B))
60C           CONTINUE
              KCS=MSV*VIVESC*DELT*INHIB
              KCB=MBV*VIVEBC*DELT*INHIB
              MS(X)=MSV*(1.+DELT*(KCS*INHIB*VIVESP*VIVESC-KDS))
              MB(X)=MBV*(1.+DELT*(KGB*INHIB*VIVEBP*VIVEBC-KDB))
C
C             BIOLOGICALLY MANIPULATED SPECIES
C
              CNH4N=CNH4(X+1)*COEF1+CNH4(X)*COEF2+CNH4(X-1)*COEF3-
     -        ALPHA*KCS
              CO2N =CO2(X+1)*COEF1+CC2X    *COEF2+CO2 (X-1)*COEF3   -
     -        LAMBDA*KCB-KAPPA*KCS
C             OXYGEN DISTRIBUTION BETWEEN GAS AND LIQUID
              BDM1=701.+(EGCX-CO2N)*PE/(PL-PE)-CGC2X
              CDM1=-701.*(CO2N*PE+CGC2X*(PL-PE))/(PL-PE)
              U2(X)=-0.5*BDM1+SQRT(0.25*BDM1*BDM1-CDM1)
              U1(X)=EGCX*U2(X)/(U2(X)+701.)
              U5(X)=CNO2(X+1)*COEF1+CNO2(X)*COEF2+CNO2(X-1)*COEF3
     -        -BETA*KCB+DELTA*KCS
              U6(X)=CNO3(X+1)*COEF1+CNO3(X)*COEF2+CNO3(X-1)*COEF3+
     -        ETA*KCB
            IF(U6(X).LT.CNO30) U6(X)=CNO30
C           THE LARGE CONCENTRATION GRADIENT FOR NITRATE LEADS TO
C           INSTABILITY AT THE INTERFACE BETWEEN THE NEWLY PERCOLATING
C           SOLUTION AND THE INTERSTITIAL SOLUTION
              U8(X)      =CCO2(X+1)*COEF1+CCO2(X)*COEF2+CCO2(X-1)*COEF3
              CAN  =CA(X+1)*COEF1+CA(X)*COEF2+CA(X-1)*COEF3+CMICRN*KCS
C
C             ION EXCHANGING SPECIES
C
```

```
                CCAN=CCA(X+1)*CCEF1+CCA(X)*CCEF2+CCA(X-1)*CCEF3
                CMGN=CMG(X+1)*CCEF1+CMG(X)*CCEF2+CMG(X-1)*CCEF3
                CNAN=CNA(X+1)*CCEF1+CNA(X)*CCEF2+CNA(X-1)*CCEF3
C               COUPLED
                UC(X)=CMGN
                UE(X)=CNAN
                U3(X)=CNH4N
                U4(X)=CCAN
                U7(X)=CAN
C               INITIAL PH GUESS
                PPH=PH(X)
C               DETERMINE IF CAN SKIP PARTS OR ALL OF CATION
C               EXCHANGE COMPUATIONS
                HSKIP=1
                IF(ABS(CNH4N-CENH4(X))/CNH4N.LT.C.C7) GO TO 10151
                CENH4(X)=CNH4N
                HSKIP=0
                IF(PH(X).GT.7.0)HSKIP=1
                GO TO 10152
10151           IF(PH(X).GT.3.9)GO TO 32156
C               NO DELTA NH4 & PH>7 THUS NOTHING BUT CONVECTIVE
C               AND DISPERSIVE MASS TRANSFER
                HSKIP=0
                CENH4(X)=CNH4(X)
C               IF DEL NH4<0.1 AND PH>4 NO ION EXCHANGE
C               IF DEL NH4>0.1 AND PH>7 NO H+ ION EXCHANGE
10152           CONTINUE
C               ION EXCHANGE EQUILIBRIUM SECTION
                SUM=0.C4990*CCAN+0.C8224*CMGN+C.04348*CNAN+C.C7143*CNH4N
     -          +CAN
                SUMD=1./SUM
                XCAI=XCA(X)
                DELPH=0.6
                CT=CCO2(X)
C               USE PREVIOUS PH AS GUESS
                CNT=-10
                Z1=CCAN*0.C499/STPV+XCAI
C               APPROXIMATE SINCE SUM CHANGES
                F1=SUM/STPV
                F2=F1
                ORDER=-1
7               Z1=Z1-0.1
                F1=F2
                F2=XDM2(Z1)
                ORDER=+1
                IF(F2) 999,999,7
999             Z2=Z1
                Z1=Z1+0.1
C               HAVE STRATTLED THE ROOT
300             Z3=Z2-F2*(Z2-Z1)/(F2-F1)
```

```
                IF(ABS(Z3-Z2).LT.5.E-4) GO TO 23334
                CNT=CNT+1
                IF(CNT) 25400,23334,23334
25400           CONTINUE
                F3=XDM2(Z3)
                IF(F3*F2) 100,200,200
100             Z1=Z3
                F1=F3
                GO TO 300
200             F1=F1*0.5
                Z2=Z3
                F2=F3
                GO TO 300
C               THE ABOVE IS THE MODIFIED REGULA FALSI SEARCH
23334           CONTINUE
                ZCA=Z3
C               GOT NEW AQUEOUS/SURFACE DISTRIBUTION
                PH(X)=PPH
C               MAKE LAST CALL TO COMPUTE XMG,XNA,ETC
                F1=XDM2(Z3)
                UD(X)=CMGN+(XMG(X)-ZMG)*STPV*12.16
                UE(X)=CNAN+(XNA(X)-ZNA)*STPV*22.99
                U3(X)=CNH4N+(XNH4(X)-ZNH4)*STPV*14.
                U4(X)=CCAN+(XCA(X)-ZCA)*STPV*20.04
                U7(X)=CAN+STPV*(XH(X)-ZH)
                XCA(X)=ZCA
                XMG(X)=ZMG
                XNH4(X)=ZNH4
                XNA(X)=ZNA
                XH(X)=ZH
32156           CONTINUE
                HSKP(X)=HSKIP
C               MUST REMEBER WHICH RESULTS DETOURED THE PH COMPUTATION
9           CONTINUE
C           AFTER ALL THE SPATIAL STEPS HAVE BEEN TAKEN
C           CONCENTRATIONS THROUGHOUT THE COLUMN HAVE BEEN COMPUTED
C           BASED ON VALUES AT TIME 'T', NOW RESET THE CONCENTRATIONS
C           TO THE VALUES AT 'T+DT'
            DO 19 X=1,PSEUDO
                CO2(X)=U1(X)
                CGO2(X)=U2(X)
                CNH4(X)=U3(X)
                CCA(X)=U4(X)
                CNO2(X)=U5(X)
                CNO3(X)=U6(X)
                CA(X)=U7(X)
                CCO2(X)=U8(X)
                CMG(X)=UD(X)
                CNA(X)=UE(X)
19          CONTINUE
```

```
C          ENACT THE BOUNDARY CONDITION THAT THE CONCENTRATION
C          GRADIENT AT 'INFINITY'    IS ZERO
           LMTD1=LIMITD+1
           LMTD2=LIMITD+2
           CMG (LMTD1)=CMG (LIMITD)
           CMG (LMTD2)=CMG (LIMITD)
           CNA (LMTD1)=CNA (LIMITD)
           CNA (LMTD2)=CNA (LIMITD)
           CO2 (LMTD1)=CO2 (LIMITD)
           CO2 (LMTD2)=CO2 (LIMITD)
           CGO2(LMTD1)=CGO2(LIMITD)
           CGO2(LMTD2)=CGO2(LIMITD)
           CNH4(LMTD1)=CNH4(LIMITD)
           CNH4(LMTD2)=CNH4(LIMITD)
           CCA (LMTD1)=CCA (LIMITD)
           CCA (LMTD2)=CCA (LIMITD)
           CNO2(LMTD1)=CNO2(LIMITD)
           CNO2(LMTD2)=CNO2(LIMITD)
           CNO3(LMTD1)=CNO3(LIMITD)
           CNO3(LMTD2)=CNO3(LIMITD)
           CA  (LMTD1)=CA  (LIMITD)
           CA  (LMTD2)=CA  (LIMITD)
           CCO2(LMTD1)=CCO2(LIMITD)
           CCO2(LMTD2)=CCO2(LIMITD)
           MS  (LMTD1)=MS  (LIMITD)
           MS  (LMTD2)=MS  (LIMITD)
           MB  (LMTD1)=MB  (LIMITD)
           MB  (LMTD2)=MB  (LIMITD)
           I4=I
           IF(MOD(I4,DUM).NE.0) GO TO 1
           WRITE(6,6) I,DELT,DELX,XSTRT,XFNL,PRNTX
6          FORMAT(/' TIME= ',I5,'*',F5.4,' HRS,DELTAZ= ',F5.4,
     -                                              ,'FT ISTDEPTH = ',
     -            F8.4,' FT,FINAL DEPTH = ',F8.4,' FT,DEPTH INCR =',
     -            F8.4,' FT'/42X,
     -            'CA   MG   NA   NH4  A'/42X,'XCA  XMG  XNA  XNH4 XH'/
     -            42X,'NO2  NO3  MS   MB   PH'/42X,'MS   MB   CO2  O2  ')
C      PH COMPUTATION FOR SITUATIONS WHERE IT WAS AVOIDED
       DO 400 X=1,XMAX
              IF(HSKP(X)) 20,400,20
20            A=CA(X)*0.001+ELEK*0.001
              RI=254.-CO2(X)
              RJ=(A+0.0051)*1000.
              INDEX2=RJ
              PPH=7.91-0.06*RJ
              IF(INDEX2.GT.40) GO TO 72722
              PPH=8.8
              IF(INDEX2.LT.1) GO TO 72722
              INDEX1=RI
C             PH WAS RECOMPUTED
```

```
                PPH=        ((LPRTCN(INDEX1+1,INDEX2)-LPRTCN(INDEX1,INDEX2)
     -          )*(RI-INDEX1)+(LPRTCN(INDEX1,INDEX2+1)-LPRTCN(INDEX1,
     -          INDEX2))*(RJ-INDEX2)+LPRTCN(INDEX1,INDEX2))
72722           CONTINUE
                PH(X)=PPH
400     CONTINUE
        WRITE(6,5) ((CCA(M),CMG(M),CNA(M),CNH4(M),CA(M))
     -     ,M=XSTRT,XEND,XSTEP)
        WRITE(6,5) ((XCA(M),XMG(M),XNA(M),XNH4(M),XH(M))
     -     ,M=XSTRT,XEND,XSTEP)
        WRITE(6,5) ((CNO2(M),CNO3(M),MS (M),MB (M),PH(M))
     -     ,M=XSTRT,XEND,XSTEP)
        WRITE (6,5) ((MS (M),MB (M),CGC2(M),CC2(M),CCC2(M))
     -     ,M=XSTRT,XEND,XSTEP)
5       FORMAT(/(T1,E11.4,T25,'* ',E11.4,T51,'* ',E11.4,T77,'* ',E11.4,
     -          T103,'* ',E11.4,T13,E11.4,T39,E11.4,T65,E11.4,T91,
     -          E11.4,T117,E11.4))
        WRITE(10) I,CCAO,CCA,CMGO,CMG,CNAO,CNA,PH(1),PH,XCA(1),XCA,
     -  XMG(1),XMG,XNA(1),XNA,XH(1),XH,XNH4(1),XNH4,CNC20,CNC2,CNO30,
     - CNO3,CNH4O,CNH4,MS(1),MS,ME(1),MB,CC20,CC2,CGC20,CGC2,CCC20,CCO2,
     - CAO,CA,CENH4(1),CENH4
        WRITE(6,60000) I
60000 FORMAT(' /GC.FT10F001 DD UNIT=SYSDA,DSN=URA.DATA,SPACE=(TRK,(1,1)'
     -,'),VOL=SER=CITSX1,DCB=(RECFM=VBS,BLKSIZE=9208),DISP=(CLD,KEEP)'
     - /'  I = ',I4)
1       CONTINUE
        STOP
        END
```

```
      IMPLICIT REAL*4 (A-Z)
      COMMON /COMPXY/ ISW,XL,YL
      COMMON /LBLCOM/ JSW,SLBL,STTL,SSCL
      COMMON /WETDRY/
     -    TMP  ,KGS  ,KGB  ,KDS  ,KCB  ,KLS  ,KMS  ,KLP  ,KMB  ,DCMBO2
     -    ,DOMSO2,DCMSI2,DOMBI2,DCMBA3,DCMSA,DCMSAM,ALPHA,BETA ,DELTA
     -    ,ETA  ,KAPPA,                    LAMBDA,CMICRN,MBMX ,MSMX,CVRPPS
     -    ,OVRPPB,CSNH4,CSO2S,CSC2B,CSNC2
     -    ,KC1  ,KC2  ,KOX  ,KEQOX,DNSND,HIST,DELX,CENH4(100)
     -    ,        CNC3O,CNC3(100),CNH4O,CNH4(100), CNC2O,CNC2(100)
     -    ,CCAO,CCA(100),CMGO,CMG(100),CNAO,CNA(100),MB (100), MS (100)
     -    ,         CCC2O,CCC2(100),CC2O,CO2(100),CAO,CA(100),PH(100)
      COMMON /ICNEX /
     -     CCAN,XCA(100),SITES,CMGN ,XMG(100)      ,CNH4N ,XNH4(100)
     -    ,      CNAN ,XNA(100),CAN,  CCCA,PL  ,PE  ,ZMG,ZNH4,ZNA
     -    ,KCM1,KCM2,KCN1,KCN2,KCA1,KCA2,KCH1,KCH2,ZH,XH(100),ELEK,STPV
      COMMON /CNSTNT/ KCH2O,KCH14C,KCH2OH
      COMMON /BLOCK1/ PPH,DMY1,DELPH,CT   ,ORDER,X    ,HSKIP
      COMMON /SLAVE /
     -    U1(100),U2(100),U3(100),U4(100),U5(100),U6(100),U7(100)
     -    ,U8(100),U9(100),UA(100),UB(100),UC(100),UD(100),UE(100)
      DIMENSION        DEPTH(100),UGS(100),UGB(100),CGC2(100)
     -    ,UPR1(10,10),UPR2(10,10),UPRTCN(10,40),UPR3(10,10),UPR4(10,10)
      INTEGER*4 JOOO,RTIME
      INTEGER*4  XMAX,I4   ,DUM ,ISW,JSW
      INTEGER*2
     -    XSTRT,XEND ,XSTEP,HSKIP,JMAX ,J    ,I    ,DUMMY,M
     -   ,      KNT ,LMTD1,LMTD2  ,PSEUDO      ,X   ,PLOTSW,INDEX1
     -    ,INDEX2,LIMITD, CNT, ORDER,HSKP(100)
C     DELX MUST BE TRANSFERED TO THE DRY PERIOD PROGRAM TO REALLIGN
C     DATA THAT PROGRAM WILL READ OFF THE DISK
      DELX=0.3
      DNSND=2.5
      SITES = 70.2
      TMP=25.
      MTP=2.E-07
C     ALL UNDER *** ARE 5-16-73
C     ***** CHEMICAL PARAMETERS
      KC1=10.**(-6.3)
      KC2=10.**(-10.25)
      KOX = 0.25
      KEQOX= 6990.*EXP(-11.41+1752./(TMP+273.2))
C     KOX,KEQOX 6OCT73,14NOV73,25APR74
      KCM1= EXP(0.8)
      KCM2=1.35
      KCN1=55950.
      KCN2=1.
```

```
      KCA1=800.
      KCA2=1.
      KCH1=.01
      KCH2=1.
      KCH2O=1./KCH2
      KCH1O=40.08/KCH1
      KCH2OH=0.5*KCH2O
C        30AG74
C
      CALL DRY
      STOP
      RETURN
      END
```

```
      SUBROUTINE DRY
      IMPLICIT REAL*4 (A-Z)
C     **** DRY PERIOD MODEL ****
      COMMON /WETDRY/
     -     TMP   ,KGS   ,KGB   ,KDS   ,KCB   ,KLS   ,KMS   ,KLB   ,KMB   ,DCMBO2
     -    ,DOMSO2,DOMSI2,DOMBI2,DCMBA3,DCMSA,DCMSAM,ALPHA,BETA ,DELTA
     -    ,ETA   ,KAPPA,                    LAMBDA,CMICRN,MBMX ,MSMX,CVRPPS
     -    ,OVRPPB,CSNH4,CSO2S,CSO2B,CSNO2
     -    ,KC1   ,KC2   ,KOX ,KEQOX,CNSND,HIST,CONCAT,CENH4(100)
     -    ,          CNO3D,CNO3(100),CNH4O,CNH4(100), CNO2O,CNO2(100)
     -    ,CCAO,CCA(100),CMGO,CMG(100),CNAO,CNA(100),MB (100), MS (100)
     -    ,          CCO2O,CCAR(100),CO2O,CO2(100),CAO,CA(100),PH(100)
      COMMON /BLOCK1/ PPH,DMY1,DELPH,CT,ORDER,X,HSKIP
      COMMON /IONEX /
     -     CCAN,XCA(100),SITES,CMGN ,XMG(100)       ,CNH4N ,XNH4(100)
     -    ,       CNAN ,XNA(100),CAN,  GCCA,PL   ,PE   ,ZMG,ZNH4,ZNA
     -    ,KCM1,KCM2,KCN1,KCN2,KCA1,KCA2,KCH1,KCH2,ZH,XH(100),ELEK,STPV
      COMMON /SLAVE /
     -    U1(100),U2(100),U3(100),U4(100),U5(100),U6(100),U7(100)
     -    ,U8(100),U9(100),UA(100),UB(100),UC(100),UD(100),UE(100)
      COMMON /O/ CGCO2O,CGCO2(100),CGO2O,CGO2(100)
C     'O' BLOCK CREATED TO ALLIGN THE ZEROTH ELEMENT OF THE ARRAYS
C     WITH THE CONCENTRATIONS AT THE COLUMN INLET
      DIMENSION PH1ST(27,12),PH2ND(9),PH1ST1(27,6),PH1ST2(27,6)
     -    ,UF(100)          ,DEPTH(100) ,PEV(100)
      INTEGER*4 TSTART
      INTEGER*4   DUMMY1,I4,TMAX
      INTEGER*2 I,HSKIP,J           ,DUMMY,XMAX ,PSEUDO,XSTRT,XEND
     -    ,XSTEP,DUM   ,X   ,M   ,CNT   ,ORDER  ,D6,D8,D1
      EQUIVALENCE  (PH1ST1(1,1),PH1ST(1,1)),(PH1ST2(1,1),PH1ST(1,6))
C     PH1ST (I,J) =PH AT:
C       (I*10-9.9996) MG TOT CARBONATE/L (I MAX =27)
C            (-0.036+J/2000.) MOLES ACID+ELEK/L (J MAX = 12
C       AT=17.6 PPM,PT=17.1 PPM
      DATA PH1ST1/
     - 11.66, 11.63, 11.60, 11.57, 11.54, 11.47, 11.44, 11.38, 11.32,
     - 11.26, 11.19, 11.13, 11.04, 10.91, 10.82, 10.69, 10.57, 10.44,
     - 10.32, 10.19, 10.10,  9.97,  9.88,  9.76,  9.63,  9.51,  9.35,
     - 11.60, 11.57, 11.54, 11.51, 11.44, 11.41, 11.35, 11.29, 11.22,
     - 11.16, 11.07, 10.97, 10.85, 10.72, 10.57, 10.44, 10.32, 10.19,
     - 10.07,  9.94,  9.82,  9.69,  9.57,  9.41,  9.19,  8.88,  8.35,
     - 11.57, 11.51, 11.47, 11.44, 11.38, 11.32, 11.26, 11.19, 11.10,
     - 11.01, 10.88, 10.76, 10.60, 10.47, 10.32, 10.19, 10.04,  9.91,
     -  9.79,  9.63,  9.44,  9.26,  8.91,  8.32,  7.72,  7.44,  7.26,
     - 11.51, 11.44, 11.41, 11.35, 11.29, 11.22, 11.13, 11.04, 10.91,
     - 10.79, 10.63, 10.47, 10.32, 10.16, 10.01,  9.88,  9.69,  9.54,
     -  9.29,  8.97,  8.29,  7.66,  7.38,  7.19,  7.07,  6.97,  6.88,
     - 11.41, 11.38, 11.32, 11.26, 11.16, 11.07, 10.97, 10.82, 10.66,
```

```
     - 10.51, 10.32, 10.16,  9.97,  9.82,  9.60,  9.38,  9.01,  8.26,
     -  7.60,  7.32,  7.13,  7.01,  6.88,  6.82,  6.72,  6.66,  6.63,
     - 11.35, 11.29, 11.19, 11.10, 11.01, 10.88, 10.72, 10.54, 10.35,
     - 10.13,  9.94,  9.72,  9.44,  9.07,  8.19,  7.54,  7.22,  7.04,
     -  6.91,  6.82,  6.72,  6.66,  6.60,  6.54,  6.47,  6.44,  6.41/
      DATA PH1ST2/
     - 11.22, 11.13, 11.04, 10.91, 10.76, 10.57, 10.35, 10.10,  9.85,
     -  9.57,  9.13,  8.13,  7.44,  7.13,  6.94,  6.82,  6.72,  6.63,
     -  6.57,  6.51,  6.44,  6.38,  6.35,  6.32,  6.26,  6.22,  6.19,
     - 11.10, 10.97, 10.82, 10.63, 10.35, 10.07,  9.72,  9.26,  8.01,
     -  7.32,  7.01,  6.82,  6.69,  6.57,  6.51,  6.41,  6.35,  6.32,
     -  6.26,  6.22,  6.16,  6.13,  6.10,  6.07,  6.04,  6.01,  6.01,
     - 10.88, 10.66, 10.38, 10.01,  9.44,  7.88,  7.16,  6.85,  6.63,
     -  6.51,  6.41,  6.32,  6.26,  6.19,  6.13,  6.07,  6.04,  6.01,
     -  5.94,  5.91,  5.88,  5.85,  5.85,  5.82,  5.79,  5.76,  5.76,
     - 10.41,  9.79,  7.69,  6.88,  6.54,  6.32,  6.19,  6.07,  6.01,
     -  5.91,  5.85,  5.82,  5.76,  5.72,  5.66,  5.63,  5.60,  5.57,
     -  5.54,  5.51,  5.47,  5.47,  5.44,  5.41,  5.41,  5.38,  5.35,
     -  4.32,  4.32,  4.29,  4.29,  4.29,  4.26,  4.26,  4.26,  4.22,
     -  4.22,  4.22,  4.19,  4.19,  4.19,  4.19,  4.19,  4.16,  4.16,
     -  4.16,  4.16,  4.16,  4.13,  4.13,  4.13,  4.13,  4.13,  4.13,
     -  3.26,  3.26,  3.26,  3.26,  3.26,  3.26,  3.26,  3.26,  3.26,
     -  3.26,  3.26,  3.26,  3.26,  3.26,  3.26,  3.26,  3.26,  3.26,
     -  3.26,  3.26,  3.26,  3.26,  3.26,  3.26,  3.26,  3.26,  3.26/
      DATA PH2ND/
C       PH2ND(I) = PH AT:
C        ((I-1)/200.) MOLAR ACID+ELEK; CT =ANYTHING
     -  3.26,  2.26,  1.97,  1.79,  1.66,  1.57,  1.51,  1.44,  1.38/
C    WILL ASSUME THE DRY COLUMN OF SOIL IS CLOSED AT ITS BASE
C
C
C     ASSUMING IT DRAINS INFINITELY FAST
C     PE = VOLUME FRACTION THAT IS SOLUTION
C     PL = VOLUME FRACTION THAT IS ~ SAND
C
C
C
C     PROGRAM CONTROL PARAMETERS
C
      PSTRT=0.5
      XFNL=8.
      PRNTT=12.
      TFNL=96.
      PRNTX=0.5
      DELT=0.1
      TSTART=1
      DELX=0.5
C
C
C     DYNAMIC FARMS
```

```
C
      U=0.
      PE=0.06
      PL=0.44
      D=0.39
C
C
C
C     ***** BIOLOGICAL PARAMETERS
      TMP = 25.0
C     **
      CSO2S = 0.4
      CSO2B = 0.8
      KGS = (10.**(0.0413*TMP-0.944))/24.
      CSNH4=(10.**(0.051*TMP-1.158))
      KGB=(10.**(0.0255*TMP-0.492))/24.
      KLS=0.00721
      KMS=KLS/10.
      KLB=0.0121
      KMB=KLB/10.
C     ABOVE ARE ASSUMED PROGS OF 14JAN74,22OCT74
      CSNO2=10.**(0.063*TMP-1.149)
      BETA=4.E-9*KGB
      KDB = 0.0121
      KDS = 0.00721
      DELTA=4.E-9*KGS
      GAMMA=5.71E-10*KGS
      KAPPA=1.37E-8*KGS
      ETA=BETA
      ALPHA=  DELTA
      LAMBDA=4.57E-9*KGB
C     11OCT74
C     BETWEEN ** AND THIS CARD ALL ARE 5-4-73; 26MY74
C     MAXIMUM BACTERIAL POPULATION DENSITIES
      MBMX=2.E9
      MSMX=2.E9
C
C
C
C     CHEMICAL PARMS
C
      KCO2=0.4
      KEQCO2=62.*10.**1.47
C
C
C     BOUNDARY CONDITIONS
C
C     THE ONLY ACIDITY IS THAT DUE TO THE BICARBONATE ION
      ELEK=-251./62.
      CGCO2O=0.648
```

```
      CGC20=299.
C
C
C     CONTROL PARMS
C
      TMAX=(TFNL/DELT+1.E-5)
      XSTRT=(PSTRT/DELX+1.E-5)
      XEND=(XFNL/DELX+1.E-5)
      XSTEP=(PRNTX/DELX+0.1)
      IF(XSTEP.LT.1) XSTEP=1
      XMAX=(XFNL/DELX+1.E-5)
      DUMMY=XMAX+20
      DUMMY1=(PRNTT/DELT+1.E-5)
      PSEUDO=XMAX+19
      DELX2=DELX*DELX
      DO 8 J=1,XMAX
          DEPTH(J)=DELX*J
8     CONTINUE
      COEF1=(D*DELT/DELX2-U*DELT/(DELX*(HIST+1.)))
      COEF2=(1.-2.*D*DELT/DELX2-(HIST-1.)*U*DELT/((HIST+1.)*DELX))
      COEF3=(HIST*U*DELT/((HIST+1.)*DELX)+D*DELT/DELX2)
      HSKIP=0
C
C
C     INITIAL CONDITIONS
C
      GO TO 50204
C     SKIP THIS, WILL PUT ACTUAL INITIAL CONDITIONS FROM THE WET PERIOD
C     INTO THE DRY PERIOD PROGRAM
60633 CONTINUE
      DO 37373 J=1,14
      READ(10) I,XDUM,CCA,XDUM,CMG,XDUM,CNA,XDUM,PH,XDUM,XCA,
     -  XDUM,XMG,XDUM,XNA,XDUM,XH,XDUM,XNH4,XDUM,CNO2,XDUM,
     -  CNO3,XDUM,CNH4,XDUM,PS,XDUM,PB,XDUM,CO2,XDUM,CGO2,XDUM,CCAR,
     -  XDUM,CA,XDUM,CENH4
37373 CONTINUE
50204 CONTINUE
      D6=(7/DELX+1.E-5)
      D7=(8/DELX+1.E-5)
      D1=(1/DELX+1.E-5)
C
C     INITIAL CONDITIONS
C
      DO 253 J=1,XMAX
          DUM=J*DELX/CONCAT+0.49
          PEV(J)=0.06
          IF(J.GT.D1) GO TO 31119
          PEV(J)=0.01+0.05*J/(D1+1.E-5)
          GO TO 31118
31119     CONTINUE
```

```
            IF(J.LT.D6) GO TO 31118
C           PEV IS THE EFFECTIVE POROSITY WHICH VARIES WITH DEPTH
            PEV(J)=0.06+0.33*(D6-J)/(D6-D7+1.E-5)
            IF(J.GT.D7) PEV(J)=0.39
31118       CONTINUE
            CNO3(J)=0.34*14.
            CNH4(J)=11.34
            CNO2(J)=0.0
            CCAR(J)=251.
            CO2(J)=8.3
            CA(J)=0.0
            PH(J)=8.3
            CCA(J)=40.
            CMG(J)=11.
            CNA(J)=120.
            MB (J)=4.E6 *3.
            MS (J)=7.E5 *3.
C       THE FOLLOWING ATTRIBUTES ARE CARRIED OVER FROM THE WET PERIOD
            XCA(J)=0.7315053
            XMG(J)=0.2250416
            XNH4(J)=.02451786
            XNA(J)=0.018892298
            XH(J)=0.000042909
253     CONTINUE
        DO 29073 J=1,DUMMY
            U7(J)=CA(J)
            U2(J)=CNH4(J)
            UF(J)=CNA(J)
            UE(J)=CMG(J)
            UC(J)=CCA(J)
29073   CONTINUE
        DO 2 J=1,DUMMY
            CGO2(J)=299.
            CGCO2(J)=0.648
            CGN2=701.
            CENH4(J)=0.
2       CONTINUE
        DUM1=(XMAX/2.+1.E-5)
        DUM2=(DUM1*DELX+1.E-5)
        WRITE(6,97793)   DUM2,XFNL
97793   FORMAT(/' CONDITIONS AT BEGINNING OF DRY PERIOD (TOP:',F4.1,' FT;'
       -     ,F4.1,' FT):'/)
        WRITE(6,97795) CCA(1),CCA(DUM1),CCA(XMAX),CMG(1),CMG(DUM1),
       -    CMG(XMAX),CNA(1),CNA(DUM1),CNA(XMAX),CCAR(1),CCAR(DUM1),
       -    CCAR(XMAX),CO2(1),CO2(DUM1),CO2(XMAX),CA(1),CA(DUM1),
       -    CA(XMAX),CNH4(1),CNH4(DUM1),CNH4(XMAX),CNO3(1),CNO3(DUM1),
       -    CNO3(XMAX),CNO2(1),CNO2(DUM1),CNO2(XMAX),SITES,XCA(1),
       -    XCA(DUM1),XCA(XMAX),XMG(1),XMG(DUM1),XMG(XMAX),XNH4(1),
       -    XNH4(DUM1),XNH4(XMAX),XNA(1),XNA(DUM1),XNA(XMAX),XH(1),
       -    XH(DUM1),XH(XMAX),MS (1),MS (DUM1),MS (XMAX),
```

```
     -              MB (1),MB (DUM1),MB (XMAX),
     -              CGC2(1),CGC2(DUM1),CGC2(XMAX),CGN2,CGN2,CGN2,
     -    CGCO2(1),CGCO2(DUM1),CGCO2(XMAX)
97795 FORMAT(
     -    ' AQUEOUS SPECIES (MG/L):'/'    CALCIUM = ',3(F7.2,';')/
     -    '    MAGNESIUM = ',3(F7.2,';')/'    SODIUM = ',3(F7.2,';')/
     -    '    TOTAL CARBONATE = ',3(F7.2,';')/'    OXYGEN = ',
     -    3(F7.2 ,';')/'    ACIDITY (MM) =',3(F7.2,';')/
     -    '    AMMONIUM (N) =',3(F7.2,';')/'    NITRATE (N) =',3(F7.2,
     -    ';')/'    NITRITE (N) =',3(F7.2,';')/
     -    ' EXCHANGABLE SPECIES (EQUV FRACTION) (',F8.2,' MEQ/L SAND):'/
     -    '    CALCIUM = ',3(F9.4,';')/'    MAGNESIUM =',3(F9.4,';')/
     -    '    AMMONIUM =',3(F9.4,';')/'    SODIUM = ',3(F9.4,';')/
     -    '    PROTON =',3(F9.7,';')/' BIOLOGICAL SPECIES (CELLS/CC ',
     -    'SAND):'/'    NITROSOMONAS (+) = ',3(E14.7,';')/
     -                                          '    NITROBACTER (+) ='
     -    ,3(E14.7,';')/
     -    ' GASEOUS SPECIES (MG/L GAS):'/
     -    '    OXYGEN = ',3(F7.2,';')/'    NITROGEN =',3(F7.2,';')/
     -    '    CARBON DIOXIDE =',3(F7.2,';')/)
C     X'ED VALUES ARE NEEDED TO PERMIT COMPUTATION OF THE EFFECT OF THE
C     BACTERIAL NITRIFICATION REACTIONS ON THE VARYING VOLUME FRACTION
C     OF INTERSTITIALLY HELD SOLUTION FILM
      ALPHX=ALPHA
      BETX=BETA
      ETX=ETA
      DELTX=DELTA
      KAPPX=KAPPA
      CMICRX=CMICRN
      LAMBDX=LAMBDA
C
C
C     'I' IS THE TIME VALUE
      DO 1 I=TSTART,TMAX
      CT=25.
      I4=I
C     I4 IS INTEGER*4,I IS INTEGER*2
C
C
C          AFTER THE TIME STEP IS TAKEN THE SPATIAL STEP 'X' IS TAKEN
C
           DO 9 X=1,XMAX
           PE=PEV(X)
C          CONVERT 'PER ML SAND' TO 'PER L SOLUTION'
           ALPHA =ALPHX *((1.-PL)/PE)*1000.
           BETA  =BETX  *((1.-PL)/PE)*1000.
           DELTA =DELTX *((1.-PL)/PE)*1000.
           ETA   =ETX   *((1.-PL)/PE)*1000.
           KAPPA =KAPPX * ((1.-PL)/PE)*1000.
           CMICRN=CMICRX* ((1.-PL)/PE)*1000.
```

```
      LAMBDA=LAMBDX* ((1.-PL)/PE)*1000.
      STPV=SITES*(1-PL)/PE
C
C
C     BIOLOGICAL SPECIES
C
      MSV=MS(X)
      MBV=MB(X)
      VIVESP=1.-MSV/MSMX
      VIVEBP=1.-MBV/MBMX
      CO2X=CO2(X)
      CGO2X=CGO2(X)
      CGCO2X=CGCO2(X)
      INHIB=1./(1.+CNO2(X)*22000.* 10.**(-PH(X)))
      VIVESC=CNH4(X)*CO2X  /((CNH4(X)+CSNH4)*(CO2X  +CSC2S))
      VIVEBC=CNO2(X)*CO2X  /((CNO2(X)+CSNO2)*(CO2X  +CSC2B))
C     IF THE OXYGEN CONTENT HAPPENS TO GO SLIGHTLY BELOW
C     ZERO THEN ASSUME THAT IT IS IDENTICALLY ZERO
      IF(CO2X.GT.0.) GO TO 36667
      VIVESC=0.
      VIVEBC=0.
36667 CONTINUE
      KCB=MBV*VIVEBC*DELT *INHIB
      KCS=MSV*VIVESC*DELT*INHIB
      KCST=(CNH4(X) 1.E-5)/ALPHA
      IF(KCS.GT.KCST) KCS=KCST
      KCBT=(CNO2(X)-1.E-5+DELTA*KCS)/BETA
      IF(KCB.GT.KCBT) KCB=KCBT
      KCST=(CO2X-1.E-5-LAMBDA*KCB)/KAPPA
      IF(KCS.GT.KCST) KCS=KCST
      VIVESC=KCS/(MSV*DELT*INHIB)
      VIVEBC=KCB/(MBV*DELT*INHIB)
      MS(X)=MSV*(1.+DELT*(KGS*INHIB*VIVESP*VIVESC-KDS))
      MB(X)=MBV*(1.+DELT*(KGB*INHIB*VIVEBP*VIVEBC-KDB))
C
C     BIOLOGICALLY MANIPULATED SPECIES
C
      CNH4(X)=CNH4(X)-ALPHA*KCS
       CO2N=CO2X-LAMBDA*KCB-KAPPA*KCS
      CGO2N=CGO2(X+1)*CCEF1+CGO2X*CCEF2+CGO2(X-1)*CCEF3
C     THE GASEOUS OXYGEN CONCENTRATION IS IN EQUILIBRIUM LOCALLY
C     WITH THE AQUEOUS OXYGEN CONTENT
      BDM1=701.+(KEQOX-CO2N)*PE/(PL-PE)-CGO2N
      CDM1=-701.*(CO2N*PE+CGO2N*(PL-PE))/(PL-PE)
      U5(X)=-0.5*BDM1+SQRT(0.25*BDM1*BDM1-CDM1)
       U6(X)=KEQOX*U5(X)/(U5(X)+701.)
C     SINCE NO HYDROSTATIC PRESSURE EQOX = KEQIX
      CNO2(X)=CNO2(X)-BETA*KCB+DELTA*KCS
      CNO3(X)=CNO3(X)+ETA*KCB
      CA(X)=CA(X)+CMICRN*KCS
```

```
C      ASSUME ALL PROCESSES OCCUR IN AQUEOUS PHASE. THUS IF CA(AQ) AND
C          NH4(AQ) HAVE NOT CHANGED THEN ION EXCHANGE WILL ¬ CHANGE.
C          IF CA(AQ) HAS ¬ CHANGED THEN PH MUST BE GREATER THAN APPROX 6
C           THEREFORE THE PROTON WILL  ¬ EFFECT THE ION EXCHANGE.
           CCAN=CCA(X)
           CMGN=CMG(X)
           CNAN=CNA(X)
           CNH4N=CNH4(X)
           CAN=CA(X)
           PPH=PH(X)
           IF(ABS(CNH4N-CENH4(X)).LT.0.01) GO TO 22156
C          THIS IS ENOUGH TO LOWER UNBUFFERED SOL'N TO PH 6
           CENH4(X)=CNH4(X)
           DELPH=0.6
           SUM=0.04990*CCAN+0.08224*CMGN+0.04348*CNAN+0.07143*CNH4N
     -     +CAN
           SUMD=1./SUM
           XCAI=XCA(X)
C          CT=CCAR(X)
           CNT=-10
           Z1=CCAN*0.0499/STPV+XCAI
           F1=SUM/STPV
           F2=F1
           ORDER=-1
7          Z1=Z1-0.1
           F1=F2
           F2=XDM2(Z1)
           ORDER=+1
           IF(F2)999,999,7
999        Z2=Z1
           Z1=Z1+0.1
C          GOT A STRATTLING Z1,Z2
300        Z3=Z2-F2*(Z2-Z1)/(F2-F1)
C          ERROR WILL BE LESS THAN 1/STPV TO AVOID LOW FREQUENCY
C          INSTABILITIES
           IF(ABS(Z3-Z2).LT.1.E-4) GO TO 23334
           CNT=CNT+1
           IF(CNT) 25400,23334,23334
25400      CONTINUE
           F3=XDM2(Z3)
           IF(F3*F2) 100,200,200
100        Z1=Z3
           F1=F3
           GO TO 300
200        F1=F1*0.5
           Z2=Z3
           F2=F3
           GO TO 300
23334      CONTINUE
           ZCA=Z3
```

```
C          MAKE A DUMMY CALL TO 'XDM2' TO EVALUATE THE OTHER X'S
           F1=XDM2(Z3)
           CNH4(X)=CNH4N+(XNH4(X)-ZNH4)*STPV*14.
           CA (X)=CAN+STPV*(XH(X)-ZH)
           CMG (X)=CMGN+(XMG(X)-ZMG)*STPV*12.16
           CNA (X)=CNAN+(XNA(X)-ZNA)*STPV*22.99
           CCA(X)=CCAN+(XCA(X)-ZCA)*STPV*20.04
           XCA(X)=ZCA
           XMG(X)=ZMG
           XNH4(X)=ZNH4
           XNA(X)=ZNA
           XH(X)=ZH
22156      CONTINUE
           H=10.**(-PPH)
           PH(X)=PPH
C          ASSUME PH WILL NOT CHANGE AS CO2 FLASHES OFF
           CDUMM=        H*H/(H*H+H*5.0118723E-7+2.818383CE-17)
           CCARN=CCAR(X)
           CGCO2N=CGCO2(X+1)*COEF1+CGCO2X*COEF2+CGCO2(X-1)*COEF3
           CCAR(X)=(CGCO2N*22.7273*(PL-PE)+CCARN*16.3934*PE)/
     -     (21.5865C*(PL-PE)*CDUMM+16.3934*PE)
           UC(X)=CCAR(X)*0.949894*CDUMM
9          CONTINUE
       DO 19 X=1,XMAX
           CGO2(X)=U5(X)
           CO2(X)=U6(X)
           CGCO2(X)=UC(X)
19     CONTINUE
       V5=U5(XMAX)
       V6=U6(XMAX)
       VC=UC(XMAX)
C      ENFORCE THE BOUNDARY CONDITION THAT THE CONCENTRATION GRADIENT
C      AT THE BOTTOM OF THE COLUMN IS ZERO
       DO 21 X=XMAX,PSEUDO
           CGO2(X)=V5
           CGCO2(X)=VC
21     CONTINUE
       IF(MOD(I4,DUMMY1).NE.0) GO TO 1
           WRITE(6,6) I,DELT,DELX,XSTRT,XFAL,PRNTX
6          FORMAT(/' TIME= ',I5,'*',F5.4,' HRS,DELTAZ= ',F5.4,
     -          1X                                  ,'FT 1STDEPTH = ',
     -            F8.4,' FT,FINAL DEPTH = ',F9.4,' FT,DEPTH INCR =',
     -            F8.4,' FT'/42X,
     -            'CA  MG  NA  NH4 CT'/42X,'XCA XMG XNA XAM CO2G'/
     -            42X,'PH  MS  MB  CA  C2'/42X,'HC2 HC3 XH  MB  C2G'  )
       PE=0.06
       X1FT=(1./DELX+1.E-5)
       FC2=(209.-CGO2(X1FT))*D*(PL-PE)*(PL-PE)*0.196*0.196*28.3/32.
       FCC2=(0.4-CGCO2(X1FT))*D*(PL-PE)*(PL-PE)*0.196*0.196*28.3/44
       WRITE(6,503) FC2,FCC2
```

```
503   FORMAT(' FLUX O2 (MM/HR) = ',E11.4,' ; FLUX CO2 (MM/HR) = ',E11.4)
      WRITE(6,5) ((CCA(M),CMG(M),CNA(M),CNH4(M),CCAR(M))
     -      ,M=XSTRT,XEND,XSTEP)
      WRITE(6,5) ((XCA(M),XMG(M),XNA(M),XNH4(M),CGCO2(M))
     -      ,M=XSTRT,XEND,XSTEP)
      WRITE(6,5) ((PH(M),MS (M),ME (M),CA(M),CO2(M))
     -      ,M=XSTRT,XEND,XSTEP)
      WRITE(6,5) ((CNO2(M),CNO3(M), XH(M),MB (M),CGO2(M))
     -      ,M=XSTRT,XEND,XSTEP)
5     FORMAT(/(T1,E11.4,T25,'* ',E11.4,T51,'* ',E11.4,T77,'* ',E11.4,
     -          T103,'* ',E11.4,T13,E11.4,T39,E11.4,T65,E11.4,T91,
     -          E11.4,T117,E11.4))
      WRITE (15) I,CCA,CMG,CNA,PH,XCA,XMG,XNA,XH,XNH4,CNO2,
     -   CNO3,CNH4,MS,MB,CO2,CGO2,CCAR,CA,CGCO2,CENH4
      WRITE(6,65656) I
65656 FORMAT(' //GO.FT15F001 DD UNIT=SYSDA,DSN=DRY.DATA,SPACE=(TRK,(1,1)
     -),DCB=SER=CITSX1,DCB=(RECFM=VBS,BLKSIZE=9208),DISP=(CLD,KEEP)',
     - 'I=',I4)
1     CONTINUE
      WRITE(6,97796) DUM2,XFNL
97796 FORMAT(' CONDITIONS AT END OF DRY PERIOD (TOP;',F4.1,' FT;',
     -    F4.1,' FT):'/)
      WRITE(6,97795) CCA(1),CCA(DUM1),CCA(XMAX),CMG(1),CMG(DUM1),
     -    CMG(XMAX),CNA(1),CNA(DUM1),CNA(XMAX),CCAR(1),CCAR(DUM1),
     -    CCAR(XMAX),CO2(1),CO2(DUM1),CO2(XMAX),CA(1),CA(DUM1),
     -    CA(XMAX),CNH4(1),CNH4(DUM1),CNH4(XMAX),CNO3(1),CNO3(DUM1),
     -    CNO3(XMAX),CNO2(1),CNO2(DUM1),CNO2(XMAX),SITES,XCA(1),
     -    XCA(DUM1),XCA(XMAX),XMG(1),XMG(DUM1),XMG(XMAX),XNH4(1),
     -    XNH4(DUM1),XNH4(XMAX),XNA(1),XNA(DUM1),XNA(XMAX),XH(1),
     -    XH(DUM1),XH(XMAX),MS (1),MS (DUM1),MS (XMAX),
     -               MB (1),MB (DUM1),MB (XMAX),
     -               CGO2(1),CGO2(DUM1),CGO2(XMAX),CGN2,CGN2,CGN2,
     -    CGCO2(1),CGCO2(DUM1),CGCO2(XMAX)
      RETURN
      END
```

```
      FUNCTION XDM2(ARGMNT)
      IMPLICIT REAL*4 (A-Z)
      COMMON /CNSTNT/ KCH2O,KCH14O,KCH2OH
      COMMON /BLOCK1/ PHNEW,ZCA,  DELPH,DUMMY1,FIRST,X,HSKIP
      COMMON /ICNEX /
     -     CCAN,XCA(100),SITES,CMGN ,XMG(100)       ,CNH4N ,XNH4(100)
     -    ,      CNAN ,XNA(100),CAN,  GCCA,PL  ,PE  ,ZMG,ZNH4,ZNA
     -    ,KCM1,KCM2,KCN1,KCN2,KCA1,KCA2,KCH1,KCH2,ZH,XH(100),ELEK,STPV
      INTEGER*2 X,KNT,FIRST,HSKIP
      ZCA =ARGMNT
C     PROCESS TIME = 8 MILLISEC
C     TRANSFER OF NEW PH BACK WILL OCCUR VIA PHNEW
      GCCA=CCAN+(XCA(X)-ZCA)*STPV*20.04
      GCCAM=0.0249501*GCCA
      ZCAPM2=ZCA**KCM2
      ZCAPN2=ZCA**KCN2
      ZCAPA2=ZCA**KCA2
      ZCAPH2=ZCA**KCH2
      A1=ZCAPM2*STPV*20.04/(KCM1*GCCA)
      B1=ZCAPM2*(-CMGN-XMG(X)*STPV*12.16)*1.648C263/(KCM1*GCCA)
      A2=STPV*SQRT(     ZCAPN2/(KCN1*GCCAM))
      B2=(-CNAN-XNA(X)*STPV*22.99)/(22.99*SQRT(KCN1*GCCAM/ZCAPN2))
      A3=STPV*SQRT(     ZCAPA2/(KCA1*GCCAM))
      B3=(-CNH4N-XNH4(X)*STPV*14.)/(14.*SQRT(KCA1*GCCAM      /ZCAPA2))
      GXMG=-B1/(XMG(X)**(KCM2-1)+A1)
      GXMGP=GXMG**KCM2
      GXMG=(GXMGP*(KCM2-1)-B1)/(GXMGP*KCM2/GXMG+A1)
      GXMGP=GXMG**KCM2
      ZMG =(GXMGP*(KCM2-1)-B1)/(GXMGP*KCM2/GXMG+A1)
      ZNA=-B2/(KCN2+A2)
      ZNH4=-B3/(KCA2+A3)
      ZH=XH(X)
      IF(HSKIP) 1010,2020,1010
2020  CONTINUE
      KNT=-10
      DPH=DELPH
      PH1=PHNEW
      PHER=0.05
      FPHER=0.001
C          ASSUME START ON +F1
      F1=FPREX (PH1)
      FIRST=0
      IF(F1) 1,1,2
C         ON -F SEARCHING FOR 1ST +F1
1     PH2=PH1
      DPH=-DPH
4     PH2=PH2+DPH
      F2=F1
```

```
      F1=FPREX(PH2)
      IF(F1*DPH) 3,3,4
C        CN +F SEARCHING FOR  1ST -F2
2     F2=F1
6     PH1=PH1+DPH
      F1=F2
      F2=FPREX(PH1)
      IF(F2*DPH) 5,5,6
5     PH2=PH1
      PH1=PH1-DPH
      GO TO 82
3     PH1=PH2
      PH2=PH2-DPH
82    CONTINUE
3000  PH3=PH2-F2*(PH2-PH1)/(F2-F1)
      IF(ABS(PH3-PH2).LT.EPSER) GO TO 200
      KNT=KNT+1
      IF(KNT) 500,400,400
500   CONTINUE
      F3=FPREX(PH3)
      IF(F3*F2) 1000,2000,2000
1000  PH1=PH3
      F1=F3
      GO TO 3000
2000  F1=F1*0.5
      PH2=PH3
      F2=F3
      GO TO 3000
400   PHNEW=PH3
      GO TO 600
200    CONTINUE
      PHNEW=(PH3+PH2)*0.5
C     GOT CORRECT PH SO NOW WILL COMPUTE ADSORBED H+
600   ZH=SQRT(ZCA)*(10.**(-2*PHNEW+6.)*KCH14C/GCCA )**KCH2CH
C     WHEN XDM2=0 WILL HAVE CORRECT ADSORBED CATION FRACTIONS
51515  CONTINUE
1010  CONTINUE
      XDM2=ZCA+ZNA+ZMG+ZNH4+ZH-1.
      RETURN
      END
```

```
      FUNCTION FPREX (PH)
      IMPLICIT REAL*4 (A-Z)
      COMMON /CNSTNT/ KCH2O,KCH14O,KCH2OH
      COMMON /BLOCK1/ DUMMY1,ZCA,  DUMMY2,CT,FIRST,X,DMY1
      COMMON /IONEX /
     -      CCAN,XCA(100),SITES,CMGN ,XMG(100)       ,CNH4N ,XNH4(100)
     -     ,      CNAN ,XNA(100),CAN,  GCCA,PL   ,PE   ,ZMG,ZNH4,ZNA
     -     ,KCM1,KCM2,KCN1,KCN2,KCA1,KCA2,KCH1,KCH2,ZH,XH(100),ELEK,STPV
      INTEGER*2 X,FIRST,DMY1
C     PROCESS TIME = 1.5 MILLISEC
C     FIRST = -1 COMPUTE EVERYTHING - NEW ZCA,CT,XH,ETC
C     FIRST = 1 ONLY ZCA AND PH CHANGED
C     FIRST = 0 ONLY PH CHANGED
      KW=1.E-8
      KC1=5.011872E-4
      KC2=5.623413E-8
      H=10.**(3-PH)
      ZH=SQRT(ZCA)*(   H*H          *KCH14O/GCCA)**KCH2OH
      FPREX=H-KW/H-CT*0.016393*(1./(H/KC1+1.+KC2/H)+2./(H*H/(KC1*KC2)
     - +H/KC2+1.))-CAN-(XH(X)-ZH)*STPV -ELEK
C     GIVEN TOT CARB.,CA AQ CONC,XCA;INITIAL ACIDITY & XH
C      THEN WHEN FPREX=0 HAVE FINAL XH AND ACIFITY
      RETURN
      END
```

MATHEMATICAL MODEL FOR THE SELECTION FUNCTION OF BALL MILLING

Proposition by

Julius Uradnisheck

(submitted April 1, 1975)

INTRODUCTION

Prediction of the unsteady weight-size distribution of particles,(F(x,t)), in a ball mill may be accomplished by solving the differential mass balance of comminution,

$$\frac{\partial^2 F(x,t)}{\partial x \partial t} = -K(x)\frac{\partial F(x,t)}{\partial x} + \int_x^{x_o} \frac{\partial B(x,\alpha)}{\partial x} K(\alpha) \frac{\partial F(\alpha,t)}{\partial x}\, d\alpha.$$

Mathematical descriptions of size reduction operations are dependent on two parameters. $B(x,\alpha)$, the distribution function, represents the size distribution of particles resulting from breakage of a specific particle size. The selection function, $K(x)$, is the fractional rate of breakage of material of size x. In a ball mill, particle sizes are reduced by the particles being trapped between balls, or between ball and mill wall, and crushed by the kinetic energy of the ball. It is the purpose of this paper to predict the selection function based on the dimensions of the ball mill and physical constants for the material to be ground.

For a fixed set of milling conditions, the selection function is assumed to be independent of time and composition of the mill's charge (Austin,1). A unique selection function value exists for each particle size. Experimental findings show that for relatively small particle sizes, the selection function increases with particle size (Kelsall,7,8,9,10),(Austin,2,3,4), (Kuwahara,11). Gaudin (6) showed that a larger particle would have a larger area of vulnerability to breakage

under a ball. Olsen (13),using Gaudin's probability of breakage,showed that the selectivity function varies directly with particle size. Actually,selectivity varies with particle size to the 1.4 to 0.6 power. The value of the selection function, however, does not increase indefinitely with particle size. The eventual decrease of the selection function with particle size is attributed to an insufficiency of energy to break all the particles entrapped under the colliding ball (Austin,4). Thus the selection function depends on the number of particles entrapped in a ball collision and the energy of that collision.

For a fixed particle size, the selection function will vary with operational characteristics of the mill. For ball collisions in which the colliding pair actually make contact Gaudin (6) predicted that the probability of breakage of a particle would be directly proportional to the ball diameter. For a fixed ball charge, then, the selection function should be inversely proportional to the ball diameter squared (Olsen,13). Kelsall's (7) experimental data show the selection function to vary inversely with the ball diameter to the 1.6 power. As the ball diameter decreases the selection function reaches a maximum value and falls thereafter due to insufficient crushing energy. The same author found that, as long as there is sufficient energy to cause complete crushing of particles under the balls,

a direct proportionality exists between the selection function and mill diameter raised to the 0.6 power. Olsen (13) reported that a specific angular velocity of the mill would give a maximum selection function. The optimal rotation rate was found to be a function of particle size and ball diameter. Data has been presented to show that the selectivity function increases directly with particle charge up to a maximum value and declines thereafter (Austin,1,4),(Bowdish,5). Other important variables affecting the selection function are ball density and ball charge.

Few authors have attempted to derive a selectivity function from the physical dimensions and operation of the ball mill. Olsen used Gaudin's probability of breakage and Langermann's (12) energy relationships of balls in the mill to derive an expression for the selection function. However he did not actually predict the value but rather fitted the equation's constants to his data. Tamura (14) also derived an expression for the selection function including the effects of particle charge. He also relied on empirical quantities based on ball mills to evaluate constants of his equation. To derive a selection function this paper will rely only on constants that characterize the particles being ground.

ANALYSIS

The mechanism for breakage of particles in a ball mill is assumed to be entrapment of particles between a ball and the mill wall or another ball. A fundamental assumption is made that the fractional rate of breakage of particles is equal to the product of ball collision frequency, quantity of particles trapped in the collision zone, and probability that the particles will break during the collision. If the number of collisions, and their energy, is computed from the physical and operational variables of a ball mill, the selection function can be calculated either by further theoretical considerations or from a minimal amount of experimental work on the characteristics of single ball collisions.

Motion of balls in a small ball mill was studied experimentally. A 2-inch Plexiglass mill was partially filled with lead pellets having diameters of 1/16 inch. Time exposures were taken down the axis of the rotating mill to permit evaluation of the velocities of pellets in the mill. Motion of the pellets can be considered to be of two types. One region of the mill is characterized by pellets moving as a single unit along with the motion of the walls of the mill (Figure 1). Because pellets in this region are not exchanging momentum it is a region of no active grinding. The other region is a region of active grinding where pellets are striking the mill wall and colliding with one another.

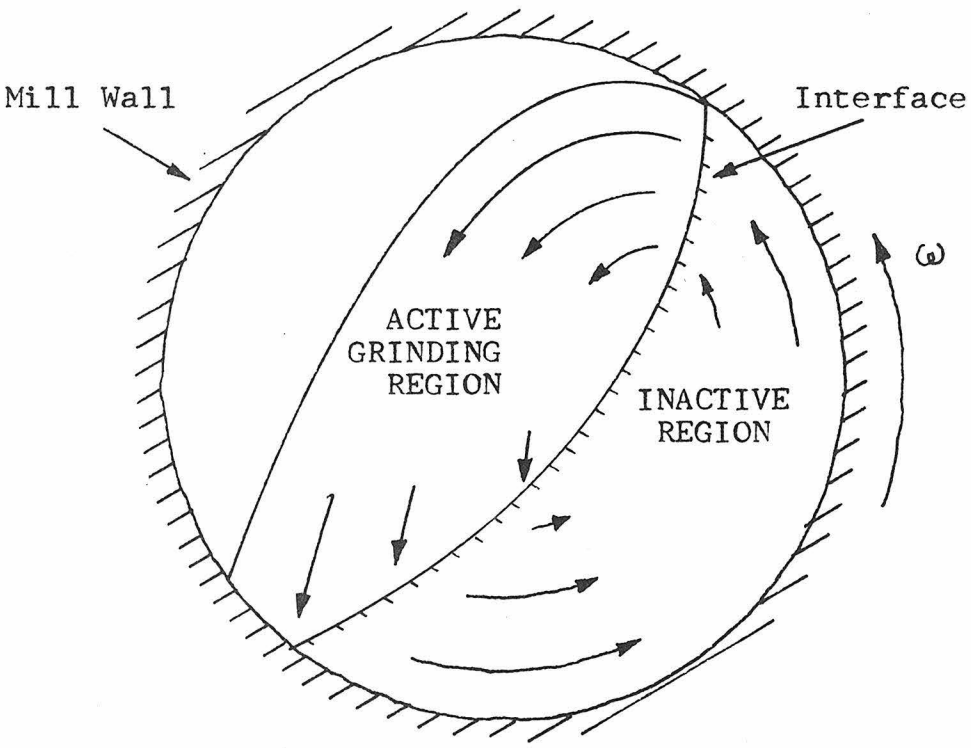

Figure 1 - Grinding Regions inside a Ball Mill

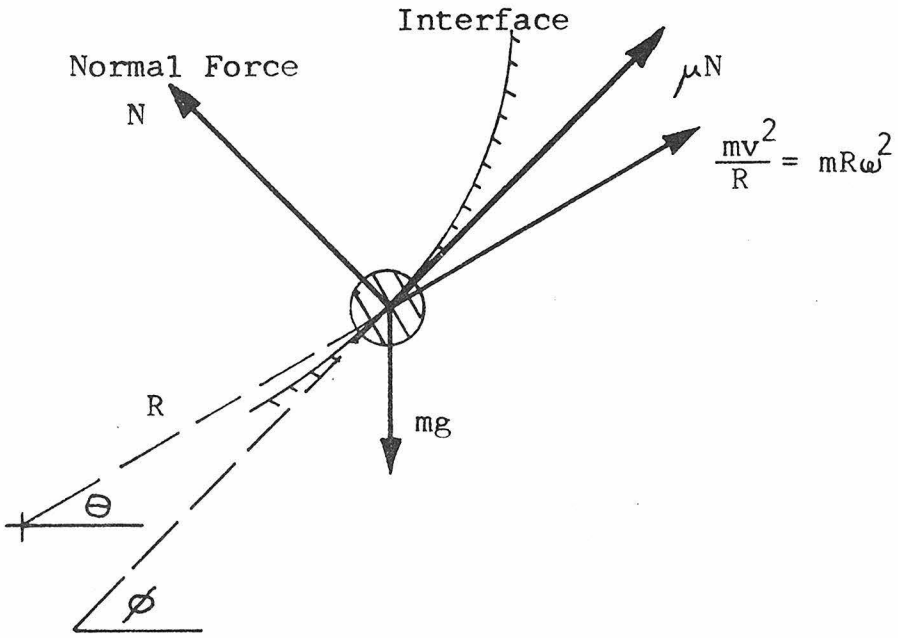

Figure 2 - Forces on an Interfacial Ball

Shape of the boundary between the active and inactive grinding regions can be characterized if it is assumed that a ball on the interface interacts only with balls on the inactive side. Consider this ball as about to slide down a slope of angle ϕ and rotating about some center (Figure 2). Assume a coefficient of static friction for the ball on the interface is μ. The ball is at equilibrium, therefore,

$$g \sin\phi = \frac{v^2}{R}\cos(\phi-\theta) + \mu g \cos(\phi) + \frac{\mu v^2}{R}\sin(\phi-\theta)$$

or,

$$1) \qquad R \sin\theta = R \cos\theta\left(\frac{1 + \mu\tan\phi}{\mu - \tan\phi}\right) + \frac{g}{\omega^2}.$$

Given a plane of angle ϕ with the horizon rotating counterclockwise with angular velocity ω, then solution of Equation 1) will give a θ for a specific R. Pellets below that position θ will slide away from that point. Pellets above position θ will not slide toward θ but could slide away from that position. A similar quation to 1), but for a ball about to slide up the plane, is

$$R \sin\theta = R \cos\theta\left(\frac{\mu\tan\phi - 1}{\tan\phi + \mu}\right) + \frac{g}{\omega^2}.$$

Except for pellets at an extreme distance away from the center of rotation, the only equation that is necessary to consider is Equation 1). Transformation of Equation 1) into an equation based on displaced polar coordinates

centered a distance g/ω^2 above the center gives,

$$R \sin\theta' = R \cos\theta'\left(\frac{1 + \tan\phi}{\mu - \tan\phi}\right)$$

or

$$2) \qquad \tan\phi = \frac{\mu\tan\theta' - 1}{\mu + \tan\theta'} \ .$$

By Equation 2) a pellet located at any position θ' in the new polar coordinate system must rest on a surface of angle ϕ with the horizon. An equation for the curve can be described that will have a tangent of angle ϕ with the horizon at the angle θ' by equating the appropriate derivatives:

$$\frac{r' + \tan\theta' \frac{dr'}{d\theta'}}{-r'\tan\theta' + \frac{dr'}{d\theta'}} = \frac{\mu\tan\theta' - 1}{\mu + \tan\theta'}$$

or

$$3) \qquad r' = \exp(-\mu\theta').$$

Equation 3) describes all the possible interfaces that could exist between the active and inactive regions of balls in a rotating ball mill (Figure 3). A ball mill with a particular dimensionless radius $\bar{R} = R\omega^2/g$ will have an interface between the active and inactive ball regions described by a particular α depending on the volume occupied by the balls. Furthermore the maximum dimensionless radius a mill with tumbling balls can have is unity. Any balls outside the dimensionless radius of one will be moving as a single mass, locked together by centrifugal force against the mill walls. As the angular velocity

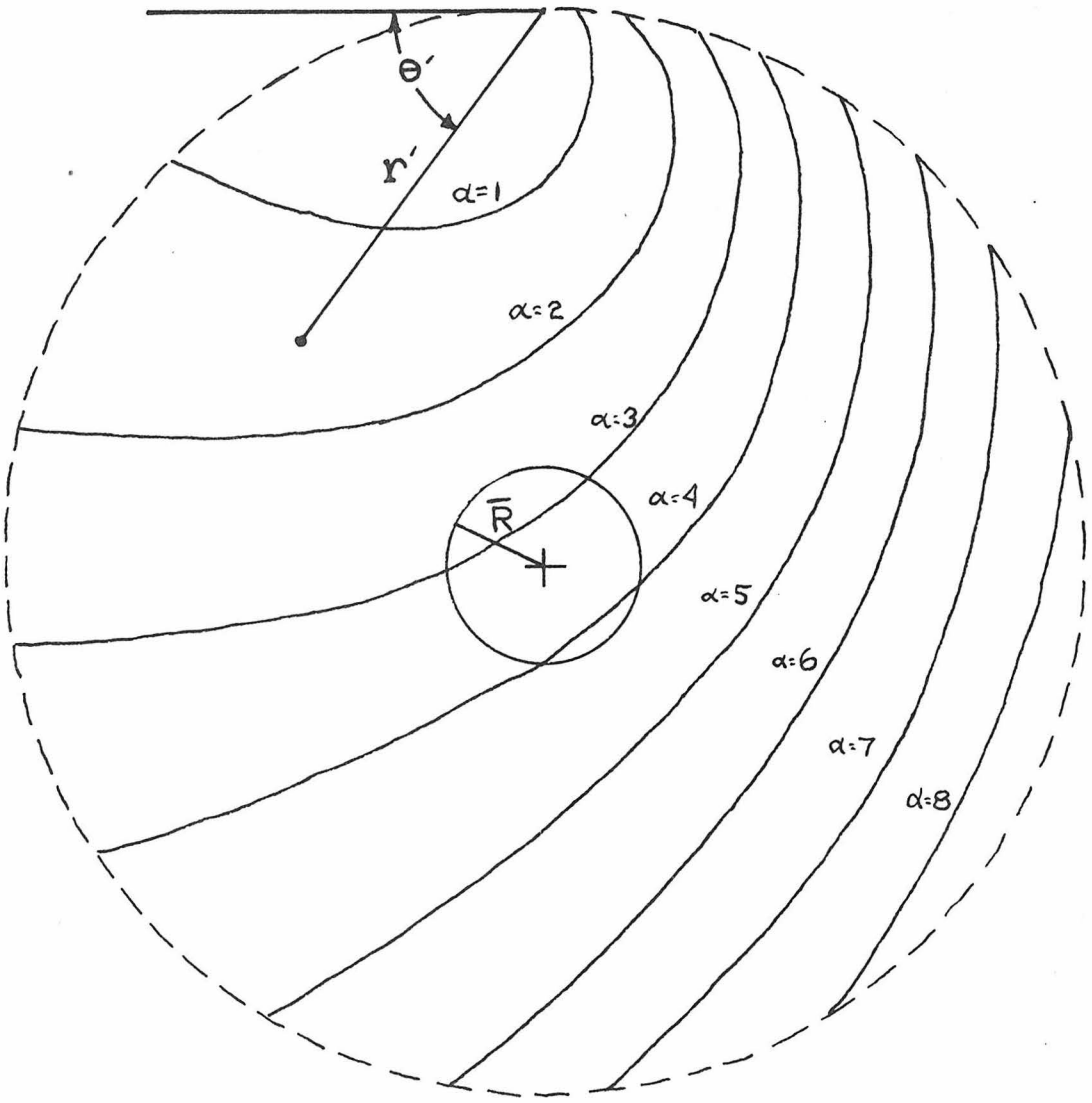

Figure 3- Possible Interfaces between Active and Inactive Grinding Regions

Interfacial curves are computed from Equation 3) with μ =0.77. A mill with dimensionless radius $\bar{R}$, as shown, has interfaces described by an α between 0.26 and 0.42 depending on the ball charge to the mill. The large dotted circle represents the radius outside of which balls will be moving as a unit fixed to the mill wall by centrifugal force.

approaches zero, the dimensionless radius of the mill approaches zero, and the shape of the interface between the active and inactive grinding regions approaches a plane. The angle of the plane above the horizon is

$$\phi_{cr} = \tan^{-1}\mu .$$

By specifying the radius and angular velocity of a ball mill, and the quantity of balls, a single value, α, will describe the interface separating balls actively grinding particles from balls in an inactive state.

An approximate analytical solution for α is possible by assuming the entire ball mass to be in the inactive region. Curves everywhere perpendicular to the interfacial curves are described by

$$r' = \beta \exp(\theta'/\mu).$$

The particular curve passing through the center of rotation of the ball mill is

$$r' = \exp((\theta' - \pi/2)\mu)$$

and will be referred to as the symmetry curve. Considering Figure 4, the symmetry curve intercepts the dimensionless mill wall at A'. The tangent line to the symmetry curve, at the center of rotation, meets the dimensionless mill wall at point A. Since

$$\psi = \pi - \phi_{cr}$$

then

$$\mathfrak{R}^2 = 1 + \bar{R}^2 + 2\bar{R}\cos\phi_{cr} .$$

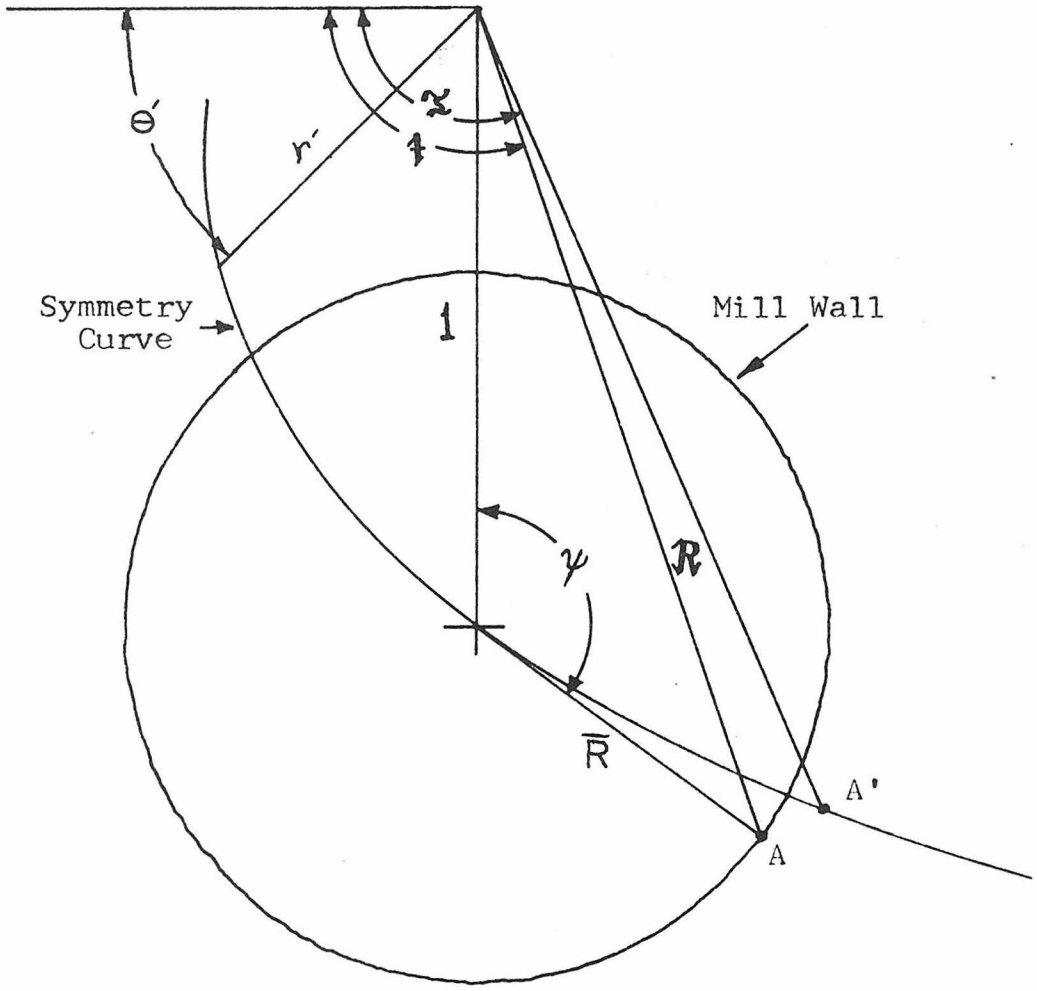

Figure 4 - Construction for Determining Approximate α

Therefore

$$\mathfrak{t} = \pi/2 + \cos^{-1}\frac{\mathfrak{R}^2 + 1 - \bar{R}^2}{2\mathfrak{R}} \quad .$$

If $\mathfrak{R}$ is the radial component of the symmetry curve then the angular component is

$$\mathfrak{T} = \pi/2 + (\ln(\mathfrak{R}))/\mu .$$

Then the angular component of the coordinate of A' will be approximately

$$\theta_o' \simeq 0.5(\mathfrak{T} + \mathfrak{t}).$$

Arc length on the symmetry curve from the dimensionless mill wall to some position defined by the angular component θ' is

$$\bar{S} = \exp(-\pi/2\mu)(\exp(\theta_o'/\mu) - \exp(\theta'/\mu))\sqrt{1 + \mu^2} \quad .$$

If a motionless ball mill of length L has a ball charge C_b, the dimensionless height to which the balls will fill the mill is approximately

$$\bar{h} \simeq \frac{\omega^2}{g}\left(\frac{0.573\ C_b}{R\ \rho_b(1-\epsilon)L} + 0.1R\right) .$$

Since the interface of the rotating ball mass is approximately symmetric about the symmetry curve then $\bar{h} \simeq \bar{S}$ .Therefore the angular component of the interception of the interface with the symmetry curve is θ_I' and

$$\exp(\theta_I'/\mu) = \exp(\theta_o'/\mu) - \bar{h}\ \exp(\pi/2\mu)/\sqrt{1 + \mu^2}.$$

The radial component is defined by

$$r'_I = \exp(\theta_I'/\mu)\exp(-\pi/2\mu).$$

Because the interface is defined by Equation 3),

4) $$\alpha = r_I' \exp(\mu\theta_I').$$

Study of balls in the grinding region reveals two zones of balls defined by the type of grinding occurring . The inner zone is characterized (Figure 5) by pellets tumbling over one another. This zone is typified undoubtedly by abundant shearing between balls. The outer region of balls are in free-flight and end their paths with impact on the mill wall or on the interface. The shearing zone is dominant at low angular velocities, but at high mill rotational rates the free flight zone is the primary cause of grinding.

As the ball mill rotates in the counterclockwise sense, the surface C'AC is repositioned. Position A (Figure 5) represents the position on the interface where balls are moved tangentially with the interface. Balls on the interface will find themselves suspended in space with an initial velocity directed away from the interface. Pellets on the interface C'A' also are susceptible to motion but are assumed not to move by virtue of their velocities being directed toward the interface and because of the rain of balls landing on the interface. Therefore the balls emanating from above the position of zero radial velocity, A, on the interface, are responsible for grinding particles. The phenomenon requires that the point B' be the same distance below A as B is above A. Clearly some balls will enter the

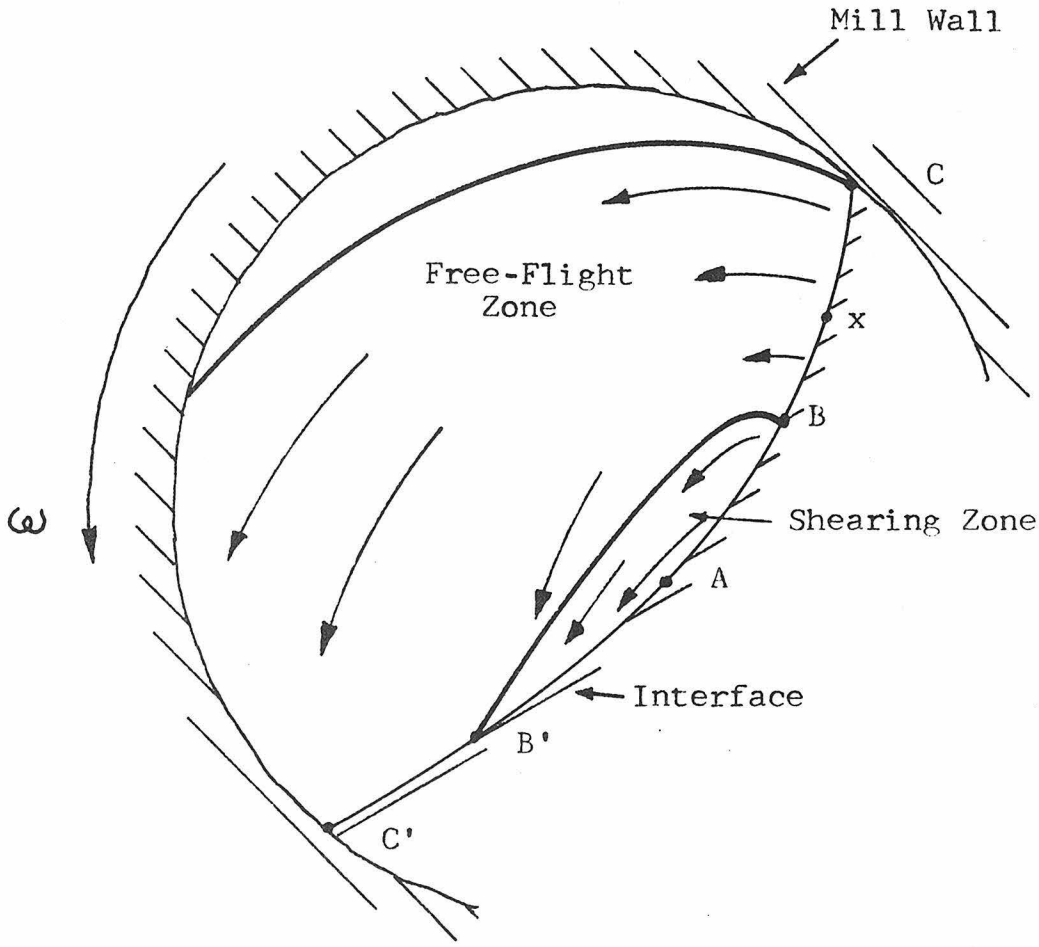

Figure 5- Zones of the Active Grinding Region

shearing zone from free-flight, and some will enter directly from the interface. To include at least half those balls entering from free-flight, B is defined as the maximum height on the interface for which a ball will take off to land at point A. Balls originating along AB are assumed to be involved in shear grinding and those along BC are responsible for pure impact grinding.

The rate at which balls are carried to the interface BC will be the same as the number of impact collisions per time. The dimensionless rate is

$$\overline{C}_{IM} = 0.5 \left(\overline{R}^2 - \overline{R}_B^2 \right),$$

where $\overline{R}_B$ is the dimensionless distance from the center of rotation of position B. A ball taking flight from position x will sustain no collisions in flight and will land with a dimensionless energy

$$\overline{E}_{IM} = 2\overline{\Delta H} + \overline{R}_x^2 ,$$

where $\overline{\Delta H}$ is the dimensionless vertical distance of fall and $\overline{R}_x$ is the dimensionless radial distance of position x from the center of rotation. It is assumed that upon landing the ball will become inactive.

Because of the conditions specified for the model and the requirement that balls must not accumulate anywhere in the ball mill, the Shearing Zone must be considered to be composed of two neighborhoods, I and II (Figure 6). Considering Neighborhood I (Figure 7),

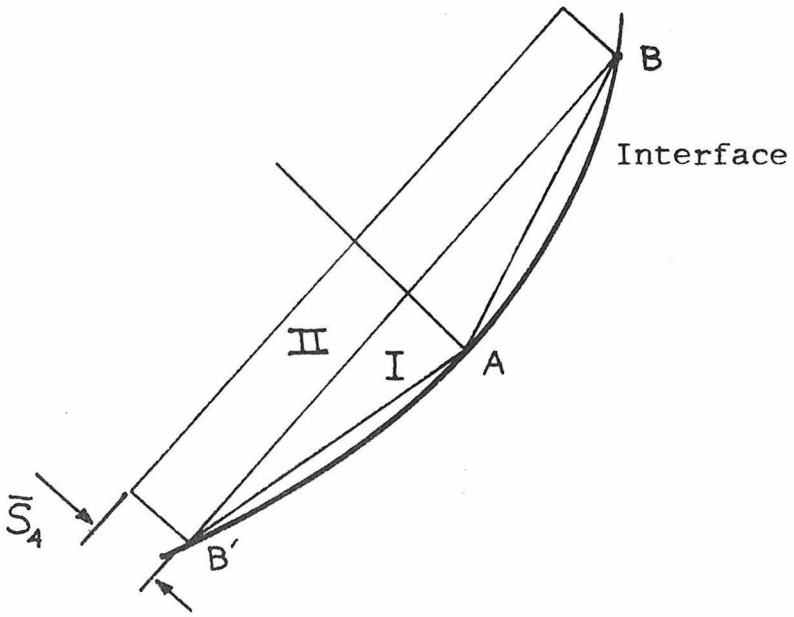

Figure 6-Neighborhoods of the Shearing Zone

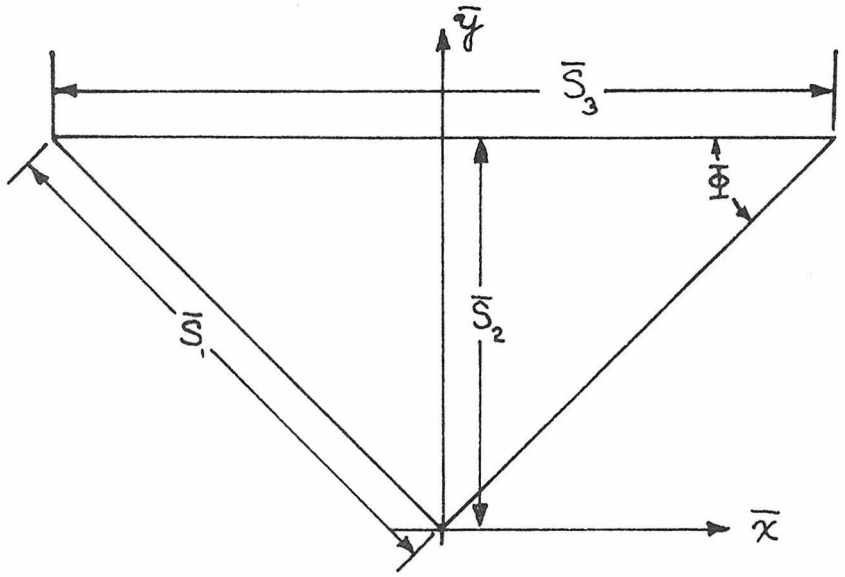

Figure 7-Dimensional Notation for Neighborhood I

$(\bar{R}_A', \theta_A')$, $(\bar{R}_B', \theta_B')$, and $(\bar{R}_{B'}', \theta_{B'}')$ are coordinates in the displaced polar coordinate system of the points A, B, and B′ respectively. Therefore

$$\bar{S}_1^2 = \bar{R}_A'^2 + \bar{R}_B'^2 - 2\bar{R}_A'\bar{R}_B' \cos(\theta_B' - \theta_A'),$$

$$\Phi \simeq 0.5\ ((\theta_B' - \theta_A')/2 + (\theta_A' - \theta_{B'}')/2),$$

$$\Phi \simeq 0.25\ (\theta_B' - \theta_{B'}').$$

Because Φ is small $\bar{S}_3 \simeq \bar{S}_1$. Inasmuch as B′ is defined such that the arc length BA′ equals AB, then

$$\theta_B' = -\ln(2\exp(-\mu\theta_A) - \exp(-\mu\theta_B))/\mu.$$

Balls presumably travel parallel to B′B with the maximum dimensionless velocity $\bar{v}_{max}$ occuring on the outermost boundary of the Shearing Zone. B′B makes an angle ϕ_1 above the horizon,

$$\phi_1 = \tan^{-1}(1/\mu) + \theta_A' .$$

The average maximum velocity on the outermost sheet is therefore

$$\bar{v}_{max} = \sqrt{(S_3 \sin\phi_1)/2} .$$

Observations of balls in the Shearing Zone suggest a parabolic velocity profile. Therefore

$$\bar{v}(\bar{y}) = \bar{v}_{max} \left(\frac{2\bar{y}}{\bar{S}_2 + \bar{S}_4} + \frac{\bar{y}^2}{(\bar{S}_2 + \bar{S}_4)^2} \right).$$

It will be assumed that very soon in its travel down through the hearing one, the ball will experience a

balance between gravitational and collisional forces and travel with constant velocity through the zone. $\bar{v}(\bar{y})$ will be assumed to be the constant velocity. The flow rate of balls through the zone is the volumetric flow rate through the plane tangent to the y-axis times the number of balls per volume. If it is assumed that the balls are packed in the Shearing Zone as they would be in a static system , then the dimensionless flow rate is

$$\bar{F}_{SH} = 0.67\bar{v}_{max} (\bar{S}_2 + \bar{S}_4).$$

The last dimension that must be specified to characterize the shape of the Shearing Zone is $\bar{S}_4$. The flow of balls into the Shearing Zone is

$$\bar{N}_{SH} = 0.5 (\bar{R}_B^2 - \bar{R}_A^2).$$

$\bar{S}_4$ is calculated by equating the flow of balls through the Shearing Zone, $\bar{F}_{SH}$, to the flow of balls into the Shearing Zone, $\bar{N}_{SH}$.

If a sheet of n_b balls of radius r_b rolls with velocity v_{rel} down another sheet of tightly packed balls of the same radius, the rate of ball-ball collisions will be

$$c = \frac{v_{rel}}{2r_b} n_b .$$

The number of ball-ball collisions between pairs of sheets in the Shearing Zone can be calculated in a similar manner. Because the centers of sheets are $2r_b$ apart, the relative velocity between sheets is

$$v_{rel} = 2r_b \frac{\partial v}{\partial y} .$$

The number of balls in a sheet is a product of the area of the sheet and the total area allotted to one ball; for Neighborhood I,

$$n_b = \frac{S_3 L y}{S_2} \frac{1}{\sigma \pi r_b^2} .$$

Total collision frequency in Neighborhood I is the summation of collision rates

$$c_I = \frac{2v_{max} S_3 L}{(S_4+S_2) S_2 \sigma \pi r_b^2} \sum_{y=0}^{S_2} y - \frac{y^2}{S_4 + S_2}$$

or

$$c_I = \frac{2v_{max} S_3 L}{(S_4+S_2) S_2 \sigma \pi r_b^2} \sum_{i=0}^{S_2/2r_b} 2r_b i - \frac{(2r_b i)^2}{S_4 + S_2} .$$

Using an approximation that

$$\int_{y=0}^{L} f(y)dy \simeq \Delta \sum_{i=0}^{L/\Delta} f(i\Delta)$$

the dimensionless collision frequency in Neighborhood I is found to be

$$\bar{c}_I = \frac{4\bar{v}_{max} \bar{S}_3 \bar{S}_2}{3\ \bar{S}_4 + \bar{S}_2} \left(0.5 - \frac{\bar{S}_2}{3(\bar{S}_4 + \bar{S}_2)} \right) .$$

Similarly, the dimensionless frequency of ball-ball collisions in Neighborhood II is

$$\bar{c}_{II} = \frac{2\bar{v}_{max}\bar{S}_3}{3(\bar{S}_4 + \bar{S}_2)}\left(\frac{\bar{S}_2^2}{\bar{S}_4 + \bar{S}_2} + \bar{S}_4 - \bar{S}_2 \right) .$$

The energy of impact is assumed to be the kinetic energy of one ball based on the relative velocity between it and its collision companion. The average collision energy throughout the Shearing Zone is

$$\bar{E}_{SH_{av}} = \frac{10\ \bar{v}_{max}^2}{3(\bar{S}_4 + \bar{S}_2)} .$$

This paper has permitted the calculation of collision frequency and energy of collision. Knowledge of these quantities free the ball mill designer from the need of operating one ball mill to design another. To determine the selection function from the number of collisions and their energies, experimentation is reduced to the observation of the number of particles crushed under a standard sphere of known collision energy.

RESULTS AND DISCUSSION

Presented are plots of dimensionless collision frequency and energy versus dimensionless mill radius at various alphas. Plots were computed on the assumption that μ =0.77. For a fixed mill radius, total impact collision frequency decreases for any alpha different from 3.4 because the number of balls entering the Active Region from the Inactive Region of the mill drops as alpha varies away from 3.4 (Figure 8).As the dimensionless mill radius decreases the impact collision frequency declines to zero at which time shearing collisions have become the dominant grinding mechanism in the mill. Of the total number of impact collisions, a fraction of collisions will occur on the mill wall (Figure 9). When the mill has a ball charge such that alpha equals approximately 5 (Figure 3)the fraction of impact collisions on the mill wall will be at a maximum. No mill wall collisions can occur at any ball charge if the dimensionless mill radius is less than 0.68. No impact collisions at all can occur in a ball mill with a dimensionless radius less than 0.32. The dominant grinding mechanism at lower dimensionless mill radii is caused by balls shearing past each other. Dimensionless shearing collision frequencies (Figure 10) are constant at high dimensionless mill radii because the geometric size of the shearing zone is fixed by the physics of ball movement. However at lower radii the dimensionless collision frequency

decreases because the Shearing Zone is forced to shrink in size, below the limits set by physics, with the smaller dimensionless mill radius. For each alpha there is a minimum dimensionless mill radius below which no collisions at all are possible. Such behavior is a consequence that certain alphas are meaningless below certain dimensionless mill radii (Figure 3). By use of Figures 8 through 10 the frequency of collisions of various types can be determined in a ball mill of known angular velocity and ball charge. The collision frequency can be used to compute the maximum value for the selection function.

Energies of collisions must be known to determine the number of particles broken under a colliding ball. The maximum dimensionless energy of impact collisions between freely flying balls and balls on the interface are plotted in Figure 11. The energy of collision that would result if a ball were dropped, from rest, from the top of the mill to the bottom is plotted. Also shown is the energy of collision of the same ball if it started to fall with the rotational kinetic energy of balls next to the mill wall. A mill filled with balls such that it has an alpha of 5 comes closely to the maximum use of potential energy because balls for such a mill will fall nearly two mill radii in distance. Curves in Figure 11 abruptly stop at certain dimensionless mill radii when the Shearing Zone has totally dominated

the mill as the grinding mechanism. Balls striking the mill wall will have smaller collision energies as they strike further and further up the wall. The maximum energy will occur for collisions of balls starting at the apex of the interface and falling to its base. The range of energies of impact collisions on the wall is drawn (Figure 12). Minimum energies approach zero as the dimensionless radius reaches one. Above a dimensionless radius of one balls can take flight and collide with the mill wall immediately with negligible energy of collision. The dimensionless energy of collision of balls in the Shearing Zone (Figure 13) is constant at high radii for the same reason that collision frequency is constant. Maximum gravitational and rotational energies are not shown on this plot because the dimensionless form of these energies would include the ball radius (see Nomenclature). Given the ball charge and rotational speed of the ball mill, the collision frequency and energies can be determined by use of the plots. Knowledge of the number of particles crushed under a standard ball of known collision energy can then be used to calculate the selection function of the mill.

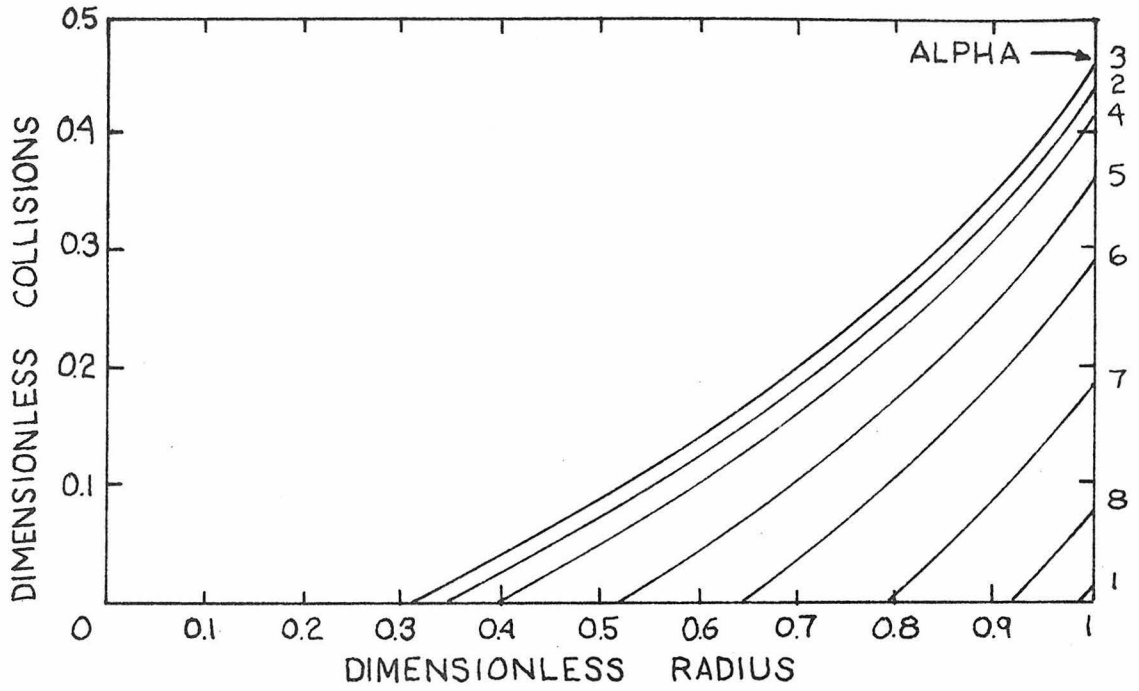

Figure 8 -Dimensionless Frequency of Total Impact Collisions Versus Radius at Different Alphas

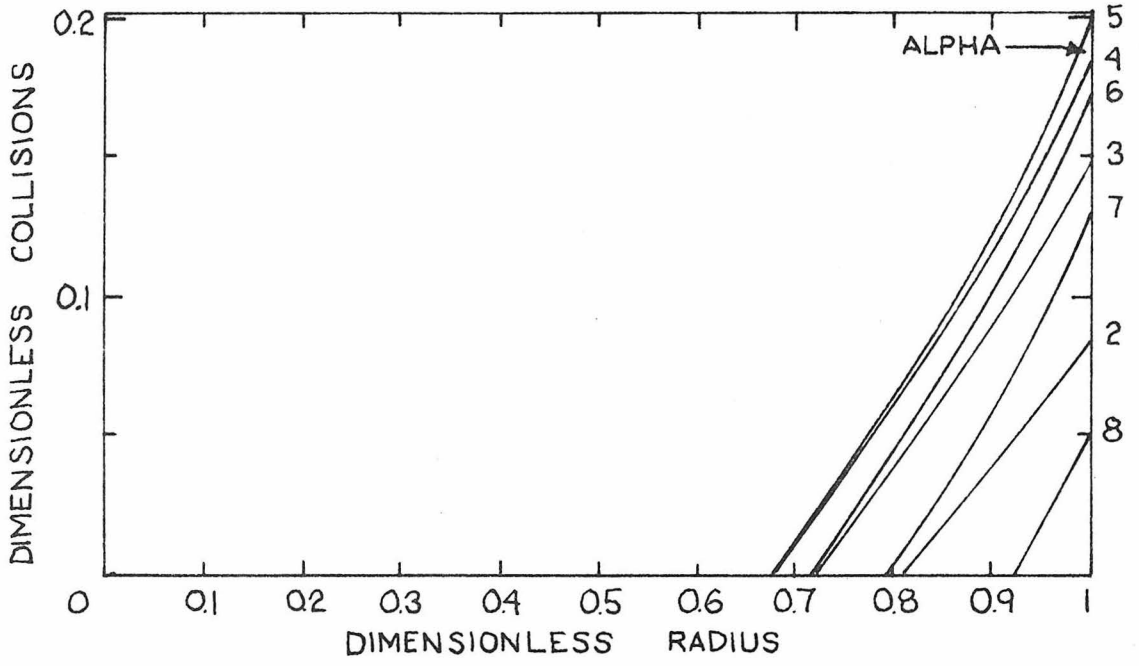

Figure 9-Dimensionless Frequency of Impact Collisions on Mill Wall Versus Dimensionless Radius at Various Alphas

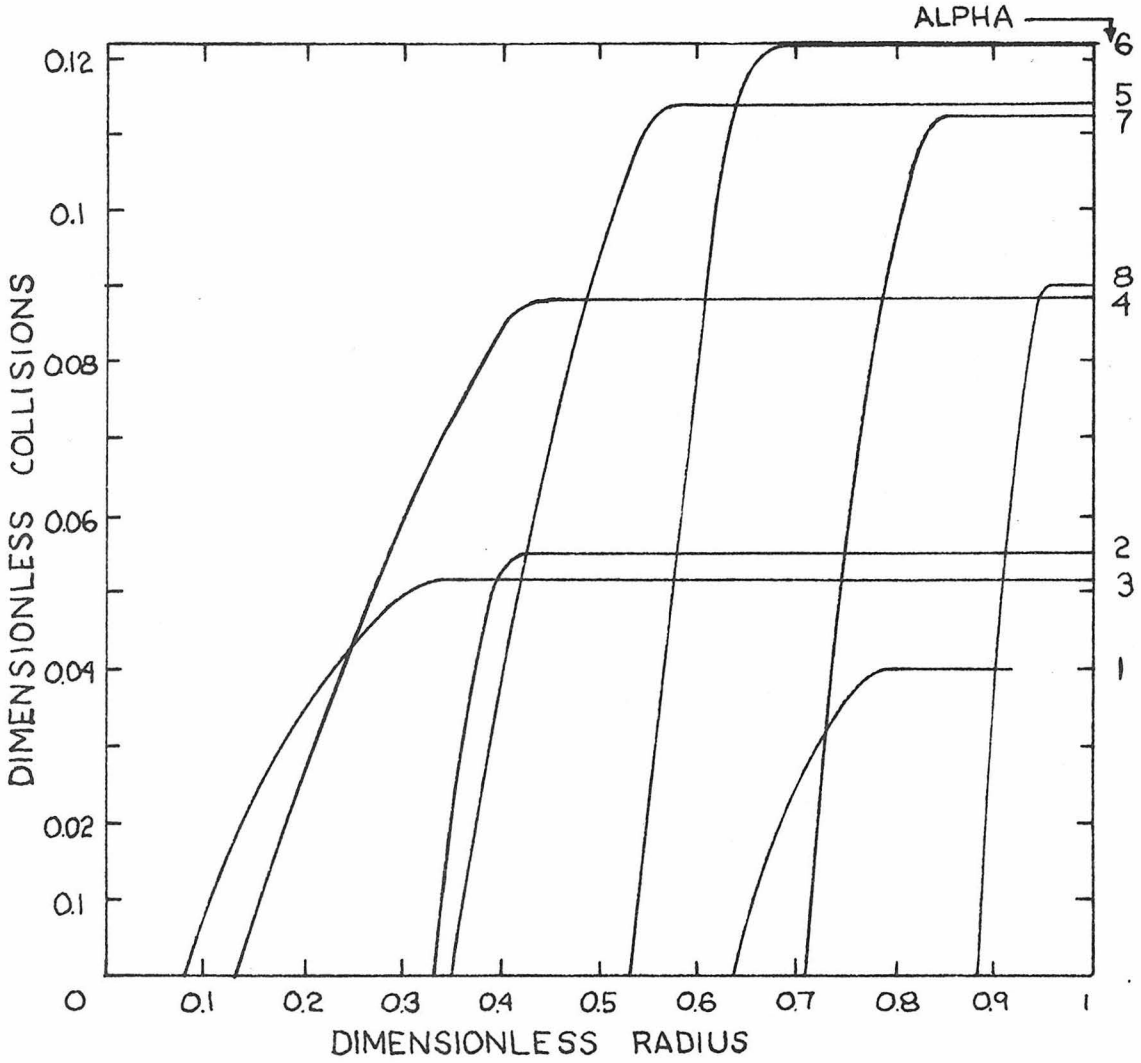

Figure 10-Dimensionless Frequency of Shearing Collisions Versus Dimensionless Mill Radius at Various Alphas

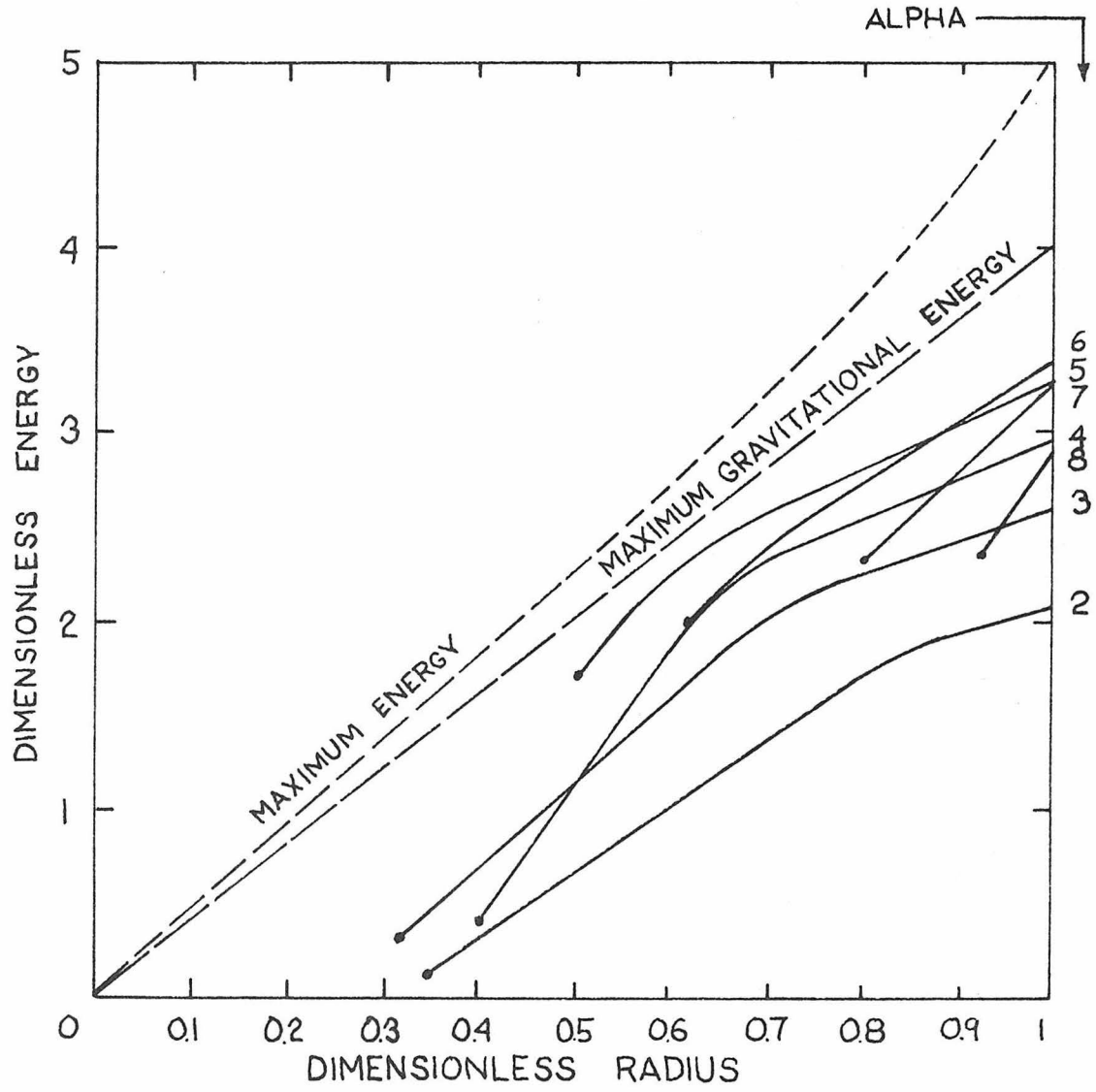

Figure 11-Maximum Dimensionless Energy of Collision of Impact between a Free-Flight Ball and an Interfacial Ball Versus Dimensionless Radius of Mill at Various Alphas

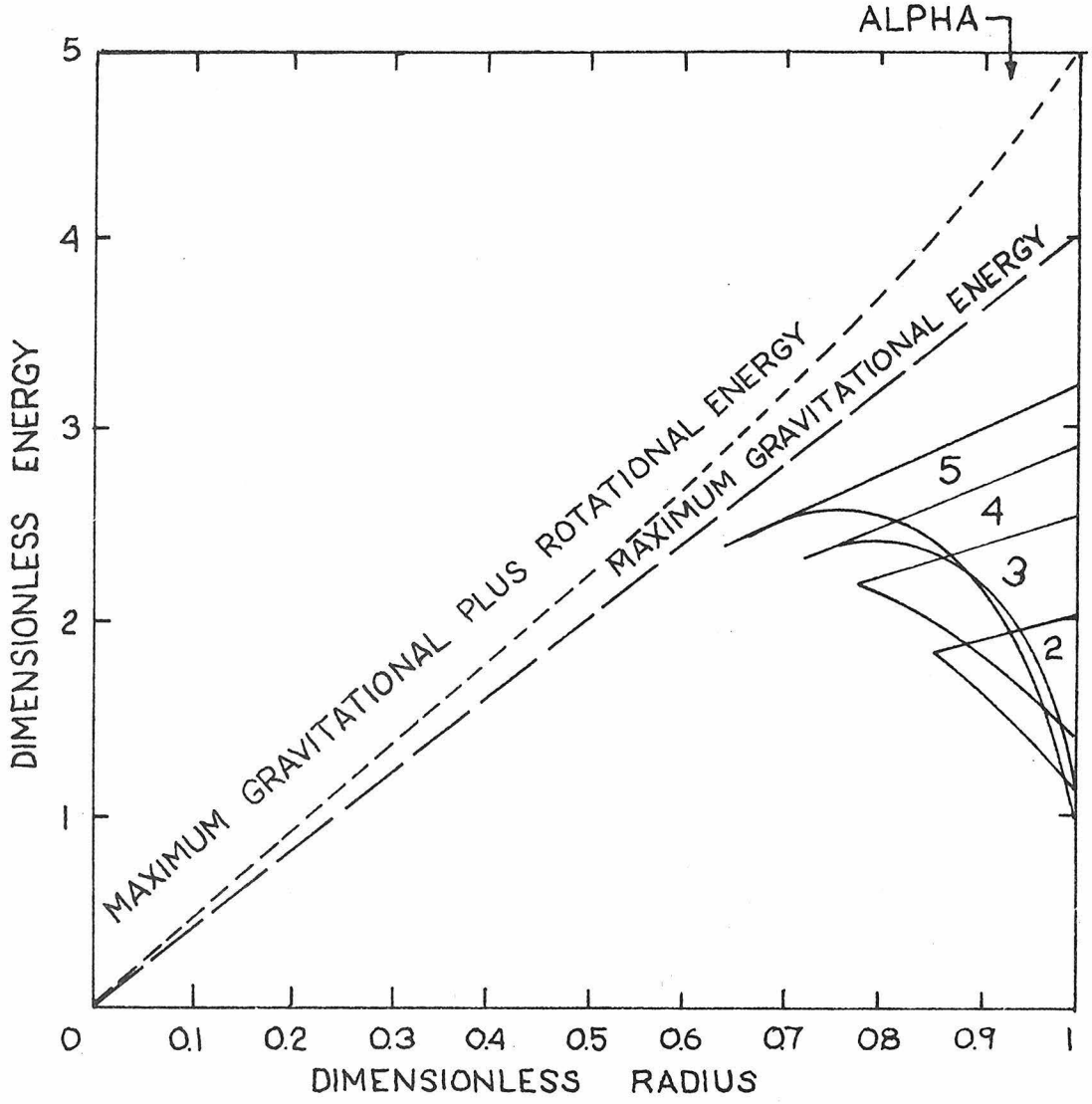

Figure12-Range of Dimensionless Energy of Collision of Impact between a Free-Flight Ball and the Mill Wall Versus Dimensionless Radius of Mill at Various Alphas

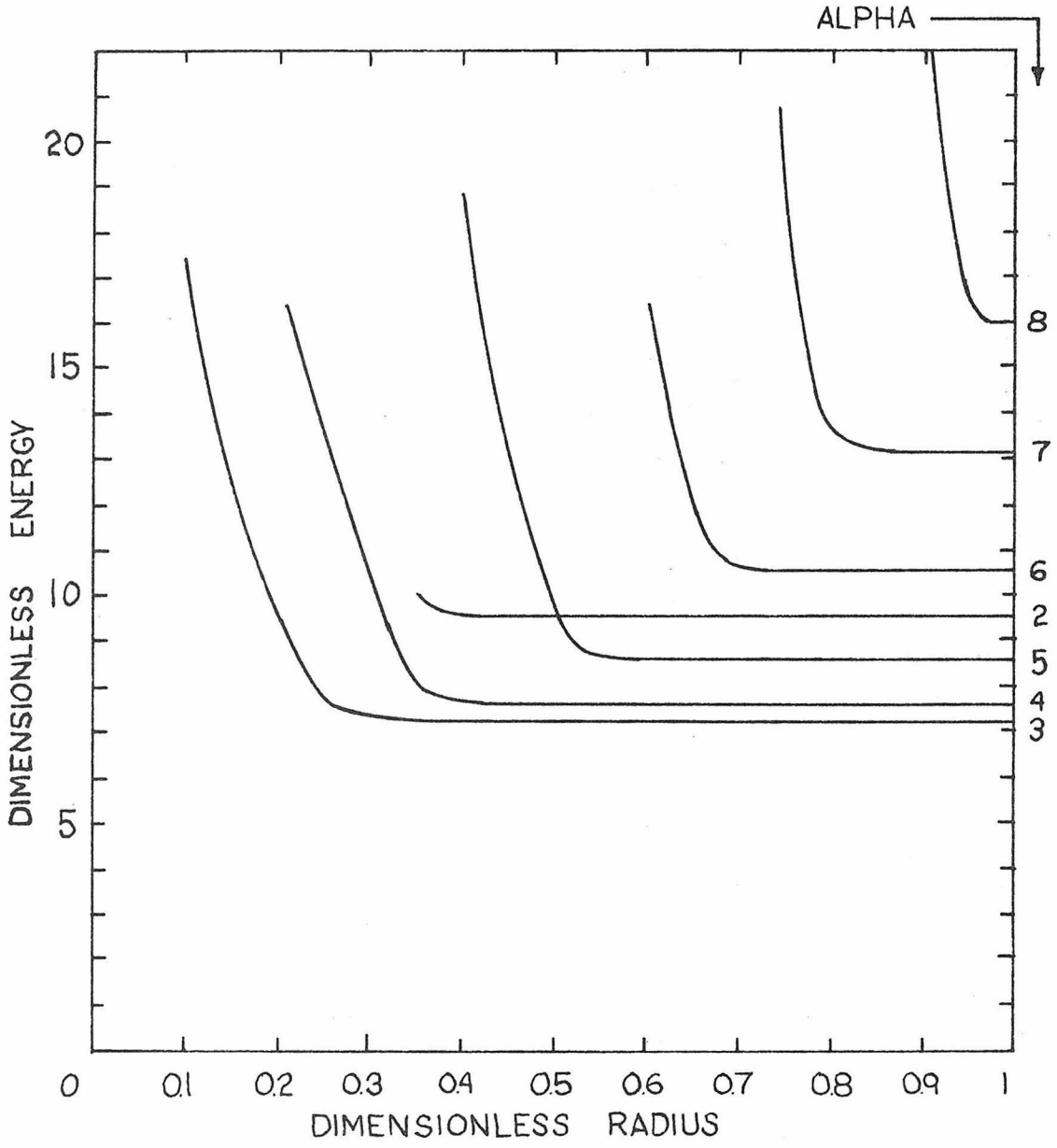

Figure13-Average Dimensionless Energy of Shearing Collisions Versus Dimensionless Mill Radius at Various Alphas

NOMENCLATURE

Dimensions of variables are given in length (l), force (f), and time (t) scales.

R = mill radius (l)

L = mill length (l)

ω = mill angular velocity (radians/t)

r_b = ball radius (l)

ρ_b = ball density (f/l^3)

C_b = mill ball charge (f)

ϵ = void fraction of balls in mill

α = constant describing shape of interface between active and inactive grinding zones

ϕ_{cr} = critical slope angle of balls

μ = internal friction of balls

g = acceleration of gravity (l/t^2)

x = particle size (l)

σ = total cross sectional area per particle area

Dimensionless quantities:

l = length (l)

$\bar{l}$ = $l\omega^2/g$ = dimensionless length

v = velocity (l/t)

$\bar{v}$ = $v\omega/g$ = dimensionless velocity

f = flow rate or collision frequency (t^{-1})

$\bar{f}$ = $f4\pi r_b^3\omega^3/(3(1-\epsilon)Lg^2)$ = dimensionless rate

E_{IM} = impact collision energy (fl)

$E_{IM}=E_{IM}3\omega^2/(2\pi r_b^3\rho_b g)$ = dimensionless impact collision energy

E_{SH}= shear collision energy (f1)

$E_{SH}= E_{SH}3g/(8\pi r_b^5\rho_s\omega^2)$ = dimensionless shear collision energy

APPENDIX A

Experimental and Theoretical Grinding Regions in a Small Ball Mill

Time exposures presented (Figure A1) show the motion of 1/32-inch lead pellets in a 1-inch radius tumbler at increasingly large rotational speeds. The theoretical position of the interface between the Active and Inactive Grinding egions based on Equation 4, with $\mu = 0.77$, is pictured in Figure A2. The approximate calculation of alpha tends to be smaller than the actual value. For angular velocities above 3.87 sec^{-1}, Neighborhood II disappears because the geometric size of Neighborhood I permits all the balls entering the Shearing Zone to be transported through Neighborhood I without the requirement of another additional neighborhood. For a rotational rate of 20.3 sec^{-1} a ring of inactive balls encircles the Free-Flight Zone because they fall outside a dimensionless radius on one.

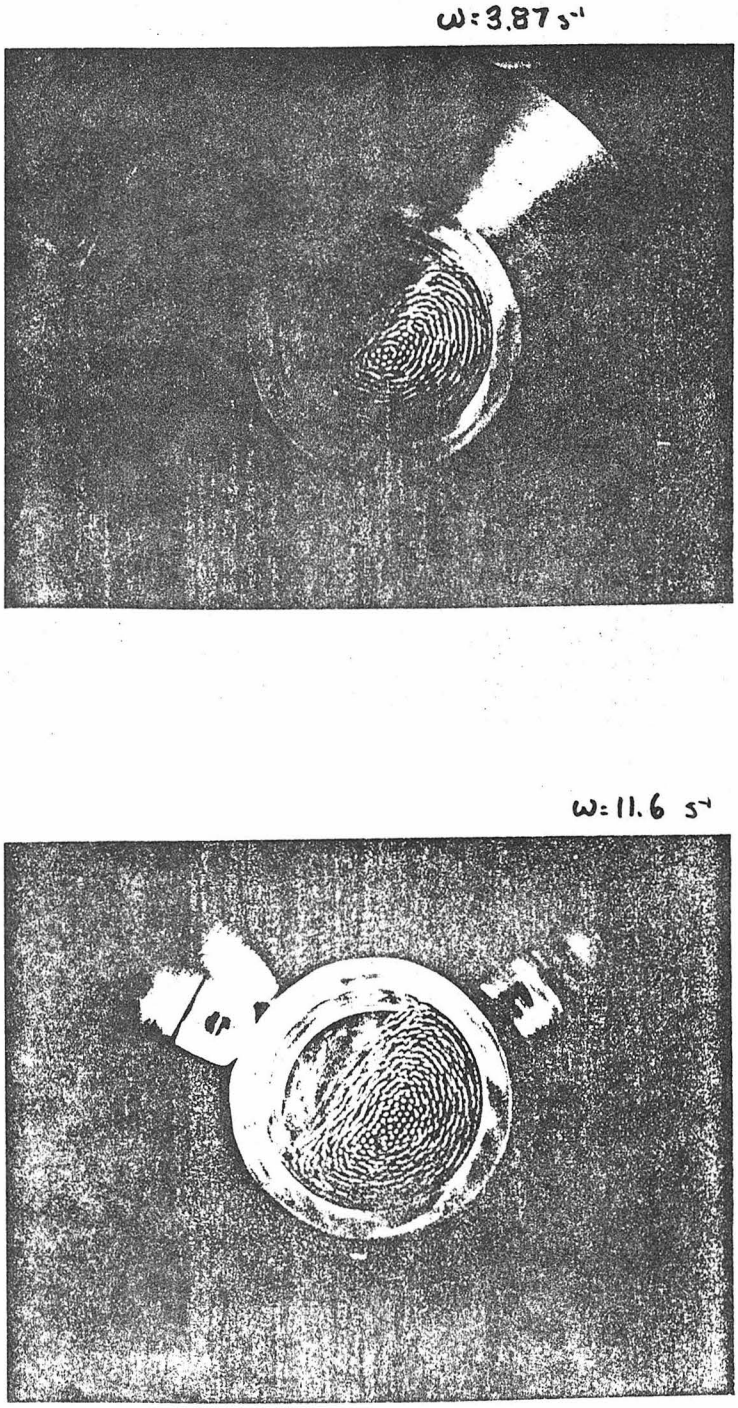

Figure A1-Motion of Pellets in a Small Tumbler

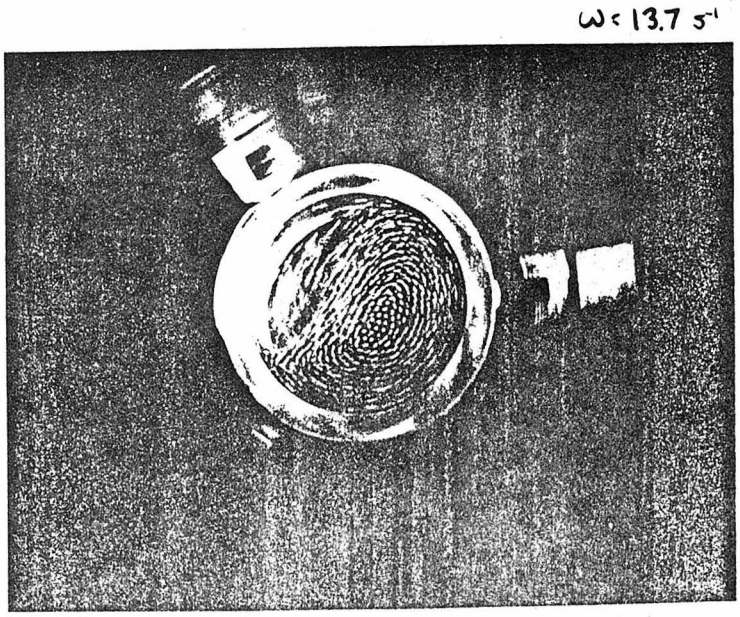

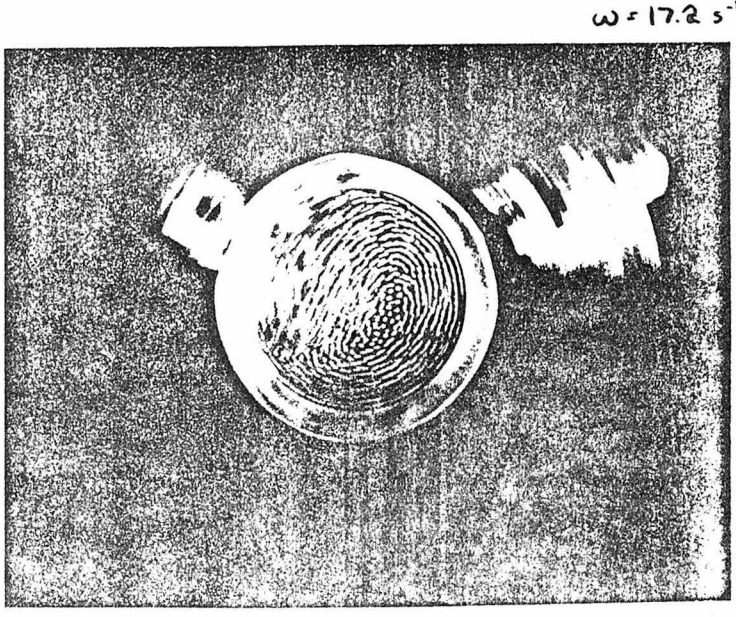

Figure A1-Motion of Pellets in a Small Tumbler

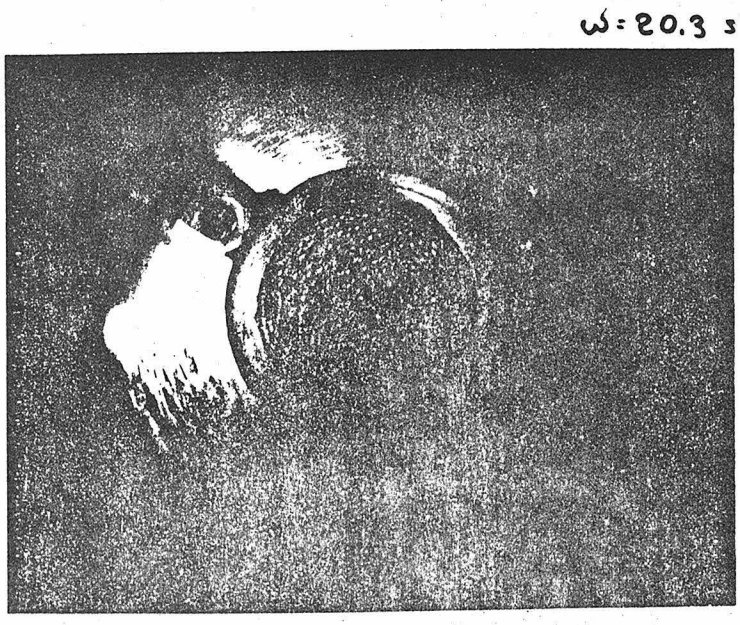

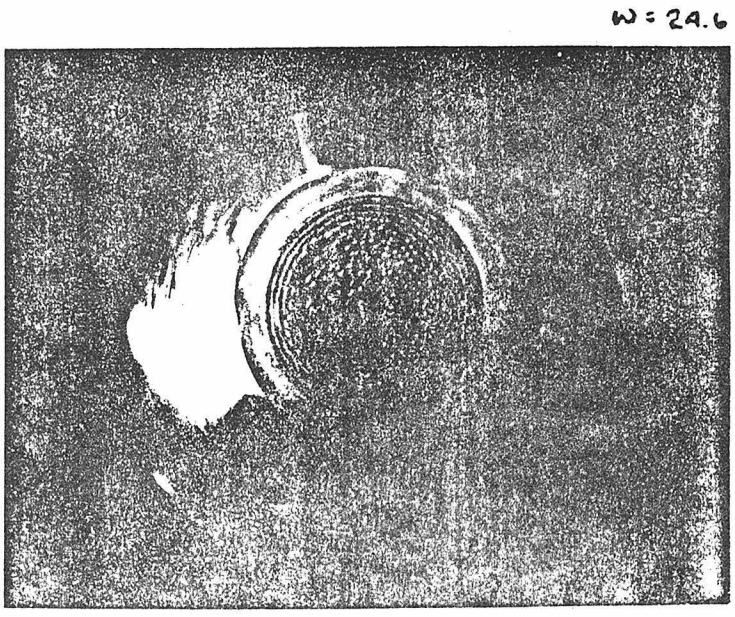

Figure A1-Motion of Pellets in a Small Tumbler

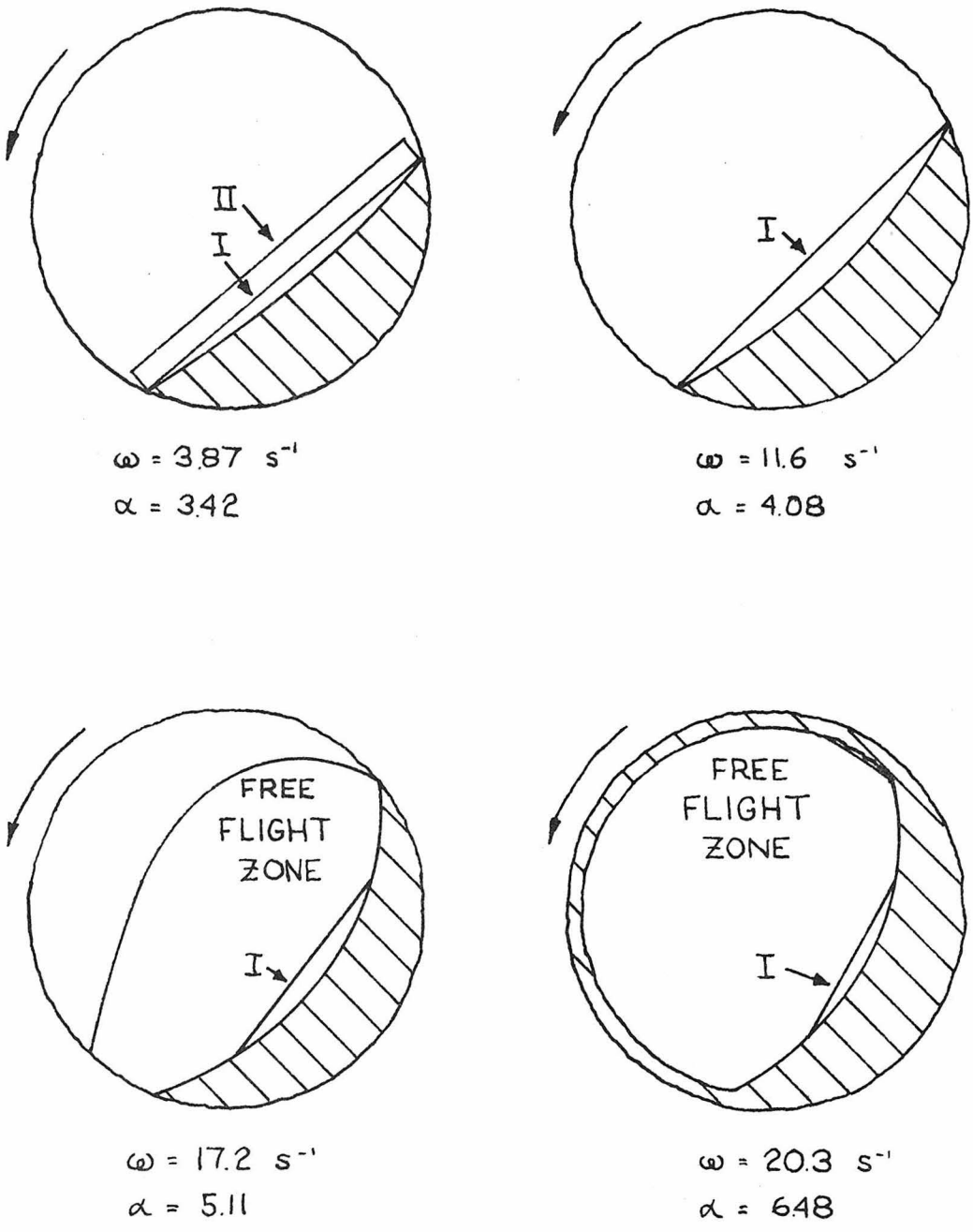

Figure A2-Theoretical Grinding Zones in a Ball Mill

Cross-hatching represents inactive balls. If present, Neighborhoods I and II and the Free-Flight Zone are labeled.

APPENDIX B

Computer Program for Calculating Alpha and Dimensionless Energy and Collision Frequency a Ball Mill

```
      IMPLICIT REAL*4 (A-Z)
      INTEGER LAYERS,L,LAYER1,LAYER2,I,KNT
      COMMON /DDTIME / W
      COMMON /BLK1/ RBAR,ALPHA,RBBALL
C      MILLING DIMENSIONS
      RMILL=1.
      G=384.
      P=0.395
      SIGMA=1.08
      E=0.26
      LNGTH=2.96/2.54
      MU=0.77
      RBALL=0.03125
      FPS=1.E-3
      MASS=4.19*RBALL**3
      TCR=ATAN(MU)
      DO 11111 I=1,70
      READ(5,10,END=9999) W,CB
10    FORMAT(8F10.0)
      WRITE(6,1000) RMILL,CB,RBALL,MU,E,P
1000  FORMAT(/' MILL RADIUS = ',F8.6,'  MILL CHARGE = ',F6.3,
     - ' PELLET RADIUS = ',F8.6,' FRIC COEF =',F6.3/' PELLET POROSITY =
     -',F6.3,' PELLET DENSITY = ',F7.4)
      RNEW=RMILL
      CNEW=CB
      RBAR=RMILL*W*W/G
      WRITE(6,1009) W,RBAR
C     INTERFACE EQUATION
1009  FORMAT(' OMEGA =',F6.2,'   DIMENSIONLESS RADIUS = ',F6.3)
      IF(RBAR.GT.1.) GO TO 100
      H=W*W*(0.573*CB/(RMILL*P*(1-E)*LNGTH)+0.1*RMILL)/G
      GR=SQRT(1+RBAR *RBAR +2*RBAR *COS(TCR))
      GT=1.571+ARCOS((GR*GR+1-RBAR *RBAR )*0.5/GR)
      KGT=1.571+ALOG(GR)/MU
      TOP=0.5*(KGT+GT)
      TP=MU*ALOG(EXP(TOP/MU)-H*EXP(1.571/MU)/SQRT(1+MU*MU))
      RP=EXP(TP/MU)*EXP(-1.571/MU)
      ALPHA=RP*EXP( MU*TP)
      WRITE(6,123) H,GR,GT,KGT,TOP,TP,RP
123   FORMAT( (1X,7E14.7) )
      WRITE(6,1001) ALPHA
1001  FORMAT(' INTERFACE DESCRIBED BY RP = ',F5.2,'*EXP(-MU*TP)',
     - T85,'  (R,T)  C.R.      (R,T)  DISPLACED')
      GO TO 20
100   RNEW=G/(W*W)
      AREA=3.14*(RMILL*RMILL-RNEW*RNEW)
      CNEW=CB-AREA*LNGTH*(1-P)*P
      RBAR=1.
      IF(CNEW.LT.0.) GO TO 30
      H=W*W*(0.573*CNEW/(RNEW*P*(1-E)*LNGTH)+0.1*RNEW)/G
      GR=SQRT(1+RBAR *RBAR +2*RBAR *COS(TCR))
      GT=1.571+ARCOS((GR*GR+1-RBAR *RBAR )*0.5/GR)
      KGT=1.571+ALOG(GR)/MU
      TOP=0.5*(KGT+GT)
      TP=MU*ALOG(EXP(TOP/MU)-H*EXP(1.571/MU)/SQRT(1+MU*MU))
      RP=EXP(TP/MU)*EXP(-1.571/MU)
      ALPHA=RP*EXP( MU*TP)
      WRITE(6,123) H,GR,GT,KGT,TOP,TP,RP
      WRITE(6,1002) CNEW,RNEW
1002  FORMAT(' SOME PELLETS CAPTURED'/' NEW TUMBLING PELLET CHARGE = ',
```

```
     -  ,F6.3,' NEW TUMBLING RADIUS = ',F6.3)
      WRITE(6,1001) ALPHA
      GO TO 20
30    WRITE(6,1010)
1010  FORMAT(' ENTIRE PELLET CHARGE IS CAPTURED ')
20    CONTINUE
      RBAR=RNEW*W*W/G
      RBBALL=RBALL*W*W/G
      F1=4.19*(RBALL*W)**3/((1-E)*LNGTH*G*G)
      WRITE(6,6550) F1
6550  FORMAT(' FLOWBAR = FLOW * ',E14.7,' (SEC)')
      F2=1./(8.3776*RBALL**5*W*W/G)
      WRITE(6,6551) F2
6551  FORMAT(' SHEARENERGYBAR = ENERGY * ',E14.7,' (LB/IN) INVERSE')
      F2=1./(2.0944*RBALL**3*P*G/W**2)
      WRITE(6,6554) F2
6554  FORMAT(' IMPACTENERGYBAR = IMPACTENERGY * ',E14.7)
      F3=W/G
      WRITE(6,6552) F3
6552  FORMAT(' VELOCITYBAR =VELOCITY * ',E14.7,' SEC/IN')
      F4=W*W/G
      WRITE(6,6553) F4
6553  FORMAT(' LENGTHBAR =LENGTH *',E14.7,' IN INVERSE')
1111   CALL MAIN1
  1    CONTINUE
9999  STOP
      END
      SUBROUTINE MAIN1
      IMPLICIT REAL*4 (A-Z)
      INTEGER LAYERS,L,LAYER1,LAYER2,I,KNT
      COMMON /DPTIME/ W
      COMMON /BLK1/ RBAR,ALPHA,RBBALL
      EPS=0.001
      G=384
      MU=0.77
      TCR=ATAN(MU)
      WRITE(6,12333) ALPHA,RBAR
12333 FORMAT(/'ALPHA =',F10.5,' RBAR = ',F10.5)
C
C     LOWER INTERCEPT
C
      KNT=0
      TP =1.571
      DTP=-0.1
      TP=TP-DTP
9000  TP=TP+DTP
       RP = ALPHA*EXP(-MU*TP)
      X=-RP*COS(TP)
      Y=1-RP*SIN(TP)
      R=SQRT(X*X+Y*Y)
      KNT=KNT+1
      IF(KNT.GT.20) GO TO 9001
      IF((R-RBAR)*DTP .GT. 0.) GO TO 9000
      IF(ABS(R-RBAR)/RBAR .LT. EPS) GO TO 9001
      DTP=-0.5*DTP
      GO TO 9000
9001  RLINT=RP
      CRLINT=R
      TLINT=TP
      CTLINT=ATAN(Y/X)
```

```
      IF(X.LT.0.) CTLINT=CTLINT-3.1415
      WRITE(6,1033) CRLINT,CTLINT,RLINT,TLINT,KNT
1033  FORMAT(' THEORETICAL BASAL CONTACT OF INTERFACIAL SURFACE',T85,
     -'(',F6.3,',',F6.3,')(',F6.3,',',F6.3,')',I3)
C
C     DISPLACED POLAR COORDINATE OF TANGENT ZONE
C
      KNT=0
      TN=0.0001
210   TO=TN
      KNT=KNT+1
      IF(KNT.GT.20) GO TO 212
      DUM=ALPHA*MU*EXP(-MU*TO)
      F=DUM-MU*SIN(TO)+COS(TO)
      FP=MU*DUM+MU*COS(TO)+SIN(TO)
      TN=TO+F/FP
      IF(ABS((TN-TO)/TO) .GT. EPS) GO TO 210
212   RTAN=ALPHA*EXP(-MU*TN)
      X=-RTAN*COS(TN)
      Y=1-RTAN*SIN(TN)
      CENT=ATAN(Y/X)
      IF(X.LT.0.) CENT=CENT+3.1416
      CRD=SQRT(X*X+Y*Y)
      WRITE(6,1004) CRD,CENT,RTAN,TN,KNT
1004  FORMAT(' POSITION OF ZERO RADIAL VELOCITY ON INTERAFCE ',T85,
     -'(',F6.3,',',F6.3,')(',F6.3,',',F6.3,')',I3)
      TTAN=TN
C
C     COORDINATES OF PEAK INTERCEPT OF INTERFACIAL ZONE
C
      KNT=0
      RN=RTAN+0.09
1003  RN=RN-0.1
      TN=-ALOG(RN/ALPHA)/MU
      X=-RN*COS(TN)
      Y=1-RN*SIN(TN)
      R=SQRT(X*X+Y*Y)
      KNT=KNT+1
      IF(KNT.GT.20) GO TO 112
      IF(R.LT.RBAR) GO TO 1003
      RN=RN+0.05
110   RO=RN
      KNT=KNT+1
      IF(KNT.GT.20) GO TO 112
      DUM=ALOG(RO/ALPHA)/MU
      F=1+RO*RO+2*RO*SIN(DUM)-RBAR*RBAR
      FP=2*RO+2*SIN(DUM)+2*COS(DUM)/MU
      RN=RO-F/FP
123   FORMAT(1X,8E14.7)
      IF(ABS((RN-RO)/RO).GT. EPS) GO TO 110
      TINTR=-ALOG(RN/ALPHA)/MU
      RINTR=RN
112   CONTINUE
      CRINTR=SQRT(1+RN*RN-2*RN*SIN(TINTR))
      CTINTR=ASIN((1-RN*COS(TINTR-1.571))/CRINTR)
      WRITE(6,1018) CRINTR,CTINTR,RN,TINTR,KNT
1018  FORMAT(' PEAK CONTACT OF INTERFACIAL SURFACE ',T85,
     -'(',F6.3,',',F6.3,')(',F6.3,',',F6.3,')',I3)
C
C   COORDINATES OF TAKEOFF POSITION
```

```
C
      XC=CRD*COS(CENT)
      YC=CRD*SIN(CENT)
      TP=TINTR
      DTP=0.25
      KNT=0
70009 TP=TP-DTP
      RP=ALPHA*EXP(-MU*TP)
      R=SQRT(1+RP*RP-2*RP*SIN(TP))
      X=-RP*COS(TP)
      Y=1-RP*SIN(TP)
      T=ATAN(Y/X)
       IF(X.LT.0.) T=T+3.14159
      TN=T
      VXO=-R*SIN(T)
      VYO=R*COS(T)
      XO=R*COS(T)
      YO=R*SIN(T)
      TM=(XC-XO)/VXO
      F=YC+TM*TM*0.5-VYO*TM-YO
      KNT=KNT+1
      IF(KNT.GT.20) GO TO 70019
      IF(F*DTP.LT.0.) GO TO 70009
      DTP=-0.5*DTP
      IF(ABS(F) .GT. 1.E-6      ) GO TO 70009
70019 CONTINUE
80109 CONTINUE
      CTTKOF=T
      CRTKOF=R
      RTKOF=RP
      TTKOF=TP
      IF(CRTKOF.LT.CRINTR) GO TO 10200
      CTTKOF=CTINTR
      RTKOF=RINTR
      CRTKOF=CRINTR
      TTKOF=TINTR
10200 CONTINUE
      IF(TTKOF.GT.TTAN) GO TO 10179
      CTTKOF=CENT
      CRTKOF=CRD
      TTKOF=TTAN
      RTKOF=RTAN
10179 CONTINUE
417   WRITE(6,1015) CRTKOF,CTTKOF,RTKOF,TTKOF,KNT
1015  FORMAT(' APPROXIMATE POSITION ON INTERFACE OF TAKEOFF',T85,
     -'(',F6.3,',',F6.3,')(',F6.3,',',F6.3,')',I3)
      KE=RP*R+(Y-YC)*2
      IF(CRTKOF.GT.(CRINTR-1.E-6)) KE=0.
      WRITE(6,4357) KE
4357  FORMAT(' DIMENSIONLESS IMPACT ENERGY MINIMUM ON PELLET MASS ',
     - T85,E14.7)
C
C  ENERGY ALLOCATION
C
C   SHEAR ZONE GEOMETRY
C
      DUM=SQRT(1+ALPHA*ALPHA*EXP(-6.28*MU))
      FLOW=0.5*(RBAR*RBAR-CRD*CRD)
      WRITE(6,1020) FLOW
1020  FORMAT(' DIMENSIONLESS FLOW OF PELLETS INTO GRINDING STATE ',
```

```
     - T70,E14.7)
      NUMS=0.5*(CRTKOF*CRTKOF-CRD*CRD)
      WRITE(6,1006) NUMS
1006  FORMAT(' DIMENSIONLESS FLOW OF PELLETS INTO PURE SHEAR ZONE ',
     - T70,E14.7)
      NUMIS=0.5*(RBAR*RBAR-CRTKOF*CRTKOF)
      WRITE(6,1007) NUMIS
1007  FORMAT(' DIMENSIONLESS FLOW OF PELLETS INTO IMPACTION ',
     - T70,E14.7)
      NUMN=3.1416*CRD*CRD
      IF(ALPHA*EXP(-MU*1.571) .GT. 1.) NUMN=0
      WRITE(6,1008) NUMN
1008  FORMAT(' DIMENSIONLESS PELLETS INERT ',T70,E14.7)
       TANINV=ATAN(-1/MU)
      PSI1=TANINV+TTAN
      THETAX=-ALOG(2*EXP(-MU*TTAN)-EXP(-MU*TTKOF))/MU
      ARC=SQRT(RTAN*RTAN+RTKOF*RTKOF-2*RTAN*RTKOF*COS(TTKOF-TTAN))
      BIGPSI=-(THETAX-TTKOF)*0.5
      H=ARC*SIN(BIGPSI)
      WRITE(6,1026) ARC
1026  FORMAT(' HALF DIMENSIOLESS ARC LENGTH OF CONTACT OF SHEAR ZONE',
     - 1X,F7.4)
      SP=2*ARC*COS(BIGPSI)
      VOMAX=SQRT(SP*0.5*SIN(PSI1))
        S2=0.667*NUMS/VOMAX-H
      IF(S2.LT.0.) S2=0.
      WRITE(6,12385) H,ARC,S2
12385 FORMAT(' DIMENSIONLESS DEPTH OF ZONE I ',T40,      E14.7
     -/' DIMENSIONLESS HALFARC OF ZONE I ',T40,E14.7
     -/' DIMENSIONLESS DEPTH OF ZONE II ',T40,E14.7)
      WRITE(6,123) PSI1,PSI3,THETAX,PSI4,BIGPSI,H,SP,S2,VOMAX
8020  CONTINUE
      COLSN1=1.33*VOMAX*SP*H*(0.5-0.33*H/(H+S2))/(H+S2)
       KE=3.33*VOMAX*VOMAX/(H+S2)
      COLSN2=0.66*VOMAX*SP*(H*H/(H+S2)+S2-H)/(H+S2)
      WRITE(6,1012) COLSN1,COLSN2,KE
1012  FORMAT(' DIMENSIONLESS SHEAR COLLISIONS ZONE I ',T70,E14.7
     -/' DIMENSIONLESS SHEAR COLLISIONS ZONE II ',T70,E14.7
     -/' DIMENSIONLESS SHEAR ENERGY ',T55,E14.7)
32151 CONTINUE
C
C
      IF(CRTKOF.GT. (CRINTR-1.E-6) ) GO TO 10101
      VYO=(CRINTR-1.E-5)*COS(CTINTR+1.E-5)
      VXO=-(CRINTR-1.E-5)*SIN(CTINTR+1.E-5)
      YO=-VXO
      XO=VYO
      TIME=0.
      DT= .2
      KNT=0
8000  TIME=TIME+DT
      IF(TIME.LT.0.) GO TO 8003
      KNT=KNT+1
      IF(KNT.GT.20) GO TO 8003
      Y=-TIME*TIME*0.5+VYO*TIME+YO
      X=VXO*TIME+XO
      RP=SQRT(X*X+(1-Y)*(1-Y))
      TP=ATAN((Y-1)/X)
      IF(X.GT.0.) TP=TP+3.14
      R=SQRT(X*X+Y*Y)
```

```
      T=ATAN(Y/X)
      IF(X.LT.0.) T=T-3.14
      FINT=RP-ALPHA*EXP(-MU*TP)
      FMILL=R-RBAR
      IF(FINT .GT. 0.) GO TO 8001
      IF(FMILL .GT. 0.) GO TO 8002
      GO TO 8000
C   HIT THE WALL
8002  IF(FINT.LT.0.) GO TO 80069
      TIME=TIME-DT
      DT=0.5*DT
      GO TO 8000
80069 IF(FMILL*DT.LT.0.) DT=-DT
80067 DT=-0.5*DT
80068 TIME=TIME+DT
      IF(TIME.LT.0.) GO TO 8003
      KNT=KNT+1
      IF(KNT.GT.20) GO TO 8003
      Y=-TIME*TIME*0.5+VYO*TIME+YO
      X=VXO*TIME+XO
      R=SQRT(X*X+Y*Y)
      T=ATAN(Y/X)
      IF(X.LT.0.) T=T-3.14
      FMILL=R-RBAR
      IF(FMILL*DT .LT.0.) GO TO 80068
      IF(ABS(DT/TIME).LT.1.E-3) GO TO 8003
      GO TO 80067
8001  IF(FMILL .LT. 0.) GO TO 80057
      TIME=TIME-DT
      DT=0.5*DT
      GO TO 8000
80057  IF(FINT*DT.LT.0.) DT=-DT
80059  DT=-0.5*DT
8007   TIME=TIME+DT
      IF(TIME.LT.0.) GO TO 8003
      Y=-TIME*TIME*0.5+VYO*TIME+YO
       X=VXO*TIME+XO
      RP=SQRT(X*X+(1-Y)*(1-Y))
      TP=ATAN((Y-1)/X)
      IF(X.GT.0.) TP=TP+3.14
      FINT=RP-ALPHA*EXP(-MU*TP)
      KNT=KNT+1
      IF(KNT.GT.20) GO TO 8008
      IF(FINT*DT.LT.0.) GO TO 8007
      IF(ABS(DT/TIME) .LT. 1.E-3) GO TO 8008
      GO TO 80059
8008  CONTINUE
      WRITE(6,1050) RP,TP  ,KNT
1050  FORMAT(' OUTERMOST PROJECTED PELLET HAS COLLIDIED WITH PELLET MASS
     - AT PRIMED COORD ',T85, '(',F6.3,',',F6.3,')',I3)
      KE=(VO-Y)*2*R*R
      WRITE(6,1613) KE
1613  FORMAT(' DIMENSIONLESS IMPACT ENERGY OF PELLET ON MASS = ',
     - T85,E14.7)
      NUMW=0.
      GO TO 8019
8003  CTCOLL=I
      WRITE(6,1032) R   ,CTCOLL,KNT
1032  FORMAT(' OUTERMOST PPROJECTED PELLEET HAS COLLIDED WITH MILL ',
     -'WALL AT CR COORDINATE ',T85,
```

```
     -'(',F6.3,',',F6.3,')',I3)
      VBAR=SQRT(VXO*VXO+(-TIME+VYO)**2)
      KE=VBAR*VBAR
      WRITE(6,1031) KE
1031  FORMAT(' DIMENSIONLESS IMPACT ENERGY ON WALL OF FURTHERST PELLET',
     - T85,E14.7)
C
C     NUMBER OF PELLETS COLLIDING WITH MILL WALL
C
      XC=CRLINT*COS(CTLINT)
      YC=CRLINT*SIN(CTLINT)
      TP=TINTR
      TN=1.E20
      DTP=0.1
      KNT=0
7000  TP=TP-DTP
      TO=TN
      RP=ALPHA*EXP(-MU*TP)
      R=SQRT(1+RP*RP-2*RP*SIN(TP))
      X=-RP*COS(TP)
      Y=1-RP*SIN(TP)
      T=ATAN(Y/X)
      IF(X.LT.0.) T=T+3.1416
      TN=T
      VXO=-R*SIN(T)
      VYO=R*COS(T)
      XO=R*COS(T)
      YO=R*SIN(T)
      TM=(XC-XO)/VXO
      F=YC+TM*TM*0.5-VYO*TM-YO
      KNT=KNT+1
      IF(KNT.GT.20) GO TO 7001
      IF(F*DTP .LT.0.) GO TO 7000
      DTP=-0.5*DTP
      IF(ABS((TN-TO)/TN) .GT. 1.E-3) GO TO 7000
7001  CONTINUE
8010  CONTINUE
      NUMW=0.5*(PBAR*RBAR-R*R)
      WRITE(6,1055) NUMW
1055  FORMAT(' DIMENSIONLESS PELLETS STRIKING WALL = ',T70,E14.7)
      KE=(YO-YC)*2*R*R
      WRITE(6,1513) KE
1513  FORMAT(' DIMENSIONLESS IMPACT ENERGY AT BASE OF INTERFACE = ',
     - T85,E14.7)
8019  CONTINUE
10101 CONTINUE
1     CONTINUE
      RETURN
      END
```

REFERENCES

1. Austin,L.G.1964.The Theory of Grinding Operations. Industrial and Engineering Chemistry.56:18-29.

2. Austin,L.G.1971/1972.Experimental Methods for Grinding Studies in Laboratory Mills.Powder Technology.5:261-266.

3. Austin,L.G.1971/1972.The Estimation of Non-Normalized Breakage Distribution Parameters from Batch Grinding Tests.Powder Technology.5:267-271.

4. Austin,L.G.1973.Understanding Ball Mill Sizing. Industrial Engineering Chemistry Process Des. Develop..12:121-129.

5. Bowdish,F.W.1960.Theoretical and Experimental Studies of the Kinetics of Grinding in a Ball Mill.AIME Trans..217:194-202.

6. Gaudin,A.M.1962.Model and Comminution Distribution Equation for Repeated Fracture. Trans. SME/AIME. 223:43

7. Kelsall,D.F.1967.Continuous Grinding in a Small Wet Ball Mill Part I. A study of the Influence of Ball Diameter.Powder Technology.1:291-300.

8. Kelsall,D.F.1968.Continuous Grinding in a Small Wet Ball Mill Part II. A Study of the Influence of Hold-Up Weight.Powder Technology.2:162-168.

9. Kelsall,D.F.1969.Continuous Grinding in a Small Wet ball Mill Part III. A Study of Distribution of Residence Time.Powder Technology.3:170-178.

10. Kelsall,D.F.1973.Continuous Grinding in a Small Wet Ball Mill Part IV. A Study of the Influence of Grinding Media Load and Density.Powder Technology. 7:293-301.

11. Kuwahara,Y.1971.Experimental Study of Selection Function and Distribution Function.Journal of Chemical Engineering of Japan.4:359-363.

12. Langemann,H.1962.Kinetik der Hertzerkleinerung. Chemie-Ing. Techn..34:615-627.

13. Olsen,T.O.1972.Mathematical Model of Grinding at Different Conditions in Ball Mills.Trans. SME/ AIME.252:452-457.

14. Tamura,K.1970.Rate of Ball Milling and Vibration Milling on the Basis of the Comminution Law. Industrial Engineering Chemistry Process Design Development.9:165-173.